In this thesis we investigate the interplay between dissipation and driving in nonlinear quantum systems for a special setup: a flux qubit read out by a DC-SQUID - a nonlinear quantum oscillator. The latter is embedded in a harmonic bath, thereby mediating dissipation to the qubit.

Two different approaches are elaborated: First we consider a composite qubit-SQUID system and add the bath afterwards. We derive analytical expressions for its eigenstates beyond rotating wave approximation (RWA), by applying Van Vleck perturbation theory (VVPT) in the qubit-oscillator coupling. The second approach is an effective bath approach based on a mapping procedure, where SQUID and bath form an effective bath seen by the qubit. Here the qubit dynamics is obtained by applying standard procedures established for the spin-boson problem. This approach requires the knowledge of the steady-state response of the dissipative Duffing oscillator, which is studied within a resonant and an off-resonant approach: The first is applicable near and at an N-photon resonance using VVPT beyond a RWA. The second is based on the exact Floquet states of the nonlinear driven oscillator.

The dissipative qubit dynamics is described analytically for weak system-bath coupling and agrees well for both approaches. We derive the effect of the nonlinearity on the qubit dynamics, on the Bloch-Siegert shift and on the vacuum Rabi splitting.

Universitätsverlag Regensburg

ISBN 978-3-86845-072-9

gefördert von:

Alumni der physikalischen Fakultät der Universität Regensburg e.V.

Universität Regensburg

Dissertationsreihe Physik - Band 19

Carmen Vierheilig

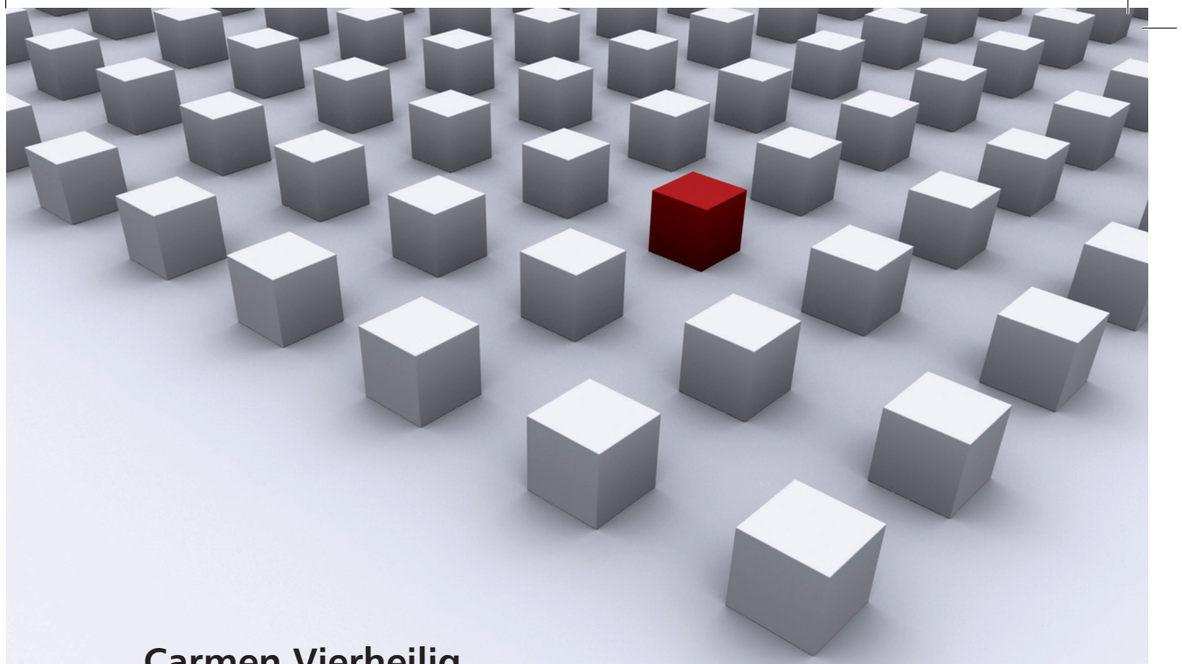

Interplay between dissipation and driving in nonlinear quantum systems

Universitätsverlag Regensburg

Carmen Vierheilig

19

Dissertationsreihe Physik

Carmen Vierheilig

Interplay between dissipation and driving in nonlinear quantum systems

Interplay between dissipation and driving in nonlinear quantum systems

Dissertation zur Erlangung des Doktorgrades der Naturwissenschaften (Dr. rer. nat.) der naturwissenschaftlichen Fakultät II - Physik der Universität Regensburg vorgelegt von

Carmen Vierheilig

aus Tegernheim
2010

Die Arbeit wurde von Prof. Dr. Milena Grifoni angeleitet.
Das Promotionsgesuch wurde am 12.01.2010 eingereicht.
Das Promotionskolloquium fand am 23.11.2010 statt.

Prüfungsausschuss: Vorsitzender: Prof. Dr. Jascha Repp
1. Gutachter: Prof. Dr. Milena Grifoni
2. Gutachter: Dr. Tobias Kramer
weiterer Prüfer: Prof. Dr. Vladimir Braun

Dissertationsreihe der Fakultät für Physik der Universität Regensburg, Band 19

Herausgegeben vom Präsidium des Alumnivereins der Physikalischen Fakultät:
Klaus Richter, Andreas Schäfer, Werner Wegscheider, Dieter Weiss

Carmen Vierheilig

Interplay between dissipation and driving in nonlinear quantum systems

Universitätsverlag Regensburg

Bibliografische Informationen der Deutschen Bibliothek.
Die Deutsche Bibliothek verzeichnet diese Publikation
in der Deutschen Nationalbibliografie. Detailierte bibliografische Daten
sind im Internet über http://dnb.ddb.de abrufbar.

1. Auflage 2011

Leibnizstraße 13, 93055 Regensburg

Konzeption: Thomas Geiger
Umschlagentwurf: Franz Stadler, Designcooperative Nittenau eG
Layout: Carmen Vierheilig
Druck: Docupoint, Magdeburg
ISBN: 978-3-86845-072-9

Weitere Informationen zum Verlagsprogramm erhalten Sie unter:
www.univerlag-regensburg.de

Interplay between dissipation and driving in nonlinear quantum systems

DISSERTATION ZUR ERLANGUNG DES DOKTORGRADES DER NATURWISSENSCHAFTEN (DR. RER. NAT.)
DER NATURWISSENSCHAFTLICHEN FAKULTÄT II - PHYSIK

DER UNIVERSITÄT REGENSBURG

vorgelegt von

Carmen Vierheilig

aus
Tegernheim

im Jahr 2010

Die Arbeit wurde angeleitet von: Prof. Dr. Milena Grifoni
Promotionsgesuch eingereicht am: 12.01.2010
Das Promotionskolloqium fand am 23.11.2010 statt.

Prüfungsausschuss: Vorsitzender: Prof. Dr. Jascha Repp
1. Gutachter: Prof. Dr. Milena Grifoni
2. Gutachter: Dr. Tobias Kramer
weiterer Prüfer: Prof. Dr. Vladimir Braun

Contents

Chapter 1

Introduction

Investigating the interplay of dissipation and driving for nonlinear systems, in particular for nonlinear oscillators, is essential to understand a large variety of physical systems, including electrical circuits, nanoresonators or SQUIDs (superconducting quantum interference device) acting as read-out devices for qubits. Dissipation affects the system dynamics in two ways: it leads to energy loss and hence to damping of the motion as well as to decoherence as a consequence of dephasing. While dissipative effects perturb or even strongly affect the motion of the system under consideration, an additional tunable driving can act as a source of energy and stabilize the dynamics. Therefore an efficient amplification that counteracts the dissipation is possible. Moreover, taking into account an external driving is more appropriate to the experimental situation, where external voltages or currents are applied. Within a quantum mechanical interpretation dissipation enters a system which is coupled to an environment. The latter is treated as a bath containing infinitely many degrees of freedom. The bath measures continuously the system thereby destructing phase correlations and causing decoherence [1]. A famous model for including environmental effects on a quantum level is the Ullersma-Zwanzig-Caldeira-Leggett model [2, 3, 4, 5]. The bath is a reservoir composed of independent harmonic oscillators, where each one is coupled bilinearily to the system of interest. This kind of coupling allows an exact elimination of the bath degrees of freedom, when the reduced dynamics of the system is considered. Understanding dissipative effects and decoherence including driving allows to construct efficient procedures in quantum computation to achieve longer coherence times. When on top of this nonlinearity comes into play, we observe new behavior of the system, like bistability, frequency doubling, higher harmonics generation and nonlinear response [6, 7]. Thus quantum computation schemes can benefit from the use of nonlinear devices, which allow for e.g. efficient amplification of signals or improved read-out schemes for qubits [8, 9, 10, 11]. To observe coherent effects a quantum description of nonlinear systems is essential. This will be elaborated in this thesis for the case of a SQUID modeled as a nonlinear oscillator in the deep quantum regime.
Imposing a nonlinearity allows insight into the classical to quantum transition of a system [12], which exists both in the deep quantum and in the classical regime. The reason for testing the transition using a nonlinear system relies on the fact that Ehren-

fest theorem does not hold any more. Ehrenfest stated [13, 14], based on the fact that the classical limit is embedded in quantum mechanics, that for a strictly linear system the classical equations of motion are valid for the expectation values:

$$M\frac{d^2}{dt^2}\langle\hat{y}\rangle \;=\; -\langle\frac{\partial}{\partial\hat{y}}V(\hat{y})\rangle, \tag{1.1}$$

where $\hat{y}$ denotes the position operator of a particle with mass M moving in a potential $V(\hat{y})$. Moreover, the expectation values of quantum mechanical observables fulfill the classical equations of motion if the replacement $\langle V(\hat{y})\rangle \rightarrow V(\langle\hat{y}\rangle)$ holds. This is exactly valid if all derivatives of the force $\frac{\partial}{\partial\hat{y}}V(\hat{y})$ from the second one on vanish, as in the case of a harmonic oscillator. It is approximately valid only when the force $\frac{\partial}{\partial\hat{y}}V(\hat{y})$ varies slowly over the spatial extent of the wavefunction, which is about the de Broglie wavelength. This is verified for extremely localized wave packets and according to the partition theorem this fact corresponds to high temperatures with respect to the other energy scales of the system. Then semiclassical or classical treatments are allowed. For a nonlinear oscillator with nonlinearity $\sim \hat{y}^n$ the exact agreement of the equations of motion does not hold anymore, as in general the following equality for the position operator $\hat{y}$ is not fulfilled: $\langle\hat{y}^n\rangle \neq \langle\hat{y}\rangle^n$, $n > 2$, such that the mean value of the system's coordinate $\langle\hat{y}\rangle$ does not obey the classical nonlinear equation of motion. This fact manifests itself e.g. in the behaviour of the Duffing oscillator, - a driven nonlinear oscillator - : while the classical Duffing oscillator exhibits hysteresis in its steady-state response, the quantum one does not [15]. In particular, the interplay of driving and nonlinearity at the quantum level allows completely new system behavior, like multiphoton-resonances and antiresonances in the response of the system [16, 17, 18, 19, 20].

We start this chapter with the presentation of the various approximation schemes and approaches elaborated in the main part of this thesis. Then we describe a classical nonlinear system and consider afterwards nonlinear quantum systems. Various experimental realizations are shown to provide insight into the state of the art and the limitations of todays experiments as well as the corresponding theoretical works. Although the variety of nonlinear systems is large, we mainly focus on nanoresonators, Josephson junction devices or SQUIDs and consider the qubit read-out via a nonlinear DC-SQUID. The next chapter is dedicated to the inclusion of dissipative effects and to the spin-boson model. Moreover, the dynamical quantity of interest characterizing the qubit dynamics is investigated.

The main goal of this thesis was to clarify the effects of the SQUID on the qubit dynamics, when the SQUID is treated as a nonlinear device in the deep quantum regime. For the tripartite setup, composed of qubit, SQUID and harmonic bath we elaborated two different approaches to determine the qubit dynamics, shown in Fig. 1.1. The first (yellow box) is perturbative in the qubit-oscillator coupling, but exact in the tunneling amplitude of the qubit. The second (red box), in contrast, is based on an effective bath description, where the qubit read-out device, the SQUID, and the harmonic bath form an effective environment. The second approach is perturbative in the tunneling amplitude and in the qubit-oscillator coupling. As will be shown in the following

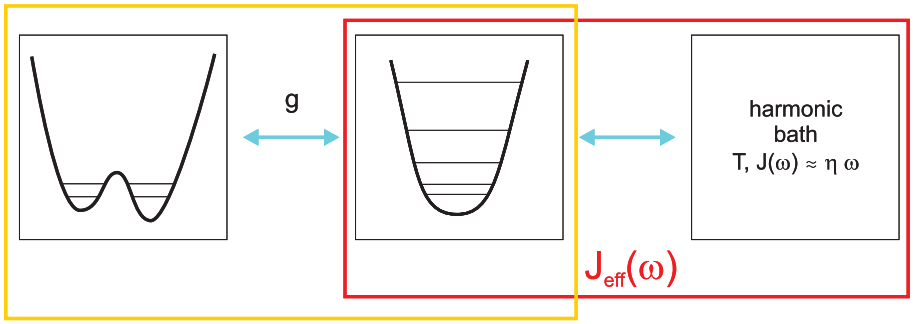

Figure 1.1: *Two different approaches for treating the tripartite system. The first is to start with diagonalizing the qubit-nonlinear oscillator system and adding the bath afterwards (yellow box). The second approach relies on building an effective bath with effective spectral density $J_{\text{eff}}(\omega)$, which includes the oscillator and the harmonic bath (red box). This composed system is then coupled to the qubit.*

chapters there is a mapping procedure for linear systems to build an effective bath composed of the read-out device and the harmonic bath, where the effective bath is characterized by an effective spectral density with structured form. We investigated an approximate mapping procedure for nonlinear systems using linear response theory to determine the effective spectral density in chapter 5. For this purpose, the knowledge of the steady-state response of the dissipative Duffing oscillator is essential. Consequently, we start in the main part of this thesis with the quantum Duffing oscillator and determine its dissipative steady-state dynamics for the one-photon resonance. We study the quantum Duffing oscillator within two different approaches in chapter 3. The first is based on the exact Floquet states of the driven harmonic oscillator and the nonlinearity is treated perturbatively. It well describes the dynamics in the off-resonant regime, i.e., when the driving frequency is far off any of the resonances of the nonlinear oscillator. The second, in contrast, is applicable at and in the vicinity of an N-photon resonance and exploits quasi-degenerate perturbation theory for the nonlinear oscillator in Floquet space. Thereby we avoid the application of a rotating wave approximation, which has always been used up to now [16, 18]. The second approach is perturbative in both driving and nonlinearity. While in the first one the linear system can be retained back at any step of the calculation, in the second the finite nonlinearity is essential for achieving a certain resonance condition and can therefore no more be set to zero. However, these two analytical treatments can be combined to yield the possibility to cover a wide range of driving frequencies. Then we calculate the dissipative steady-state dynamics of a quantum Duffing oscillator near and at the one-photon resonance and observe a characteristic antiresonance in the amplitude of the response. Finally we investigate the case of an off-resonant approach for the dissipative dynamics of the quantum Duffing oscillator, based on the solution for the corresponding linear system. We demonstrate the difficulties, when both nonlinearity and driving have to be considered without applying a resonance condition. In the next step, chapter 4, the composite system of a qubit and a nonlinear undriven os-

cillator, the latter embedded in an Ohmic bath, is considered following the approach indicated by the yellow box in Fig. 1.1. Here, first the energy spectrum of qubit plus oscillator is investigated and afterwards the effects of the bath are included via a Born-Markov master equation. In particular, by treating the nonlinearity up to first order and applying Van Vleck perturbation theory up to second order in the qubit-oscillator coupling, we derive an analytical expression for the eigenstates and eigenfunctions of the coupled qubit-NLO system beyond the rotating wave approximation. We derive the effect of the nonlinearity on the qubit dynamics and on the Bloch-Siegert shift and present a nonlinearity-decreased vacuum Rabi splitting. The second part of chapter 4 deals with the dissipative dynamics. In the regime of weak coupling to the thermal bath, analytical expressions for the time evolution of the qubit's populations are derived: they describe a multiplicity of damped oscillations superimposed on a complex relaxation part towards thermal equilibrium. The long-time dynamics is characterized by a single relaxation rate, which is maximal when the qubit is tuned to one of the resonances with the nonlinear oscillator. In chapter 5 we focus on an effective bath description, indicated by the red box in Fig. 1.1 and investigate the qubit dynamics. The read-out SQUID, modeled as a nonlinear quantum oscillator, and an Ohmic bath form an effective bath, which is then coupled to the qubit. This composed system can be mapped onto that of a qubit coupled to an effective bath. An approximate mapping procedure to determine the spectral density of the effective bath is given. Specifically, within a linear response approximation the effective spectral density is given by the knowledge of the linear susceptibility of the nonlinear quantum oscillator. To determine the actual form of the susceptibility, we consider its periodically driven counterpart, the problem of the quantum Duffing oscillator within linear response theory in the driving amplitude. Knowing the effective spectral density, which includes all effects of the bath, the qubit dynamics is investigated. In particular, an analytic formula for the qubit's population difference is derived. Within the regime of validity of our theory, a very good agreement is found with predictions obtained from a Bloch-Redfield master equation approach applied to the composite qubit-nonlinear oscillator system, i.e., the two complementary approximation schemes in Fig. 1.1 agree very well. Furthermore a comparison of the dynamics of the qubit coupled to a harmonic oscillator with the nonlinear one using the effective bath description in the non-interacting blip approximation (NIBA) is put forward. In chapter 6 conclusions are drawn. Parts of this thesis have already been published in [20, 21, 22, 23, 24].

1.1 Classical nonlinear systems

In this section we give an insight into the rich dynamics of classical nonlinear systems and their differences compared to the underlying linear systems. Exemplarily we mention a LCR-circuit with either nonlinear inductivity or capacitance [25] and the well-known damped pendulum equation with harmonic forcing. Their equation of motion is the famous one of the Duffing oscillator, which is approximated by a sinusoidal driven and damped harmonic oscillator with mass M, eigenfrequency Ω, damping constant γ and cubic nonlinearity denoted by α [6, 26]:

$$\ddot{y} + \gamma\dot{y} + \Omega^2 y + \frac{\alpha}{M}y^3 \;=\; -\frac{F}{M}\cos\omega_{ex}t. \tag{1.2}$$

The driving amplitude is denoted by F and the driving frequency by ω_{ex}. In case of small amplitudes we can neglect the nonlinear term and the response reduces to the one of the *underlying linear system* [25, 6], which is determined by a superposition of the solution for the homogeneous and a special solution for the inhomogeneous differential equation obtained e.g. by the complex variable method [27, 26]:

$$\begin{aligned} y(t) &= y_{\text{hom}}(t) + y_{\text{inhom}}(t) \qquad (1.3)\\ &= \exp\left(-\frac{\gamma}{2}t\right)\left\{C_1\sin\left[\sqrt{\Omega^2-\frac{\gamma^2}{4}}t\right] + C_2\cos\left[\sqrt{\Omega^2-\frac{\gamma^2}{4}}t\right]\right\} - A\cos(\omega_{ex}t+\phi_0), \end{aligned}$$

where C_1 and C_2 are determined by initial conditions. The first part shows exponential damping, while the second, the so-called steady-state, oscillates at the driving frequency and is therefore harmonic. The amplitude of the steady-state is determined by the frequency-amplitude relation:

$$\frac{F^2}{M^2} \;=\; A^2\left[(-\omega_{ex}^2+\Omega^2)^2 + \gamma^2\omega_{ex}^2\right].$$

The additional phase ϕ_0 in the steady-state oscillation originates from the damping and the deviation of driving and eigenfrequency:

$$\tan\phi_0 \;=\; \frac{-\gamma\omega_{ex}}{-\omega_{ex}^2+\Omega^2}. \tag{1.4}$$

The amplitude of the steady-state response increases rapidly close to $\omega_{ex} \approx \Omega$ or for large driving amplitudes. As a consequence we can not disregard the nonlinearity [6]. According to Hayashi [28] there is no general method for the solution of nonlinear differential equations. Consequently, various types of approximation procedures are applied, for example Lindstedt-Poincare perturbation method [7], restricting to a perturbation around $\Omega = \omega_{ex}(1+\epsilon)$, where ϵ denotes the detuning. This perturbative approach effectively couples the free part of the oscillation with the steady-state part. Therefore the general decomposition procedure in a homogeneous and a special solution fails when finite nonlinearity and detunings are considered. In this case we apply Lindstedt perturbation theory, whose main advantages are [6]: first the solution for the dynamics of the system is a periodic one based on the underlying linear system, which is the starting point for the perturbative approach [7]. Second the requirement to have a periodic solution and to avoid secular terms leading to divergences determines the frequency-amplitude relation. Third a systematic inclusion of higher harmonics is possible by considering higher orders in the perturbation theory.
Lindstedt perturbation theory provides a solution of a nonlinear differential equation around the *underlying linear equation* [7, 28] via a perturbative treatment of F, α, γ and $\Omega - \omega_{ex}$ leading in lowest order to:

$$y(t) \;=\; A\cos(\omega_{ex}t+\phi_0), \tag{1.5}$$

where

$$\tan\phi_0 = \frac{-\gamma\Omega}{-\omega_{ex}^2 + \Omega^2 + \frac{3\alpha}{4M}A^2} \tag{1.6}$$

and

$$A^2\left[\gamma^2\omega_{ex}^2 + \left(\Omega^2 - \omega_{ex}^2 + \frac{3\alpha}{4M}A^2\right)^2\right] = \frac{F^2}{M^2}. \tag{1.7}$$

The last equation is the frequency-amplitude relation leading to a characteristic phenomenon of the Duffing system: the occurrence of a bistable region. When plotting the amplitude versus the driving frequency, shown in Fig. 1.2, a backbone curve arises, exhibiting hysteretic behaviour: Depending on the initial starting point on one of the two branches of the backbone curve for fixed driving amplitude F the amplitude jumps discontinuously when the driving frequency is continuously increased or decreased [7, 25]. The points where the amplitude jumps determine the bistable region, where in principle three values of the amplitude A are possible, but the central one is unstable and is never observed in experiments. The peak position of the backbone curve is determined by the dissipation in the system and is located nearly on the curve defined by [7]: $\omega_{ex}^2 = \Omega^2 + \frac{3\alpha}{4M}A^2$, if the damping is weak. In case of vanishing damping the response of the system diverges - a situation known from non-dissipative resonantly driven systems: the resonance catastrophe. The main effect of a finite and weak damping is to prevent the divergence and to give a finite peak at resonance [25]. The higher the dissipation, the lower is the height of the resonance peak. If dissipation becomes too large, the bistable region disappears and one obtains the corresponding linear response.

1.2 Nonlinear quantum systems

The experimental achievements during the last years allow to fabricate devices which can potentially reach the quantum regime. The latter achieve non negligible nonlinear behaviour as a consequence of their size or due to their incorporation of nonlinear elements, like Josephson junctions. Promising examples are nanoresonators, Josephson junctions embedded in a cavity or SQUIDs acting as Josephson bifurcation amplifiers to improve qubit read-out.
As this thesis considers first the very generic dissipative quantum Duffing oscillator and focusses later on the effect of a nonlinear undriven oscillator on a qubit, we split this section into two parts: the first is a representation of nonlinear driven and undriven quantum oscillators in their various experimental realizations, including single systems and composed architectures and the related theoretical works. The second is dedicated to the qubit read-out via a nonlinear undriven quantum oscillator. We clarify the different regimes, for example semiclassical or deep quantum, and linear or nonlinear systems in both theory and experiment and demonstrate the integration of the results of this thesis in the scientific development.

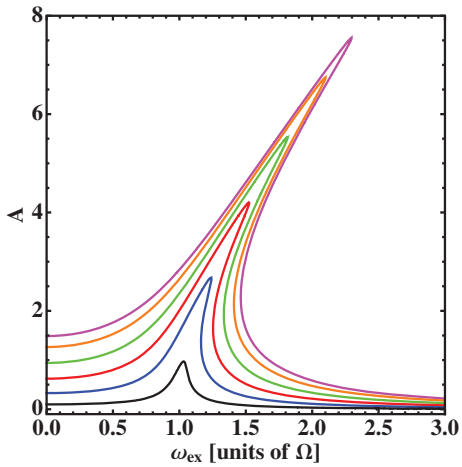

Figure 1.2: *Amplitude A for fixed driving amplitude F, oscillator frequency Ω and positive nonlinearity $\alpha > 0$, resulting in a bending to the right. We vary the external driving frequency for different values of the damping strength increasing from magenta to black. The amplitude shows a bistable region, depending on the actual values of the parameters.*

1.2.1 Nanoresonators, Josephson junctions and SQUIDs in the nonlinear regime

Starting with single nonlinear oscillator systems we present the experimental status and the corresponding theoretical works. Then we consider composed systems allowing to achieve entanglement as well as to improve measurement schemes by using for example a cavity including a nonlinear element as bifurcation amplifier[1].
Nowadays nanoresonators of submicron length [29], for example double-clamped beams, nanocantilevers or torsional resonators, are constructed. Due to their size the effects of nonlinearities become relevant, as the measure for the influence of nonlinearities, the so-called dynamic range scales with system size [30]. The dynamic range is defined by the kinetic energy at the critical amplitude divided by the thermomechanical energy. Nanoresonators are highly tunable and consequently make it possible to cover various dynamic ranges. Due to their high quality factor ($10^2 - 10^4$), being a signature of their weak dissipation, their high frequency [31, 32, 33, 34, 35], and their large variability they can be used for detecting weak forces, masses, charges [33, 36, 35, 37] and displacements [32], for stabilizing frequencies [30], signal amplification [38] and noise reduction [39, 40, 41, 42]. Although the experimental realizations are not yet in the deep quantum regime, where bistability in the amplitude response is no more observed, it is in our opinion only a matter of time, when a nonlinear driven quantum

[1]Principle of a bifurcation amplifier: At the jump points, where the bistable regime sets in, as shown in Fig 1.2, the derivative with respect to the driving frequency becomes infinite, i.e., a small change in the driving frequency results in a large amplitude change. This allows an efficient amplification of signals [29].

resonator is achieved.
Moreover nanoresonators provide an insight into the classical to quantum transition of nonlinear systems [43, 44, 45, 46, 12]. In a semiclassical regime, where the bistability is still present, there exists the idea of creating a quantum mechanical superposition of the two steady-states of motion or of observing tunneling or switching between these [47, 48, 49]. This regime requires intermediate temperatures, so that mechanisms like thermal activation, quantum tunneling or thermal switching are possible. In the deep quantum regime, however, thermal effects are strongly suppressed and the bistability in the response of the system is no more observed [15], which is also shown in chapter 3.
From the theoretical side single nonlinear quantum oscillators were predominantly studied within the quantum Duffing oscillator model [16, 17, 18, 19], where the oscillator is subject to an external AC driving force. Dynamical tunneling for a Duffing oscillator based on a semiclassical Wentzel-Kramers-Brillouin (WKB) scheme was investigated in [49], while a detailed analysis near the bifurcation point using Wigner functions was carried out in [50, 46, 12]. Motivated by the experimental achievements the deep quantum regime of the Duffing oscillator has also been widely investigated theoretically: Within a quantum diffusion model Rigo et al. [15] demonstrated that in the steady-state the quantum Duffing oscillator, in contrast to the classical one, does not exhibit any bistability or hysteresis in its mean excitation number as a function of the driving frequency. In particular, the nonlinear quantum Duffing oscillator exhibits a very special degeneracy of its eigenenergy spectrum [16]. This is the origin of the oscillator's response amplitude that displays antiresonant dips and peaks [16, 17, 18, 19], depending on the frequency of the driving field. While the nonlinear response shows resonant behavior for high damping, resembling the response of a linear oscillator at a shifted frequency, an antiresonance arises for zero damping and persists even for a weak Ohmic bath [18, 20].
From the theoretical point of view composed quantum systems including nanoresonators are of high interest within the framework of quantum computation: By coupling a micromechanical resonator to a Cooper-Pair Box the resonator states can be entangled and environmental decoherence can be probed [51]. In [52] entanglement and qubit storage is achieved by a nanomechanical resonator coupled to Josephson junction phase qubits. In both cases the resonator is modeled by a linear quantum oscillator. To achieve these coherence effects a quantum mechanical behaviour of at least one of the systems is essential. However, there has been to date no experimental realization of such composed systems in the deep nonlinear quantum regime, while the semiclassical regime, where the underlying classical bistability dominates the dynamics, is already observed in a novel class of devices combining SQUIDs and resonators. For example, a micromechanical resonator embedded in a nonlinear DC-SQUID, which is strongly damped to avoid bistability, is used to acquire cooling and squeezing of the resonator modes and to achieve quantum-limited position detection [53]. Such a kind of composed system can also be coupled to a qubit. Other setups are cavities incorporating a Josephson junction [54, 55] constituting a bifurcation amplifier, which can be used for amplification at the quantum limit therefore determining for

example qubit decoherence. Theoretically a semiclassical approach [56] is put forward to use a DC-SQUID embedded into a cavity as a bifurcation amplifier in its nonlinear regime allowing displacement detection and cooling. All these approaches rely in principle on treating the nanoresonator, the composed systems including Josephson junctions and the SQUID as a classical nonlinear system. To our knowledge there has been to date no experimental realization of these in the nonlinear quantum regime.

1.2.2 Flux qubit

A qubit is a quantum bit, having two states, which correspond to the two logical states 0 and 1 of a classical bit used as unit for information storage. Due to its quantum nature, in contrast to the classical bit, which is exclusively in one of the two states, the quantum bit allows also for superpositions of both, allowing parallel computing, which is not possible for a classical computer [57].
In the last years there have been various implementations of qubits involving cavities, ion traps [58] or nuclear spins [59]. Within cavity quantum electrodynamics we exemplarily refer to experiments of two-level quantum dots in photonic crystal nanocavities [60, 61], a quantum dot exciton in a microcavity [62], or single atoms with a large dipole moment interacting with photons in a microwave cavity [63]. In this thesis we focus on solid state realizations of qubits exhibiting macroscopic quantum behaviour because they are, compared to atomic, photonic or nuclear qubit realizations, highly scalable and tunable allowing therefore to cover various coupling regimes and an easy integration into electrical circuits [64]. Solid state qubits, however, are more affected by noise and decoherence than the qubit realizations mentioned above. So they have to be decoupled from the environment by properly manipulating system parameters. Within the framework of quantum computation two prominent solid-state realizations of a qubit-oscillator system are found: a Cooper-pair box [65, 66, 67, 68] coupled to a transmission line resonator [69, 70, 71, 72, 73, 74] and the Josephson flux qubit [75] read-out by a DC-SQUID [76, 77, 78]. These devices exhibit macroscopic quantum behaviour, as the measured state is fully characterized by a macroscopic variable. In case of the Cooper-pair box this is the charge state and for the flux qubit the supercurrent carried by the Cooper pairs [79]. The Cooper-pair box setup has been used to perform non-demolition measurements or to transfer information between qubits via the transmission line resonator [69, 80, 72, 81, 82, 83]. In the second experimental realization the flux qubit is usually read out via a damped DC-SQUID, which is represented by either a linear or a nonlinear oscillator. As demonstrated in [77] the quantum limit is within the experimental reach as well. A non-demolition read-out procedure, based on the measurement of the Josephson inductance, is given by Lupaşcu et al. [84].
At present the effort to exploit the nonlinearity of a qubit read-out device, for example, a DC-SQUID or a Josephson bifurcation amplifier (JBA) [9, 8], is increasing, as nonlinear effects lead to advantages in various measurement schemes and to new physical observations. The SQUID in the nonlinear regime acting as bifurcation amplifier optimizes qubit read-out allowing a fast read-out with high fidelity [10, 11] and causing

little dissipation. Due to the bifurcation of the read-out device a higher sensitivity, when determining the qubit states, and, due to the nonlinear Josephson inductance, a high quality factor for the resonance is achieved [8]. Though there are many advantages for driving the system to the nonlinear regime also new channels of relaxation might arise [11]. A quantum non-demolition read-out has been demonstrated for a quatronium qubit [85] using a Josephson bifurcation amplifier as well as for a flux qubit [86] coupled to a nonlinear resonator.
Despite the numerous theoretical works on coupled qubit-linear oscillator systems [87, 88, 89, 90, 91, 92, 93, 94, 95] composed qubit-Josephson bifurcation amplifier systems have only been investigated in [96, 97, 98]. In particular, Nakano et al. [98] looked at the composed qubit-Duffing oscillator dynamics during read-out process and Kakuyanagi et al. determined the optimal read-out pulse [99]. But the theoretical attempts up to now where either based on semiclassical analysis, where the bifurcation dominates, or on approximating the Duffing oscillator by applying a rotating wave approximation [98]. In this thesis we consider the deep quantum regime of a nonlinear driven or undriven oscillator without applying a rotating wave approximation. In the remaining part of this chapter we concentrate on the flux qubit and its read-out by a DC-SQUID by introducing the basic physical mechanism needed as well as the relevant quantities and the theoretical modelling. As both the qubit and the SQUID are incorporating Josephson junctions, we first present a short overview on the Josephson effects.

The Josephson effects

For an extensive derivation we refer to [100, 101]. A Josephson junction contains two strongly coupled superconducting electrodes either interrupted by a thin oxide or normal conducting layer or connected via a weak link. Such a kind of system exhibits the Josephson effect. The DC Josephson effect is that at zero voltage a supercurrent

$$I_s = I_c \sin \Upsilon \tag{1.8}$$

arises, which depends on the critical current I_c the junction sustains and the phase difference Υ of the two electrodes. The magnitude of I_c determines the coupling strength of the phases of the two electrodes across the weak link.
The AC Josephson effects predicts for a finite voltage difference V across the junction that the time evolution of the phase difference behaves as:

$$\dot{\Upsilon} \equiv \frac{d}{dt}\Upsilon = \frac{(2e)V}{\hbar}, \tag{1.9}$$

resulting in an alternating current of amplitude I_c and frequency $\frac{(2e)V}{\hbar}$ corresponding to the transfer of one Cooper pair, which is carrying twice the elementary charge e, across the junction. To describe the AC Josephson effect we introduce the RCSJ (resistively and capacitively shunted junction) model. The bias current I is equal to the total current in the junction, which is for parallel channels according to Kirchhoff:

$$I = I_c \sin \Upsilon + \frac{V}{R} + C\frac{d}{dt}V. \tag{1.10}$$

Expressing the last equation in terms of the phase we obtain using the second Josephson relation Eq. (1.9):

$$\left(\frac{\hbar}{2e}\right)^2 C\ddot{\Upsilon} + \left(\frac{\hbar}{2e}\right)^2 \frac{1}{R}\dot{\Upsilon} + \left(\frac{\hbar}{2e}\right) I_c \sin\Upsilon - \left(\frac{\hbar}{2e}\right) I = 0. \tag{1.11}$$

This equation of motion is nonlinear, having exactly the form of the Duffing equation, when expanding $\sin\Upsilon \simeq \Upsilon - \Upsilon^3/6$. It can be interpreted as a velocity-dependent damped particle with mass $\left(\frac{\hbar}{2e}\right)^2 C$ moving in a tilted washboard potential:

$$U(\Upsilon) \;=\; E_J - E_J\cos\Upsilon - \left(\frac{\hbar}{2e}\right) I\Upsilon, \tag{1.12}$$

where we introduced the Josephson coupling energy $E_J = \left(\frac{\hbar}{2e}\right) I_c$. The classical Hamiltonian accompanied by the above equation of motion at zero damping is:

$$H = \frac{Q^2}{2C} + U(\Upsilon), \tag{1.13}$$

where both the second Josephson relation and $V = Q/C$ have been inserted.
To classify the charging or superconducting regime of the junction we introduce the corresponding quantum Hamiltonian:

$$\hat{H} = \frac{\hat{Q}^2}{2C} + U(\hat{\Upsilon}). \tag{1.14}$$

We define the number operator counting Cooper pairs as $\hat{N} = \hat{Q}/(2e) = i\partial/(\partial\hat{\Upsilon})$. As in the corresponding particle picture, where $\hat{Q}$ refers to the generalized momentum and $\hat{\Upsilon}$ to the coordinate, these are conjugate operators, therefore fulfilling:

$$[\hat{\Upsilon}, \hat{N}] = i. \tag{1.15}$$

Setting $E_C = \frac{e^2}{2C}$ the Hamiltonian is:

$$\hat{H} = -4E_C\frac{\partial^2}{\partial\hat{\Upsilon}^2} + U(\hat{\Upsilon}). \tag{1.16}$$

The fraction $4E_C/E_J \gg 1$ determines the charging regime where, in analogy to a free particle motion, the coordinate $\hat{\Upsilon}$ is equally partitioned corresponding to a delocalized phase. In the superconducting regime $4E_C/E_J \ll 1$ the phase is localized. The conjugate operators fulfill the uncertainty principle:

$$\Delta\hat{\Upsilon}\Delta\hat{N} \gtrsim 1. \tag{1.17}$$

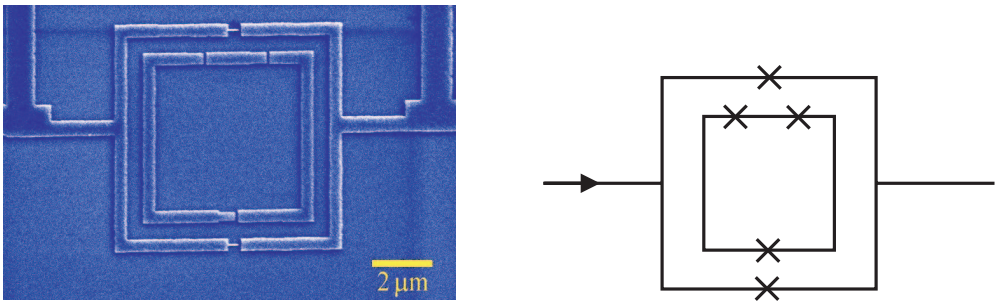

Figure 1.3: *On the left: Scanning electron microscope picture of a flux qubit read-out by a DC-SQUID. The qubit is the inner ring interrupted by three Josephson junctions, the outer is the DC-SQUID, containing two Josephson junctions. Picture courtesy of J. E. Mooij [75]. On the right: Schematic circuit, where crosses denote the junctions.*

The superconducting persistent-current qubit

In Fig. 1.3 a flux qubit, the so-called persistent current qubit, is depicted. It is a mesoscopic system of μm size with a superconducting island connected to tunnel junctions. Due to its size it is insensitive to background charges in the substrate and is effectively decoupled from the electrostatic environment, therefore allowing decoherence times of more than $1ms$ [75, 64, 89]. The charge on each island and the current through the junction behave quantum mechanically in the low temperature regime ($T \sim 30mK$).
A persistent-current qubit [64, 75] is built of three Josephson junctions embedded in a superconducting loop and controlled by applying a magnetic field with magnetic flux

$$\Phi_{ex} = f\Phi_0, \tag{1.18}$$

where f is the so-called magnetic frustration, giving the applied flux in terms of the flux quantum $\Phi_0 = h/2e$. The external flux results in a persistent current in the loop. Requiring a negligible inductance of the loop the flux generated by this circulating current is as small as $10^{-3}\Phi_0$ and the whole flux is reduced to the external applied one. In the superconducting limit ($E_J > E_C$) the phase is a good quantum number and the charge fluctuates. The ith junction is determined by its charging energy E_{Ci} and its Josephson coupling energy E_{Ji}, while the resistive channel originating in the RCSJ model is assumed to be disregarded. To calculate the total Josephson energy U we model two Josephson junctions to be equal $E_{J1} = E_{J2} = E_J$, while the third is by a factor δ smaller: $E_{J3} = \delta E_J$, $0.5 < \delta < 1$ and consider each of them contributing to the total energy with:

$$U_i = E_{Ji}(1 - \cos\Upsilon_i), \tag{1.19}$$

where Υ_i is the gauge-invariant phase different across the junction i. Using fluxoid quantization [101] arising for the superconducting loop:

$$\Upsilon_1 - \Upsilon_2 + \Upsilon_3 = -2\pi f + 2\pi n, \quad n \text{ integer}, \tag{1.20}$$

the total Josephson energy is characterized by two phases:

$$\frac{U}{E_J} = 2 + \delta - \cos\Upsilon_1 - \cos\Upsilon_2 - \delta\cos(2\pi f + \Upsilon_1 - \Upsilon_2). \tag{1.21}$$

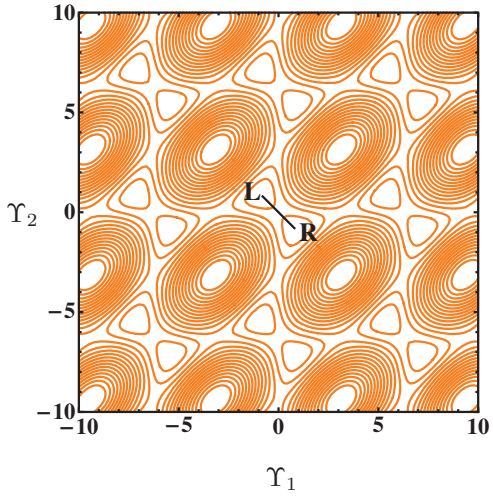

Figure 1.4: *Contourplot of the Josephson energy U in terms of the two dominating phases, using: $f = 0.5$ and $\delta = 0.8$. The periodic pattern with two degenerate minima in one unit cell is due to choosing $f = 1/2$. L and R denote the minima in one unit cell. The black line determines the intracell potential, shown in Fig. 1.5.*

In Fig. 1.4 we show the energy contour for fixed δ and $f = 1/2$. We observe a periodic pattern corresponding to two minima per unit cell within the eight-shaped contour, while the circular contours correspond to maxima. Plotting U along the connection of the minima within this eight-shaped contour (indicated by the black line in Fig. 1.4), which corresponds to choosing $\Upsilon_1 = -\Upsilon_2$, a double well potential is obtained if the external flux is close to 1/2. For further interpretation we use the analogy of a particle being either localized in the right, denoted by $|R\rangle$, or left well $|L\rangle$. Because the minima of the potential correspond to stable solutions, they can be interpreted as the two qubit states, i.e., states with opposite current flow (about $300nA$ in real devices [75, 64, 89]). Classically the minimal energy in each well is [102]:

$$\varepsilon = \pm I_p(\Phi_{ex} - \Phi_0/2), \tag{1.22}$$

where I_p is the magnitude of the classical currents and lies very close to the critical current of the weakest junction. Analog to a particle, whose mass is proportional to the capacitance and which moves in the double well potential, quantum tunneling between the wells can occur if the mass is low enough. Tunneling can occur also between minima belonging not to the same unit cell, but according to [64, 75] a proper parameter regime allows to prevent this. This suppression effectively results in the fact that the qubit is not influenced by charge effects. Requiring that the barrier height of the double well potential is much larger than the energy splitting between ground

state and first excited state in each well, which is also large compared to the tunneling amplitude [1], the system can be represented by a two level system Hamiltonian:

$$\begin{aligned} \hat{H}_{\mathrm{TLS}} &= -\frac{\hbar}{2}\begin{pmatrix} \varepsilon & \Delta_0 \\ \Delta_0 & -\varepsilon \end{pmatrix} \\ &= -\frac{\hbar}{2}\left(\varepsilon\hat{\sigma}_z + \Delta_0\hat{\sigma}_x\right), \end{aligned} \tag{1.23}$$

where $|L\rangle$ and $|R\rangle$ form the so-called localized basis. In case of zero tunneling, $\Delta_0 = 0$, they reduce to the eigenstates of the system [1], corresponding to clockwise and counterclockwise currents. $\hat{\sigma}_z = |R\rangle\langle R| - |L\rangle\langle L|$ and $\hat{\sigma}_x = |R\rangle\langle L| - |L\rangle\langle R|$ are the Pauli matrices. As the localized basis is not an eigenbasis for $\hat{H}_{\mathrm{TLS}}$, an eigenbasis is given

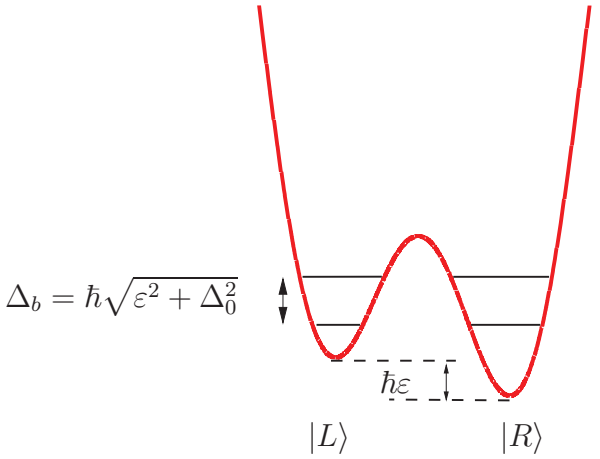

Figure 1.5: *Double well potential arising when $U(\Upsilon_1, \Upsilon_2)$ is plotted along the line connecting two minima in a unit cell as shown in Fig. 1.4. The two lowest lying energy levels are separated by the energy amount Δ_b.*

by their superposition:

$$\begin{aligned} |\mathrm{g}\rangle &= \cos(\Theta/2)|R\rangle - \sin(\Theta/2)|L\rangle, \\ |\mathrm{e}\rangle &= \sin(\Theta/2)|R\rangle + \cos(\Theta/2)|L\rangle, \end{aligned} \tag{1.24}$$

with $\tan\Theta = -\Delta_0/\varepsilon$ and $-\frac{\pi}{2} \leq \Theta < \frac{\pi}{2}$.
This is the so-called energy basis, where $|\mathrm{g}\rangle$ is the groundstate and $|\mathrm{e}\rangle$ the excited state accompanied by eigenenergies $E_{\mathrm{g/e}} = \mp\frac{\hbar}{2}\sqrt{\varepsilon^2 + \Delta_0^2}$. Applying the transformation:

$$R(\Theta) = \begin{pmatrix} \cos(\Theta/2) & \sin(\Theta/2) \\ -\sin(\Theta/2) & \cos(\Theta/2) \end{pmatrix}, \tag{1.25}$$

the TLS Hamiltonian becomes diagonal: $\hat{\tilde{\mathcal{H}}}_{\mathrm{TLS}} = R^T(\Theta)\hat{H}_{\mathrm{TLS}}R(\Theta) = -\frac{\hbar\Delta_b}{2}\tilde{\sigma}_z$, where $\tilde{\sigma}_z$ is the Pauli matrix in the energy basis and $\hbar\Delta_b = \hbar\sqrt{\varepsilon^2 + \Delta_0^2}$ is the energy splitting. The energy bias ε can be tuned for a superconducting flux qubit by application of an

external flux Φ_{ex}, see Eq. (1.22), and vanishes at the so-called degeneracy point: $\Phi_{ex} = \Phi_0/2$ [74]. Consequently at the degeneracy point the double well potential is symmetric and the eigenstates acquire the simple form:

$$\begin{aligned} |\mathrm{g}\rangle &= \tfrac{1}{\sqrt{2}}\left(|R\rangle - |L\rangle\right), \\ |\mathrm{e}\rangle &= \tfrac{1}{\sqrt{2}}\left(|R\rangle + |L\rangle\right). \end{aligned} \tag{1.26}$$

While for $\varepsilon \gg \Delta_0$, the states $|L\rangle$ and $|R\rangle$ are eigenstates of the TLS, which correspond to a localization in one well, at the degeneracy point the eigenstates $|\mathrm{g}\rangle$, $|\mathrm{e}\rangle$ are given by symmetric and antisymmetric superpositions, respectively, of the two logical states. The experimental verification of a Josephson junction loop behaving as macroscopic quantum two level system is provided in [102] using resonance measurements and spectroscopy. Coherent dynamics of a persistent current qubit [76] have been observed by coherent manipulation of the quantum state in the loop using microwave pulses of variable frequency and amplitude. The read-out of the pulsed SQUID showed quantum state oscillations with high fidelity. A coherent superposition of current states has been approached by spectroscopic measurements in [89]. Within these experiments Leggett's proposal [103] to achieve superposition of macroscopic quantum states and therefore macroscopic quantum coherence has been achieved.

The SQUID

SQUIDs are superconducting quantum interference devices allowing highly sensitive detection of magnetic flux using interference. Two realizations are widely used: The DC-SQUID, built of a superconducting loop intersected by two Josephson junctions, and the RF-SQUID, containing only one junction. As the qubit read-out in our considerations is based on the DC-setup, we focus on the description of the DC-SQUID. For a detailed description see [101, 88, 89].
The principle is as follows: To determine the flux the switching current I_{SW}, which is the current where the SQUID is driven to the normal conducting state resulting in a finite voltage drop, is measured when a certain bias current is applied. The larger this applied bias is, the more the washboard potential in the particle picture is tilted, as shown in Fig. 3 of [89]. As long as the bias current cannot overcome the switching current, the particle is trapped in one well. In the opposite case, the particle is in the so-called running mode, corresponding to escape out of a well. Then a finite voltage is detected. Averaging over several measurements allows to minimize fluctuations and external noise, which leads to $I_{SW} < I_m$. The maximal supercurrent I_m is directly related to the flux Φ by:

$$I_m = 2I_c \left|\cos\left(\frac{\pi\Phi}{\Phi_0}\right)\right|. \tag{1.27}$$

It therefore allows to determine the flux very accurately. In the last formula a symmetric SQUID with equal critical current is assumed.

According to [89] a DC-SQUID can be treated as a single Josephson junction with a flux-tunable critical current. Consequently the equation of motion for the flux can be obtained by the one of the Josephson junction, where on top the selfinductance of the loop, which arises due to the flux induced by the circulating current, and an external applied bias and flux are considered [1]:

$$C\ddot{\Phi} + \frac{1}{R}\dot{\Phi} + \frac{1}{L}(\Phi - \Phi_{ex}) + I_c \sin(2e\Phi/\hbar) = I_{ex}\cos(\omega_{ex}t). \tag{1.28}$$

The SQUID behaves as a linear inductor with inductance $L = \frac{\hbar}{2e}I_c$ if $\sin(2e\Phi/\hbar) \backsimeq 2e\Phi/\hbar$. It becomes hysteretic and acquires a Duffing type form if higher orders in the trigonometric expansion have to be taken into account, corresponding to $LI_c 2e/\hbar > 1$ [104, 1]. A driving contribution is either achieved by applying an external periodic bias, as given above, or by periodic modification of the external flux [105].
The SQUID can be modeled in the supercurrent regime, where the particle is trapped in one well, by a harmonic oscillator. Including nonlinear effects corresponds to taking into account higher oscillations in the well corresponding to a modified potential, which is not simple harmonic. The nonlinear Hamiltonian is determined by:

$$\begin{aligned}
\hat{H}_{\mathrm{NLO}} &= \frac{\hat{P}_y^2}{2M} + \frac{M}{2}\Omega^2\hat{y}^2 + \frac{\alpha}{4}\hat{y}^4 \\
&= \hbar\Omega\left(\hat{j} + \frac{1}{2}\right) + \frac{\alpha y_0^4}{16}\left(\hat{a} + \hat{a}^\dagger\right)^4 \\
&= \hbar\Omega\left(\hat{j} + \frac{1}{2}\right) + \frac{3}{8}\alpha y_0^4 \hat{j}\left(\hat{j} + 1\right) + \mathcal{O}(\alpha^2) \\
&:= \hbar\Omega\left(\hat{j} + \frac{1}{2}\right) + \frac{3}{2}\overline{\alpha}\hat{j}\left(\hat{j} + 1\right) + \mathcal{O}(\overline{\alpha}^2).
\end{aligned} \tag{1.29}$$

The third line is the first order perturbation theory in the nonlinearity, where $\hat{j} = \hat{a}^\dagger\hat{a}$ and $\hat{a}$ and $\hat{a}^\dagger$ are the annihilation and creation operators of the linear oscillator. In the last line a convenient notation is introduced, which will be used in the chapters 4 and 5.
When on top an external driving comes into play via an external applied flux or bias, we obtain the Hamiltonian of the quantum Duffing oscillator:

$$\hat{H}_{\mathrm{DO}}(t) = \hat{H}_{\mathrm{NLO}} + F\hat{y}\cos\omega_{ex}t. \tag{1.30}$$

The inclusion of nonlinear effects resembles not only the experimental situation more accurately but has direct advantages: In the linear regime the qubit state is determined by detecting the switching current to the normal state. The switching read-out is very efficient, but due to driving the system to the finite voltage state a high level of dissipation destroys the qubit state. Moreover, this results also in an increase of the temperature for the junction and the substrate during the time of the finite voltage state ($1\mu s$), while the equilibrium is not restored for about $1ms$. This limits the measurement rate and leads to long data acquisition times [79]. These negative

effects are avoided if a Josephson bifurcation amplifier (JBA) [106, 79] is used, which allows read-out without dissipation, as the SQUID remains in its superconducting regime. By explicit use of the SQUID nonlinearity and application of certain driving frequencies or currents, the JBA is forced to switch to the high or the low amplitude state of the classical Duffing oscillator, depending on the qubit state. Moreover for such experiments a quantum non-demolition measurement, which is essential for quantum computation, has been shown in [9].

The qubit read-out via a DC-SQUID

As shown in Fig. 1.7 the qubit is inductively coupled to the DC-SQUID, so that the interaction term depends on the magnetic flux and is therefore proportional to σ_z [107]:

$$\begin{aligned} \hat{H}_{\rm Int} &= g\hat{y}\hat{q} \\ &= g\left(\frac{q_0}{2}\sigma_z\right)\frac{y_0}{\sqrt{2}}\left(\hat{a}+\hat{a}^\dagger\right) \\ &:= \hbar\overline{g}\sigma_z(\hat{a}+\hat{a}^\dagger). \end{aligned} \tag{1.31}$$

In the last line we introduced a convenient notation, as already indicated in Eq. (1.29). In reality the qubit and its read-out device are never completely decoupled from their surrounding electromagnetic environment in any experimental situation. Therefore we have also to take into account environmental effects, which lead due to the coupling of the three composite parts to dissipation and decoherence in the qubit dynamics, as indicated in Figs. (1.6) and (1.7).

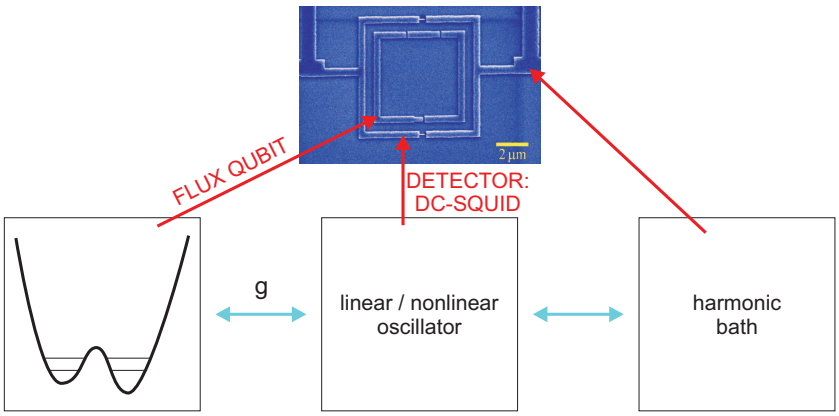

Figure 1.6: *Experimental realization of a flux qubit read-out by a DC-SQUID and its theoretical modeling. Experimental picture in the middle courtesy of J. E. Mooij [75].*

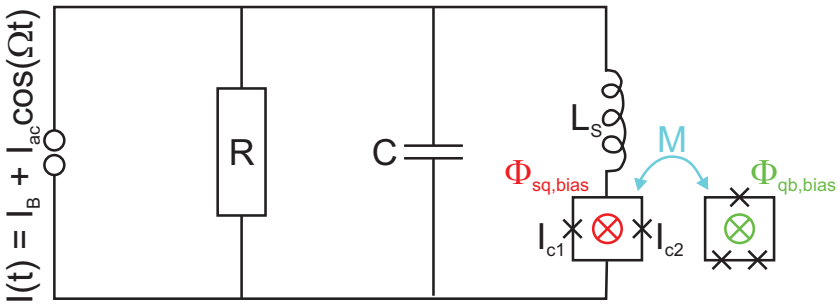

Figure 1.7: *Schematic representation of the circuit describing the situation in Fig. 1.6. The qubit (denoted by qb) is coupled inductively via M to a DC-SQUID. The Josephson junctions are depicted by crosses. The DC-SQUID is driven by an AC current and coupled to an electromagnetic reservoir of LC-oscillators, represented by harmonic oscillators [5].*

The inclusion of dissipation on a quantum level is represented in the next chapter, by representing the bath as a reservoir of uncoupled harmonic oscillators.

Chapter 2

Dissipative quantum systems

A classical example for a dissipative system is the dissipative motion of a Brownian particle moving in a liquid and exhibiting friction and a force orginating from collisions of the particle with molecules in the liquid. The equation of motion describing this situation is the Langevin-equation, which includes environmental effects via a frictional velocity-dependent and a fluctuating force [1]:

$$\mu\ddot{q}(t) + \mu\gamma\dot{q}(t) + \frac{d}{dq}U(q) \;=\; \xi(t), \tag{2.1}$$

where $q(t)$ is the position of the particle with mass μ, $U(q)$ an external potential and the friction term is $\gamma\dot{q}(t)$. The fluctuating force $\xi(t)$ obeys Gaussian statistics:

$$\langle\xi(t)\rangle \;=\; 0 \tag{2.2a}$$
$$\langle\xi(t)\xi(t')\rangle \;=\; 2\mu\gamma k_B T\delta(t-t'), \tag{2.2b}$$

leading to white or δ-correlated noise. The second relation is the classical fluctuation-dissipation theorem (FDT)[1] .
The inclusion of a friction term and a fluctuating force to model dissipation in classical systems is rather phenomenological. In this chapter we want to clarify the microscopic origin of dissipation and how it is obtained within a full quantum description. Without explicit time-dependence of the system's Hamiltonian the principle of energy conservation is valid and consequently there is no dissipation. According to [1] there have been several attempts to introduce dissipative effects in the equation of motion of a quantum particle: First a time-dependent mass is embedded in the Lagrangian allowing a damping term in the classical equation of motion. However, within this treatment the uncertainty principle is violated. The second realization of damping is modifying the quantization procedure, requiring some ad hoc assumptions for the occurrence of certain noise terms. Third due to the violation of the quantum mechanical superposition principle considering a nonlinear Schrödinger equation failed. The most famous and successful method is the system-bath approach, where the system of

[1]The response of a system to a small external perturbation is related to the spontaneous equilibrium fluctuations of the system.

interest, consisting only of few degrees of freedom, is coupled to a large bath (reservoir) with many degrees of freedom. The first is therefore treated as an open system, while the composed system is closed and the origin of dissipation in the small system is associated with the exchange of energy with the large one. The major advantage of the system-bath approach is that first the dynamical equation resulting from the system-bath model describes a stochastic process, represented by a quantum Langevin equation with a memory-friction force and an operator-valued random force. Second, due to the special character of the coupling and the actual form of the bath, an exact elimination of the bath degrees of freedom is possible. The details are found in the following sections, where we introduce the system-bath model and derive the time evolution of the system of interest within two different approaches. We introduce the quantum Langevin equation and apply the path integral formalism, where the bath degrees of freedom are eliminated and the influence of the bath is captured in the so-called Feynman-Vernon influence functional, allowing to go beyond the weak coupling limit.

2.1 System plus bath model

The modelling of the environment is captured within the Ullersma-Zwanzig-Caldeira-Leggett model [2, 3, 4, 5]. The bath is assumed to be large in order to treat it as a reservoir compared with the relevant system. Consequently the energy disappears in the environment and is not fed back into the system within any time of physical interest, i.e., Poincare recurrences are physically irrelevant. This behaviour describes a dissipative process [5, 1]. The generic assumption that any bath degree of freedom is only weakly perturbed by the system allows us to represent the bath as an ensemble of uncoupled harmonic oscillators, as the equilibrium bath state is almost not affected by the system. The spectrum of the oscillators is smooth and dense, so that each oscillator is only weakly coupled to the system of interest. Specifically, the coupling of system and bath is linear in the bath as well as in the system position coordinates. This allows an exact elimination of the bath degrees of freedom when we consider the reduced dynamics of the system. However, as stressed in [5], the weak coupling does not at all imply that the interaction seen by the system is weak, as the number of bath modes interacting with the system is large.
Caldeira and Leggett proposed the following ansatz for the Hamiltonian:

$$\hat{H} \;=\; \hat{H}_S + \hat{H}_B, \tag{2.3}$$

where $\hat{H}_S$ is the system and $\hat{H}_B$ the bath Hamiltonian:

$$\hat{H}_S \;=\; \frac{\hat{p}^2}{2\mu} + U(\hat{q}), \tag{2.4a}$$

$$\hat{H}_B \;=\; \sum_{j=1}^{\mathcal{N}} \left(\frac{\hat{p}_j^2}{2m_j} + \frac{1}{2} m_j \omega_j^2 \left[\hat{x}_j - \frac{c_j}{m_j \omega_j^2} \hat{q} \right]^2 \right). \tag{2.4b}$$

In Eq. (2.4a) μ is the particle's mass and $U(q)$ a one-dimensional potential. In Eq. (2.4b) the bath is composed of $\mathcal{N}$ harmonic oscillators, each determined by its mass m_j, frequency ω_j, its momentum $\hat{p}_j$ and position operator $\hat{x}_j$. The strength of the coupling is determined by the coefficients c_j. In the definition of the bath Hamiltonian we added a counter term $\propto c_j^2$ which compensates a renormalization of the potential $U(\hat{q})$ originating from the linear system-bath coupling [1].
To determine the time-evolution, we have to specify the initial conditions of the composed system by choosing the system and bath to be uncoupled at time $t = 0$. This corresponds to factorizing initial conditions for the density operator of system and bath $\hat{\rho}_{S+B}$:

$$\hat{\rho}_{S+B}(0) \;=\; \hat{\rho}_S(0) \otimes \hat{\rho}_B^0(0), \tag{2.5}$$

where $\hat{\rho}_S(0)$ is the density operator of the system at time $t = 0$ and

$$\hat{\rho}_B^0(0) \;=\; \frac{\exp(-\hat{H}_B^0/k_BT)}{\mathrm{Tr}\exp(-\hat{H}_B^0/k_BT)}, \tag{2.6}$$

the corresponding one of the canonically distributed bath at zero coupling ($c_j = 0$), respectively. From the experimental point of view, these conditions, where initial correlations of system and bath are disregarded, are rather artificial, but from the theoretical side very simple. A more realistic condition is to start from the equilibrium state of system and bath including the coupling [108]. However, initial preparation effects disappear in the stationary limit mainly considered in this work, if the temperature is finite, so that the simple choice of the initial conditions is appropriate.

2.1.1 Quantum Langevin equation

The Hamiltonian in Eq. (2.3) leads to coupled Heisenberg equations of motion [1]:

$$\begin{aligned} \mu\ddot{\hat{q}}(t) + U'(\hat{q}) + \sum_{j=1}^{\mathcal{N}} \left(\frac{c_j^2}{m_j\omega_j^2}\hat{q} \right) &= \sum_{j=1}^{\mathcal{N}} c_j\hat{x}_j, \\ m_j\ddot{\hat{x}}_j + m_j\omega_j^2\hat{x}_j &= c_j\hat{q}, \end{aligned} \tag{2.7}$$

where $U'(\hat{q}) = \frac{d}{d\hat{q}}U(\hat{q})$. When integrating formally the second equation of motion and inserting this result into the first one, we obtain the operatorial Langevin equation:

$$\mu\ddot{\hat{q}}(t) + \mu\int_0^t dt'\gamma(t-t')\dot{\hat{q}}(t') + U'(\hat{q}) \;=\; \hat{\xi}(t), \tag{2.8}$$

where the memory friction kernel $\gamma(t-t')$ and the fluctuating force $\hat{\xi}(t)$ are related to the bath via:

$$\gamma(t-t') = \theta(t-t')\frac{1}{\mu}\sum_{j=1}^{\mathcal{N}}\frac{c_j}{m_j\omega_j^2}\cos(\omega_j(t-t')), \tag{2.9}$$

$$\hat{\xi}(t) = \sum_{j=1}^{\mathcal{N}} c_j\left[\hat{x}_j^{(0)}\cos(\omega_j t) + \frac{\hat{p}_j^{(0)}}{m_j\omega_j}\sin(\omega_j t)\right] - \mu\gamma(t)\hat{q}(0). \tag{2.10}$$

The force $\hat{\xi}(t)$ is determined in terms of the initial conditions of the bath and by the transient term $\mu\gamma(t)\hat{q}(0)$ originating from the factorizing initial conditions. The time evolution of $\hat{\xi}(t)$ is given by Eq. (2.10) and *not* by the Heisenberg equations of motion. Moreover, note that $\hat{\xi}(t)$ is a fluctuating force with colored noise[2] and Gaussian statistics, if the average is taken with respect to $\hat{\rho}_B$ and not to $\hat{\rho}_B^0$:

$$\begin{aligned}\langle\hat{\xi}(t)\rangle_{\hat{\rho}_B} &= 0, \\ \langle\hat{\xi}(t)\hat{\xi}(0)\rangle_{\hat{\rho}_B} &= \frac{\hbar\mu}{\pi}\int_0^\infty d\omega\omega\gamma'(\omega)\left[\coth(\omega\hbar\beta/2)\cos(\omega t) - i\sin(\omega t)\right] \\ &\equiv \hbar L(t),\end{aligned} \tag{2.11}$$

where $\gamma'(\omega)$ represents the real and $\gamma''(\omega)$ the imaginary part of the damping kernel in Fourier space. The last relation is the quantum mechanical extension of the fluctuation-dissipation theorem (FDT), where we used the fact that for $\mathcal{N}\to\infty$ the Poincare recurrence time tends towards infinity, such that the spectrum of the oscillators is smooth and continuous allowing us to replace the sum over the oscillator degrees of freedom by a integral over a continuous spectral density [1].
Defining the spectral density as

$$J(\omega) = \frac{\pi}{2}\sum_{j=1}^{\mathcal{N}}\frac{c_j^2}{m_j\omega_j}\delta(\omega-\omega_j), \tag{2.12}$$

leads in Fourier space to the simple relation with the real part of the memory-friction kernel:

$$\gamma'(\omega) = \frac{J(\omega)}{\mu\omega}. \tag{2.13}$$

[2]This means that the noise has a finite correlation time [109].

In the time-domain this quantity, the noise kernel $K(t)$ and the autocorrelation function $L(t)$ are related to the spectral density via:

$$\gamma(t) = \theta(t)\frac{2}{\pi\mu}\int_0^\infty d\omega \frac{J(\omega)}{\omega}\cos(\omega t), \tag{2.14a}$$

$$\begin{aligned} K(t) &= \frac{1}{2\hbar}\langle[\hat{\xi}(t),\hat{\xi}(0)]_+\rangle = \frac{1}{2}\sum_{j=1}^{\mathcal{N}}\frac{c_j^2}{m_j\omega_j}\coth\left(\frac{\hbar\omega_j\beta}{2}\right)\cos(\omega_j t) \\ &= \frac{1}{\pi}\int_0^\infty d\omega J(\omega)\coth\left(\frac{\hbar\omega\beta}{2}\right)\cos(\omega t). \end{aligned} \tag{2.14b}$$

$$\begin{aligned} L(t) &= L'(t) + iL''(t) \\ &= \frac{1}{\pi}\int_0^\infty d\omega J(\omega)\left[\coth\left(\frac{\hbar\omega\beta}{2}\right)\cos(\omega t) - i\sin(\omega t)\right], \end{aligned} \tag{2.14c}$$

where $L'(t) = K(t)$ and $L''(t) = \frac{\mu}{2}\frac{d\gamma(t)}{dt}$. From here we see that the influence of the bath on the system is fully described by the spectral density $J(\omega)$. Therefore, the dynamics of the system is determined by the potential of the system $U(\hat{q})$ and the knowledge of the spectral density of the bath.
The time for the decay of the correlation function is $\tau_B = \hbar/k_BT$, giving an upper boundary for relevant system-bath correlations. In the classical limit $\hbar\omega \ll k_BT$ Eq. (2.14b) reduces to its classical analogue in Eq. (2.2b). Moreover, for a linear harmonic oscillator coupled bilinearly to a linear environment the spectral density is determined by quantities that appear already in the classical phenomenological equation of motion. For nonlinear system this argument is not valid anymore.

Forms of the spectral density

Now we want to consider two examples, the first corresponding to a *unstructured bath* (Ohmic bath) and the second corresponding to a *structured bath*. The spectral density of the bath, which we will refer to as unstructured bath, is well described by a power-law form with exponential cutoff:

$$J(\omega) = M\gamma\frac{\omega^s}{\Omega^{s-1}}\exp(-\omega/\omega_c). \tag{2.15}$$

In particular, we consider in the following chapters the Ohmic bath ($s = 1$)

$$J(\omega) = \eta\omega = \mu\gamma\omega, \tag{2.16}$$

where the damping is independent of the frequency $\gamma(\omega) = \gamma$ and the cutoff is sent to infinity. This type of spectral density corresponds to the ideal case of memoryless friction, which leads in the equation of motion to a term proportional to $\gamma\dot{\hat{q}}$ and can be interpreted accordingly to Ohmic's law as Ohmic. Due to the δ-correlation of the second cumulant of the force in the limit $\hbar \to 0$ in Eq. (2.11), it corresponds to a white noise source in the classical limit.
We obtain an example of a structured environment if we consider the experiment

described in the introduction, namely a qubit coupled to a read-out SQUID, where the SQUID itself is coupled to a bath of harmonic oscillators. In the appropriate regime of parameters [88, 89] the SQUID can be described as a harmonic oscillator with frequency Ω corresponding to the SQUID's plasma frequency. Therefore we can schematically visualize the problem as in Fig. 2.1, where we couple a two level system with the potential $U(\hat{q})$ (qubit) via an intermediate harmonic oscillator with eigenfrequency Ω to an Ohmic bath, which is characterized by its temperature T and its damping coefficient η.

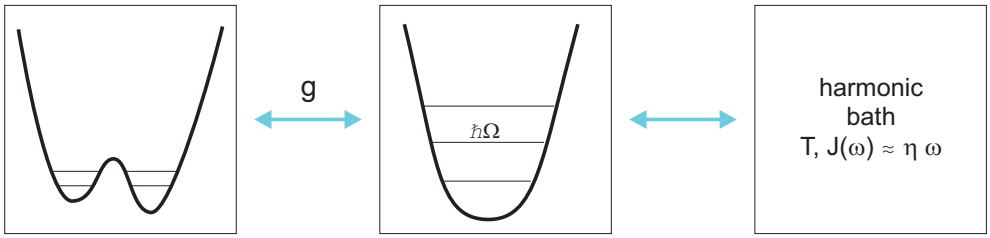

Figure 2.1: *Schematic representation of a qubit (two level system with potential $U(q)$) coupled to an intermediate harmonic oscillator with eigenfrequency Ω. The oscillator itself is coupled to an Ohmic bath.*

According to [87] there exists a mapping of the first description onto one, where the influence of both the intermediate harmonic oscillator and the bath is embedded into an effective spectral density, see Fig. 2.2.

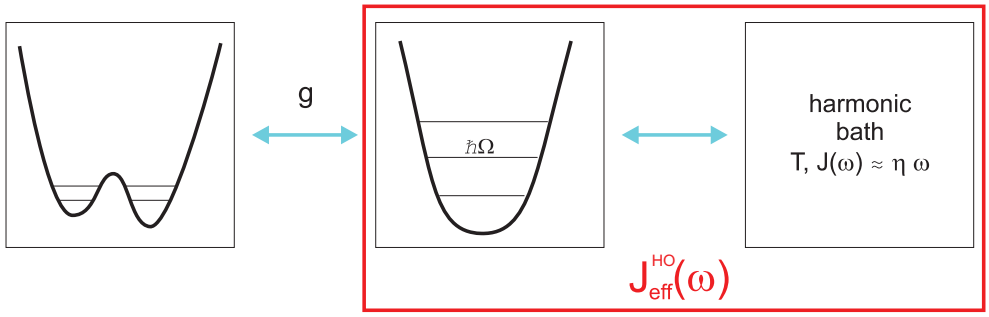

Figure 2.2: *The intermediate oscillator and the Ohmic bath build a composed system with an effective spectral density $J_{\text{eff}}^{HO}(\omega)$. This composed system is then coupled to the qubit.*

The effective spectral density is given by:

$$J_{\text{eff}}^{\text{HO}}(\omega) \quad = \quad \frac{g^2\gamma\omega}{M(\Omega^2-\omega^2)^2+M\gamma^2\omega^2}. \tag{2.17}$$

In the limit of vanishing frequency we obtain an Ohmic behaviour for the effective spectral density: $J_{\text{eff}}^{\text{HO}}(\omega) \xrightarrow[\omega\to 0]{} g^2\gamma\omega/(M\Omega^4)$.

2.1.2 The influence functional and the Markovian master equation (MME)

Although the quantum Langevin equation is simple, a direct integration can only be performed for very special cases. Feynman and Vernon [110] systematically determined the dynamics of the system of interest, which is subject to dissipation, that originates due to the coupling to a reservoir, by using real-time path integral methods. This procedure allows to capture environmental effects in a general class of functionals depending on coordinates of the system of interest only [110]. This corresponds to effectively eliminating the bath degrees of freedom of the full density matrix of the composed system and considering the reduced dynamics, where the bath degrees of freedom have been traced out. For a basic introduction to path integrals we refer to the book of Kleinert [111].
We consider the time evolution of the density operator of the composed system:

$$\hat{\rho}_{S+B}(t) \;=\; \exp[-i\hat{H}t/\hbar]\hat{\rho}_{S+B}(0)\exp[+i\hat{H}t/\hbar], \tag{2.18}$$

which reads in coordinate representation:

$$\begin{aligned}\langle q_f,\mathbf{x}_f|\hat{\rho}_{S+B}(t)|q_f',\mathbf{x}_f'\rangle &= \langle q_f,\mathbf{x}_f|\hat{U}(t,0)\hat{\rho}_{S+B}(0)\hat{U}^{-1}(t,0)|q_f',\mathbf{x}_f'\rangle \qquad (2.19)\\ &= \int dq_i dq_i' \mathbf{x}_j\mathbf{x}_i \hat{U}(q_f,\mathbf{x}_f,t;q_i,\mathbf{x}_i,0)\langle q_i,\mathbf{x}_i|\hat{\rho}_{S+B}(0)|q_i',\mathbf{x}_i'\rangle U^*(q_f',\mathbf{x}_f',t;q_i',\mathbf{x}_i',0).\end{aligned}$$

We introduced the shorthand notation $\mathbf{x}_i = \{x_{i,1},\ldots,x_{i,\mathcal{N}}\}$ including all bath coordinates and

$$U(q_f,\mathbf{x}_f,t;q_i,\mathbf{x}_i,0) = \langle q_f,\mathbf{x}_f|\mathcal{T}\exp\left[-i\int_0^t ds\hat{H}(s)\right]|q_i,\mathbf{x}_i\rangle \tag{2.20}$$

is the propagator for the system plus bath connecting the initial state $|q_i,\mathbf{x}_i\rangle$ at time $t=0$ and the final state $|q_f,\mathbf{x}_f\rangle$ at time t. Moreover, the completeness relations have been used: $\mathbb{1} = \int dq_i|q_i\rangle\langle q_i|$ and $\mathbb{1} = \int d\mathbf{x}_i|\mathbf{x}_i\rangle\langle\mathbf{x}_i|$. The idea is to split the time evolution operator over a finite time t into N short time intervals $\Delta t = t/N$, where $N\to\infty$. Decomposing into kinetic and potential parts as well as applying Trotter's formula [112, 111] allows us to derive a discretized version of the action entering the propagator as a functional. This applies only if the system has a classical analogue, which is not the case for a qubit. In general, the propagator is described by

$$U(q_f,t,q_i,0) \;=\; \int_{q(0)=q_i}^{q(t)=q_f}\mathcal{D}qA[q], \tag{2.21}$$

where $A[q]$ is the weight of a path for the non-dissipative system fulfilling the boundary conditions. If a classical counterpart exists, according to Feynman and Vernon, the propagator is expressed in terms of a real-time functional integral over all paths connecting start and end point, denoted by $\mathcal{D}x$:

$$U(q_f,\mathbf{x}_f,t;q_i,\mathbf{x}_i,0) = \int_{q(0)=q_i}^{q(t)=q_f}\mathcal{D}q\int_{\mathbf{x}(0)=\mathbf{x}_0}^{\mathbf{x}(t)=\mathbf{x}_f}\mathcal{D}\mathbf{x}A[q]\exp\left\{\frac{i}{\hbar}(S_S[q]+S_B[q,\mathbf{x}])\right\}, \tag{2.22}$$

where $S_S[q]$ and $S_B[q,\mathbf{x}]$ are the classical actions, which are related to the classical Lagrangian by $S[q] = \int ds \Lambda(q,\dot{q},s)$ and expressed in terms of our composite system by the the paths $q(s)$ and $x_j(s)$:

$$\begin{aligned} S_S[q] &= \int_0^t ds \left\{ \frac{\mu}{2}\dot{q}^2(s) - V(q(s)) \right\} \\ S_B[q,\mathbf{x}] &= \sum_{j=1}^{\mathcal{N}} \int_0^t ds \left\{ \frac{m_j}{2}\dot{x}_j^2(s) - \frac{m_j}{2}\omega_j^2[x_j(s) - \frac{c_j}{m_j\omega_j^2}q(s)]^2 \right\}. \end{aligned} \tag{2.23}$$

Since we are only interested in the system dynamics, we eliminate the bath degrees of freedom by taking the trace and end up with the reduced density matrix:

$$\hat{\rho}(t) \equiv \mathrm{Tr}_B \hat{\rho}_{S+B}(t). \tag{2.24}$$

With the help of the factorizing initial conditions, Eq. (2.5), the path integral over the bath degrees of freedom can be performed exactly, as only Gaussian integrals occur. Due to the bilinear coupling of system and each harmonic oscillator of the bath, the elimination of the bath yields an influence phase for linear systems being quadratic in the system coordinates [110], as shown below. The reduced density operator acquires then this form in position representation [1, 5, 110]:

$$\begin{aligned} \rho(q_f,q_f',t) &= \int d\mathbf{x}_f \langle q_f \mathbf{x}_f | \hat{\rho}_{S+B}(t) | q_f' \mathbf{x}_f \rangle \\ &= \int dq_i dq_i' \rho_S(q_i,q_i',0) \int d\mathbf{x}_i d\mathbf{x}_i' d\mathbf{x}_f U(q_f,\mathbf{x}_f,t,q_i,\mathbf{x}_i,0)\rho_B(\mathbf{x}_i,\mathbf{x}_i',0) \\ &\quad \times U^*(q_f',\mathbf{x}_f,t,q_i',\mathbf{x}_i',0) \\ &= \int dq_i \int dq_i' \mathcal{G}(q_f,q_f',t;q_i,q_i',0)\rho_S(q_i,q_i',0), \end{aligned} \tag{2.25}$$

where

$$\begin{aligned} \mathcal{G}(q_f,q_f',t;q_i,q_i',0) &= \int_{q(t_0)=q_i}^{q(t)=q_f} \mathcal{D}q \int_{q'(t_0)=q_i'}^{q'(t)=q_f'} \mathcal{D}q' A[q]A^*[q'] \exp\left[\frac{i}{\hbar}(S_S[q] - S_S[q'])\right] \\ &\quad \times \exp\{-\Phi_{FV}[q,q']/\hbar\}, \end{aligned} \tag{2.26}$$

is the propagating function for the reduced density operator depending on q, q' alone and describing how the dissipative system evolves with time. The last term in Eq. (2.26) is the Feynman-Vernon influence functional, which includes all the influence of the bath, as we want to emphasize. It includes the influence phase:

$$\begin{aligned} \Phi_{FV}[q,q'] &= \int_0^t dt' \int_0^{t'} dt'' [q(t') - q'(t')][L(t'-t'')q(t'') - L^*(t'-t'')q'(t'')] \\ &\quad + \frac{i}{2}\sum_{j=1}^{\mathcal{N}} \frac{c_j^2}{m_j\omega_j^2} \int_0^t dt' [q^2(t') - q'^2(t')]. \end{aligned} \tag{2.27}$$

Therefore the influence of the bath is fully characterized by the autocorrelation function of the fluctuating force $L(t)$, given in Eq. (2.14c), and consequently by the spectral density. Imposing the relations given after Eqs. (2.14a-2.14c) and integrating by parts, the potential renormalization cancels and we obtain in symmetric and antisymmetric terms:

$$\begin{aligned}\Phi_{FV}[q,q'] &= \int_0^t dt' \int_0^{t'} dt''[q(t')-q'(t')]K(t'-t'')[q(t'')-q'(t'')] \\ &+\frac{i\mu}{2}\int_0^t dt' \int_0^{t'} dt''[q(t')-q'(t')]\gamma(t'-t'')[\dot{q}(t'')+\dot{q}'(t'')] \\ &+\frac{i\mu}{2}\int_0^t dt'[q(t')-q'(t')]\gamma(t')[q(0)+q'(0)].\end{aligned} \tag{2.28}$$

The last term is the initial slip term, which occurs also in the quantum Langevin equation Eq. (2.8). It is omitted in the following chapters, for the same reasons as explained in detail in section 2.1.1. Besides the quadratic form in the system coordinate, which originates due to the bilinear coupling, the effect of the bath is to add a nonlocal contribution, in particular a selfinteraction. The real part of $\Phi_{FV}[q,q']$, the so-called noise functional, represents a pure phase, whose argument is strongly fluctuating. It is antisymmetric in q and q' so that it connects the offdiagonal parts of the reduced density matrix, the coherences. Therefore this part gives rise to decoherence. An explanation is that the bath is continuously measuring the system's position, therefore suppressing quantum interference between the different system states [1]. The imaginary part of $\Phi_{FV}[q,q']$ is an exponential decaying function coupling both symmetric and asymmetric paths and leads to friction in the system. The main effects of the influence phase, whose real and imaginary part are related via the fluctuation-dissipation theorem given in the second part of Eq. (2.11), are to introduce friction and dissipation in a systematic way.

Because an analytical treatment of the functional integral is very complicated or even not possible, for example for nonlinear systems, we impose an additional approximation by restricting to the weak coupling limit: $\gamma \ll k_B T/\hbar = 1/\tau_B, \Delta E/\hbar$, where τ_B is the bath correlation time and ΔE refers to any energy difference in the system, so that the smallest frequency scale is the damping strength.

Therefore we expand the propagator for the reduced density matrix in terms of the damping strength γ up to first order $\mathcal{G}_1(q_f,q'_f,t;q_i,q'_i,0)$ using

$$\exp(-\Phi_{FV}[q,q']/\hbar) \approx 1-\Phi_{FV}[q,q']/\hbar. \tag{2.29}$$

The lowest order contribution $\mathcal{G}_0(q_f,q'_f,t;q_i,q'_i,0)$ of the propagator is given by approximating $\exp\{-\Phi_{FV}[q,q']/\hbar\} \simeq 1$ and is represented by the propagator for the Schrödinger equation of the system alone, $U_0(q_f,t;q_i,0)$:

$$\mathcal{G}_0(q_f,q'_f,t;q_i,q'_i,0) = U_0(q_f,t;q_i,0)U_0^*(q'_f,t;q'_i,0). \tag{2.30}$$

Thus an expansion up to first order in the damping strength, which corresponds to second order in the coupling constants c_j, is effectively the so-called Born approximation.

Moreover, the resulting master equation is of Markovian form, if the damping is the smallest frequency scale of the problem, as shown below [113, 114, 115, 116, 117, 118]. The reduced density matrix in terms of the expanded propagators is:

$$\begin{aligned}\rho(q_f,q_f',t) &= \int dq_i dq_i' \mathcal{G}_0(q_f,q_f',t;q_i,q_i',0)\rho(q_i,q_i',0) \\ &-\frac{1}{\hbar}\int_0^t dt' \int_0^{t'} dt'' \int dq_1 dq_1' dq_2 dq_2' \mathcal{G}_0(q_f,q_f',t;q_1,q_1',t')(q_1-q_1') \\ &\times \mathcal{G}_0(q_1,q_1',t';q_2,q_2',t'')K(t'-t'')(q_2-q_2')\rho(q_2,q_2',t'') \\ &-\frac{i\mu}{2\hbar}\int_0^t dt' \int_0^{t'} dt'' \int dq_1 dq_1' dq_2 dq_2' \mathcal{G}_0(q_f,q_f',t;q_1,q_1',t')(q_1-q_1') \\ &\times \mathcal{G}_0(q_1,q_1',t';q_2,q_2',t'')\gamma(t'-t'')(\dot{q}_2+\dot{q}_2')\rho(q_2,q_2',t''),\end{aligned} \tag{2.31}$$

where additionally, due to the dependence of $\Phi_{FV}[q,q']$ on t' and t'', the path integral is split into a free time evolution and an integral over $q(t')=q_1$ and $q(t'')=q_2$ assuming that the path integral commutes with the integrations over t' and t'' [119, 120]. The term $\rho(t'')$ can be rewritten in terms of $\rho(t)$ by using the zeroth order propagator:

$$\rho(q_2,q_2',t'') = \int dq dq' U_0(q_2,t'',q,t)U_0^*(q_2',t'';q',t)\rho(q,q',t). \tag{2.32}$$

Inserting this expression into Eq. (2.31), taking the full time derivative with respect to t and rewriting the result in terms of $\tau = t - t''$, we obtain a Markovian master equation. It is characterized by the fact that no memory effects are included, as the derivative for the reduced density matrix $\dot{\rho}(t)$ depends only on the density matrix $\rho(t)$ at equal time [121]:

$$\begin{aligned}\dot{\rho}(q_f,q_f',t) \equiv \frac{d}{dt}\rho(q_f,q_f',t) &= -\frac{i}{\hbar}(H_S(q_f)-H_S(q_f'))\rho(q_f,q_f',t) \\ &-\frac{1}{\hbar}\int_0^t d\tau K(\tau)\int dq_2 dq_2' dq dq' (q_f-q_f')U_0(q_f,t;q_2,t-\tau)U_0^*(q_f',t;q_2',t-\tau) \\ &\times (q_2-q_2')U_0(q_2,t-\tau,q,t)U_0^*(q_2',t-\tau;q',t)\rho(q,q',t) \\ &-\frac{i\mu}{2\hbar}\int_0^t d\tau\gamma(\tau)\int dq_2 q_2' dq dq' U_0(q_f,t,q_2,t-\tau)U_0^*(q_f',t,q_2',t-\tau) \\ &\times (q_f-q_f')(\dot{q}_2+\dot{q}_2')U_0(q_2,t-\tau,q,t)U_0^*(q_2',t-\tau,q',t)\rho(q,q',t).\end{aligned} \tag{2.33}$$

In the last derivations we used the rule for differentiating products and the completeness relations.
The master equation can also be represented in operatorial form as:

$$\frac{d}{dt}\hat{\rho} = -\frac{i}{\hbar}[\hat{H}_S,\hat{\rho}] + \hat{\mathcal{L}}\hat{\rho}, \tag{2.34}$$

where the influence of the bath comes in via the superoperator:

$$\hat{\mathcal{L}}\hat{\rho} = -[\hat{q},[\hat{P}(t),\hat{\rho}]_+] - [\hat{q},[\hat{Q}(t),\hat{\rho}]], \tag{2.35}$$

with the correlators:

$$\hat{P}(t) = \frac{i}{2\hbar}\int_0^\infty d\tau\gamma(\tau)\hat{U}_0^\dagger(t-\tau,t)\hat{p}\hat{U}_0(t-\tau,t), \tag{2.36}$$

$$\hat{Q}(t) = \frac{1}{\hbar}\int_0^\infty d\tau K(\tau)\hat{U}_0^\dagger(t-\tau,t)\hat{q}\hat{U}_0(t-\tau,t), \tag{2.37}$$

and $\hat{U}_0(t,t') = \exp[-i\hat{H}_S(t-t')/\hbar]$ [121]. In the last lines we assumed that the integration kernel and the friction kernel are practically zero after a finite time τ_B and extended the upper integration limit to infinity, thereby implicitly considering the time distance t from the preparation to be much larger than τ_B, so that the master equation involving the above quantities describes an almost equilibrium situation of the system dynamics [121, 122].
In chapter 3 we solve the master equation in Floquet basis, where the driving is taken into account, as well as in chapter 4 in a composite basis based on a time-independent spin-boson Hamiltonian.

2.2 Spin-boson-model

This bath approach is used for the spin-boson model [103, 123, 1]. It is composed of a two-level system (TLS), which exhibits constructive and destructive quantum interference effects, coupled to a harmonic reservoir. The TLS is modeled by a double well potential with finite barrier. Although the bath degrees of freedom can be traced out exactly, analytical solutions are only possible within two different perturbative schemes. Spin-boson dynamics are usually perturbative in either the tunneling through the barrier of the TLS (NIBA, Non-Interacting-Blip-Approximation) [1, 124, 125] or in the bath coupling (WCA, Weak-Coupling-Approximation) [126, 127]. Those perturbative in the coupling of the TLS to the bath are typically obtained within a Born-Markov treatment of the Liouville equation for the TLS density matrix [128, 116] or within the path integral formalism [1]. The equivalence of both methods has been demonstrated in [129] restricting to low temperatures and damping strengths. An alternative approach is to perform perturbation theory in the tunneling amplitude of the two-level system. Within the so-termed non-interacting blip approximation (NIBA) [125, 130, 1] it yields equations of motion for the TLS reduced density matrix enabling to capture the case of strong TLS-bath coupling.
As argued above, a two level system, termed as 'spin' system, provides one of the simplest situations to study quantum interference effects. When environmental effects are modeled as in the previous sections by harmonic oscillators which are bilinearily coupled to the spin system, we obtain the spin-boson Hamiltonian [1]:

$$\hat{H} = \hat{H}_{\mathrm{TLS}} + \hat{H}_{\mathrm{TLS-B}} + \hat{H}_{\mathrm{B}}, \tag{2.38}$$

where

$$\hat{H}_{TLS} = -\frac{\hbar}{2}\left(\varepsilon\sigma_z + \Delta_0\sigma_x\right) \tag{2.39}$$

and

$$\hat{H}_{\rm TLS-B} = -\frac{q_0}{2}\sigma_z \sum_{j=1}^{\mathcal{N}} c_j \hat{x}_j. \tag{2.40}$$

Notice that the generic system Hamiltonian defined before, see section 2.1, has been replaced by the corresponding one of the two level system, using $\hat{q} \to \frac{q_0}{2}\sigma_z$, where $q_0/2$ are the eigenvalues of the localized states. We obtain:

$$\hat{H} = -\frac{\hbar}{2}\left(\varepsilon\sigma_z + \Delta_0\sigma_x\right) - \frac{q_0}{2}\sigma_z \sum_{j=1}^{\mathcal{N}} c_j\hat{x}_j + \sum_{j=1}^{\mathcal{N}}\left(\frac{\hat{p}_j^2}{2m_j} + \frac{m_j}{2}\omega_j^2\hat{x}_j^2\right). \tag{2.41}$$

Expressing the position and momentum operators in second quantization

$$\hat{x}_j = \sqrt{\frac{\hbar}{2m_j\omega_j}}(\hat{b}_j + \hat{b}_j^\dagger), \qquad \hat{p}_j = i\sqrt{\frac{\hbar m_j\omega_j}{2}}(\hat{b}_j - \hat{b}_j^\dagger), \tag{2.42}$$

we obtain:

$$\hat{H} = -\frac{\hbar}{2}\left(\varepsilon\sigma_z + \Delta_0\sigma_x\right) + \sum_{j=1}^{\mathcal{N}}\hbar\omega_j\hat{b}_j^\dagger\hat{b}_j - \frac{1}{2}\sigma_z\sum_{j=1}^{\mathcal{N}}\hbar\lambda_j(\hat{b}_j + \hat{b}_j^\dagger), \tag{2.43}$$

where

$$\lambda_j = q_0 c_j\left(\frac{1}{2m_j\omega_j\hbar}\right)^{1/2}. \tag{2.44}$$

This allows to define the spin-boson spectral density:

$$G(\omega) = \sum_{j=1}^{\mathcal{N}}\lambda_j^2\delta(\omega-\omega_j) = \frac{q_0^2}{2\hbar}\sum_{j=1}^{\mathcal{N}}\frac{c_j^2}{m_j\omega_j}\delta(\omega-\omega_j). \tag{2.45}$$

Comparing with Eq. (2.12) we find the relation:

$$G(\omega) = \frac{q_0^2}{\pi\hbar}J(\omega). \tag{2.46}$$

2.3 Population difference of a qubit

The dynamical quantity of interest is the population difference of the two-level system:

$$\begin{aligned} P(t) &= \langle\sigma_z(t)\rangle = {\rm Tr}_{\rm TLS}\{\sigma_z\hat{\rho}(t)\} \\ &= \langle R|\sigma_z\hat{\rho}(t)|R\rangle - \langle L|\sigma_z\hat{\rho}(t)|L\rangle, \end{aligned} \tag{2.47}$$

where $\hat{\rho}(t)$ is the reduced density matrix. According to section 2.1.2, the reduced density matrix can be expressed via a real-time path integral:

$$\rho_{\sigma,\sigma'}(t) = \int \mathcal{D}q \int \mathcal{D}q' A[q]A^*[q] \exp(-\Phi_{FV}[q,q']/\hbar). \tag{2.48}$$

It is evaluated using the initial state $\rho_{\sigma,\sigma'}(0) = \delta_{\sigma,1}\delta_{\sigma',1}$ and by summing over all spin paths $q(t)$ and $q'(t')$ which fulfill the boundary conditions $q(0) = q'(0) = \frac{q_0}{2}$, $q(t') = q_0\sigma/2$ and $q'(t') = q_0\sigma'/2$ [131]. In our case this corresponds to starting and ending in the right well. $\int \mathcal{D}qA[q]$ is the propagator of the non-dissipative TLS, which includes the probability amplitude of the TLS to follow the path $q(t)$. The propagator can be directly calculated for a TLS, fixing initial and final conditions. Then the propagator is split into propagators at many successive time steps, corresponding to taking into account all possible paths. The TLS paths consist of contributions where the TLS can remain in its state or jump between the two states. The last process is always proportional to the tunneling amplitude Δ_0. According to [132, 1] the population difference including this propagator is obtained in an exact analytic form by summing over all paths containing a certain number of transitions and is therefore expressed as a power series in the tunneling amplitude.
Following [132] the time evolution of the population difference is given by a generalized master equation (GME):

$$\dot{P}(t) = -\int_0^t dt' K^{(a)}(t-t') + K^{(s)}(t-t')P(t'), \quad t \geq 0, \tag{2.49}$$

where the superscripts $\{(a),(s)\}$ refer to the asymmetric or symmetric kernel with respect to the external bias. For an extensive and detailed derivation we refer to [132, 131, 1]. The kernels contain arbitrary orders in Δ_0^2. An analytical calculation of the GME including all these non-local terms originating from the correlations is too complicated. Therefore we restrict ourselves for the calculations in chapter 5 to the well-established Non-Interacting-Blip-Approximation (NIBA), allowing to truncate the infinite sum in the kernels to first order in Δ_0^2 [124, 1]:

$$K^{(s)}(\tau) = \Delta_0^2 \exp(-S(\tau)) \cos(R(\tau)) \cos(\varepsilon\tau), \tag{2.50}$$

$$K^{(a)}(\tau) = \Delta_0^2 \exp(-S(\tau)) \sin(R(\tau)) \sin(\varepsilon\tau), \tag{2.51}$$

where we introduced:

$$Q(\tau) = S(\tau) + iR(\tau) \tag{2.52}$$

$$= \int_0^\infty d\omega \frac{G(\omega)}{\omega^2} \left[\coth\left(\frac{\hbar\omega\beta}{2}\right)(1-\cos\omega t) + i\sin\omega t \right], \tag{2.53}$$

which is related to the autcorrelation function of the force by: $\ddot{Q}(\tau) = q_0^2 L(\tau)/\hbar$. By rewriting the kernels in terms of the time difference $\tau = t - t'$ and without external time-dependent driving the master equation depends only on convolutive integrals. Therefore the GME is solved using Laplace transform:

$$P(\lambda) = \frac{1 + K^{(a)}(\lambda)}{\lambda + K^{(s)}(\lambda)}. \tag{2.54}$$

Then the poles of $P(\lambda)$ determine the dynamics. An inverse Laplace transform finally yields $P(t)$.
The NIBA approximation becomes exact for $\langle\sigma_z(t)\rangle$ using an unbiased TLS in the weak damping regime. Moreover, it is in general applicable for the Ohmic case using large damping and/or high temperatures [1].

Chapter 3

The dissipative quantum Duffing oscillator

Parts of the results presented here have been published in [20].

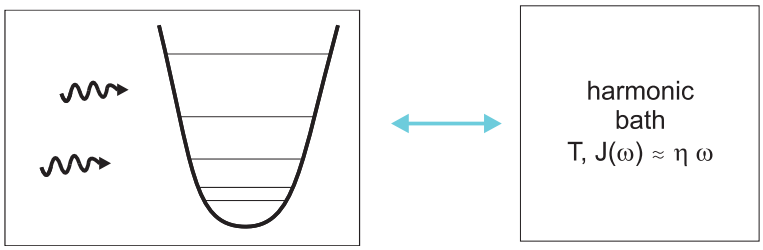

Figure 3.1: *The nonlinear quantum oscillator to whom a periodic external driving (denoted by the wiggled arrows) is applied is the so-called Duffing oscillator indicated by the left box. Dissipation enters the oscillator by coupling it to a harmonic bath with temperature T and Ohmic spectral density $J(\omega) = \eta\omega$.*

In this chapter we investigate the deep quantum limit of the dissipative quantum Duffing oscillator and present two different approaches covering different parameter regimes. The first approach is based on the exact Floquet energies and states of the driven linear oscillator with the nonlinearity treated perturbatively. As there is no restriction on the driving amplitude, this scheme can also be applied to the regime where the driving amplitude is larger than the nonlinearity. The second approach treats both the driving and the nonlinearity perturbatively. It is applicable for driving frequencies which can resonantly excite two states of the nonlinear oscillator, requiring that the energy scale associated with the driving amplitude cannot overcome the energy shift introduced by the nonlinearity. In general a combination of both approaches allows to cover a wide range of driving frequencies. Exemplarily we consider in the first part of this chapter the dynamics of the Duffing oscillator near the one-photon resonance, where the oscillator dynamics is described analytically. As in [16, 17,

18, 19] we obtain that for weak dissipation the amplitude of the oscillations displays an antiresonance rather than a resonance. We find a characteristic asymmetry of the antiresonance lineshape. In contrast to [16, 17, 18, 19], our analytic results are obtained without applying a rotating wave approximation (RWA) on the Duffing oscillator. In the second part of this chapter, we do not impose a resonance condition but investigate, based on the first approach, the dissipative dynamics of the Duffing oscillator, using the solution for the dissipative dynamics of the corresponding linear system, the driven harmonic oscillator.
The chapter is organized as follows: In section 3.1 we introduce the Hamiltonian of the non-dissipative Duffing oscillator and in section 3.2 the two Floquet based approximation schemes to treat it. Moreover we derive the Floquet states of the driven harmonic oscillator. The energy spectrum and eigenstates of the non-dissipative Duffing oscillator are calculated with the two different schemes in section 3.3 and section 3.4 and both approaches are compared in section 3.5. Afterwards dissipative effects are included within a Born-Markov-Floquet master equation in section 3.6. Section 3.7 addresses the special case of the one-photon resonance including dissipative effects. In section 3.8 we derive the dissipative steady-state dynamics of the driven harmonic oscillator and compare the results to its classical analogue. Afterwards the extension to the nonlinear case is elaborated. In section 3.9 conclusions are drawn.

3.1 Quantum Duffing oscillator

A quantum Duffing oscillator is described by the Hamiltonian:

$$\hat{H}_{\mathrm{DO}}(t) = \frac{\hat{P}_y^2}{2M} + \frac{M\Omega^2}{2}\hat{y}^2 + \frac{\alpha}{4}\hat{y}^4 + \hat{y}F\cos(\omega_{ex}t), \tag{3.1}$$

where M and Ω are the mass and frequency of the Duffing oscillator which is driven by a monochromatic field of amplitude F and frequency ω_{ex}. For later convenience we introduce the oscillator length $y_0 := \sqrt{\frac{\hbar}{M\Omega}}$. In the following we will consider the case of hard nonlinearities, $\alpha > 0$, such that the undriven potential is monostable.
To treat the quantum Duffing oscillator problem we observe that the Hamiltonian can be rewritten as:

$$\begin{aligned} \hat{H}_{\mathrm{DO}}(t) &= \hat{H}_{\mathrm{LO}}(t) + \frac{\alpha}{4}\hat{y}^4 && \text{(3.2a)} \\ &= \hat{H}_{\mathrm{NLO}} + \hat{y}F\cos(\omega_{ex}t), && \text{(3.2b)} \end{aligned}$$

where $\hat{H}_{\mathrm{LO}}(t)$ describes a driven linear oscillator, while $\hat{H}_{\mathrm{NLO}}$ is the Hamiltonian of an undriven nonlinear oscillator. Due to the periodic driving Floquet theory [133, 134, 135, 130] can be applied, as reviewed in the following section 3.1.1.

3.1.1 Floquet theory

The Floquet theorem states that a Schrödinger equation involving a time-periodic Hamiltonian ($\hat{H}_{\mathrm{DO}}(t) = \hat{H}_{\mathrm{DO}}(t + T_{\omega_{ex}})$ with period $T_{\omega_{ex}} = 2\pi/\omega_{ex}$) [133, 134, 135, 130,

118]:

$$i\hbar\partial_t|\psi(t)\rangle = \hat{H}_{\rm DO}(t)|\psi(t)\rangle \tag{3.3}$$

has a complete set of solutions:

$$|\psi_j(t)\rangle = \exp(-i\epsilon_j t/\hbar)|\phi_j(t)\rangle, \tag{3.4}$$

where $|\phi_j(t)\rangle = |\phi_j(t+T_{\omega_{ex}})\rangle$. The quasienergies ϵ_j and Floquet states $|\phi_j(t)\rangle$ solve the eigenvalue equation of the Floquet Hamiltonian:

$$\hat{\mathcal{H}}(t)|\phi_j(t)\rangle = \left[\hat{H}_{\rm DO}(t) - i\hbar\frac{\partial}{\partial t}\right]|\phi_j(t)\rangle = \epsilon_j|\phi_j(t)\rangle. \tag{3.5}$$

Defining $|\phi_{j,n}(t)\rangle = \exp(-in\omega_{ex}t)|\phi_j(t)\rangle$ and inserting into Eq. (3.5) we find that $|\phi_{j,n}(t)\rangle$ is also an eigenstate of the Floquet Hamiltonian, but with the eigenvalue $\epsilon_{j,n} = \epsilon_j - n\hbar\omega_{ex}$ differing by a multiple integer of $\hbar\omega_{ex}$. These Floquet states are therefore physically identical. In other words the spectrum of the Floquet Hamiltonian has a Brillouin zone structure, each Brillouin zone being of size ω_{ex}. To find a complete set of solutions $\{|\psi_j(t)\rangle\}$, it is sufficient to consider only those Floquet states and quasienergies which lie within a single Brillouin zone, i.e., $-\hbar\omega_{ex}/2 \leq \epsilon_j < \hbar\omega_{ex}/2$. Moreover $\epsilon_j \equiv \epsilon_{j,0}$ and $|\phi_j(t)\rangle := |\phi_{j,0}(t)\rangle$. The eigenstates $|\psi_j(t)\rangle$ as well as the Floquet states $|\phi_j(t)\rangle$ are elements of the Hilbert space $\mathcal{R}$. For convenience we also define $\mathcal{T}$ as the space of $T_{\omega_{ex}}$-periodic functions with the inner product:

$$(f,g) \;=\; \frac{1}{T_{\omega_{ex}}}\int_0^{T_{\omega_{ex}}} dt f^*(t)g(t). \tag{3.6}$$

An orthonormalized basis of $\mathcal{T}$ is given by the functions: $\varphi_n(t) = \exp(-in\omega_{ex}t)$, n integer. The basis set $\{\varphi_n\}$ is orthonormalized and complete:

$$(\varphi_n, \varphi_n') \;=\; \delta_{n,n'}, \tag{3.7}$$

$$\frac{1}{T_{\omega_{ex}}}\sum_n \varphi_n^*(t)\varphi_n(t') \;=\; \delta_{T_{\omega_{ex}}}(t-t'), \tag{3.8}$$

where $\delta_{T_{\omega_{ex}}}$ is the $T_{\omega_{ex}}$-periodic delta function. The scalar product in the composite Hilbert space $\mathcal{R}\otimes\mathcal{T}$ is then given by:

$$\langle\langle\phi_j|\phi_k\rangle\rangle \;:=\; \frac{1}{T_{\omega_{ex}}}\int_0^{T_{\omega_{ex}}} dt\langle\phi_j(t)|\phi_k(t)\rangle. \tag{3.9}$$

The decomposition of $|\phi_j(t)\rangle$ into basis functions $\varphi_n(t)$ is equivalent to an expansion in Fourier series:

$$|\phi_{j,n}(t)\rangle \;=\; \sum_l \exp(-il\omega_{ex}t)|\phi_j^{(l-n)}\rangle, \tag{3.10}$$

$$\begin{aligned}|\phi_j^{(n)}\rangle \;&=\; \frac{1}{T_{\omega_{ex}}}\int_0^{T_{\omega_{ex}}} dt\exp(in\omega_{ex}t)|\phi_j(t)\rangle \\ &=\; \frac{1}{T_{\omega_{ex}}}\int_0^{T_{\omega_{ex}}} dt|\phi_{j,-n}(t)\rangle.\end{aligned} \tag{3.11}$$

For a basis independent notation we introduce the state vectors $|n)$ with $(t|n) := \varphi_n(t)$. Then, in the composite Hilbert space $\mathcal{R} \otimes \mathcal{T}$ we define the state:

$$|\phi_{j,n}\rangle\rangle = \sum_l |\phi_j^{(l-n)}\rangle \otimes |l), \tag{3.12}$$

and $|\phi_{j,n}(t)\rangle = (t|\phi_{j,n}\rangle\rangle$. In particular, due to the orthogonality of the Floquet states $|\phi_{j,m}(t)\rangle$, also the orthonormality relation is valid:

$$\langle\langle\phi_{i,n}|\phi_{j,m}\rangle\rangle = \frac{1}{T_{\omega_{ex}}} \int_0^{T_{\omega_{ex}}} dt \langle\phi_{i,n}(t)|\phi_{j,m}(t)\rangle = \delta_{ij}\delta_{nm}. \tag{3.13}$$

Additionally we define:

$$\mathcal{H}_{ij}^{nm} \equiv \langle\langle\phi_{i,n}|\hat{\mathcal{H}}|\phi_{j,m}\rangle\rangle = \frac{1}{T_{\omega_{ex}}} \int_0^{T_{\omega_{ex}}} dt \langle\phi_{i,n}(t)|\hat{\mathcal{H}}(t)|\phi_{j,m}(t)\rangle. \tag{3.14}$$

Hence through the expansion of the Hilbert space it is possible to treat the time-dependent problem in Eq. (3.3) as a time-independent one by expressing the Floquet Hamiltonian in a basis of $\mathcal{R} \otimes \mathcal{T}$. Which basis of $\mathcal{R} \otimes \mathcal{T}$ is the most convenient to express $\mathcal{H}$ depends on the specific problem. For example in the basis $\{|\phi_{j,n}\rangle\rangle\}$ of the Floquet states the eigenvalue equation reads:

$$\hat{\mathcal{H}}|\phi_{j,m}\rangle\rangle = \epsilon_{j,m}|\phi_{j,m}\rangle\rangle. \tag{3.15}$$

Equivalently, using the expansion in Eq. (3.12) it also follows from Eqs. (3.14) and (3.15)

$$\sum_{l'} \left(\hat{H}^{(l-l')} - l'\hbar\omega_{ex}\delta_{ll'}\right) |\phi_j^{(l'-m)}\rangle = \epsilon_{j,m}|\phi_j^{(l-m)}\rangle, \tag{3.16}$$

where $\hat{H}^{(l)}$ are the Fourier components in the Fourier expansion of $\hat{H}(t)$.
The eigenenergies and eigenstates of $\hat{\mathcal{H}}$ are known only in very few cases, among which the case of the driven linear oscillator, see section 3.2.1. For a generic time-periodic Hamiltonian only approximated solutions of Eqs. (3.14) or (3.15) can be found.

3.2 Complementary approaches for the quantum Duffing oscillator

In this section we discuss two complementary approximation schemes to treat the quantum Duffing oscillator. Eqs. (3.2a) and (3.2b) describe two different approaches, shown in Fig. 3.2, to solve the eigenvalue problem described by Eqs. (3.15) and (3.16): In the first one, called App I, we start with the exact Floquet states and eigenenergies of the driven linear oscillator $\hat{H}_{\mathrm{LO}}(t)$, see Eq. (3.2a). The nonlinearity is treated as a perturbation. A similar problem was considered by Tittonen et al. [136]. This approach is convenient if the Floquet states of the time-dependent Hamiltonian are

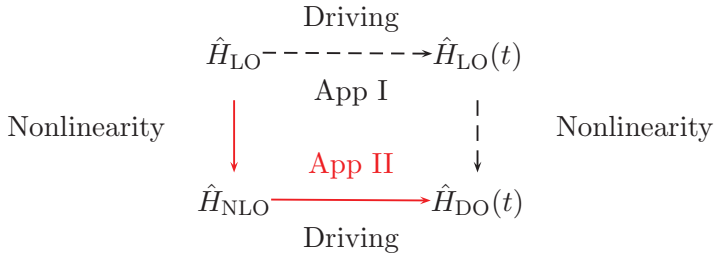

Figure 3.2: *Different procedures to incorporate driving and nonlinearity. In App I starting point are the exact Floquet states and eigenenergies of the driven linear oscillator $\hat{H}_{\mathrm{LO}}(t)$. The nonlinearity is the perturbation. In App II the driving is a perturbation expressed on the basis of the Floquet states of the undriven nonlinear oscillator $\hat{H}_{\mathrm{NLO}}$.*

known.
For the driven harmonic oscillator they have been derived by Husimi and Perelomov [137, 138] and are given in section 3.2.1.
In the second approach, which we call App II, one considers as unperturbed system the undriven nonlinear oscillator (NLO) and the driving is the perturbation, see Eq. (3.2b).
As we shall see, the different ways of treating the infinite dimensional Floquet Hamiltonian result in crucial differences when evaluating observables of the Duffing oscillator.

3.2.1 Floquet states of the driven harmonic oscillator

In this section we want to consider the case of the driven harmonic oscillator as according to Husimi, Perelomov and Breuer [137, 138, 139] the quasienergy spectrum can be determined exactly for a periodically driven harmonic oscillator.
Due to the special form of the driving, proportional to the position operator, and the special properties of the non-dissipative harmonic oscillator, possessing an equidistant energy spectrum, the time-dependent Schrödinger equation

$$i\hbar\frac{\partial\psi(y,t)}{\partial t} = -\frac{\hbar^2}{2M}\frac{\partial^2\psi(y,t)}{\partial y^2} + \frac{M}{2}\Omega^2 y^2\psi(y,t) - f(t)y\psi(y,t) \tag{3.17}$$

is exactly solvable. According to Husimi [137] and Ref. [140] the last equation can be formally solved by introducing a time-dependent translation $y_1 = y - \xi(t)$, such that the Schrödinger equation becomes:

$$\begin{aligned} i\hbar\frac{\partial\psi(y_1,t)}{\partial t} = {} & i\hbar\dot{\xi}(t)\frac{\partial\psi(y_1+\xi(t),t)}{\partial y_1} - \frac{\hbar^2}{2M}\frac{\partial^2\psi(y_1+\xi(t),t)}{\partial y_1^2} + \frac{M}{2}\Omega^2(y_1+\xi(t))^2 \times \\ & \psi(y_1+\xi(t),t) + F\cos(\omega_{ex}t)(y_1+\xi(t))\psi(y_1+\xi(t),t). \end{aligned} \tag{3.18}$$

Applying moreover the unitary transformation $\psi(y,t) = \exp(iM\dot{\xi}(t)y/\hbar)\varphi(y,t)$ and requiring that $\xi(t)$ is the steady-state solution of the classical equation of motion, the

term linear in y_1 can be eliminated, so that the wave equation reads:

$$i\hbar\frac{\partial\varphi}{\partial t} = -\frac{\hbar^2}{2M}\frac{\partial^2\varphi}{\partial y_1^2} + \frac{M}{2}\Omega^2 y_1^2\varphi - \Lambda\varphi + M\ddot{\xi}(t)\xi(t)\varphi + M\dot{\xi}(t)^2\varphi, \tag{3.19}$$

where Λ is the classical Lagrangian:

$$\Lambda = \frac{M}{2}\dot{\xi}(t)^2 - \frac{M}{2}\Omega^2\xi(t)^2 + f(t)\xi(t). \tag{3.20}$$

A further transformation

$$\varphi = \chi\exp\left[\frac{i}{\hbar}\int_0^t dt'\left(\Lambda - M\ddot{\xi}(t)\xi(t) - M\dot{\xi}(t)^2\right)\right] \tag{3.21}$$

reduces the wave equation to the one of the undriven harmonic oscillator:

$$i\hbar\frac{\partial\chi}{\partial t} = \left[-\frac{\hbar^2}{2M}\frac{\partial^2}{\partial y^2} + \frac{M}{2}\Omega^2(y-\xi(t))^2\right]\chi(y,t). \tag{3.22}$$

Consequently the driven system is rewritten in terms of the wave equation for the undriven harmonic oscillator weighted with a complex phase, depending on the Lagrangian of the classical system:

$$\begin{aligned}\psi(y,t) &= \chi(y-\xi(t))\exp\left[i\frac{M}{\hbar}\dot{\xi}(y-\xi) + \frac{i}{\hbar}\int_0^t \Lambda dt\right] \qquad (3.23)\\ &= \overline{\phi}_j(y-\xi(t))\exp\left[\frac{i}{\hbar}\left(\int_0^t \Lambda dt' - \frac{t}{T_{\omega_{ex}}}\int_0^{T_{\omega_{ex}}}\Lambda dt' + M\dot{\xi}(y-\xi)\right)\right]\times\\ &\quad \exp\left[-\frac{i}{\hbar}\left(E_j^{(0)} - \frac{1}{T_{\omega_{ex}}}\int_0^{T_{\omega_{ex}}}\Lambda dt'\right)t\right],\end{aligned}$$

where we replaced in the last step: $\chi(y-\xi(t)) = \overline{\phi}_j(y-\xi(t))\exp(-iE_j^{(0)}t/\hbar)$. Therefore by applying the above transformations the well-known equidistant eigenenergies $E_j^{(0)} = \hbar\Omega(j+1/2)$ and eigenstates $|j\rangle_0$ of the undriven harmonic oscillator together with their orthonormality relation can be used. Remember that the states in position representation are Hermite-Polynomials $H_j\left(\frac{y}{y_0}\right)$ weighted with Gaussian functions:

$$\overline{\phi}_j(y) = \langle y|j\rangle_0 = \frac{1}{\sqrt{y_0}}\frac{1}{\sqrt{2^j j!\sqrt{\pi}}}\exp\left(-\frac{y^2}{2y_0^2}\right)H_j\left(\frac{y}{y_0}\right). \tag{3.24}$$

The solution $\langle y|\psi_j(t)\rangle = \psi_j(y,t)$ of Eq. (3.5) for the time-dependent Hamiltonian $\hat{H}_{\mathrm{LO}}(t)$, see Eq. (3.2a), is:

$$\begin{aligned}\psi_j(y,t) &= \overline{\phi_j}(y-\xi(t))\exp\left\{-i\left[\left(j+\frac{1}{2}\right)\Omega t - \frac{1}{2\hbar}\int_0^t f(t')\xi(t')dt'\right]\right\}\times\\ &\quad \exp\left(\frac{i}{\hbar}\left[-\frac{M}{2}\xi(t)\dot{\xi}(t) + M\dot{\xi}(t)y\right]\right)\\ &\equiv \phi_j^{(0)}(y,t)\exp(-i\epsilon_j^{(0)}t/\hbar),\end{aligned} \tag{3.25}$$

Finally $\xi(t)$ is the steady-state solution of the corresponding classical equation,

$$M\ddot{\xi}(t) + M\Omega^2\xi(t) = f(t), \tag{3.26}$$

which is for a driving of the form $f(t) = -F\cos(\omega_{ex}t)$:

$$\xi(t) = \frac{F}{M(\omega_{ex}^2 - \Omega^2)}\cos(\omega_{ex}t). \tag{3.27}$$

The quasienergy spectrum for the harmonic oscillator is for a cosine-like driving term:

$$\epsilon_j^{(0)} = \epsilon_{j,0}^{(0)} = \hbar\Omega\left(j + \frac{1}{2}\right) + \frac{F^2}{4M(\omega_{ex}^2 - \Omega^2)}. \tag{3.28}$$

Finally,

$$\phi_j^{(0)}(y,t) = \overline{\phi}_j(y - \xi(t))\exp(-i\theta(F^2,t))\exp\left(\frac{i}{\hbar}\left[-\frac{M}{2}\xi(t)\dot{\xi}(t) + M\dot{\xi}(t)y\right]\right) \tag{3.29}$$

with

$$\theta(F^2,t) = -\frac{1}{2\hbar}\left[\int_0^t dt' f(t')\xi(t') - \frac{t}{T_{\omega_{ex}}}\int_0^{T_{\omega_{ex}}} dt' f(t')\xi(t')\right]. \tag{3.30}$$

In the following section we use this results to determine perturbatively the Floquet states of the quantum Duffing oscillator.

3.3 Perturbation theory for a time-periodic Hamiltonian with time-independent perturbation

The starting point of the perturbative treatment App I is the Floquet equation for the full Floquet Hamiltonian $\hat{\mathcal{H}}$ in the extended Hilbert space $\mathcal{R}\otimes\mathcal{T}$, see Eq. (3.15),

$$\hat{\mathcal{H}}|\phi_{j,m}\rangle\rangle = \epsilon_{j,m}|\phi_{j,m}\rangle\rangle, \tag{3.31}$$

where $\hat{\mathcal{H}} = \hat{\mathcal{H}}_0 + \hat{V}_\alpha$. Moreover, the Floquet states of the Floquet Hamiltonian $\hat{\mathcal{H}}_0$ satisfying the eigenvalue equation in Eq. (3.15) are known, see e.g. Eq. (3.25) and Eq. (3.28):

$$\hat{\mathcal{H}}_0|\phi_{j,m}\rangle\rangle_0 = \epsilon_{j,m}^{(0)}|\phi_{j,m}\rangle\rangle_0. \tag{3.32}$$

We look for an expression of $\epsilon_{j,m}$ and $|\phi_{j,m}\rangle\rangle$ in first order in $\hat{V}_\alpha$. Consequently we introduce the first order corrections $\epsilon_{j,m}^{(1)}$ and $|\phi_{j,m}\rangle\rangle_1$ as:

$$\begin{aligned}\epsilon_{j,m} &= \epsilon_{j,m}^{(0)} + \epsilon_{j,m}^{(1)},\\ |\phi_{j,m}\rangle\rangle &= |\phi_{j,m}\rangle\rangle_0 + |\phi_{j,m}\rangle\rangle_1.\end{aligned} \tag{3.33}$$

Additionally, we introduce the Fourier coefficients:

$$ {}_0\langle\langle\phi_{k,n}|\hat{V}_\alpha|\phi_{j,m}\rangle\rangle_0 \equiv v_{kj}^{(n-m)}. \tag{3.34} $$

As in the case of conventional stationary perturbation theory, the perturbed states are written as a linear combination of the unperturbed states:

$$ |\phi_{j,m}\rangle\rangle = |\phi_{j,m}\rangle\rangle_0 + \sum_{(k,n)\neq(j,m)} c_{kj}^{nm}|\phi_{k,n}\rangle\rangle_0, \tag{3.35} $$

where (k,n) denotes the couple of quantum numbers k and n. Inserting ansatz Eq. (3.33) in the Floquet equation, Eq. (3.31), we obtain:

$$ \left(\hat{\mathcal{H}}_0 + \hat{V}_\alpha - \epsilon_{j,m}^{(0)} - \epsilon_{j,m}^{(1)}\right)\left(|\phi_{j,m}\rangle\rangle_0 + |\phi_{j,m}\rangle\rangle_1\right) = 0. \tag{3.36} $$

Because $\epsilon_{j,m}^{(0)}$ and $|\phi_{j,m}\rangle\rangle_0$ solve the Floquet equation for $\hat{\mathcal{H}}_0$ the last equation reduces to:

$$ \left(\hat{V}_\alpha - \epsilon_{j,m}^{(1)}\right)|\phi_{j,m}\rangle\rangle_0 + \left(\hat{\mathcal{H}}_0 - \epsilon_{j,m}^{(0)}\right)|\phi_{j,m}\rangle\rangle_1 = 0. \tag{3.37} $$

This equation allows to determine the modification to the quasienergy $\epsilon_{j,m}^{(1)}$ and the actual form of the coefficients c_{kj}^{nm}. To calculate $\epsilon_{j,m}^{(1)}$ we multiply it from the left with ${}_0\langle\langle\phi_{j,m}|$. It follows:

$$ \epsilon_{j,m}^{(1)} = {}_0\langle\langle\phi_{j,m}|\hat{V}_\alpha|\phi_{j,m}\rangle\rangle_0. \tag{3.38} $$

To determine the coefficients for the states we multiply Eq. (3.37) from the left with ${}_0\langle\langle\phi_{k,n}|$, where the couple $(k,n)\neq(j,m)$. Moreover, we exclude the case of degenerate quasienergies and impose: $\epsilon_{k,n}^{(0)} \neq \epsilon_{j,m}^{(0)}$. In case of $\epsilon_{k,n}^{(0)} = \epsilon_{j,m}^{(0)}$ degenerate perturbation theory should be applied. We obtain:

$$ 0 = {}_0\langle\langle\phi_{k,n}|\hat{V}_\alpha|\phi_{j,m}\rangle_0 + (\epsilon_{k,n}^{(0)} - \epsilon_{j,m}^{(0)})c_{kj}^{nm}, \tag{3.39} $$

yielding:

$$ c_{kj}^{nm} = \frac{{}_0\langle\langle\phi_{k,n}|\hat{V}_\alpha|\phi_{j,m}\rangle\rangle_0}{\epsilon_{j,m}^{(0)} - \epsilon_{k,n}^{(0)}} \equiv c_{kj}^{(n-m)}. \tag{3.40} $$

Notice that in order to apply perturbation theory, we have to require that $|c_{kj}^{nm}| < 1$, which imposes restrictions on the allowed values of driving and nonlinearity. Moreover, if we set the driving to zero the quasienergy and the states reduce to the ones obtained by applying conventional stationary perturbation theory on the unforced system.

3.3.1 Application to the quantum Duffing oscillator

We can now determine the actual form of the quasienergy spectrum and the corresponding expansion coefficients for the case of the quantum Duffing oscillator using as perturbation $\hat{V}_\alpha = \frac{\alpha}{4}\hat{y}^4$. The matrix elements Eq. (3.34) defined as:

$$v_{kj}^{(n-m)} = \frac{1}{T_{\omega_{ex}}}\int_0^{T_{\omega_{ex}}} dt \exp(i(n-m)\omega_{ex}t)_0\langle\phi_k(t)|\hat{V}_\alpha|\phi_j(t)\rangle_0 \tag{3.41}$$

are given in Appendix A. The quasienergies of the quantum Duffing oscillator up to first order in the nonlinearity read:

$$\begin{aligned}\epsilon_{j,m} &= \hbar\Omega\left(j+\frac{1}{2}\right)+\frac{F^2}{4M(\omega_{ex}^2-\Omega^2)}+\frac{\alpha}{4}\left[\frac{3}{2}(2j+1)y_0^2\left(\frac{F}{M(\omega_{ex}^2-\Omega^2)}\right)^2\right.\\ &\left.+\frac{3}{2}\left(j(j+1)+\frac{1}{2}\right)y_0^4+\frac{3}{8}\left(\frac{F}{M(\omega_{ex}^2-\Omega^2)}\right)^4\right]-\hbar\omega_{ex}m\\ &+\mathcal{O}(\alpha^2).\end{aligned} \tag{3.42}$$

In the limit of no driving Eqs. (3.35) and (3.42) yield:

$$E_j = \lim_{F\to 0}\epsilon_j = \hbar\Omega\left(j+\frac{1}{2}\right)+\frac{3}{8}\alpha y_0^4\left(j(j+1)+\frac{1}{2}\right), \tag{3.43a}$$

$$\begin{aligned}|j\rangle &= \lim_{F\to 0}|\phi_j(t)\rangle = \lim_{F\to 0}(t|\phi_j\rangle\rangle \\ &= |j\rangle_0+\frac{\alpha y_0^4}{4}\left[\frac{\sqrt{j(j-1)}(j-\frac{1}{2})}{2\hbar\Omega}|j-2\rangle_0\right.\\ &+\frac{\sqrt{(j+1)(j+2)}(j+\frac{3}{2})}{-2\hbar\Omega}|j+2\rangle_0\\ &+\frac{\frac{1}{4}\sqrt{j(j-1)(j-2)(j-3)}}{4\hbar\Omega}|j-4\rangle_0+\\ &\left.\frac{\frac{1}{4}\sqrt{(j+1)(j+2)(j+3)(j+4)}}{-4\hbar\Omega}|j+4\rangle_0\right],\end{aligned} \tag{3.43b}$$

such that the modifications due to the nonlinearity are exactly those obtained by conventional stationary perturbation theory [21], where $\{|\ j\rangle_0\}$ are the eigenstates of the undriven harmonic oscillator. Expanding up to second order in the driving

amplitude we obtain from Eq. (3.35) for $|\phi_j(t)\rangle = (t|\phi_j\rangle\rangle$ the result:

$$
\begin{aligned}
|\phi_j(t)\rangle \;=\; & |\phi_j(t)\rangle_0 + \frac{\alpha}{4}\left[+ \frac{[y_0^4(j+\frac{3}{2}) + \frac{3}{2}y_0^2A_\xi^2]\sqrt{(j+1)(j+2)}}{-2\hbar\Omega}|\phi_{j+2}(t)\rangle_0 \right. \\
& + \frac{[y_0^4(j-\frac{1}{2}) + \frac{3}{2}y_0^2A_\xi^2]\sqrt{j(j-1)}}{2\hbar\Omega}|\phi_{j-2}(t)\rangle_0 \\
& + \frac{\frac{y_0^4}{4}\sqrt{(j+1)(j+2)(j+3)(j+4)}}{-4\hbar\Omega}|\phi_{j+4}(t)\rangle_0 \\
& + \frac{\frac{y_0^4}{4}\sqrt{j(j-1)(j-2)(j-3)}}{4\hbar\Omega}|\phi_{j-4}(t)\rangle_0 \\
& + \frac{3}{4}(2j+1)y_0^2A_\xi^2\left[\frac{\exp(-i2\omega_{ex}t)}{\hbar 2\omega_{ex}} + \frac{\exp(i2\omega_{ex}t)}{-2\hbar\omega_{ex}}\right]|\phi_j(t)\rangle_0 \\
& + \frac{3!\sqrt{2}}{4}(j+1)\sqrt{j+1}A_\xi y_0^3\left[\frac{\exp(-i\omega_{ex}t)}{\hbar\omega_{ex}-\hbar\Omega} - \frac{\exp(i\omega_{ex}t)}{\hbar\omega_{ex}+\hbar\Omega}\right]|\phi_{j+1}(t)\rangle_0 \\
& + \frac{3!\sqrt{2}}{4}j\sqrt{j}A_\xi y_0^3\left[\frac{\exp(-i\omega_{ex}t)}{\hbar\omega_{ex}+\hbar\Omega} + \frac{\exp(i\omega_{ex}t)}{-\hbar\omega_{ex}+\hbar\Omega}\right]|\phi_{j-1}(t)\rangle_0 \\
& + \sqrt{(j+3)(j+2)(j+1)}\frac{2^{3/2}}{4}y_0^3A_\xi\left[\frac{\exp(-i\omega_{ex}t)}{\hbar\omega_{ex}-3\hbar\Omega} - \frac{\exp(+i\omega_{ex}t)}{\hbar\omega_{ex}+3\hbar\Omega}\right]|\phi_{j+3}(t)\rangle_0 \\
& + \sqrt{j(j-1)(j-2)}\frac{2^{3/2}}{4}y_0^3A_\xi\left[\frac{\exp(-i\omega_{ex}t)}{\hbar\omega_{ex}+3\hbar\Omega} + \frac{\exp(+i\omega_{ex}t)}{-\hbar\omega_{ex}+3\hbar\Omega}\right]|\phi_{j-3}(t)\rangle_0 \\
& + \frac{3}{4}y_0^2A_\xi^2\sqrt{(j+1)(j+2)}\left[\frac{\exp(-i2\omega_{ex}t)}{\hbar 2\omega_{ex}-2\hbar\Omega} + \frac{\exp(i2\omega_{ex}t)}{-\hbar 2\omega_{ex}-2\hbar\Omega}\right]|\phi_{j+2}(t)\rangle_0 \\
& \left. + \frac{3}{4}y_0^2A_\xi^2\sqrt{j(j-1)}\left[\frac{\exp(-i2\omega_{ex}t)}{\hbar 2\omega_{ex}+2\hbar\Omega} + \frac{\exp(i2\omega_{ex}t)}{-\hbar 2\omega_{ex}+2\hbar\Omega}\right]|\phi_{j-2}(t)\rangle_0 \,\right],
\end{aligned}
\tag{3.44}
$$

where we used the abbreviation $A_\xi \equiv F/[M(\omega_{ex}^2 - \Omega^2)]$ and $|\phi_j(t)\rangle_0$ are the Floquet states of the linear oscillator. The coefficients c_{kj}^{nm} have to be small compared to one, so that a perturbative treatment is adequate. Depending on the actual value of the driving amplitude, the vicinity of ω_{ex} to Ω and the order of the divergence at exact resonance, we can give a lower boundary for the validity of App I. In the vicinity of a one-photon resonance ($\omega_{ex} \propto \Omega$) the condition that the coefficients c_{kj}^{nm} are smaller than one becomes:

$$
\left| c\frac{(\alpha y_0^4)^1(y_0F)^m}{\hbar^{1+m}\Omega^l} \right| < |\omega_{ex} - \Omega|^{1+m-l}, \tag{3.45}
$$

where c is a dimensionless constant with $|c| < 1$. Up to second order in the driving combinations of $m = 1, 2$ and $l = 0, 1$ occur. This allows us to cover two different regimes of validity for App I:

$$
\left| \frac{(y_0F/\hbar)^{m+1}}{\Omega^l} \right| < |\omega_{ex} - \Omega|^{1+m-l}, \qquad c\alpha y_0^4 < y_0F, \tag{3.46a}
$$

$$
\left| \frac{(c\alpha y_0^4/\hbar)^{1+m}}{\Omega^l} \right| < |\omega_{ex} - \Omega|^{1+m-l}, \qquad c\alpha y_0^4 > y_0F. \tag{3.46b}
$$

3.4 Perturbative approach for the one-photon resonance

When the nonlinearity becomes a relevant perturbation to the equidistant spectrum of the linear oscillator, it becomes preferable to use the second approximation scheme, App II, based on the decomposition Eq. (3.2b).
In this case it is convenient to express the Floquet Hamiltonian $\hat{\mathcal{H}}_{\rm DO}$ in the composite Hilbert space $\mathcal{R}\otimes\mathcal{T}$ spanned by the vectors $|j,n\rangle\rangle \equiv |j\rangle\otimes|n)$, where $|j\rangle$ is an eigenstate of the nonlinear oscillator $\hat{H}_{\rm NLO}$ given in Eq. (3.43b). Therefore in this basis the Floquet Hamiltonian of the nonlinear oscillator $\hat{\mathcal{H}}_{\rm NLO}$, see Eq. (3.48) below at vanishing driving amplitude, is diagonal. In contrast, the perturbation $\hat{V}_F = \hat{y}F\cos(\omega_{ex}t)$ is time-dependent and thus non-diagonal also in the Hilbert space $\mathcal{T}$. From the relation:

$$\langle\langle j,n|\hat{\mathcal{H}}_{\rm DO}|k,n'\rangle\rangle \;=\; (\hat{H}_{\rm DO})^{(n-n')}_{jk} - \hbar\omega_{ex}n\delta_{jk}\delta_{nn'}, \tag{3.47}$$

where $(\hat{H}_{\rm DO})^{(n-n')}_{jk}$ are the Fourier coefficients of the matrix $\langle j|\hat{H}_{\rm DO}(t)|k\rangle$, it follows

$$\langle\langle j,n|\hat{\mathcal{H}}_{\rm DO}|k,n'\rangle\rangle \;=\; E_{j,n}\delta_{kj}\delta_{nn'} + \frac{F}{2}\langle j|\hat{y}|k\rangle(\delta_{n,n'+1}+\delta_{n,n'-1}), \tag{3.48}$$

with $E_{j,n} = E_j - \hbar n\omega_{ex}$ and E_j the energies of the nonlinear oscillator Eq. (3.43a). From Eq. (3.48) it is thus apparent that two eigenstates $|j,n\rangle\rangle$, $|k,m\rangle\rangle$ of $\hat{\mathcal{H}}_{\rm NLO}$ become degenerate when $E_{j,n} = E_{k,n'}$, i.e., for a driving frequency ω_{ex} satisfying

$$\hbar\omega_{ex}(n'-n) \;=\; E_k - E_j. \tag{3.49}$$

Setting $N = n' - n$ one speaks of an N-photon resonance. From Eq. (3.43a) for the energies E_j it follows, with $k = j + M$,

$$\hbar\omega_{ex}N \;=\; E_{j+M} - E_j = M\left[\hbar\Omega + \frac{3}{8}\alpha y_0^4\,(M+1+2j)\right]. \tag{3.50}$$

In the following we restrict to the case $\omega_{ex} \sim \Omega$ such that $N = M$ and to the one-photon resonance $N = 1$, i.e., the quasienergies $E_{j,n}$ and $E_{j+1,n+1}$ are degenerate if $\omega_{ex} = \Omega + \frac{3\alpha y_0^4(j+1)}{4\hbar} \equiv \Omega_j$.
Moreover, due to the arbitrariness in the choice of the Brillouin zone index n, we fix it in the following to the zeroth Brillouin zone, i.e., $n = 0$. For our perturbative treatment we further require that the nonlinearity is large enough that if $E_{j,0}$ is resonant with $E_{j+1,+1}$ the remaining quasi-energy levels are off resonance and not involved in the doublet spanned by the two degenerate levels. Having this in mind, we have to restrict ourselves to a certain range of possible values of ω_{ex}, namely to the resonance region such that the chosen doublet remains degenerate or almost degenerate, i.e., for the one-photon resonance: $|\omega_{ex} - \Omega_j| < \frac{3}{4\hbar}\alpha y_0^4$. This results from the fact that if $E_{j,0} = E_{j+1,+1}$, the closest lying levels $E_{j+2,2}$ and $E_{j-1,-1}$ are by $\frac{3}{4}\alpha y_0^4$ away. Because of the manifold (doublet) structure of the quasi-energy spectrum, we apply in the

following Van Vleck perturbation theory [141, 142] and treat the driving as a small perturbation, i.e., $\frac{y_0 F}{2\sqrt{2}} \ll \frac{3}{4}\alpha y_0^4 \ll \hbar\Omega$. Consequently, a consistent treatment in App II requires that either F^2 contributions are neglected if we consider the nonlinearity only up to first order, or that both driving and nonlinearity are treated up to second order. As the second order in both parameters is very involved, we restrict to the first order in the nonlinearity and neglect quadratic contributions in the driving strength, as long as their reliability cannot be verified within a different approach, i.e., App I.
Within Van Vleck perturbation theory we construct an effective Floquet Hamiltonian $\hat{\mathcal{H}}_{\rm eff} = \exp(i\hat{S})\hat{\mathcal{H}}_{\rm DO}\exp(-i\hat{S})$ having the same eigenvalues as the original Hamiltonian $\hat{\mathcal{H}}_{\rm DO}$ and not containing matrix elements connecting states belonging to different manifolds. Therefore it is block-diagonal with all quasi-degenerate energy states in one common block. To determine the transformation $\hat{S}$ and the effective Hamiltonian $\hat{\mathcal{H}}_{\rm eff}$ we write both as a power series in the driving:

$$\hat{S} = \hat{S}^{(0)} + \hat{S}^{(1)} + \hat{S}^{(2)} + \dots \tag{3.51}$$

$$\hat{\mathcal{H}}_{\rm eff} = \hat{\mathcal{H}}_{\rm eff}^{(0)} + \hat{\mathcal{H}}_{\rm eff}^{(1)} + \hat{\mathcal{H}}_{\rm eff}^{(2)} + \dots \ . \tag{3.52}$$

In Appendix C the general formulas for the energies and the states up to second order are provided [141, 142, 143, 144].
The zeroth order energies are $E_{j,0}$ and $E_{j+1,+1}$ and the corresponding (quasi)-degenerate Floquet states are: $|j,0\rangle\rangle$ and $|j+1,+1\rangle\rangle$.
The quasi-degenerate block of the effective Hamiltonian in this basis up to second order in the driving strength acquires the form:

$$\hat{\mathcal{H}}_{\rm eff} = \begin{pmatrix} E_{j,0} + E_j^{(2)--} & E_j^{(1)} \\ E_j^{(1)} & E_{j+1,+1} + E_j^{(2)++} \end{pmatrix}, \tag{3.53}$$

where

$$E_j^{(1)} = \langle\langle j,0|\hat{V}_F|j+1,+1\rangle\rangle = \langle\langle j+1,+1|V_F|j,0\rangle\rangle = n_1(j)\frac{y_0 F}{2\sqrt{2}}, \tag{3.54}$$

and

$$E_j^{(2)--} = \frac{y_0^2 F^2}{8}\left[\frac{n_1^2(j-1)}{E_{j,0}-E_{j-1,-1}} + \frac{n_1^2(j-1)}{E_{j,0}-E_{j-1,+1}} + \frac{n_1^2(j)}{E_{j,0}-E_{j+1,-1}}\right], \tag{3.55}$$

$$E_j^{(2)++} = \frac{y_0^2 F^2}{8}\left[\frac{n_1^2(j+1)}{E_{j+1,+1}-E_{j+2,+2}} + \frac{n_1^2(j+1)}{E_{j+1,+1}-E_{j+2,0}} + \frac{n_1^2(j)}{E_{j+1,+1}-E_{j,2}}\right],$$

with

$$n_1(j) = \sqrt{j+1}\left[1 - \frac{3}{8\hbar\Omega}\alpha y_0^4 (j+1)\right]. \tag{3.56}$$

Notice that the unperturbed quasienergies $E_{j,0}$ and $E_{j+1,1}$ are correct up to first order in the nonlinearity. For consistency also $n_i^2(j)$ has to be treated up to first order in α

only.
As shown by Eq. (3.57) below it is essential to determine the eigenenergies of $\hat{\mathcal{H}}_{\text{eff}}$ up to second order in F. They are also the eigenenergies of $\hat{\mathcal{H}}_{\text{DO}}$ and read:

$$\begin{aligned}\epsilon_j^{\mp} &= \frac{1}{2}\left(E_{j,0}+E_{j+1,+1}+E_j^{(2)--}+E_j^{(2)++}\right) \pm \frac{1}{2}\left[(E_{j,0}-E_{j+1,+1})^2\right. \\ &\quad \left. +2(E_{j,0}-E_{j+1,+1})(E_j^{(2)--}-E_j^{(2)++})+4E_j^{(1)^2}\right]^{1/2}. \end{aligned} \tag{3.57}$$

The convention $\epsilon_j^{\mp}$ is chosen such that $\epsilon_j^- < \epsilon_j^+$ for $\omega_{ex} < \Omega_j$, whereas it jumps at resonance such that $\epsilon_j^- > \epsilon_j^+$ for $\omega_{ex} > \Omega_j$. Because the first order correction in the driving $E_j^{(1)}$ enters Eq. (3.57) quadratically, a calculation of the quasienergies up to first order in F merely yields (when $E_{j,0} \neq E_{j+1,1}$) the zeroth order results. Consequently to be consistent one has to take into account also the second order corrections $E_j^{(2)--}$ and $E_j^{(2)++}$ to the energies.
The eigenstates of the block, Eq. (3.53), are determined by:

$$\begin{aligned}|-_{j,0}\rangle\rangle_{\text{ eff}} &:= -\sin\frac{\eta_j}{2}|j+1,+1\rangle\rangle + \cos\frac{\eta_j}{2}|j,0\rangle\rangle, \\ |+_{j,1}\rangle\rangle_{\text{ eff}} &:= \sin\frac{\eta_j}{2}|j,0\rangle\rangle + \cos\frac{\eta_j}{2}|j+1,+1\rangle\rangle, \end{aligned} \tag{3.58}$$

where

$$\tan\eta_j = \frac{2|E_j^{(1)}|}{-(E_{j,0}-E_{j+1,+1}+E_j^{(2)--}-E_j^{(2)++})}. \tag{3.59}$$

In conventional Van Vleck perturbation theory the eigenstates of $\hat{\mathcal{H}}_{\text{DO}}$ are obtained by applying a back transformation:

$$|\mp_{j,n}\rangle\rangle = \exp(-i\hat{S})|\mp_{j,n}\rangle\rangle_{\text{eff}}. \tag{3.60}$$

Expanding the exponential up to first order we obtain for the eigenstates:

$$\begin{aligned}|\mp_{j,n}\rangle\rangle &= |\mp_{j,n}\rangle\rangle_{\text{eff}} - i\hat{S}^{(1)}|\mp_{j,n}\rangle\rangle_{\text{eff}}, \\ &= |\mp_{j,n}\rangle\rangle_{\text{eff}} + \hat{R}\hat{V}_F|\mp_{j,n}\rangle\rangle_{\text{eff}}. \end{aligned} \tag{3.61}$$

As anticipated above Eq. (3.51) we do not determine the second order correction for the states coming from the second order contribution to $\hat{S}$. For consistency the trigonometric functions in Eq. (3.62) below should be expanded in F, when certain orders in perturbation theory are considered. However, for the matter of analytical convenience and because of the agreement of the quasienergies in both approaches up to order $\mathcal{O}(\alpha F^2)$, see section 3.5.1, we prefer not to expand them.
In the second line of Eq. (3.61) we used the fact that we can express the transformation $\hat{S}$ by introducing the reduced resolvent $\hat{R}$, allowing a nice connection to conventional degenerate perturbation theory as shown in Appendix C. From Eq. (3.61) it follows:

$$\begin{aligned}|-_{j,0}\rangle\rangle &= -\sin\frac{\eta_j}{2}(1+\hat{R}\hat{V}_F)|j+1,+1\rangle\rangle + \cos\frac{\eta_j}{2}(1+\hat{R}\hat{V}_F)|j,0\rangle\rangle, \\ |+_{j,1}\rangle\rangle &= \sin\frac{\eta_j}{2}(1+\hat{R}\hat{V}_F)|j,0\rangle\rangle + \cos\frac{\eta_j}{2}(1+\hat{R}\hat{V}_F)|j+1,+1\rangle\rangle, \end{aligned} \tag{3.62}$$

where

$$
\begin{aligned}
\hat{R}\hat{V}_F|j,0\rangle\rangle &= \sum_{(k,n)\neq\{(j,0),(j+1,+1)\}} \frac{|k,n\rangle\rangle\langle\langle k,n|\hat{V}_F|j,0\rangle\rangle}{E_{j,0}-E_{k,n}} \qquad (3.63)\\
&= \frac{y_0F}{2\sqrt{2}}\left(\frac{n_1(j-1)}{E_{j,0}-E_{j-1,-1}}|j-1,-1\rangle\rangle+\frac{n_1(j)}{E_{j,0}-E_{j+1,-1}}|j+1,-1\rangle\rangle\right.\\
&\quad+\frac{n_1(j-1)}{E_{j,0}-E_{j-1,+1}}|j-1,+1\rangle\rangle+\frac{n_3(j,\alpha)}{E_{j,0}-E_{j+3,+1}}|j+3,+1\rangle\rangle\\
&\quad+\frac{n_3(j-3,\alpha)}{E_{j,0}-E_{j-3,+1}}|j-3,+1\rangle\rangle+\frac{n_3(j,\alpha)}{E_{j,0}-E_{j+3,-1}}|j+3,-1\rangle\rangle\\
&\quad\left.+\frac{n_3(j-3,\alpha)}{E_{j,0}-E_{j-3,-1}}|j-3,-1\rangle\rangle\right),\\
\hat{R}\hat{V}_F|j+1,+1\rangle\rangle &= \sum_{(k,n)\neq\{(j,0),(j+1,+1)\}} \frac{|k,n\rangle\rangle\langle\langle k,n|\hat{V}_F|j+1,+1\rangle\rangle}{E_{j+1,+1}-E_{k,n}}\\
&= \frac{y_0F}{2\sqrt{2}}\left(\frac{n_1(j)}{E_{j+1,1}-E_{j,2}}|j,+2\rangle\rangle+\frac{n_1(j+1)}{E_{j+1,1}-E_{j+2,2}}|j+2,+2\rangle\rangle\right.\\
&\quad+\frac{n_1(j+1)}{E_{j+1,1}-E_{j+2,0}}|j+2,0\rangle\rangle+\frac{n_3(j-2,\alpha)}{E_{j+1,1}-E_{j-2,0}}|j-2,0\rangle\rangle\\
&\quad+\frac{n_3(j-2,\alpha)}{E_{j+1,1}-E_{j-2,2}}|j-2,+2\rangle\rangle+\frac{n_3(j+1,\alpha)}{E_{j+1,1}-E_{j+4,0}}|j+4,0\rangle\rangle\\
&\quad\left.+\frac{n_3(j+1,\alpha)}{E_{j+1,+1}-E_{j+4,2}}|j+4,+2\rangle\rangle\right),
\end{aligned}
$$

and

$$
n_3(j,\alpha) = \frac{\alpha y_0^4}{16\hbar\Omega}\sqrt{(j+3)(j+2)(j+1)}.
$$

The effect of the transformation is to yield a contribution from states outside the manifold. Notice that in order to obtain the states to first order in F the trigonometric functions $\sin\frac{\eta_j}{2}$ and $\cos\frac{\eta_j}{2}$ should be expanded in powers of F.

We conclude this section by mentioning that eigenenergies and eigenstates of the Duffing oscillator have been calculated near and at resonance also by Peano et al. [18]. However in [18] the nonlinear undriven Hamiltonian $\hat{H}_{\rm NLO}=\frac{\hat{P}_y^2}{2M}+\frac{M\Omega^2}{2}\hat{y}^2+\frac{\alpha}{4}\hat{y}^4$ is approximated by $\hat{H}_{\rm NLO}\simeq\hbar\Omega\hat{j}+\frac{3}{8}\alpha y_0^4\hat{j}(\hat{j}+1)$, where $\hat{j}$ is the occupation number operator of the undriven linear oscillator. This approximated Hamiltonian is diagonal in the linear oscillator basis and yields the result Eq. (3.43a) for the energies of $\hat{H}_{\rm NLO}$. However, further corrections of order α contained in the eigenstates (3.43b) are neglected. The results of [18] at finite driving can be retained from Eqs. (3.57) and (3.62) by treating the driving up to first order, by replacing $n_1(j)$ by $\sqrt{j+1}$ and by setting $n_3(j)=0$.

3.5 Comparison of the outcomes of the two approaches

The approximation scheme in section 3.3, App I, is valid when the quasienergy spectrum of the linear oscillator is non-degenerate and if conditions (3.46a-3.46b) are fulfilled, i.e., away of an N-photon resonance. In contrast, the perturbative approach of section 3.4, denoted as App II, works at best near and at an N-photon resonance in the quasienergy spectrum of the undriven nonlinear oscillator: $0 \leq |\omega_{ex} - \Omega_j| < \frac{3}{4\hbar}\alpha y_0^4$. Thus a comparison of the outcomes of the two approaches is possible in the frequency regime near resonance, i.e., within an intermediate regime, where both approaches are valid. Additionally, as the Van Vleck-based approximation scheme is perturbative in the driving, remember $\frac{y_0 F}{2\sqrt{2}} \ll \frac{3}{4}\alpha y_0^4$, a comparison requires an expansion in F of the results from App I. This implies that Eq. (3.46b) has to be used for the comparison. As the one-photon resonance $\omega_{ex} \sim \Omega$ for the levels $j = 0$ and $j = 1$ is considered, the largest prefactor arises for $j = 1$, such that the condition for applying perturbation theory is determined by:

$$\frac{3(\alpha y_0^4)(y_0 F)}{4\hbar^2} < |\omega_{ex} - \Omega|^2. \tag{3.64}$$

In this case Eq. (3.46b) with $y_0 F < \frac{3}{4}\alpha y_0^4$ becomes:

$$\frac{3}{4}\alpha y_0^4/\hbar < |\omega_{ex} - \Omega|. \tag{3.65}$$

This section is organized as follows: first the energies and then the matrix elements of the position operator are compared.

3.5.1 Comparison of the quasienergies

We start with the off resonant case $|E_{j,0} - E_{j+1,+1}| = \hbar|\omega_{ex} - \Omega_j| > E_j^{(1)}$ and expand the result in Eq. (3.57) up to second order in the driving amplitude F:

$$\begin{aligned} \epsilon_j^- &= E_{j,0} + E_j^{(2)--} + E_j^{(1)2}/(E_{j,0} - E_{j+1,+1}), \\ \epsilon_j^+ &= E_{j+1,+1} + E_j^{(2)++} - E_j^{(1)2}/(E_{j,0} - E_{j+1,+1}). \end{aligned} \tag{3.66}$$

Expanding further for consistency the eigenvalues up to first order in the nonlinearity we obtain:

$$\begin{aligned} \epsilon_j^- &= E_{j,0} + \frac{y_0^2 F^2}{8}\left[\frac{2\Omega}{\hbar(\omega_{ex}^2 - \Omega^2)} + \frac{3\alpha y_0^4}{\hbar^2}(2j+1)\frac{\Omega^2}{(\omega_{ex}^2 - \Omega^2)^2}\right] \\ &\quad + \mathcal{O}(F^3, \alpha^2) \\ \epsilon_j^+ &= E_{j+1,+1} + \frac{y_0^2 F^2}{8}\left[\frac{2\Omega}{\hbar(\omega_{ex}^2 - \Omega^2)} + \frac{3\alpha y_0^4}{\hbar^2}\frac{(2j+3)\Omega^2}{(\omega_{ex}^2 - \Omega^2)^2}\right] + \mathcal{O}(F^3, \alpha^2). \end{aligned} \tag{3.67}$$

Inserting $y_0 = \sqrt{\hbar/(M\Omega)}$, these are exactly the results obtained from App I for $\epsilon_{j,0}$ and $\epsilon_{j+1,1}$ upon expanding Eq. (3.42) up to second order in the driving amplitude.

Consequently, as the quasienergies, Eq. (3.42), coincide with the quasienergies from App II away from the resonance, we conclude that Eq. (3.57) describes the frequency dependence of the quasienergies up to $\mathcal{O}(F^4)$, also far from resonance. Moreover, because the contribution of order $\mathcal{O}(F^4)$ to the quasienergies obtained in App I is state-independent, see Eq. (3.42), it drops when differences of quasienergies are considered. In other words the difference of quasienergies coincides in both approaches.

3.5.2 Matrix element $y_{lk}(t)$

Due to the agreement (in second order in F) for the quasienergies and the disagreement for the Floquet states shown in Appendix D, the question arises whether expectation values of observables also differ in the two approaches. We shall answer this question in the following at the level of the expectation value of the position operator $\hat{y}$.

$y_{lk}(t)$ in App I

For the linear oscillator the exact result holds:

$$\begin{aligned} y_{lk}^{(0)}(t) &:= {}_0\langle\phi_l(t)|\hat{y}|\phi_k(t)\rangle_0 \\ &= \int dy'dy''\ {}_0\langle\phi_l(t)|y'\rangle\langle y'|\hat{y}|y''\rangle\langle y''|\phi_k(t)\rangle_0 \\ &= \int dy\overline{\phi}_l(y-\xi(t))y\overline{\phi}_k(y-\xi(t)) \\ &= \int dy\overline{\phi}_l(y)(y+\xi(t))\overline{\phi}_k(y) \\ &= \frac{y_0}{\sqrt{2}}\left[\sqrt{k+1}\delta_{l,k+1}+\sqrt{k}\delta_{l,k-1}\right]+\xi(t)\delta_{lk}. \end{aligned} \tag{3.68}$$

where the function $\overline{\phi}_l(y)$ is introduced in Eq. (3.24). Notice that there is *no* second order contribution in the driving to the matrix element $y_{lk}^{(0)}(t)$. This observation will be important later on. We now look at the matrix elements of $\hat{y}$ on Floquet states of the driven nonlinear oscillator from App I. We define for the following:

$$y_{lk}(t) := \langle\phi_l(t)|\hat{y}|\phi_k(t)\rangle = \sum_n \exp(-in\omega_{ex}t)y_{lk}^{(n)}, \tag{3.69}$$

where

$$y_{lk}^{(n)} = \frac{1}{T_{\omega_{ex}}}\int_0^{T_{\omega_{ex}}} \exp(+in\omega_{ex}t)\langle\phi_l(t)|\hat{y}|\phi_k(t)\rangle = \langle\langle\phi_{l,n}|\hat{y}|\phi_{k,0}\rangle\rangle. \tag{3.70}$$

Moreover:

$$y_{lk,mn}(t) := \langle\phi_{l,m}(t)|\hat{y}|\phi_{k,n}(t)\rangle = \exp(-i\omega_{ex}t(n-m))y_{lk}(t). \tag{3.71}$$

We calculate the matrix elements within App I. In particular, from Eq. (3.35) we obtain:

$$\begin{aligned}
y^{\text{App I}}_{01,01}(t) &= \frac{y_0}{\sqrt{2}}\Big[\sqrt{1}+\sqrt{2}\left(c^{(0)}_{20}+c^{(+2)}_{20}\exp(i2\omega_{ex}t)+c^{(-2)}_{20}\exp(-i2\omega_{ex}t)\right)\\
&\quad +\sqrt{1}\left(\exp(-2i\omega_{ex}t)(c^{(-2)}_{00}+c^{(2)}_{11})+\exp(2i\omega_{ex}t)(c^{(2)}_{00}+c^{(-2)}_{11})\right)\Big]\times\\
&\quad \exp(-i\omega_{ex}t),\\
y^{\text{App I}}_{00,00}(t) &= \xi(t)+\frac{y_0}{\sqrt{2}}\left[2\cos(\omega_{ex}t)(c^{(1)}_{10}+c^{(-1)}_{10})+2\cos(3\omega_{ex}t)(c^{(3)}_{10}+c^{(-3)}_{10})\right],\\
y^{\text{App I}}_{10,10}(t) &= \left(y^{\text{App I}}_{01,01}(t)\right)^*,\\
y^{\text{App I}}_{11,11}(t) &= \xi(t)+\frac{y_0}{\sqrt{2}}\Big[2\cos(\omega_{ex}t)(c^{(1)}_{01}+c^{(-1)}_{01})+2\cos(3\omega_{ex}t)(c^{(3)}_{01}+c^{(-3)}_{01})\\
&\quad +2\sqrt{2}\cos(\omega_{ex}t)(c^{(1)}_{21}+c^{(-1)}_{21})+2\sqrt{2}\cos(3\omega_{ex}t)(c^{(3)}_{21}+c^{(-3)}_{21})\Big].
\end{aligned}$$

In the last derivations we used the coefficients $c^{(n)}_{kj}$ introduced in Eq. (3.40) and the symmetry relations:

$$\begin{aligned}
c^{(\pm 4)}_{jj} &= c^{(\pm 4)}_{kk}, \quad j\neq k\\
c^{(n)}_{kj} &= -c^{(-n)}_{jk}.
\end{aligned} \tag{3.72}$$

Inserting the actual form of the coefficients $c^{(n)}_{kj}$ we obtain:

$$y^{\text{App I}}_{00,00} = \frac{F}{M(\omega^2_{ex}-\Omega^2)}\cos(\omega_{ex}t)\left[1+\frac{3\alpha y_0^4\Omega}{2\hbar(\omega^2_{ex}-\Omega^2)}\right] +\mathcal{O}(\alpha F^2), \tag{3.73a}$$

$$y^{\text{App I}}_{10,10} = \frac{y_0}{\sqrt{2}}\sqrt{1}\left(1-\frac{3\alpha y_0^4}{8\hbar\Omega}\right)\exp(+i\omega_{ex}t)+\mathcal{O}(\alpha F^2), \tag{3.73b}$$

$$y^{\text{App I}}_{11,11} = \frac{F}{M(\omega^2_{ex}-\Omega^2)}\cos(\omega_{ex}t)\left[1+\frac{9\alpha y_0^4\Omega}{2\hbar(\omega^2_{ex}-\Omega^2)}\right] +\mathcal{O}(\alpha F^2). \tag{3.73c}$$

We observe that, as it is well known from the driven linear oscillator, terms of order F^2 or higher are absent at zero nonlinearity. The nonlinearity introduces a correction of $\mathcal{O}(\alpha F^2)$ in Eqs. (3.73a)-(3.73c), which we neglect in the following.

$y_{lk}(t)$ in the perturbative approach App II

We calculate $y_{lk}(t)$ for the one-photon resonance for the case $j=0$. In the following we define $|\phi_{0,0}(t)\rangle \equiv (t|-_{0,0}\rangle\rangle$ and $|\phi_{1,1}(t)\rangle \equiv (t|+_{0,1}\rangle\rangle$. Then

$$\begin{aligned}
y^{\text{App II}}_{00,00}(t) &\equiv \langle\phi_{0,0}(t)|\hat{y}|\phi_{0,0}(t)\rangle\\
&= \sum_n \exp(-in\omega_{ex}t)y^{(n)}_{00}\\
&= \sum_n \exp(-in\omega_{ex}t)\langle\langle -_{0,n}|\hat{y}|-_{0,0}\rangle\rangle.
\end{aligned} \tag{3.74}$$

To proceed we use Eqs. (3.62) and (3.63) for $j = 0$. Using the relation $\hat{y} = \frac{y_0}{\sqrt{2}}(\hat{a} + \hat{a}^\dagger)$, where $\hat{a}$ and $\hat{a}^\dagger$ are the annihilation and creation operators of the linear oscillator, we calculate the matrix elements:

$$\begin{aligned}\langle\langle 0,n|(1+\hat{R}\hat{V}_F)^\dagger(\hat{a}+\hat{a}^\dagger)(1+\hat{R}\hat{V}_F)|0,0\rangle\rangle &= \frac{y_0 F}{2\sqrt{2}}\frac{n_1^2(0)}{E_{0,0}-E_{1,-1}}(\delta_{n,1}+\delta_{n,-1}) \\ &\equiv A_{--}(F)(\delta_{n,1}+\delta_{n,-1}),\end{aligned}$$

$$\begin{aligned}\langle\langle 1,n+1|(1+\hat{R}\hat{V}_F)^\dagger(\hat{a}+\hat{a}^\dagger)(1+\hat{R}\hat{V}_F)|1,1\rangle\rangle &= \frac{y_0 F}{2\sqrt{2}}\left[\frac{n_1^2(0)}{E_{1,1}-E_{0,2}}\right. \\ \left.+\frac{n_1^2(1)}{E_{1,1}-E_{2,2}}+\frac{n_1^2(1)}{E_{1,1}-E_{2,0}}\right](\delta_{n,1}+\delta_{n,-1})) &\equiv A_{++}(F)(\delta_{n,1}+\delta_{n,-1}),\end{aligned}$$

$$\begin{aligned}\langle\langle 1,n+1|(1+\hat{R}\hat{V}_F)^\dagger(\hat{a}+\hat{a}^\dagger)(1+\hat{R}\hat{V}_F)|0,0\rangle\rangle &= n_1(0)\delta_{n,-1} \equiv A_{+-}\delta_{n,-1}, \\ \langle\langle 0,n|(1+\hat{R}\hat{V}_F)^\dagger(\hat{a}+\hat{a}^\dagger)(1+\hat{R}\hat{V}_F)|1,1\rangle\rangle &= n_1(0)\delta_{n,1} \equiv A_{-+}\delta_{n,1}.\end{aligned} \tag{3.75}$$

Note that $A_{+-} = A_{-+} = n_1(0)$ is independent of the driving. Consequently, we find the result:

$$y_{00,00}^{\text{App II}}(t) = y_{00}^{(+1)}\exp(-i\omega_{ex}t) + y_{00}^{(-1)}\exp(i\omega_{ex}t), \tag{3.76}$$

with

$$\begin{aligned}y_{00}^{(+1)} &= y_{00}^{(-1)} \\ &\equiv \frac{y_0}{\sqrt{2}}\left(\sin^2\frac{\eta_0}{2}A_{++}(F) - \sin\frac{\eta_0}{2}\cos\frac{\eta_0}{2}A_{+-} + \cos^2\frac{\eta_0}{2}A_{--}(F)\right).\end{aligned} \tag{3.77}$$

The other matrix elements are obtained in the same way. We give only the results:

$$\begin{aligned}y_{11,11}^{\text{App II}}(t) &= \langle\phi_{1,1}(t)|\hat{y}|\phi_{1,1}(t)\rangle = \sum_n \exp(-in\omega_{ex}t)\langle\langle +_{0,n+1}|\hat{y}|+_{0,1}\rangle\rangle \\ &= y_{11}^{(+1)}\exp(-i\omega_{ex}t) + y_{11}^{(-1)}\exp(i\omega_{ex}t)\end{aligned} \tag{3.78}$$

with

$$\begin{aligned}y_{11}^{(+1)} &= y_{11}^{(-1)} \\ &\equiv \frac{y_0}{\sqrt{2}}\left(\sin^2\frac{\eta_0}{2}A_{--}(F) + \sin\frac{\eta_0}{2}\cos\frac{\eta_0}{2}A_{+-} + \cos^2\frac{\eta_0}{2}A_{++}(F)\right),\end{aligned} \tag{3.79}$$

$$\begin{aligned}y_{10,10}^{\text{App II}}(t) &= \langle\phi_{1,1}(t)|\hat{y}|\phi_{0,0}(t)\rangle = \sum_n \exp(-in\omega_{ex}t)\langle\langle +_{0,n+1}|\hat{y}|-_{0,0}\rangle\rangle \\ &= y_{10}^{(+1)}\exp(-i\omega_{ex}t) + y_{10}^{(-1)}\exp(i\omega_{ex}t)\end{aligned} \tag{3.80}$$

with

$$y_{10}^{(+1)} \equiv \frac{y_0}{\sqrt{2}}\left(-\sin^2\frac{\eta_0}{2}A_{-+}+\sin\frac{\eta_0}{2}\cos\frac{\eta_0}{2}[A_{--}(F)-A_{++}(F)]\right), \quad (3.81)$$
$$y_{10}^{(-1)} \equiv \frac{y_0}{\sqrt{2}}\left(+\sin\frac{\eta_0}{2}\cos\frac{\eta_0}{2}[A_{--}(F)-A_{++}(F)]+\cos^2\frac{\eta_0}{2}A_{+-}\right),$$

and

$$y_{01,01}^{\text{App II}}(t) = \langle\phi_{0,0}(t)|\hat{y}|\phi_{1,1}(t)\rangle = \sum_n \exp(-in\omega_{ex}t)\langle\langle -_{0,n}|\hat{y}|+_{0,1}\rangle\rangle \quad (3.82)$$
$$= y_{01}^{(+1)}\exp(-i\omega_{ex}t)+y_{01}^{(-1)}\exp(i\omega_{ex}t)$$

with

$$y_{01}^{(+1)} = y_{10}^{(-1)}, \quad (3.83)$$
$$y_{01}^{(-1)} = y_{10}^{(+1)}.$$

Consequently, $y_{10,10}^{\text{App II}}(t) = \left(y_{01,01}^{\text{App II}}(t)\right)^*$.
To compare we now expand the matrix elements in the driving strength and in the nonlinearity up to first order, using:

$$\sin\frac{\eta_j}{2} = \frac{y_0 F n_1(j)}{2\sqrt{2}(E_{j+1,+1}-E_{j,0})}+\mathcal{O}(F^3,\alpha^2), \quad (3.84)$$
$$\cos\frac{\eta_j}{2} = 1-\frac{1}{16}\frac{y_0^2F^2n_1^2(j)}{(E_{j+1,+1}-E_{j,0})^2}+\mathcal{O}(F^4,\alpha^2). \quad (3.85)$$

Consequently Eqs. (3.76)- (3.83) yield:

$$y_{00,00}^{\text{App II}}(t) = \frac{F}{M(\omega_{ex}^2-\Omega^2)}\cos(\omega_{ex}t)\left[1+\frac{3\alpha y_0^4\Omega}{2\hbar(\omega_{ex}^2-\Omega^2)}\right] \quad (3.86)$$
$$+\mathcal{O}(\alpha^2,F^2),$$
$$y_{10,10}^{\text{App II}}(t) = \frac{y_0}{\sqrt{2}}\left(1-\frac{3\alpha y_0^4}{8\hbar\Omega}\right)\exp(i\omega_{ex}t)+\mathcal{O}(\alpha^2,F^2), \quad (3.87)$$
$$y_{11,11}^{\text{App II}}(t) = \frac{F}{M(\omega_{ex}^2-\Omega^2)}\cos(\omega_{ex}t)\left[1+\frac{9\alpha y_0^4\Omega}{2\hbar(\omega_{ex}^2-\Omega^2)}\right] \quad (3.88)$$
$$+\mathcal{O}(\alpha^2,F^2),$$

Therefore App I reproduces the expressions for the matrix elements $y_{lk}(t)$ obtained in App II up to first order in the driving F near the one-photon resonance. Note that, as in App I, the difference between $y_{00,00}^{\text{App II}}(t)$ and $y_{11,11}^{\text{App II}}(t)$ in the nonlinear contribution arises due to the contribution of states neighbouring the (quasi)-degenerate states. App I is not valid at resonance, as the generated degeneracy is not included in the perturbative treatment. For App II the resonance condition is essential for generating a doublet of degenerate levels, requiring a finite nonlinearity. However the resulting energies and matrix elements can be expanded in the off-resonant regime and coincide with the results obtained within App I. Combining both approaches we can describe a large range of possible driving frequencies, using Eqs. (3.76)-(3.83).

3.6 Dissipative dynamics

To include dissipative effects, as presented in chapter 2, we use the system-bath approach introduced by Caldeira and Leggett [5], where the bath is composed by $\mathcal{N}$ harmonic oscillators with coordinate $\hat{x}_j$, momentum $\hat{p}_j$ and frequency ω_j and is coupled bilinearily to the system degrees of freedom. The interaction between system and bath is encapsulated in the coupling constants c_j. We have also introduced a counter term, proportional to $\hat{y}^2$, which accounts for the renormalization of the potential of the system due to the coupling.
The total Hamiltonian of the system plus bath is given by:

$$\hat{H}(t) = \hat{H}_{\rm DO}(t) + \hat{H}_{\rm B} + \hat{H}_{\rm DO+B}, \tag{3.89}$$

where

$$\begin{aligned}\hat{H}_{\rm B} &= \sum_{j=1}^{\mathcal{N}} \left[\frac{\hat{p}_j^2}{2m_j} + \frac{1}{2} m_j \omega_j^2 \hat{x}_j^2 \right] \\ \hat{H}_{\rm DO+B} &= -\hat{y} \sum_{j=1}^{\mathcal{N}} c_j \hat{x}_j + \hat{y}^2 \sum_{j=1}^{\mathcal{N}} \frac{c_j^2}{2m_j\omega_j^2}.\end{aligned}$$

In order to specifiy the effect of the bath it is convenient to introduce the spectral density of the bath, see Eq. (2.12):

$$J(\omega) = \frac{\pi}{2} \sum_{j=1}^{\mathcal{N}} \frac{c_j^2}{m_j\omega_j} \delta(\omega - \omega_j). \tag{3.90}$$

For a large number of bath oscillators the spectral density will become a smooth function and in the following calculations we use the Ohmic case: $J(\omega) = M\gamma\omega$, leading to memoryless friction and white noise in the classical limit. We will assume for the further calculation that the Duffing oscillator (DO) and bath are uncorrelated at time $t = 0$:

$$\hat{\rho}_{\rm DO+B}(0) = \hat{\rho}_{\rm DO}(0) \otimes \frac{\exp(-\hat{H}_{\rm B}/k_BT)}{{\rm Tr}_{\rm B} \exp(-\hat{H}_{\rm B}/k_BT)}, \tag{3.91}$$

where $\hat{\rho}_{\rm DO}(0)$ is the density operator of the Duffing oscillator at time $t = 0$. Because the bath consists of infinite degrees of freedom we assume the effects of the interaction with the DO system on the bath to dissipate away quickly, such that the bath remains in thermal equilibrium for all times t.
We wish to obtain an equation of motion for the reduced density operator $\hat{\rho}_{\rm DO}(t) = {\rm Tr}_{\rm B}\hat{\rho}_{\rm DO+B}(t)$. Following [113, 114, 115, 116, 117, 118] a Born-Markov approximation is applied and a Floquet-Markov master equation for the reduced density operator expressed in the Floquet basis of the DO, as presented in general form in

chapter 2, is derived:

$$\begin{aligned}\dot{\rho}_{\alpha\beta}(t) &= -\frac{i}{\hbar}(\epsilon_\alpha-\epsilon_\beta)\rho_{\alpha\beta}(t) \\ &+\sum_{\alpha'\beta'}\sum_{nn'}\exp[-i(n+n')\omega_{ex}t][(N_{\alpha\alpha',-n}+N_{\beta\beta',n'})y^{(n)}_{\alpha\alpha'}y^{(n')}_{\beta'\beta}\rho_{\alpha'\beta'} \\ &-N_{\beta'\alpha',-n}y^{(n')}_{\alpha\beta'}y^{(n)}_{\beta'\alpha'}\rho_{\alpha'\beta}-N_{\alpha'\beta',n'}y^{(n')}_{\beta'\alpha'}y^{(n)}_{\alpha'\beta}\rho_{\alpha\beta'}],\end{aligned} \tag{3.92}$$

where $\rho_{\alpha\beta}(t)=\langle\phi_\alpha(t)|\hat{\rho}_{\rm DO}(t)|\phi_\beta(t)\rangle$. A Lamb-shift contribution was disregarded. The other quantities entering Eq. (3.92) are

$$\begin{aligned}N_{\alpha\beta,n} &= N(\epsilon_\alpha-\epsilon_\beta+\hbar n\omega_{ex}), \\ N(\epsilon) &= \frac{J(|\epsilon|)}{\hbar}[n_{th}(|\epsilon|)+\theta(-\epsilon)],\end{aligned} \tag{3.93}$$

where $\theta(x)$ is the Heaviside function and n_{th} is the bosonic thermal occupation number $n_{th}(\epsilon)=\frac{1}{2}\left[\coth\left(\frac{\epsilon}{2k_BT}\right)-1\right]$. Additionally, $y^{(n)}_{\alpha\beta}$ are the Fourier coefficients defined by the matrix elements calculated in section 3.5.2 , see Eq. (3.70). For additional simplification we perform a moderate rotating-wave approximation consisting in averaging the time-dependent terms in the bath part over the driving period $T_{\omega_{ex}}=2\pi/\omega_{ex}$ [117, 118]:

$$\dot{\overline{\rho}}_{\alpha\beta}(t) = -\frac{i}{\hbar}(\epsilon_\alpha-\epsilon_\beta)\overline{\rho}_{\alpha\beta}(t)+\sum_{\alpha'\beta'}\mathcal{L}_{\alpha\beta,\alpha'\beta'}\overline{\rho}_{\alpha'\beta'}, \tag{3.94}$$

where $\overline{\rho}$ indicates the time average and the dissipative transition rates are:

$$\begin{aligned}\mathcal{L}_{\alpha\beta,\alpha'\beta'} &= \sum_n(N_{\alpha\alpha',-n}+N_{\beta\beta',-n})y^{(n)}_{\alpha\alpha'}y^{(-n)}_{\beta'\beta} \\ &-\delta_{\alpha\alpha'}\sum_{\alpha'',n}N_{\alpha''\beta',-n}y^{(-n)}_{\beta'\alpha''}y^{(n)}_{\alpha''\beta}-\delta_{\beta\beta'}\sum_{\beta'',n}N_{\beta''\alpha',-n}y^{(-n)}_{\alpha\beta''}y^{(n)}_{\beta''\alpha'}.\end{aligned} \tag{3.95}$$

The reason for its application is that it yields a time-independent stationary solution $\rho^{\rm st}_{\alpha\beta}=\lim_{t\to\infty}\overline{\rho}_{\alpha\beta}(t)$, which can be obtained by solving the linear system of equations:

$$0 = -\frac{i}{\hbar}(\epsilon_\alpha-\epsilon_\beta)\rho^{\rm st}_{\alpha\beta}+\sum_{\alpha'\beta'}\mathcal{L}_{\alpha\beta,\alpha'\beta'}\rho^{\rm st}_{\alpha'\beta'}. \tag{3.96}$$

3.7 Observable for the nonlinear response

Using Eq. (3.96) corresponds to describe the long time limit, where the system has already reached the steady-state. We calculate the mean value of the position operator in the stationary state, the nonlinear response:

$$\langle\hat{y}\rangle_{\rm st} = \lim_{t\to\infty}{\rm Tr}\{\hat{\overline{\rho}}_{\rm DO}(t)\hat{y}\}=\sum_{\alpha\beta}\rho^{\rm st}_{\alpha\beta}y_{\beta\alpha}(t), \tag{3.97}$$

where Tr{} denotes the trace over the oscillator degrees of freedom. Upon focussing on driving frequencies near and at the first resonance, the solution in the long time limit for a driven system is given by:

$$\langle \hat{y} \rangle_{\rm st} \simeq A \cos(\omega_{ex} t + \phi), \tag{3.98}$$

where higher harmonics have been neglected. We introduce the amplitude:

$$A = 2|\sum_{\alpha\beta} \rho^{\rm st}_{\alpha\beta} y^{(+1)}_{\beta\alpha}|, \tag{3.99}$$

and phase shift

$$\phi = +\pi\theta \left(-{\rm Re} \sum_{\alpha\beta} \rho^{\rm st}_{\alpha\beta} y^{(+1)}_{\beta\alpha} \right) - \arctan \left[\frac{{\rm Im} \sum_{\alpha\beta} \rho^{\rm st}_{\alpha\beta} y^{(+1)}_{\beta\alpha}}{{\rm Re} \sum_{\alpha\beta} \rho^{\rm st}_{\alpha\beta} y^{(+1)}_{\beta\alpha}} \right]. \tag{3.100}$$

3.7.1 One-photon resonance using PSA

We solve the master equation close to resonance in the low temperature regime, imposing a partial secular approximation (PSA) which amounts to take only coherences of the involved resonant levels into account. For an intermediate damping strength, i.e., the damping is of the order of the splitting of the one-photon resonance or larger, the system of equations is:

$$\begin{aligned} 0 &= \mathcal{L}_{00,00}\rho_{00}(t) + \mathcal{L}_{00,11}\rho_{11}(t) + 2\mathcal{L}_{00,01}{\rm Re}\left[\rho_{01}(t)\right], \\ 0 &= -i(\epsilon_0 - \epsilon_1)\rho_{01} + \mathcal{L}_{01,00}\rho_{00} + \mathcal{L}_{01,11}\rho_{11} + \mathcal{L}_{01,01}\rho_{01} + \mathcal{L}_{01,10}\rho^*_{01}, \\ \rho_{11} &= 1 - \rho_{00}, \end{aligned} \tag{3.101}$$

where for simplicity we omit the superscript 'st'.
If the damping γ is smaller than the smallest splitting we can even neglect the coherences completely:

$$0 = \sum_{\beta} \mathcal{L}_{\alpha\alpha,\beta\beta}\rho_{\beta\beta}. \tag{3.102}$$

Note that we use as shorthand abbreviations: $\epsilon_0 := \epsilon_0^-$ with eigenstate $|0\rangle = |\phi_{0,0}(t)\rangle$ and $\epsilon_1 := \epsilon_0^+$ with $|1\rangle = |\phi_{1,1}(t)\rangle$, respectively. Solving the system of equation for the stationary solution, we obtain:

$$\begin{aligned} \rho_{00} &= \left\{ -\mathcal{L}_{00,11}[\mathcal{L}^2_{01,01} - \mathcal{L}^2_{01,10} + (\epsilon_0 - \epsilon_1)^2/\hbar^2] + 2\mathcal{L}_{00,01}\mathcal{L}_{01,11}(\mathcal{L}_{01,01} \right. \\ &\quad \left. -\mathcal{L}_{01,10}) \right\} / \left\{ (\mathcal{L}_{00,00} - \mathcal{L}_{00,11})[\mathcal{L}^2_{01,01} - \mathcal{L}^2_{01,10} + (\epsilon_0 - \epsilon_1)^2/\hbar^2] \right. \\ &\quad \left. -2\mathcal{L}_{00,01}(\mathcal{L}_{01,00} - \mathcal{L}_{01,11})(\mathcal{L}_{01,01} - \mathcal{L}_{01,10}) \right\}, \\ {\rm Re}\rho_{01} &= \frac{-(\mathcal{L}_{01,01} - \mathcal{L}_{01,10})[\mathcal{L}_{01,11} + (\mathcal{L}_{01,00} - \mathcal{L}_{01,11})\rho_{00}]}{\mathcal{L}^2_{01,01} - \mathcal{L}^2_{01,10} + (\epsilon_0 - \epsilon_1)^2/\hbar^2}, \\ {\rm Im}\rho_{01} &= \frac{(\epsilon_0 - \epsilon_1)/\hbar}{(\mathcal{L}_{01,01} - \mathcal{L}_{01,10})} {\rm Re}\rho_{01}. \end{aligned} \tag{3.103}$$

To simplify the rates and obtain analytic results we restrict to low temperatures, $k_BT \ll \hbar\omega_{ex}$. Moreover, we consider the vicinity of a resonance, such that $|\epsilon_\alpha - \epsilon_\beta|$ is of the order of the minimal splitting, proportional to F, and within the limit of validity of App II, we obtain $|\epsilon_\alpha - \epsilon_\beta| \ll \hbar\omega_{ex}$. This corresponds to consider only spontaneous emission (see Eq. (3.93)): $N_{\alpha\beta,-1} \simeq J(|\omega_{ex}|)$ and $N_{\alpha\beta,1} \simeq 0$.
So we obtain:

$$\begin{aligned}\mathcal{L}_{\alpha\beta,\alpha'\beta'} &= J(|\omega_{ex}|)\Bigg[2y^{(1)}_{\alpha\alpha'}y^{(-1)}_{\beta'\beta} - \delta_{\alpha\alpha'}\sum_{\alpha''} y^{(-1)}_{\beta'\alpha''}y^{(1)}_{\alpha'',\beta} \\ &\quad -\delta_{\beta\beta'}\sum_{\beta''} y^{(-1)}_{\alpha\beta''}y^{(1)}_{\beta''\alpha'}\Bigg],\end{aligned} \tag{3.104}$$

with $J(|\omega_{ex}|) = M\gamma|\omega_{ex}|$.

3.7.2 One-photon resonance versus antiresonance

We use these approximate low temperature rates and solve the master equation near the one-photon resonance to calculate the amplitude and phase of the steady-state. The amplitude A in Eq. (3.99) is calculated for the one-photon resonance using the energies Eq. (3.57) up to second order in the driving and first in the nonlinearity and the expectation values Eqs. (3.76)-(3.83) up to both first order in the driving and in the nonlinearity.

The amplitude in lowest order of the damping

First we start with the analytical result for very low damping, where we only have to solve Eq. (3.102) resulting in:

$$\begin{aligned}\rho_{00} &= \frac{-\mathcal{L}_{00,11}}{(\mathcal{L}_{00,00} - \mathcal{L}_{00,11})} = \frac{y^2_{01,1}}{(y^2_{10,1} + y^2_{01,1})} + \mathcal{O}(\gamma) \\ \rho_{11} &= 1 - \rho_{00} + \mathcal{O}(\gamma).\end{aligned} \tag{3.105}$$

Therefore the amplitude Eq. (3.99) in lowest order, i.e., zeroth order, in the damping is determined to be:

$$\begin{aligned}A &= 2\Big|\big[y_0\left(2\sin\eta_0 4A_{+-}\cos\eta_0 A^2_{--}(F)\right. \\ &\quad + \left((5\cos(2\eta_0)+3)A^2_{+-} - 4A_{++}(F)\sin(2\eta_0)A_{+-}\right)A_{--}(F) \\ &\quad \left.+6A^2_{+-}A_{++}(F)\sin^2\eta_0 - 2A^3_{+-}\sin(2\eta_0)\right)\big] \\ &\quad / \Big[2\sqrt{2}\left((\cos(2\eta_0)+3)A^2_{+-} + 2(A_{--}(F) - A_{++}(F))\sin(2\eta_0)A_{+-}\right. \\ &\quad \left.+2(A_{--}(F) - A_{++}(F))^2\sin^2(\eta_0)\right)\big]\Big|.\end{aligned} \tag{3.106}$$

The actual form for the amplitude is shown in Fig. 3.3. Interestingly, an antiresonance occurs, as already predicted in [16, 18]. For comparison we show the result obtained

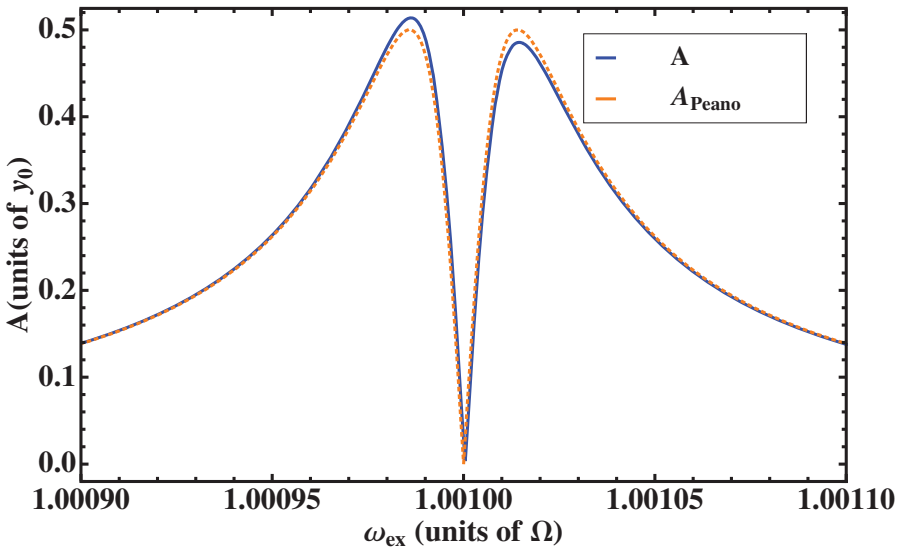

Figure 3.3: *Amplitude A at low damping ($\hbar\gamma \ll y_0 F n_1(0)/\sqrt{2}$) versus the driving frequency ω_{ex}. Chosen parameters are: $\Omega = 1$, $y_0^4\alpha/(\hbar\Omega) = 4/3 \cdot 10^{-3}$, $y_0 F/(\hbar\Omega) = 2^{3/2} \cdot 10^{-5}$, $k_b T/(\hbar\Omega) = 10^{-3}$ and $\gamma/\Omega = 10^{-7}$. For comparison we give also the result obtained by Peano et al. in Eq. (43) in [18].*

by Peano et al. [18]. We see that both curves show an exact antiresonance, but the dip position is slightly different and our result shows an asymmetric line shape. The reason for the differences are explained in the following. The condition for an exact antiresonance, $A = 0$, is $\rho_{00} y_{00}^{(1)} = -\rho_{11} y_{11}^{(1)}$. As the result of [18] is given in lowest order without back transformation, the dip position occurs at the one-photon resonance, when the driving is such that $\sin\frac{\eta_0}{2} = \cos\frac{\eta_0}{2} = 1/\sqrt{2}$. This corresponds to resonance in [18] due to $\rho_{00} = \rho_{11} = \frac{1}{2}$ and with $y_{00}^{(+1)} = -y_{11}^{(1)} = -\sin\frac{\eta_0}{2}\cos\frac{\eta_0}{2}\frac{y_0}{\sqrt{2}}$, yielding a symmetric shape of the amplitude, seen in Fig. 3.3. When all contributions linear in α are included, we find at resonance:

$$\rho_{00} = \frac{(A_{+-} + A_{--}(F) - A_{++}(F))^2}{2\left[A_{+-}^2 + (A_{--}(F) - A_{++}(F))^2\right]} \neq \frac{1}{2}, \tag{3.107}$$

and $y_{00}^{(+1)} \neq -y_{11}^{(1)}$. Moreover $A_{\eta_0=\pi/4} \neq 0$. The reason for not obtaining an equal population of the involved levels at resonance is due to the back transformation leading to the dressing of the eigenstates by states outside the quasi-degenerate doublet. In general, the dip position is determined by minimizing the amplitude A, Eq. (3.106), with respect to the external driving frequency. As the driving enters in both $A_{++}(F)$, $A_{--}(F)$ and in η_0, the amplitude acquires a nontrivial ω_{ex}-dependence, such that the minimization can only be done numerically. The antiresonance does not occur exactly at $\eta_0 = \pi/4$, but it is shifted to little larger values (deviation $\propto 10^{-7}$) with respect to the resonant case. This deviation arises due to the interplay of terms involving trigonometric functions of η_0 and explicitly driving-dependent prefactors, $A_{++}(F)$ and

$A_{--}(F)$, resulting from the back transformation.

Solution for the amplitude including higher orders in the damping

We compute the amplitude in the low temperature regime, for fixed driving amplitude and varying damping strengths by solving Eq. (3.103) for the one-photon resonance $E_{0,0} = E_{1,1}$. Depending on the actual value of the damping, introduced by the bath, either an antiresonant behaviour, at small damping, or a resonant one, at large damping, is observed. The resonant/ antiresonant lineshape depends on the ratio of damping and minimal splitting: $\hbar\sqrt{2}\gamma / \left[1 - \frac{3y_0^4}{8\hbar\Omega}\alpha\right] F y_0$. In case of high damping, the amplitude is very small and broad showing resonant behaviour, where the asymmetry is smeared out completely. If we decrease the damping, the amplitude increases and the width shrinks until we reach a critical value for the damping. This critical value occurs when damping and minimal splitting are almost equal. Lowering the damping below the critical value, a cusp-like profile arises: the antiresonance. The treatment of higher orders in the driving and the interplay of driving and nonlinearity introduce additionally an asymmetry in the response with respect to $\omega_{ex} = \Omega + \frac{3}{4\hbar}\alpha y_0^4$. For very large damping we observe the corresponding linear response (LR) of a linear oscillator with eigenfrequency $\Omega + \frac{3}{4\hbar}\alpha y_0^4$, indicated by the black dashed line in Fig. 3.4. So we can make the connection to the linear response of a driven damped harmonic oscillator, which is resonant at the frequency $\omega_{ex} = \Omega + \frac{3}{4\hbar}\alpha y_0^4$, if considering first order perturbation theory in the nonlinearity.

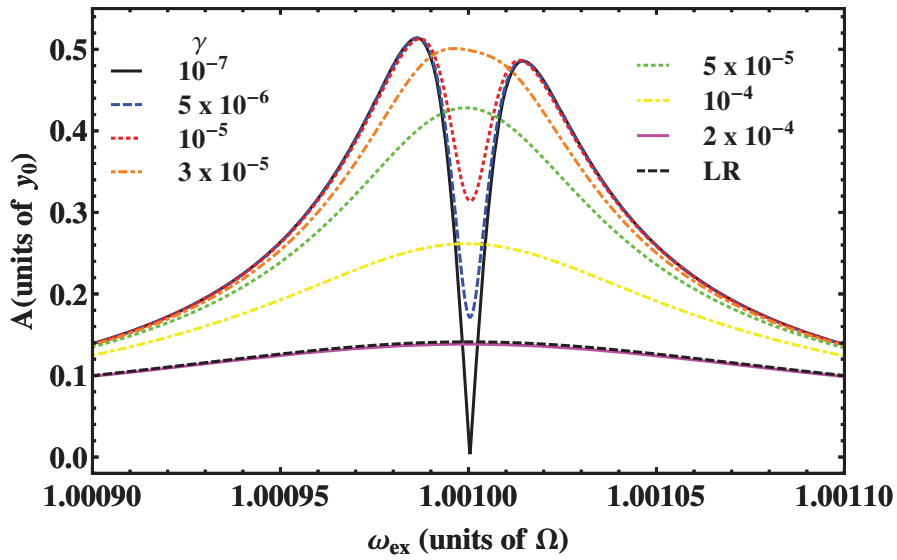

Figure 3.4: *Amplitude A versus driving frequency at low temperature $k_B T/(\hbar\Omega) = 10^{-3}$ for different damping strengths γ. For the rest of the parameters we take $y_0^4\alpha/(\hbar\Omega) = 4/3 \cdot 10^{-3}$, $y_0 F/(\hbar\Omega) = 2^{3/2} \cdot 10^{-5}$, $\Omega = 1$ and varying damping: $\gamma/\Omega = 10^{-7}, 5\cdot 10^{-6}, 1\cdot 10^{-5}, 3\cdot 10^{-5}, 5\cdot 10^{-5}, 1\cdot 10^{-4}, 2\cdot 10^{-4}$.*

3.7.3 Phase

The phase for the one-photon resonance is given in Fig. 3.5. It jumps by π at the one-photon resonance and the step becomes smoother the larger the damping is.

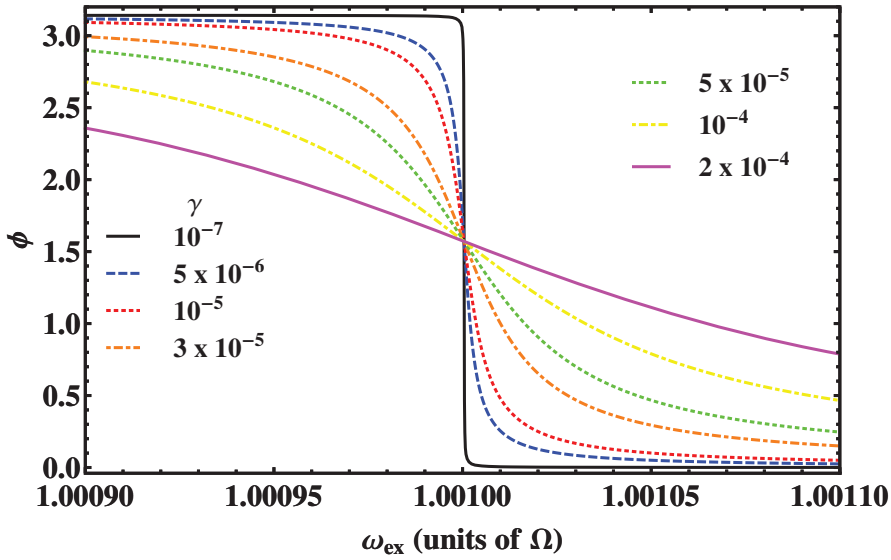

Figure 3.5: *Phase ϕ versus driving frequency at low temperature $k_BT/(\hbar\Omega) = 10^{-3}$ for different damping strengths γ. For the rest of the parameters we take $y_0^4\alpha/(\hbar\Omega) = 4/3 \cdot 10^{-3}$, $y_0F/(\hbar\Omega) = 2^{3/2} \cdot 10^{-5}$, $\Omega = 1$ and varying damping: $\gamma/\Omega = 10^{-7}, 5 \cdot 10^{-6}, 1 \cdot 10^{-5}, 3 \cdot 10^{-5}, 5 \cdot 10^{-5}, 1 \cdot 10^{-4}, 2 \cdot 10^{-4}$.*

3.8 Off-resonant approach based on the dissipative driven harmonic oscillator

As the driven harmonic oscillator is exactly solvable we use it in the following in order to first specify the differences to the corresponding undriven case, and second to show that the quantum treatment of the dissipative system is much more involved than the solution of the corresponding classical system. We show in Appendix B that treating the driven harmonic oscillator within a rotating wave approximation does not give the correct results. Then we present, based on the exact solution, how to account for dissipation in the quantum case. In a second step we extend the derivation for the dissipative linear oscillator to the nonlinear case.

3.8.1 The steady-state dynamics for the dissipative driven harmonic oscillator

Before starting we want to make a short excursion: As the quantum Duffing oscillator has mainly be considered within a rotating wave approximation (RWA) directly applied to the Hamiltonian, we consider the effect of this approximation on the underlying linear system, the driven harmonic oscillator. For completeness and for the comparison with RWA directly applied to the driven harmonic oscillator Hamiltonian, shown in Appendix B, we give the result for the matrix element $y_{lk}(t)$, based on the exact Floquet states:

$$\begin{aligned} y_{lk}(t) &= \langle\psi_l(t)|\hat{y}|\psi_k(t)\rangle \\ &= \sum_{y',y''}\langle\psi_l(t)|y'\rangle\langle y'|\hat{y}|y''\rangle\langle y''|\psi_k(t)\rangle \\ &= \exp(-i\Omega t(k-l))\int_{-\infty}^{\infty} dy\overline{\phi}_l(y-\xi(t))y\overline{\phi}_k(y-\xi(t)) \\ &= \frac{y_0}{\sqrt{2}}\left[\sqrt{l}\delta_{l,k+1}\exp(i\Omega t)+\sqrt{k}\delta_{l,k-1}\exp(-i\Omega t)+\right]+\xi(t)\delta_{lk}. \end{aligned} \tag{3.108}$$

This result is obtained in the ψ-basis and compared with results obtained in the RWA approach, see Eq. (B.8). A detailed derivation together with the corresponding equations is given in Appendix B. The main results are the following: first we obtain a different time-dependence for the undriven contributions in the RWA treatment, as they are no more slowly oscillating. Second the weights for the driven terms in the RWA approach are only proportional to $\omega_{ex}-\Omega$ and not to $\omega_{ex}^2-\Omega^2$, which is essential for making the proper connection to the classical case. Moreover, as a certain resonance condition involving only two levels, as in the nonlinear oscillator case, cannot be chosen due to the equidistant energy spectrum of the linear oscillator a different procedure is elaborated below. For the above reasons and the fact that an exact solution is available we focus in the following on the solution of the master equation using the exact expressions obtained for the driven harmonic oscillator.

The solution of the dissipative dynamics of a driven harmonic oscillator is based on this observation: In the regime where the driving frequency is in the vicinity of the eigenfrequency of the oscillator we observe resonant excitation, leading in the dissipation-free case to the so-called resonance catastrophe. This results in the fact that the system can no more be truncated, such that infinitely many oscillator levels have to be taken into account. Therefore to account for the dissipative dynamics we have to solve the full problem, which corresponds to do a summation over the infinite Hilbert space. Usually this is a very nasty task. However, in the special case of a driven harmonic oscillator, the master equation containing infinitely many levels can be solved analytically. This fact is very crucial and is directly related to the very special properties of the equidistant energy spectrum and the fact that there are analytical results for infinite sums containing the Laguerre-Polynomials weighted with Gaussians.

As the Floquet states $|\psi_l(t)\rangle$ of the undamped system solve the Schrödinger equation, the master equation can be simplified as follows. Expressing the density matrix in the

ψ-basis, the part containing the free dynamics, see the first term in Eq. (3.92), drops out compared to the representation in the ϕ-basis, so that the master equation reduces to:

$$\begin{aligned}\dot{\rho}_{lk}(t) &= \sum_{l'k'} \mathcal{L}_{lk,l'k'}\rho_{l'k'}(t) \qquad (3.109)\\ &= \sum_{l'k'}\sum_{nn'} \exp[-i\omega_{ex}(n+n')t] \\ &\quad \Big\{\exp[i(\epsilon_l-\epsilon_k-\epsilon_{l'}+\epsilon_{k'})t/\hbar](N_{ll',-n}+N_{kk',n'})y^{(n)}_{ll'}y^{(n')}_{k',k}\rho_{l'k'} \\ &\quad -\exp[i(\epsilon_l-\epsilon_{l'})t/\hbar]N_{k'l',-n}y^{(n')}_{l'k'}y^{(n)}_{k',l'}\rho_{l'k} \\ &\quad -\exp[i(\epsilon_{k'}-\epsilon_k)t/\hbar]N_{l'k',n'}y^{(n)}_{l'k}y^{(n')}_{k',l'}\rho_{lk'}\Big\},\end{aligned}$$

where $\rho_{lk}(t) = \langle\psi_l(t)|\hat{\rho}|\psi_k(t)\rangle$. To solve this master equation a rotating wave approximation is applied. Usually the RWA consists of neglecting fast oscillating terms, where $\{l,k,n\} \neq \{l',k',n'\}$. However, this argument holds only for systems without degeneracies or quasidegeneracies. For the linear oscillator with its equidistant energy spectrum, additional terms have to be taken into account: $\{l-k,n\} \neq \{l'-k',n'\}$, resulting in two possibilities: First $\Omega \ll \omega_{ex}$ or $\Omega \gg \omega_{ex}$, i.e., both frequencies deviate strongly from each other, such that we can treat them independently in a rotating wave approximation: $l-k = l'-k'$ and $n = n'$. Second if the driving frequency is close to the oscillator resonance frequency $\Omega \sim \omega_{ex}$ we cannot treat these two frequencies independently and have therefore to account for additional terms: $(l-k-l'+k')\Omega \cong (n-n')\omega_{ex}$. To obtain the master equation we insert the actual form of $y^{(n)}_{lk}$ in Eq. (3.109) and apply a rotating wave approximation, by neglecting rapidly oscillating terms ($\exp(2i\Omega t)$ or $\exp(\pm(\Omega + k\omega_{ex}))$, $k \geq 0$). Hence the remaining terms can maximally oscillate with $\exp(\pm i(\Omega - k\omega_{ex}))$, $k \geq 0$, which corresponds to take into account the resonant driving of the oscillator. Note that at this level, i.e. without dissipation, an exact resonance must be avoided, such that $\xi(t)$ does not diverge [145]. The master equation reduces then to:

$$\begin{aligned}\dot{\rho}_{lk}(t) &= \frac{y_0^2}{2\hbar}\Big\{J(|\Omega|)[n_{th}(|\Omega|)+1][-(l+k)\rho_{lk}+2\sqrt{(l+1)(k+1)}\rho_{l+1,k+1}] \qquad (3.110)\\ &\quad +n_{th}(|\Omega|)[(-l-k-2)\rho_{lk}+2\sqrt{lk}\rho_{l-1,k-1}]\Big\} \\ &\quad +\frac{y_0^2}{2\hbar}\exp(i\Omega t)\exp(-i\omega_{ex}t)\frac{F\sqrt{2}}{2y_0M(\Omega^2-\omega_{ex}^2)}J(|\omega_{ex}|)\left[\sqrt{l+1}\rho_{l+1,k}-\sqrt{k}\rho_{l,k-1}\right] \\ &\quad +\frac{y_0^2}{2\hbar}\exp(-i\Omega t)\exp(i\omega_{ex}t)\frac{F\sqrt{2}}{2y_0M(\Omega^2-\omega_{ex}^2)}J(|\omega_{ex}|)\left[\sqrt{k+1}\rho_{l,k+1}-\sqrt{l}\rho_{l-1,k}\right],\end{aligned}$$

where

$$\begin{aligned}J(|\omega|) &= M\gamma\omega, \qquad (3.111)\\ \frac{y_0^2}{2\hbar}J(|\omega_{ex}|) &= \frac{\gamma}{2}|\omega_{ex}|/\Omega.\end{aligned}$$

Interestingly all higher contributions in the driving amplitude F vanish from the second order on in the master equation. The solution for the above master equation has been derived in [145]:

$$\begin{aligned}
\rho_{lk}(t) &= \exp[-i(\epsilon_k-\epsilon_l)t/\hbar]\sqrt{\frac{k!}{l!}}\frac{\sigma^k}{(\sigma+1)^{l+1}}\exp(-|A(t)|^2/(\sigma+1)) \\
&\quad A(t)^{l-k}L_k^{l-k}\left(-\frac{|A(t)|^2}{\sigma(\sigma+1)}\right), \quad \text{if } l\geq k \qquad (3.112a)\\
A(t) &= a_0\exp(-i\Omega t-\gamma t/2)+\left[\gamma_1(a_{\mathrm{st},1}-a^0_{\mathrm{st},1})+\gamma_{-1}(a^*_{\mathrm{st},-1}-a^{0*}_{\mathrm{st},-1})\right] \\
&\quad \exp(-i\omega_{ex}t), \qquad (3.112b)\\
\sigma &= n_{th}(1-\exp(-\gamma t)), \qquad (3.112c)
\end{aligned}$$

where

$$\begin{aligned}
\gamma_1 &= \gamma_{-1}=|\omega_{ex}|/\Omega, \\
a_{\mathrm{st},\pm 1} &= \frac{-F}{2\sqrt{2}y_0M\Omega}\frac{1}{\Omega\mp\omega_{ex}-i\gamma/2}. \qquad (3.113)
\end{aligned}$$

Note that: $\xi(t)=\frac{y_0}{\sqrt{2}}\left[a^0_{\mathrm{st}}+a^{0*}_{\mathrm{st}}\right]$ and $a_{\mathrm{st}}=\sum_k a_{\mathrm{st},k}\exp(-ik\omega_{ex}t)=a_{\mathrm{st},+1}\exp(-i\omega_{ex}t)+a_{\mathrm{st},-1}\exp(+i\omega_{ex}t)$. Here we already evaluated the formulas given by Graham [145] for a cosine-like driving term, allowing to take only the Fourier components associated to $k=\pm 1$. $A(t)$ denotes the classical complex trajectory. As in the case of the derivation of the quasienergies and Floquet states of the driven harmonic oscillator, the master equation can be solved in terms of classical quantities, namely the solution of the classical equation of motion.
The steady-state dynamics for the driven harmonic oscillator is obtained as:

$$\begin{aligned}
y_{\mathrm{st}}(t) &= \lim_{t\to\infty}\langle\hat{y}\rangle=\lim_{t\to\infty}\sum_{lk}\rho_{lk}(t)y_{kl}(t) \qquad (3.114)\\
&\equiv \sum_{lk}\rho^{\mathrm{st}}_{lk}\frac{y_0}{\sqrt{2}}\left[\sqrt{k}\exp(i\Omega t)\delta_{k,l+1}+\sqrt{l}\exp(-i\Omega t)\delta_{k,l-1}+\frac{\sqrt{2}\xi(t)}{y_0}\delta_{lk}\right] \\
&= \sum_{l}\frac{y_0}{\sqrt{2}}\left[\sqrt{k}\exp(i\Omega t)\rho^{\mathrm{st}}_{l,l+1}+\sqrt{l}\exp(-i\Omega t)\rho^{\mathrm{st}}_{l,l-1}+\frac{\sqrt{2}\xi(t)}{y_0}\rho^{\mathrm{st}}_{ll}\right] \\
&= \sum_{l}\frac{y_0}{\sqrt{2}}\left[\frac{n^l_{th}}{(n_{th}+1)^{l+2}}\exp(-|A_{\mathrm{st}}(t)|^2/(n_{th}+1))A^*_{\mathrm{st}}(t)L^1_l\left(-\frac{|A_{\mathrm{st}}(t)|^2}{n_{th}(n_{th}+1)}\right)\right. \\
&\quad +A_{\mathrm{st}}(t)\exp(-|A_{\mathrm{st}}(t)|^2/(n_{th}+1))\frac{n^{l-1}_{th}}{(n_{th}+1)^{l+1}}L^1_{l-1}\left(-\frac{|A_{\mathrm{st}}(t)|^2}{n_{th}(n_{th}+1)}\right) \\
&\quad \left.+\frac{n^l_{th}}{(n_{th}+1)^{l+1}}\exp(-|A_{\mathrm{st}}(t)|^2/(n_{th}+1))L^0_{l-1}\left(-\frac{|A_{\mathrm{st}}(t)|^2}{n_{th}(n_{th}+1)}\right)\frac{\xi(t)\sqrt{2}}{y_0}\right],
\end{aligned}$$

where $A_{\mathrm{st}}=\lim_{t\to\infty}A(t)$. Then we use the sum rule [146]:

$$\sum_{n=0}^{\infty}L^a_n(x)z^n = (1-z)^{-a-1}\exp\left(\frac{xz}{z-1}\right), \quad |z|<1. \qquad (3.115)$$

This formula is used to evaluate the three different sums; the first is given here explicitly, while the calculation for the other two is similar:

$$\begin{aligned}
&\sum_l \frac{n_{th}^{l-1}}{(n_{th}+1)^{l+1}} L_{l-1}^1\left(-\frac{|A_{\rm st}(t)|^2}{n_{th}(n_{th}+1)}\right) \qquad (3.116)\\
&\quad = \sum_l \frac{1}{n_{th}+1}\left(\underbrace{\frac{n_{th}}{n_{th}+1}}_{z}\right) L_l^0\left(\underbrace{-\frac{|A_{\rm st}(t)|^2}{n_{th}(n_{th}+1)}}_{x}\right)\\
&\quad = \frac{1}{n_{th}+1-n_{th}} \exp\left(\frac{|A_{\rm st}(t)|^2 n_{th}}{n_{th}(n_{th}+1)}\right)\\
&\quad = \exp\left(\frac{|A_{\rm st}(t)|^2}{n_{th}+1}\right).
\end{aligned}$$

The other summations are also proportional to this exponential factor, so that the summation over all oscillator states cancels exactly with the exponential prefactor in Eq. (3.114). Consequently, we obtain a temperature independent steady-state solution for the harmonic oscillator:

$$\begin{aligned}
y_{\rm st}(t) &= \frac{y_0}{\sqrt{2}}\left[A_{\rm st}(t) + A_{\rm st}^* + \frac{\sqrt{2}}{y_0}\xi(t)\right] \qquad (3.117)\\
&= \frac{y_0}{\sqrt{2}}\Big[\big[\gamma_1(a_{{\rm st},1} - a_{{\rm st},1}^0) + \gamma_{-1}(a_{{\rm st},-1}^* - a_{{\rm st},-1}^{*0})\big]\exp(-i\omega_{ex}t)\\
&\quad + \big[\gamma_1^*(a_{{\rm st},1}^* - a_{{\rm st},1}^{0*}) + \gamma_{-1}^*(a_{{\rm st},-1} - a_{{\rm st},-1}^0)\big]\exp(+i\omega_{ex}t) + \frac{\sqrt{2}\xi(t)}{y_0}\Big]\\
&\cong \frac{y_0}{\sqrt{2}}\sum_{k=\pm1}\big[a_{{\rm st},k}\exp(-ik\omega_{ex}t) + a_{{\rm st},-k}^*\exp(+ik\omega_{ex}t)\big]\\
&\quad \underbrace{-\frac{y_0}{\sqrt{2}}\left(a_{\rm st}^0 + a_{\rm st}^{0*}\right) + \xi(t)}_{=0}.
\end{aligned}$$

The undamped steady-state terms drop out exactly if $\gamma_k = 1$. However, in our case $\gamma_k = |\omega_{ex}|/\Omega$, which is not exactly 1. Therefore this cancellation is not exact. However, we required for the application of the rotating wave approximation that the driving frequency is in the vicinity of the eigenfrequency Ω, such that this cancellation is approximately fulfilled. Note that the solution of the classical equation of motion does not at all require to treat the resonance regime of the oscillator. The explicit form for

the steady-state of the driven quantum harmonic oscillator is:

$$\begin{aligned} y_{\rm st}(t) &= \frac{y_0}{\sqrt{2}}\left(\frac{-F}{2\sqrt{2}y_0 M\Omega}\right)\left[2\cos(\omega_{ex}t)\left(\frac{\Omega-\omega_{ex}}{(\Omega-\omega_{ex})^2+\frac{\gamma^2}{4}}+\frac{\Omega+\omega_{ex}}{(\Omega+\omega_{ex})^2+\frac{\gamma^2}{4}}\right)\right. \\ &\quad \left.+2\sin(\omega_{ex}t)\left(\frac{\gamma/2}{(\Omega-\omega_{ex})^2+\frac{\gamma^2}{4}}-\frac{\gamma/2}{(\Omega+\omega_{ex})^2+\frac{\gamma^2}{4}}\right)\right] \\ &= -\frac{F}{M}\left[\cos(\omega_{ex}t)\frac{\gamma^2/4+(\Omega^2-\omega_{ex}^2)}{[(\Omega-\omega_{ex})^2+\frac{\gamma^2}{4}][(\Omega+\omega_{ex})^2+\frac{\gamma^2}{4}]}\right. \\ &\quad \left.+\sin(\omega_{ex}t)\frac{\gamma\omega_{ex}}{[(\Omega-\omega_{ex})^2+\frac{\gamma^2}{4}][(\Omega+\omega_{ex})^2+\frac{\gamma^2}{4}]}\right] \\ &\equiv -\frac{F}{M\sqrt{[(\Omega-\omega_{ex})^2+\frac{\gamma^2}{4}][(\Omega+\omega_{ex})^2+\frac{\gamma^2}{4}]}}[\cos(\omega_{ex}t)\cos\phi_0 \\ &\quad -\sin(\omega_{ex}t)\sin\phi_0] \\ &= -\frac{F}{M\sqrt{[(\Omega-\omega_{ex})^2+\frac{\gamma^2}{4}][(\Omega+\omega_{ex})^2+\frac{\gamma^2}{4}]}}\cos(\omega_{ex}t+\phi_0), \end{aligned} \tag{3.118}$$

where

$$\tan\phi_0 = -\frac{\gamma\omega_{ex}}{(\gamma^2/4+(\Omega^2-\omega_{ex}^2))}. \tag{3.119}$$

Within the derivation of Graham [145] a small energy shift has been neglected assuming weak damping: $\gamma/\Omega \ll 1$. Therefore in the master equation the shifted frequency $\sqrt{\Omega^2-\gamma^2/4}$ is replaced by Ω. Inverting this replacement for the steady-state solution of the position operator in the quantum harmonic oscillator, we obtain exactly the same result as in the steady-state of the corresponding classical system, given in Eqs. (1.3) and (1.4).

3.8.2 Extension to the nonlinear quantum Duffing oscillator

As the driven harmonic oscillator is solved in this elegant form, we extend this procedure to the nonlinear case using App I, whose states and energies are based on a perturbative expansion using the exact Floquet energies and states of the driven

harmonic oscillator. The matrix element entering the rates is:

$$\begin{aligned} y_{lk}(t) &= \langle\psi_l(t)|\hat{y}|\psi_k(t)\rangle \qquad (3.120)\\ &= \frac{y_0}{\sqrt{2}}\exp[-i(\epsilon_k-\epsilon_l)t/\hbar]\left\{\left[\sqrt{l}\delta_{l,k+1}+\sqrt{k}\delta_{l,k-1}+\frac{\sqrt{2}}{y_0}\xi(t)\delta_{lk}\right]\times\right.\\ &\quad [1+c^*_{ll}(t)+c_{kk}(t)]\\ &\quad +\sum_{k\neq r}\left[\sqrt{l}\delta_{l,r+1}+\sqrt{r}\delta_{l,r-1}+\frac{\sqrt{2}}{y_0}\xi(t)\delta_{l,r}\right]c_{rk}(t)\\ &\quad \left.+\sum_{l\neq s}\left[\sqrt{s}\delta_{s,k+1}+\sqrt{k}\delta_{s,k-1}+\frac{\sqrt{2}}{y_0}\xi(t)\delta_{k,s}\right]c^*_{sl}(t)\right\}+\mathcal{O}(\alpha^2), \end{aligned}$$

where $c_{jk}(t)=\sum_{n=0}^{\infty}c^{(n)}_{jk}\exp(-in\omega_{ex}t)$. The expression Eq. (3.120) has only been evaluated up to first order in the nonlinearity. As in the linear case we rewrite it in terms of a Fourier expansion:

$$y_{lk}(t) = \exp[-i(\epsilon_k-\epsilon_l)t/\hbar]\sum_n\exp(-in\omega_{ex}t)y^{(n)}_{lk}, \qquad (3.121)$$

where

$$\begin{aligned} y^{(n)}_{lk} &= \frac{y_0}{\sqrt{2}}\left\{\sqrt{l}\delta_{l,k+1}\delta_{n,0}+\sqrt{k}\delta_{l,k-1}\delta_{n,0}+\lambda\delta_{n,1}\delta_{lk}+\lambda\delta_{n,-1}\delta_{lk}\right. \qquad (3.122)\\ &\quad \left[\sqrt{l}\delta_{l,k+1}+\sqrt{k}\delta_{l,k-1}\right][c^{(n)}_{kk}+c^{(-n)}_{ll}]\\ &\quad +\lambda\delta_{lk}\left[c^{(n-1)}_{kk}+c^{(-n-1)}_{ll}+c^{(n+1)}_{kk}+c^{(-n+1)}_{ll}\right]\\ &\quad +\sum_{k\neq r}\left[\sqrt{l}\delta_{l,r+1}+\sqrt{r}\delta_{l,r-1}\right]c^{(n)}_{rk}+\sum_{k\neq r}\lambda\left[c^{(n-1)}_{rk}+c^{(n+1)}_{rk}\right]\delta_{lr}\\ &\quad \left.+\sum_{l\neq s}\left[\sqrt{s}\delta_{s,k+1}+\sqrt{k}\delta_{s,k-1}\right]c^{(-n)}_{sl}+\sum_{l\neq s}\lambda\delta_{sk}\left[c^{(-n-1)}_{sl}+c^{(-n+1)}_{sl}\right]\right\}, \end{aligned}$$

and $\lambda=\frac{F\sqrt{2}}{2y_0M(\omega^2_{ex}-\Omega^2)}$. In contrast to the linear case $y^{(n)}_{lk}$ contains up to first order in the nonlinearity twenty terms and not only the three known from the linear case. Consequently, we obtain 144 possible combinations $y^{(n)}_{lk}y^{(n')}_{sr}$ entering each of the four contributions to the rate $\mathcal{L}$. Hence the master equation for the nonlinear driven oscillator up to first order in the nonlinearity consists of 576 terms. The nonlinearity enters either via the quasienergies in the exponential prefactor or as direct prefactor of the density matrix. Note that we avoid to expand the exponential containing the nonlinear quasienergies. As we have seen in the considerations for the driven linear harmonic oscillator, we have to take into account all contributions within the rotating wave approximation introduced by Graham. We use first that at least one Fourier index is already determined by the linear oscillator case, as always one factor of $y^{(n)}_{lk}y^{(n')}_{sr}$ is of zeroth and one of first order in the nonlinearity, such that their combination is

also at most of first order in the nonlinearity. Second, we recognize that the actual form of $y_{lk}^{(n)}$ restricts the possible combinations of l and k, determining in this way the quasienergy difference. A combination of both allows to choose the indices such that we obtain a minimal oscillation, resulting in:

$$\begin{aligned}
\dot{\rho}_{lk} = \frac{y_0^2}{2} \qquad & (3.123)\\
&\Big\{\rho_{lk}\Big[-(k+1)N\left(\hbar\Omega+\frac{3}{4}\alpha y_0^4[1+k]+A_\xi^2\frac{3}{4}\alpha y_0^2\right)-lN\left(-\hbar\Omega-\frac{3}{4}\alpha y_0^4 l-A_\xi^2\frac{3}{4}\alpha y_0^2\right)\\
&-(l+1)N\left(\hbar\Omega+\frac{3}{4}\alpha y_0^4[1+l]+A_\xi^2\frac{3}{4}\alpha y_0^2\right)-kN\left(-\hbar\Omega-\frac{3}{4}\alpha y_0^4 k-A_\xi^2\frac{3}{4}\alpha y_0^2\right)\Big]\\
&+\rho_{l+1,k+1}\exp(it\frac{3}{4}\alpha y_0^4[1+k-l]/\hbar)\sqrt{(l+1)(k+1)}\Big[N\left(-\hbar\Omega-\frac{3}{4}\alpha y_0^4 l-A_\xi^2\frac{3}{4}\alpha y_0^2\right)\\
&+N\left(-\hbar\Omega-\frac{3}{4}\alpha y_0^4 k-A_\xi^2\frac{3}{4}\alpha y_0^2\right)\Big]\\
&+\rho_{l-1,k-1}\exp(it\frac{3}{4}\alpha y_0^4[1+l-k]/\hbar)\sqrt{lk}\Big[N\left(\hbar\Omega+\frac{3}{4}\alpha y_0^4(l+1)+A_\xi^2\frac{3}{4}\alpha y_0^2\right)\\
&+N\left(\hbar\Omega+\frac{3}{4}\alpha y_0^4(k+1)+A_\xi^2\frac{3}{4}\alpha y_0^2\right)\Big]\\
&+J(|\omega_{ex}|)\exp(i\omega_{ex}t)\frac{F\sqrt{2}}{\hbar y_0 2M(\omega_{ex}^2-\Omega^2)}\Big[-\exp(it[-\hbar\Omega-\frac{3}{4}\alpha y_0^4 k-A_\xi^2\frac{3}{4}\alpha y_0^2]/\hbar)\sqrt{k}\rho_{l,k-1}\\
&+\sqrt{l+1}\exp(it[-\hbar\Omega-\frac{3}{4}\alpha y_0^4 l-A_\xi^2\frac{3}{4}\alpha y_0^2]/\hbar)\rho_{l+1,k}\Big]\\
&+J(|\omega_{ex}|)\exp(-i\omega_{ex}t)\frac{F\sqrt{2}}{\hbar y_0 2M(\omega_{ex}^2-\Omega^2)}\Big[\exp(it[\hbar\Omega+\frac{3}{4}\alpha y_0^4(k+1)\\
&+A_\xi^2\frac{3}{4}\alpha y_0^2]/\hbar)\sqrt{k+1}\rho_{l,k+1}\\
&-\sqrt{l}\exp(it[\hbar\Omega+\frac{3}{4}\alpha y_0^4(l+1)+A_\xi^2\frac{3}{4}\alpha y_0^2]/\hbar)\rho_{l-1,k}\Big]\Big\}+\ldots \quad .
\end{aligned}$$

In the last equation we disregarded the contributions coming from the modification of the states due to the nonlinearity, i.e., we neglect terms proportional to $c_{jk}(t)$ and consider only modifications due to the nonlinear quasienergies. The reason is, that although the resulting master equation including these terms can be calculated, it is very hard to find an analytical solution as in the linear case, as the resulting master equation still contains a lot of terms. Moreover, in contrast to the linear case, where only $\rho_{l,k}$, $\rho_{l+1,k}$, $\rho_{l,k+1}$, $\rho_{l-1,k-1}$, $\rho_{l+1,k+1}$ and $\rho_{l-1,k-1}$ occurred, in the nonlinear case including the modifications to the states much more combinations are possible, for example terms with $\rho_{l+x_1,k+x_2}$ where $|x_1 - x_2| = 0, 1, 2, 3$. Additionally, the master equation contains now $\lambda^2\alpha$ terms, such that also higher orders of the driving occur in the master equation, while in the linear case, as seen in Eq. (3.110), all the orders proportional to F^2 cancel exactly. This cancellation for the linear case is based on the fact that we have a linear perturbation for the harmonic oscillator, which can be diagonalized exactly. As we want to reproduce the underlying linear case at any step of our calculation, we are not allowed to truncate the possible os-

cillator levels, but we have really to perform the summation over all oscillator levels as in the linear case. As this is a very hard task, we look at least for an analytical solution for the part of master equation, given in Eq. (3.123), where only nonlinear effects in the quasienergies have been taken into account. Therefore we compare the two master equations for the linear and nonlinear case, Eqs. (3.110) and (3.123), and observe that first the rates become level dependent due to the nonlinearity and can therefore no more be combined to give a global prefactor as in the linear case. For example the term $\rho_{l+1,k+1}$ changes due to the nonlinearity according to: $2J(|\Omega|)n_{th}(|\Omega|) \rightarrow N\left(-\hbar\Omega - \frac{3}{4}\alpha y_0^4 l - A_\xi^2 \frac{3}{4}\alpha y_0^2\right) + N(-\hbar\Omega - \frac{3}{4}\alpha y_0^4 k - A_\xi^2 \frac{3}{4}\alpha y_0^2)$. Second we want to point out that the level dependence due to the nonlinear non-equidistant energy spectrum is also seen in the remaining oscillating contributions. While in the linear case the undriven part of the master equation was showing no oscillation, the nonlinearity gives rise to a weak level-dependent oscillation.
To find an analytical solution, we first have to understand the derivation of the corresponding linear case. As shown in the appendix of Ref. [145], the easiest way is to start using the solution and take its derivative with respect to time to determine the master equation. This allows to show how the time-dependent complex trajectory enters the master equation and how the temperature-dependence is embedded. To show that the solution (3.112a) solves the master equation (3.110) we have to use the following conditions:

$$\frac{\partial}{\partial t}\sigma(t) = \gamma(n_{th} - \sigma(t)), \tag{3.124a}$$

$$\frac{\partial}{\partial t}A(t) = -\left(i\Omega + \frac{\gamma}{2}\right)A(t) - \frac{\gamma}{2}\Gamma(t), \tag{3.124b}$$

where $A(t)$ is given in Eq. (3.112b) and

$$\Gamma(t) = [\gamma_1 a^0_{\mathrm{st},1} + \gamma_{-1} a^{0*}_{\mathrm{st},-1}] \exp(-i\omega_{ex} t). \tag{3.125}$$

To derive the master equation of the form given in Eq. (3.110), we need moreover the relations:

$$\frac{d}{dx}L_n^a(x) = -L_{n-1}^{a+1}(x), \tag{3.126}$$

$$L_n^{a-1} = L_n^a(x) - L_{n-1}^a(x), \tag{3.127}$$

$$x\frac{d}{dx}L_n^a(x) = nL_n^a(x) - (n+a)L_{n-1}^a(x). \tag{3.128}$$

To solve the nonlinear master equation we have to account for the nonlinearity-induced level dependence. This could be achieved by replacing the linear quasienergies by their corresponding nonlinear ones. Moreover to solve the linear case it is essential that Eqs. (3.124a) and (3.124b) are fulfilled. The easiest ansatz is to use a superposition:

$$\sigma(t) = \sigma(t, \Delta\epsilon_l) + \sigma(t, \Delta\epsilon_k), \tag{3.129}$$

where

$$\sigma(t,\Delta\epsilon_l) \equiv n_{th}(\Delta\epsilon_l)[1-\exp(-\gamma(\Delta\epsilon_l)t)] \tag{3.130}$$

$$\gamma = \frac{1}{2}\left[\gamma(\Delta\epsilon_l)+\gamma(\Delta\epsilon_k)\right], \tag{3.131}$$

$$\gamma(\Delta\epsilon_l) = \frac{J(|\Delta\epsilon_l|)}{M\hbar\Omega}. \tag{3.132}$$

Unfortunately, using the superposition does not allow to rewrite the result due to the level dependence into the form given by Graham. In the master equation this kind of superposition results in additional admixtures described in the following: The nonlinear master equation contains only certain combinations: the level-dependence of the normalization factor is related to the one occurring in the rate, i.e., $(l+1)N(\hbar\Omega+3\alpha y_0^4(l+1)/4+3A_\xi^2 y_0^2/4)$. Imposing the superposition, we obtain terms in the master equation where the level dependent normalization factors are weighted with rates depending on both levels l and k. Additional modifications using a weighted superposition $\sigma(t)=c_1\sigma(t,\Delta\epsilon_l)+c_2\sigma(t,\Delta\epsilon_k)$, with coefficients chosen to fulfill the nonlinear master equation, have not been successful.

3.9 Conclusions

In the first part of this chapter we have discussed two perturbative approaches, App I and App II, to calculate the Floquet quasienergies and states of the quantum Duffing oscillator beyond a RWA approach. Additionally, the stationary dynamics of the expectation value of the oscillator position was obtained. Specifically, analytical results where derived *off* and near resonance with App I and *at* the one-photon resonance within App II. For App II, based on Van Vleck perturbation theory, we also assumed that the driving is much weaker than the nonlinearity. We showed that in the parameter regime near resonance the Van Vleck approach recovers the results of App I based on the exact Floquet states of the driven linear oscillator, for both the eigenfrequencies in second order in the driving strength F and the matrix elements of the position operator in the Floquet basis to first order in F. The comparison allows to treat the quantum Duffing oscillator for a wide range of frequencies near and at the one-photon resonance. Our approach, however, also applies nearby a generic N-photon resonance.

As an application of our formalism we considered the dynamics of a quantum Duffing oscillator coupled to an Ohmic bath and calculated its response near a one-photon resonance. Dissipative effects strongly affect the behaviour of the Duffing oscillator in the resonance region. In agreement with [18] we observe upon variation of the damping strength a transition from antiresonant to resonant behaviour and that the shape of the antiresonance with respect to the one-photon resonance condition is asymmetric.

In the second part of this chapter we investigated the dissipative dynamics of a quantum Duffing oscillator using the App I based on the driven harmonic oscillator. We

want to point out that the properties of the driven harmonic oscillator, for example the equidistant energy spectrum, allow the construction of the solution of a master equation containing all orders in the driving. Within the construction of the solution, these properties allow for large simplifications, as the quasienergy differences, occurring both in the rates and in the phase factors entering the master equation, are level independent. As this very generic behaviour is absent in the nonlinear case, the underlying solution for the harmonic oscillator can no more be used or has to be strongly modified. Consequently, a full solution including all oscillator levels has to be found for the nonlinear case. Whether this is possible at all, as the nonlinearity enters in a special nontrivial way, remains an open question, because already the solution of the master equation for the driven linear system is quite complicated and requires some analytical effort.

Chapter 4

Qubit-nonlinear oscillator system coupled to an Ohmic bath

The results presented here have been published in [21].

In this chapter the dissipative dynamics of a qubit coupled to a nonlinear oscillator (NLO) embedded in an Ohmic environment is investigated. We study the SQUID as a nonlinear, undriven oscillator acting as a read-out device for a qubit. We consider weak nonlinearities such that the corresponding linear system can be retained at any step of our calculation. With the help of Van Vleck perturbation theory in the TLS-oscillator coupling $\overline{g}$ we determine the eigenstates and spectrum of the coupled system and the corresponding dynamics in analytic form. Thus we can quantitatively characterize the influence of the coupling $\overline{g}$ and of the nonlinearity on the dynamics of the composed system. The overall effects of the nonlinearity are the following: (i) a shift of the transition frequencies to higher values compared to the linear case; (ii) the amplitudes associated to the transition frequencies are modified. In particular the vacuum Rabi splitting is decreased by the interplay of coupling and nonlinearity. To account for dissipative effects we add a weak Ohmic environment. Then the dynamics of the reduced density matrix of the composed system can be described in terms of a set of coupled differential equations for its matrix elements in the energy basis (Bloch-Redfield equations). We discuss a partial secular approximation (PSA) to those equations as well as two more stringent approximations, the full secular approximation in the low temperature approximation (LTA) and the smallest eigenvalue approximation (SEA) accounting for the long time dynamics. All these three approximation schemes allow for an analytical solution of the dynamics of the TLS, which we compare with predictions obtained by numerically solving the Bloch-Redfield equations. It turns out that the most accurate PSA should be used when investigating strong nonlinearities. The long-time approximation enables us nevertheless to extract the correct relaxation rate within the regime of validity of our perturbative approach. The chapter is organized as follows: In section 4.1 we introduce the model with the relevant dynamical quantities.

In section 4.2 the energy spectrum and the dynamics of the non-dissipative coupled system are investigated. Section 4.3 addresses the dissipative effects, while in section 4.4 results are presented. In section 4.5 conclusions are drawn.

4.1 Qubit-nonlinear oscillator-bath system

In this section we consider a TLS coupled to a nonlinear oscillator, which itself is coupled to an Ohmic bath. This model mimics, e.g., the situation of a flux qubit, made of three Josephson junctions, which is coupled inductively to a damped DC-SQUID [10, 11]. The qubit with its two logical states, the clockwise and counterclockwise currents, represents a two-level system. Because the SQUID itself is coupled to an environment, it transfers environmental influences which lead to the dissipation in the qubit. Hence the total Hamiltonian reads:

$$\hat{H} = \hat{H}_{\mathrm{TLS-NLO}} + \hat{H}_{\mathrm{NLO-B}} + \hat{H}_{\mathrm{B}}, \tag{4.1}$$

with $\hat{H}_{\mathrm{TLS-NLO}}$ describing the coupled TLS-nonlinear oscillator system, while $\hat{H}_{\mathrm{NLO-B}}$ and $\hat{H}_{\mathrm{B}}$ are the coupling between the oscillator and bath and the bath Hamiltonian, respectively. For later convenience we write

$$\hat{H}_{\mathrm{TLS-NLO}} = \underbrace{\hat{H}_{\mathrm{TLS}} + \hat{H}_{\mathrm{NLO}}}_{\hat{H}_0} + \hat{H}_{\mathrm{Int}} \tag{4.2}$$

with coupling Hamiltonian $\hat{H}_{\mathrm{Int}}$.

Two-level system

First we consider the Hamiltonian of the TLS, introduced in chapter 1,

$$\hat{H}_{\mathrm{TLS}} = -\frac{\hbar}{2}\left(\varepsilon\sigma_z + \Delta_0\sigma_x\right), \tag{4.3}$$

represented in the localized basis $\{|L\rangle, |R\rangle\}$ [1], corresponding to clockwise and counterclockwise currents in the superconducting ring, respectively. The σ_i, $i = x, z$, are the corresponding Pauli matrices. The energy bias ε can be tuned for a superconducting flux qubit by application of an external flux Φ_{ext} and vanishes at the so-called degeneracy point [74].
For $\varepsilon \gg \Delta_0$, where Δ_0 is the tunneling amplitude, the states $|L\rangle$ and $|R\rangle$ are eigenstates of the TLS, while at the degeneracy point the eigenstates $|\mathrm{g}\rangle$, $|\mathrm{e}\rangle$ are given by symmetric and antisymmetric superpositions, respectively, of the two logical states. In general the states $|R\rangle$ and $|L\rangle$ become in the energy basis:

$$\begin{aligned} |R\rangle &= \cos(\Theta/2)|\mathrm{g}\rangle + \sin(\Theta/2)|\mathrm{e}\rangle, \\ |L\rangle &= -\sin(\Theta/2)|\mathrm{g}\rangle + \cos(\Theta/2)|\mathrm{e}\rangle, \end{aligned} \tag{4.4}$$

with $\tan\Theta = -\Delta_0/\varepsilon$ and $-\frac{\pi}{2} \leq \Theta < \frac{\pi}{2}$. Moreover in this basis the TLS Hamiltonian is: $\hat{\tilde{H}}_{\mathrm{TLS}} = -\frac{\hbar\Delta_b}{2}\tilde{\sigma}_{\mathrm{z}}$, where $\tilde{\sigma}_z$ is the Pauli matrix in the energy basis and $\hbar\Delta_b = \hbar\sqrt{\varepsilon^2 + \Delta_0^2}$ is the energy splitting.

Nonlinear oscillator

The Hamiltonian for the nonlinear oscillator, already introduced in chapter 1, is composed of a linear harmonic oscillator modified with a quartic term in the position operator,

$$\hat{H}_{\rm NLO} \;=\; \hbar\Omega\hat{j} + \frac{\overline{\alpha}}{4}(\hat{a}+\hat{a}^\dagger)^4, \tag{4.5}$$

where $\hat{j} = \hat{a}^\dagger\hat{a}$ is the occupation number operator of the linear oscillator and $\hat{a}$ and $\hat{a}^\dagger$ are the corresponding annihilation and creation operators. In the following we restrict to the case of hard nonlinearities, i.e., $\overline{\alpha} > 0$. Using time-independent perturbation theory we consider small nonlinearities $\overline{\alpha} \ll \hbar\Omega$ and evaluate the eigenvalues E_j and eigenfunctions $|j\rangle$ of Eq. (4.5) to lowest order in the nonlinearity,

$$E_j \;:=\; \hbar\Omega j + \frac{3}{2}\overline{\alpha}j(j+1), \quad j = 0,\ldots,\infty \tag{4.6}$$

$$\begin{aligned} |j\rangle \;:=\; & |j\rangle_0 + a_{-2}^{(j)}|j-2\rangle_0 + a_2^{(j)}|j+2\rangle_0 + \\ & a_{-4}^{(j)}|j-4\rangle_0 + a_4^{(j)}|j+4\rangle_0, \end{aligned} \tag{4.7}$$

where $|\rangle_0$ denotes the eigenstate of the corresponding linear oscillator. The expansion coefficients for the jth state of the nonlinear oscillator are given by:

$$\begin{aligned} a_{-4}^{(j)} &= \frac{\sqrt{(j-3)(j-2)(j-1)j}\overline{\alpha}}{16\hbar\Omega}, \\ a_4^{(j)} &= -\frac{\sqrt{(j+1)(j+2)(j+3)(j+4)}\overline{\alpha}}{16\hbar\Omega}, \\ a_{-2}^{(j)} &= \frac{\left(j-\frac{1}{2}\right)\sqrt{(j-1)j}\overline{\alpha}}{2\hbar\Omega}, \\ a_2^{(j)} &= -\frac{\left(j+\frac{3}{2}\right)\sqrt{(j+1)(j+2)}\overline{\alpha}}{2\hbar\Omega}. \end{aligned} \tag{4.8}$$

We notice that two arbitrary eigenstates $|j\rangle$, $|k\rangle$ are orthonormal up to first order in the nonlinearity.

Perturbation theory for a nonlinear oscillator has to be elaborated carefully. Due to the special form of the nonlinear term, proportional to $(\hat{a}+\hat{a}^\dagger)^4$ the energy corrections acquire a strong level dependence: $E_j^{(1)} = \frac{3}{2}\overline{\alpha}j(j+1)$ for the first, see Eq. (4.6), and $E_j^{(2)} = -\frac{1}{8\hbar\Omega}\overline{\alpha}^2(34j^3+51j^2+59j+21)$ for the second order. Depending on the actual level number the second order can be as large as the first order for fixed nonlinearity. To avoid this, one has to choose the nonlinearity parameter $\overline{\alpha}$ such that the oscillator levels under consideration are well represented by the first order result. The error done by disregarding the nth order perturbation theory is estimated in the following by introducing $Er^{(n)}(j) = |E_j^{(n)}|/E_j^{(0)}$ for different nonlinearities (see Table 4.1). Taking only first order perturbation theory into account, the error is determined

Error	$\overline{\alpha}/\hbar\Omega = 10^{-3}$	$\overline{\alpha}/\hbar\Omega = 0.01$	$\overline{\alpha}/\hbar\Omega = 0.02$
$Er^{(1)}(1)$	$3 \cdot 10^{-3}$	0.03	0.06
$Er^{(2)}(1)$	$2.06 \cdot 10^{-5}$	$2.06 \cdot 10^{-3}$	$8.25 \cdot 10^{-3}$
$Er^{(1)}(2)$	$4.5 \cdot 10^{-3}$	0.045	0.09
$Er^{(2)}(2)$	$3.84 \cdot 10^{-5}$	$3.8 \cdot 10^{-3}$	0.015
$Er^{(1)}(3)$	$6 \cdot 10^{-3}$	0.06	0.12
$Er^{(2)}(3)$	$6.56 \cdot 10^{-5}$	$6.56 \cdot 10^{-3}$	0.026
$Er^{(1)}(4)$	$7.5 \cdot 10^{-3}$	0.075	0.15
$Er^{(2)}(4)$	$1.02 \cdot 10^{-4}$	$1.02 \cdot 10^{-2}$	0.041
$Er^{(1)}(5)$	$9 \cdot 10^{-3}$	$9 \cdot 10^{-2}$	0.18
$Er^{(2)}(5)$	$1.46 \cdot 10^{-4}$	$1.46 \cdot 10^{-2}$	0.058

Table 4.1: *Error estimation for different values of the nonlinearity for the six lowest levels.*

by $Er^{(2)}(j_{\max})$, where $j_{\max}$ is the highest level under consideration. The error made by using first order perturbation theory is in case of $\overline{\alpha}/\hbar\Omega = 0.02$ around 6% for the $j = 5$ level.
Finally we consider a coupling Hamiltonian of the form:

$$\hat{H}_{\rm Int} \;=\; \hbar\overline{g}\sigma_z(\hat{a} + \hat{a}^\dagger). \tag{4.9}$$

This kind of coupling arises due to the inductive coupling of the TLS to the SQUID [107].

Harmonic bath

Following Caldeira and Leggett [5], we model the environmental influences originating from the circuitry surrounding the qubit and the oscillator as a bath of harmonic oscillators being coupled bilinearily to the nonlinear oscillator. Thus, the environment is described by $H_{\rm B} = \sum_k \hbar\omega_k \hat{b}_k^\dagger \hat{b}_k$ and the interaction Hamiltonian is

$$\hat{H}_{\rm NLO-B} = (\hat{a}^\dagger + \hat{a}) \sum_k \hbar\nu_k (\hat{b}_k^\dagger + \hat{b}_k) + (\hat{a}^\dagger + \hat{a})^2 \sum_k \hbar\frac{\nu_k^2}{\omega_k}. \tag{4.10}$$

The operators $\hat{b}_k^\dagger$ and $\hat{b}_k$ are the creation and annihilation operators, respectively, for the kth bath oscillator, ω_k is its frequency, and ν_k gives the coupling strength. The whole bath can be described by its spectral density, which we consider to be Ohmic,

$$G_{\rm Ohm}(\omega) = \sum_k \nu_k^2 \delta(\omega - \omega_k) = \kappa\omega, \tag{4.11}$$

where κ is a dimensionless coupling strength.

4.1.1 Population difference

We wish to describe the dynamics $P(t)$ of the TLS described by the population difference

$$\begin{aligned} P(t) &= \mathrm{Tr}_{\mathrm{TLS}}\{\sigma_{\mathrm{z}}\hat{\rho}_{\mathrm{red}}(t)\} \\ &= \langle \mathrm{R}|\hat{\rho}_{\mathrm{red}}(t)|\mathrm{R}\rangle - \langle \mathrm{L}|\hat{\rho}_{\mathrm{red}}(t)|\mathrm{L}\rangle \end{aligned} \tag{4.12}$$

between the $|R\rangle$ and $|L\rangle$ states of the qubit. The reduced density matrix of the TLS,

$$\hat{\rho}_{\mathrm{red}}(t) = \mathrm{Tr}_{\mathrm{NLO}}\mathrm{Tr}_{\mathrm{B}}\{\hat{W}(t)\} = \mathrm{Tr}_{\mathrm{NLO}}\{\hat{\rho}(t)\}, \tag{4.13}$$

is found after tracing out the oscillator and bath degrees of freedom from the total density matrix $\hat{W}(t) = \exp^{-\frac{\mathrm{i}}{\hbar}\hat{H}t}\hat{W}(0)\exp^{\frac{\mathrm{i}}{\hbar}\hat{H}t}$. For vanishing nonlinearities it is possible to map the problem described by the Hamiltonian in Eq. (4.1) onto a spin-boson model [87] with an effective peaked spectral density depending on the coupling $\overline{g}$, the frequency Ω, and the damping strength κ. This mapping hence allows the evaluation of the population difference $P(t)$ of the TLS using standard approximations developed for the spin-boson model [91, 92, 147]. Such a mapping, however, is possible in the nonlinear oscillator case within a linear response approximation, as shown in chapter 5. In this chapter here we consider therefore the TLS and the nonlinear oscillator as central quantum system and describe dissipative effects by solving the Bloch-Redfield master equations for the reduced density matrix $\hat{\rho}(t) = \mathrm{Tr}_{\mathrm{B}}\{\hat{W}(t)\}$ of the qubit-NLO system. In a second step we perform the trace over the NLO degrees of freedom to obtain the reduced dynamics of the TLS. An expression for $P(t)$ is then given in terms of diagonal and off-diagonal elements of $\hat{\rho}(t)$ in the $\hat{H}_{\mathrm{TLS-NLO}}$ Hamiltonian's eigenbasis $\{|n\rangle\}$. It reads [148]:

$$P(t) = \sum_{n} p_{nn}(t) + \sum_{\substack{n,m \\ n>m}} p_{nm}(t), \tag{4.14}$$

where

$$p_{nn}(t) = \sum_{j}\left\{\cos\Theta\left[\langle j\mathrm{g}|n\rangle^2 - \langle j\mathrm{e}|n\rangle^2\right] + 2\sin\Theta\langle j\mathrm{g}|n\rangle\langle j\mathrm{e}|n\rangle\right\}\rho_{nn}(t), \tag{4.15}$$

$$\begin{aligned} p_{nm}(t) &= 2\sum_{j}\Big\{\cos\Theta\Big[\langle j\mathrm{g}|n\rangle\langle m|j\mathrm{g}\rangle - \langle j\mathrm{e}|n\rangle\langle m|j\mathrm{e}\rangle\Big] \\ &\quad + \sin\Theta\Big[\langle j\mathrm{e}|n\rangle\langle m|j\mathrm{g}\rangle + \langle j\mathrm{e}|m\rangle\langle n|j\mathrm{g}\rangle\Big]\Big\}\mathrm{Re}\{\rho_{nm}(t)\}, \end{aligned}$$

and $\rho_{nm}(t) = \langle n|\hat{\rho}(t)|m\rangle$. The TLS-NLO eigenstates are derived in the next section.

4.2 Energy spectrum and dynamics of the non-dissipative TLS-NLO system

In the following section we derive the eigenenergies and eigenstates of the unperturbed TLS-NLO Hamiltonian $\hat{H}_{\mathrm{TLS-NLO}}$ using Van Vleck perturbation theory [141, 142],

which has already been introduced in chapter 3. This approach allows us to deal with spectra containing almost exactly degenerate levels organized in manifolds (here doublets), as it is the case if the TLS and nonlinear oscillator are close to resonance, $\Delta_b \approx \Omega$, and the coupling $\overline{g}$ is small compared to the energy separation of the manifolds.

4.2.1 Energy spectrum

The eigenstates of the uncoupled TLS-NLO system Hamiltonian $\hat{\tilde{H}}_0$ are $\{|j\rangle \otimes |\mathrm{g}\rangle; |j\rangle \otimes |\mathrm{e}\rangle\} \equiv \{|j\mathrm{g}\rangle; |j\mathrm{e}\rangle\}$. The associated energies, denoted by $E_{j,\{\mathrm{g,e}\}}$, are depicted by the dotted lines in Fig. 4.1. At the resonance condition of the TLS with two neighboring nonlinear oscillator levels,

$$\hbar\Omega \;=\; \hbar\Delta_b - 3\overline{\alpha}(j+1), \tag{4.16}$$

where j denotes the lower oscillator level involved, the states $|(j+1)\mathrm{g}\rangle$ and $|j\mathrm{e}\rangle$ are exactly degenerate except for the ground state $|0\mathrm{g}\rangle$. For finite coupling the full Hamiltonian $\hat{H}_{\mathrm{TLS-NLO}}$ acquires in the basis $\{|j\mathrm{g}\rangle; |j\mathrm{e}\rangle\}$ the form

$$\begin{aligned}\hat{\tilde{H}}_{\mathrm{TLS-NLO}} &= \hat{\tilde{H}}_0 + \hat{\tilde{H}}_{\mathrm{Int}} \\ &= -\frac{\hbar\Delta_b}{2}\tilde{\sigma}_z + \hbar\Omega\hat{j} + \frac{3}{2}\overline{\alpha}\hat{j}(\hat{j}+1) + \frac{\hbar\overline{g}}{\Delta_b}\left(\epsilon\tilde{\sigma}_z - \Delta_0\tilde{\sigma}_x\right)\left(\hat{a}+\hat{a}^\dagger\right).\end{aligned} \tag{4.17}$$

To find the eigenvalues of the Hamiltonian $\hat{\tilde{H}}_{\mathrm{TLS-NLO}}$, we treat $\hat{\tilde{H}}_{\mathrm{Int}} \propto \overline{g}$ as a small perturbation, which is satisfied for $\overline{g} \ll \Delta_b, \Omega$. Using Van Vleck perturbation theory [141, 142] we can construct an effective Hamiltonian by applying an unitary transformation to $\hat{\tilde{H}}_{\mathrm{TLS-NLO}}$,

$$\hat{\tilde{H}}_{\mathrm{eff}} \;=\; \exp(i\hat{S})\hat{\tilde{H}}_{\mathrm{TLS-NLO}}\exp(-i\hat{S}). \tag{4.18}$$

$\hat{\tilde{H}}_{\mathrm{eff}}$ has the same eigenvalues as $\hat{\tilde{H}}_{\mathrm{TLS-NLO}}$ but does not involve matrix elements connecting states which are far away from degeneracy. Consequently, it is block-diagonal with all quasi-degenerate energy levels being in one common block. Because the quasi-degenerate states form doublets, each block of $\tilde{H}_{\mathrm{eff}}$ is given by a 2×2 matrix. The latter can be diagonalized easily. To calculate $\hat{S}$ and $\hat{\tilde{H}}_{\mathrm{eff}}$ we write both as a power series up to first order in the nonlinearity $\overline{\alpha}$ and up to second order in the coupling $\overline{g}$,

$$\hat{S} \;=\; \hat{S}^{(0)} + \hat{S}^{(1)} + \hat{S}^{(2)} + \mathcal{O}(\overline{\alpha}^2, \overline{g}^3), \tag{4.19}$$

$$\hat{\tilde{H}}_{\mathrm{eff}} \;=\; \hat{\tilde{H}}^{(0)}_{\mathrm{eff}} + \hat{\tilde{H}}^{(1)}_{\mathrm{eff}} + \hat{\tilde{H}}^{(2)}_{\mathrm{eff}} + \mathcal{O}(\overline{\alpha}^2, \overline{g}^3), \tag{4.20}$$

where $\exp(i\hat{S}^{(0)}) = \mathbb{1}$. The upper index in the above equation denotes the actual order in $\overline{g}$. Consequently, in the following we assume that $\overline{\alpha}/\hbar\Omega \sim \overline{g}^2/\Omega^2 \ll 1$. To calculate $\hat{S}^{(1/2)}$ and $\hat{\tilde{H}}^{(1/2)}_{\mathrm{eff}}$ we use both that $\hat{H}_{\mathrm{eff}}$ acts only inside a manifold and that

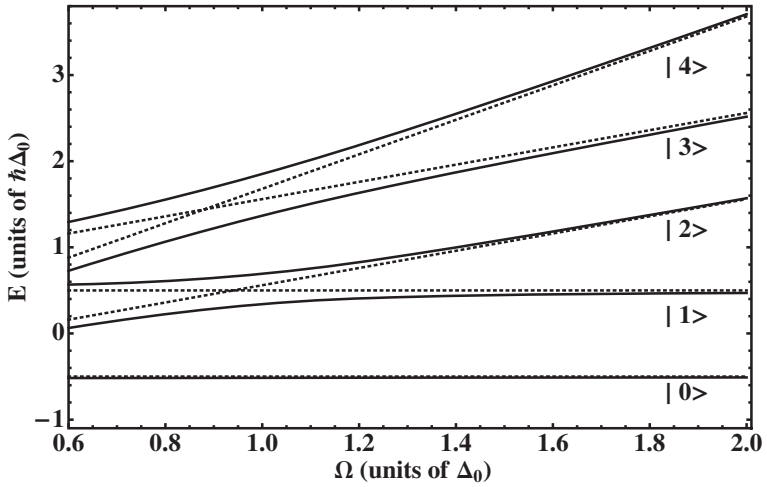

Figure 4.1: *Energy spectrum of the coupled qubit-nonlinear-oscillator system versus the linear oscillator frequency* Ω *(in units of the TLS tunneling splitting* Δ_0*). Solid lines show the energy levels for the five lowest energy states* ($|0\rangle$, $|1\rangle$, $|2\rangle$, $|3\rangle$, $|4\rangle$) *with the TLS-NLO coupling being switched on,* $\overline{g} = 0.18\Delta_0$*, and for finite nonlinearity,* $\overline{\alpha} = 0.02\hbar\Delta_0$*. The TLS is unbiased,* $\varepsilon = 0$*. The energy levels for the uncoupled case are given by the dotted lines. Due to the non-equidistant level spacing of the nonlinear oscillator the resonance condition (crossing of dotted lines), given in Eq. (4.16), is different for each doublet. This causes a shift of the exact crossings with respect to the linear case at zero coupling to lower frequencies. For finite coupling the spectrum exhibits avoided crossings around resonance, whereas it approaches the uncoupled case away from resonance.*

$\hat{S}$ has no matrix elements within a manifold. The general formulas are found e.g. in [148, 141, 142] and in Appendix C.
The results for the effective Hamiltonian and the transformation matrix are given in Appendix C.1. The non-vanishing matrix elements of the effective Hamiltonian, apart from the zeroth-order contributions in $\overline{g}$, are

$$\left(\hat{\tilde{H}}_{\text{eff}}\right)^{(1)}_{j\text{e};(j+1)\text{g}} = -\frac{\hbar\overline{g}\Delta_0}{\Delta_b} n_1(j) \equiv \hbar\Delta(j), \tag{4.21}$$

and

$$\left(\hat{\tilde{H}}_{\text{eff}}\right)^{(2)}_{j\text{e};j\text{e}} = \hbar\left[W_1(j,\Omega) - W_0(j,\Omega)\right], \tag{4.22}$$

$$\left(\hat{\tilde{H}}_{\text{eff}}\right)^{(2)}_{j\text{g};j\text{g}} = \hbar\left[W_1(j,\Omega) + W_0(j+1,\Omega)\right]. \tag{4.23}$$

We used as abbreviation

$$\begin{aligned} n_1(j) &= \sqrt{\mathrm{j}+1}\left(1+\frac{\sqrt{j}a_{-2}^{(j+1)}}{\sqrt{j+1}}+\frac{a_2^{(j)}\sqrt{j+2}}{\sqrt{j+1}}\right) \\ &= \sqrt{j+1}\left[1-\frac{3\overline{\alpha}}{2\hbar\Omega}(j+1)\right]+\mathcal{O}(\overline{\alpha}^2), \end{aligned} \tag{4.24}$$

and

$$W_1(j,\Omega) = -\frac{\overline{g}^2\varepsilon^2}{\Delta_b^2\Omega}+\frac{6\overline{\alpha}\,\overline{g}^2(2j+1)\varepsilon^2}{\hbar\Delta_b^2\Omega^2}+\mathcal{O}\left(\overline{\alpha}^2\right), \tag{4.25}$$

$$W_0(j,\Omega) = -\frac{\overline{g}^2\Delta_0^2 j}{\Delta_b^2(\Delta_b+\Omega)}\left[1-\frac{3\overline{\alpha}j(\Delta_b+2\Omega)}{\hbar\Omega(\Delta_b+\Omega)}\right]+\mathcal{O}\left(\overline{\alpha}^2\right). \tag{4.26}$$

Therefore the effective Hamiltonian acquires in first order in the nonlinearity and in second order in the coupling the form:

$$\hat{\tilde{H}}_{\mathrm{eff}} = \hbar\cdot \tag{4.27}$$

$$\left(\begin{array}{c|cc|c} \ddots & & & \\ \hline & \frac{\Delta_b}{2}+j\Omega+\frac{3}{2\hbar}\overline{\alpha}j(j+1) & \Delta(j) & \\ & +W_1(j,\Omega)-W_0(j,\Omega) & & \\ & & -\frac{\Delta_b}{2}+(j+1)\Omega+\frac{3}{2\hbar}\overline{\alpha}(j+1)(j+2) & \\ & \Delta(j) & +W_1(j+1,\Omega)+W_0(j+2,\Omega) & \\ \hline & & & \ddots \end{array}\right)$$

for the states $|j\mathrm{e}\rangle$ and $|(j+1)\mathrm{g}\rangle$. The ground state $|0\rangle_{\mathrm{eff}} \equiv |0\mathrm{g}\rangle$ is an eigenstate of $\hat{\tilde{H}}_{\mathrm{eff}}$ with eigenenergy:

$$\mathcal{E}_0 = \hbar(-\Delta_b/2+W_1(0,\Omega)+W_0(1,\Omega)). \tag{4.28}$$

Due to the doublet structure the blocks of the effective Hamiltonian are 2×2 matrices and the corresponding eigenvectors are for $j \geq 0$:

$$\begin{aligned} |2j+1\rangle_{\mathrm{eff}} &= \cos\left(\frac{\eta_j}{2}\right)|(j+1)\mathrm{g}\rangle+\sin\left(\frac{\eta_j}{2}\right)|j\mathrm{e}\rangle, \\ |2j+2\rangle_{\mathrm{eff}} &= -\sin\left(\frac{\eta_j}{2}\right)|(j+1)\mathrm{g}\rangle+\cos\left(\frac{\eta_j}{2}\right)|j\mathrm{e}\rangle, \end{aligned} \tag{4.29}$$

where $\tan\eta_j = \frac{2|\Delta(j)|}{\delta_j}$ and $0 \leq \eta_j < \pi$. Moreover,

$$\delta_j = \Delta_b-\Omega-\frac{3\overline{\alpha}(j+1)}{\hbar}+W_1(j,\Omega)-W_1(j+1,\Omega)-W_0(j,\Omega)-W_0(j+2,\Omega). \tag{4.30}$$

In turn the eigenstates of the qubit-nonlinear oscillator system are obtained from the transformation

$$|n\rangle = \exp(-i\hat{S})|n\rangle_{\rm eff}. \tag{4.31}$$

Finally, the eigenenergies are then

$$\begin{aligned}\mathcal{E}_{2j+1/2j+2} &= \hbar(j+\frac{1}{2})\Omega + \frac{3}{2}\overline{\alpha}(j+1)^2 + \hbar(W_1(j,\Omega)+W_1(j+1,\Omega))/2 \\ &\quad -\hbar W_0(j,\Omega)/2 + \hbar W_0(j+2,\Omega)/2 \mp \frac{\hbar}{2}\sqrt{\delta_j^2 + 4|\Delta(j)|^2}. \end{aligned}\tag{4.32}$$

These eigenenergies are also eigenenergies of $\hat{\tilde{H}}_{\rm TLS-NLO}$ by construction and are depicted in Fig. 4.1 (solid lines) for the case of an unbiased TLS, $\varepsilon = 0$. At finite coupling the degeneracy is lifted and we observe avoided crossings (solid lines in Fig. 4.1). Due to the coupling the resonance condition acquires a shift compared to Eq. (4.16), the so-called Bloch-Siegert shift [149],

$$\begin{aligned}\Omega &= \Delta_b - \frac{3}{\hbar}\overline{\alpha}(j+1) + W_1(j,\Delta_b) - W_1(j+1,\Delta_b) - W_0(j,\Delta_b) - W_0(j+2,\Delta_b) \\ &\quad +3\frac{\overline{\alpha}\,\overline{g}^2\Delta_0^2}{2\hbar\Delta_b^4}(j+1)^2 + \mathcal{O}(\overline{\alpha}^2,\overline{g}^4). \end{aligned}\tag{4.33}$$

The resonance corresponds to $\delta_j = 0$. We notice that the effect of the nonlinearity on the Bloch-Siegert shift is very weak, namely at least of order $\mathcal{O}(\overline{\alpha}\,\overline{g}^2)$ and negligible for the values of nonlinearity and coupling we consider in the following.
At resonance, Eq. (4.33), the minimal splitting of the former degenerate gap is:

$$\mathcal{E}_{2j+2} - \mathcal{E}_{2j+1} = \hbar\sqrt{j+1}\overline{g}\frac{\Delta_0}{\Delta_b}\left[2 - \frac{3}{\hbar\Omega}\overline{\alpha}(j+1)\right] + \mathcal{O}(\overline{\alpha}^2,\overline{g}^3). \tag{4.34}$$

We notice that at any point of our calculation we can set the nonlinearity to zero and reproduce the results obtained for the TLS-linear oscillator system [148].

4.2.2 Dynamics of the qubit for the non-dissipative case

The time evolution of the qubit-nonlinear-oscillator system without bath is given by $\hat{\rho}(t) = \exp(-\frac{i}{\hbar}\hat{\tilde{H}}_{\rm TLS-NLO})\hat{\rho}(0)\exp(+\frac{i}{\hbar}\hat{\tilde{H}}_{\rm TLS-NLO})$ and therefore

$$\rho_{nm}(t) = \langle n|\hat{\rho}(t)|m\rangle = \exp(-i\omega_{nm}t)\rho_{nm}(0), \tag{4.35}$$

where $\omega_{nm} = \frac{1}{\hbar}(\mathcal{E}_n - \mathcal{E}_m)$. Consequently, we obtain for the population difference in Eq. (4.14)

$$P(t) = p_0 + \sum_{\substack{n,m \\ n>m}} p_{nm}(0)\cos\omega_{nm}t, \tag{4.36}$$

where we introduced $p_0 \equiv \sum_n p_{nn}(0)$. We observe from Eq. (4.36) that the dynamics of the TLS is determined by an infinite number of oscillation frequencies rather than showing a single Rabi oscillation. To set the initial conditions we assume that the qubit starts in the state $|R\rangle$ and that the occupation numbers of the NLO are Boltzmann distributed:

$$\hat{\rho}(0) = |R\rangle\langle R| \frac{1}{Z_{\rm NLO}} \exp(-\beta \hat{H}_{\rm NLO}), \tag{4.37}$$

where

$$Z_{\rm NLO} = \sum_{j=0}^{\infty} \exp[-\beta(\hbar\Omega j + \frac{3}{2}\overline{\alpha} j(j+1))] \tag{4.38}$$

is the partition function of the oscillator and $\beta = (k_B T)^{-1}$ is the inverse temperature. In the TLS-NLO eigenbasis we get:

$$\begin{aligned} \rho_{nm}(0) &= \langle n|\hat{\rho}(0)|m\rangle \qquad (4.39)\\ &= \frac{1}{Z_{\rm NLO}} \sum_{j=0}^{\infty} \exp[-\beta(\hbar\Omega j + \frac{3}{2}\overline{\alpha} j(j+1))] \left[\cos\left(\frac{\Theta}{2}\right)\langle n|j{\rm g}\rangle + \sin\left(\frac{\Theta}{2}\right)\langle n|j{\rm e}\rangle\right] \\ &\quad \times \left[\cos\left(\frac{\Theta}{2}\right)\langle j{\rm g}|m\rangle + \sin\left(\frac{\Theta}{2}\right)\langle j{\rm e}|m\rangle\right]. \end{aligned}$$

Low temperature approximation

Eq. (4.36) allows us to describe the non-dissipative dynamics in terms of the approximate eigenenergies and eigenstates, Eqs. (4.31) and (4.32), which involve in this way all nonlinear oscillator states. Therefore the Hilbert space under consideration is infinite. To calculate $p_{nm}(0)$ and $p_{nn}(0)$ we need to know the structure of a matrix element such as $\langle j, \{{\rm g/e}\}|n\rangle = \langle j, \{{\rm g/e}\}| \exp(-i\hat{S})|n\rangle_{\rm eff}$. The $|n\rangle_{\rm eff}$ are themselves linear combinations of the uncoupled states $|j, \{{\rm g/e}\}\rangle$, see Eq. (4.29). Because we calculated $\exp(-iS)$ up to second order in the coupling Hamiltonian $\hat{H}_{\rm Int}$, we find that the oscillator index j can at most change by four, see Appendix C.1. For typical experiments on qubits the temperature is restricted to the regime of $\beta^{-1} \ll \hbar\Omega, \hbar\Delta_b$. Due to the exponential function in Eq. (4.39) high levels of the NLO are only weakly populated and consequently we can truncate the infinite sum in Eq. (4.39) for the matrix elements of the density matrix at initial time to $j = 1$. This means that the lowest 12 $\{|n\rangle\}$ states enter Eq. (4.39).
After a close analysis we observe, by inserting Eq. (4.39) into Eq. (4.15), that the coefficients $p_{nm}(0)$ with $n \geq 7$ are of higher than second order in $\overline{g}$. The same is valid for p_{50}, p_{60}, p_{55} and p_{66}. Thus those terms do not occur in the calculation of $P(t)$. Of the remaining contributions we observe that those with $n = 5, 6$ are either at least of order $\overline{g}\exp[-\beta(\hbar\Omega + 3\overline{\alpha})]$ or of order $\overline{g}^2 \exp[-\beta(\hbar\Omega + 3\overline{\alpha})]$ or of order $\overline{\alpha}\,\overline{g}^2$. Thus we can also disregard contributions from p_{nm} for $n \geq 5$ for the parameters chosen in the following, i.e., in the considered low temperature regime it is enough to restrict to

the five lowest eigenstates of $\hat{\tilde{H}}_{\mathrm{TLS-NLO}}$. Therefore the number of possible oscillation frequencies ω_{nm} is reduced to 10, where $n, m = 0, 1, \ldots, 4$ and $n > m$.
In the following we show the dynamics of an unbiased TLS ($\varepsilon = 0$), which results in vanishing of p_0, $p_{30}(0)$, $p_{40}(0)$, $p_{21}(0)$ and $p_{43}(0)$. Therefore we obtain:

$$\begin{aligned} P(t) &= p_{10}\cos(\omega_{10}t) + p_{20}\cos(\omega_{20}t) + p_{31}\cos(\omega_{31}t) + p_{41}\cos(\omega_{41}t) \\ &\quad + p_{32}\cos(\omega_{32}t) + p_{42}\cos(\omega_{42}t). \end{aligned} \tag{4.40}$$

Exemplarily we consider the resonant case for the corresponding linear oscillator, where $\Omega = \Delta_b = \Delta_0$. This corresponds to a slightly detuned nonlinear-oscillator system. The resulting transition frequencies using Eq. (4.32) are:

$$\begin{aligned} \omega_{10} &= \Omega - \overline{g} + \frac{3\overline{\alpha}}{2\hbar} + \frac{9\overline{\alpha}\,\overline{g}}{4\hbar\Omega} + \frac{9\overline{\alpha}\,\overline{g}^2}{4\hbar\Omega^2}, \\ \omega_{20} &= \Omega + \overline{g} + \frac{3\overline{\alpha}}{2\hbar} - \frac{9\overline{\alpha}\,\overline{g}}{4\hbar\Omega} + \frac{9\overline{\alpha}\,\overline{g}^2}{4\hbar\Omega^2}, \\ \omega_{31} &= \Omega + \overline{g}(1-\sqrt{2}) + \frac{9\overline{\alpha}}{2\hbar} + \frac{9\overline{\alpha}\,\overline{g}}{4\hbar\Omega}\left[2\sqrt{2}-1\right] + \frac{9\overline{\alpha}\,\overline{g}^2}{2\hbar\Omega^2}, \\ \omega_{41} &= \Omega + \overline{g}(1+\sqrt{2}) + \frac{9\overline{\alpha}}{2\hbar} - \frac{9\overline{\alpha}\,\overline{g}}{4\hbar\Omega}\left[2\sqrt{2}+1\right] + \frac{9\overline{\alpha}\,\overline{g}^2}{2\hbar\Omega^2}, \\ \omega_{32} &= \Omega - \overline{g}(1+\sqrt{2}) + \frac{9\overline{\alpha}}{2\hbar} + \frac{9\overline{\alpha}\,\overline{g}}{4\hbar\Omega}\left[2\sqrt{2}+1\right] + \frac{9\overline{\alpha}\,\overline{g}^2}{2\hbar\Omega^2}, \\ \omega_{42} &= \Omega - \overline{g}(1-\sqrt{2}) + \frac{9\overline{\alpha}}{2\hbar} - \frac{9\overline{\alpha}\,\overline{g}}{4\hbar\Omega}\left[2\sqrt{2}-1\right] + \frac{9\overline{\alpha}\,\overline{g}^2}{2\hbar\Omega^2}. \end{aligned} \tag{4.41}$$

Due to the nonlinearity the six different oscillation frequencies in Eq. (4.41) are shifted to higher frequencies compared to the linear oscillator case $\overline{\alpha} = 0$. In contrast to the linear case they are no longer located symmetrically around $\Omega = \Delta_0$. The reason for this lies in the non-equidistant energy levels of the nonlinear oscillator alone and in the interplay of coupling and nonlinearity. The population difference $P(t)$ and its Fourier transform are shown in Fig. 4.2. As in the linear case, the dominating frequencies are ω_{10} and ω_{20}. These correspond to transitions between the first and the second state of the qubit-NLO-system and the ground state. In the linear oscillator case the weight of their peaks is almost equal, whereas with weak nonlinearities the peak corresponding to ω_{10} is more pronounced. This is due to the fact that the frequency corresponding to the more pronounced peak fits more accurately the resonance condition, which includes the Bloch-Siegert shift in Eq. (4.33). The weight of the peaks can additionally be influenced by allowing a finite bias of the qubit, $\varepsilon \neq 0$. The zero bias case was chosen here for simplicity.
From these graphs and Eqs. (4.34) and (4.41) we can read off first that the vacuum Rabi splitting is decreased for finite nonlinearity and second that the overall frequency shifts compared to the linear case are larger the higher the oscillator levels are involved if the coupling $\overline{g}$ is not too large to overcome the effects caused by the nonlinearity.

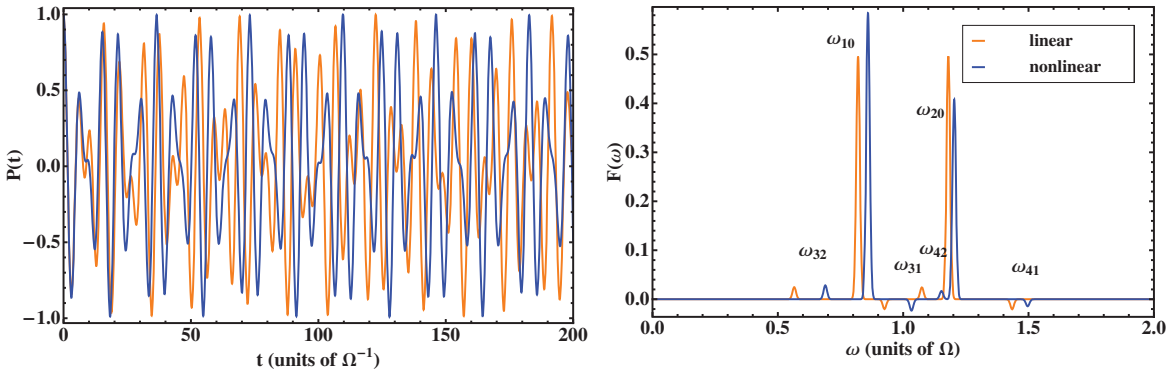

Figure 4.2: *Left: Dynamics of the population difference $P(t)$ for the unbiased, $\varepsilon = 0$, qubit-nonlinear oscillator system at linear resonance ($\Omega = \Delta_0$) (blue line). We choose a nonlinearity $\overline{\alpha} = 0.02\hbar\Omega$, a TLS-NLO coupling $\overline{g} = 0.18\Omega$, and inverse temperature $\beta = 10(\hbar\Omega)^{-1}$. For comparison we plotted the corresponding linear case (orange line). Right: Fourier transform $F(\omega)$ of $P(t)$ for the unbiased system. The dominating frequencies are ω_{10} and ω_{20}. To visualize the delta-functions, finite widths have been introduced artificially.*

4.3 Influence of the environment

The knowledge about decoherence and dissipation processes entering in the qubit dynamics is essential for quantum computation. Therefore we consider now the qubit-nonlinear-oscillator system to be coupled to an environment and treat the full Hamiltonian $\hat{H}$.

4.3.1 Master equation for the qubit-NLO system

As shown in section 4.1.1, Eq. (4.14), we need for the calculation of $P(t)$ the density matrix $\hat{\rho}(t)$ of the qubit-nonlinear oscillator system. To take into account the effect of the bath we start from the Liouville equation for the full density matrix $\hat{W}(t)$ of $\hat{H}$,

$$i\hbar\frac{\partial\hat{W}_{\rm I}(t)}{\partial t} = \left[\hat{H}_{\rm NLO-B,I}(t),\hat{W}_{\rm I}(t)\right], \tag{4.42}$$

where the index I denotes the interaction picture. Following [116, 113] and the derivations in chapter 2 we arrive at a Born-Markov master equation for $\hat{\rho}(t)$ being in the Schrödinger picture and expressed in the basis of the eigenstates of $\hat{\tilde{H}}_{\rm Q-NLO}$:

$$\dot{\rho}_{nm}(t) = -i\omega_{nm}\rho_{nm}(t) + \pi\sum_{k,l}\mathcal{L}_{nm,kl}\rho_{kl}(t). \tag{4.43}$$

The first term includes the free dynamics, whereas the second accounts for the dissipative one. The Bloch-Redfield tensors are defined by:

$$\begin{aligned}\mathcal{L}_{nm,kl} &= [G(\omega_{nk})N_{nk} - G(\omega_{lm})N_{ml}]\, y_{nk}y_{lm} - \delta_{ml}\sum_{l'} G(\omega_{l'k})N_{l'k}y_{nl'}y_{l'k} \\ &\quad +\delta_{nk}\sum_{k'} G(\omega_{lk'})N_{k'l}y_{lk'}y_{k'm},\end{aligned} \tag{4.44}$$

with $N_{nm} = \frac{1}{2}\left[\coth(\hbar\beta\omega_{nm}/2) - 1\right]$ and $y_{nm} = \langle n|(\hat{a} + \hat{a}^\dagger)|m\rangle$.
In the following we assume to have an Ohmic bath described by the spectral density $G(\omega) \equiv G_{\mathrm{Ohm}}(\omega) = \kappa\omega$.
For the derivation of the master equation besides the Born-Markov approximation more assumptions have been made. We only mention them briefly: first, we assume that the system and bath are initially uncorrelated (at $t = 0$), i.e., $\hat{W}(0) = \hat{\rho}_{\mathrm{I}}(0)\hat{\rho}_{\mathrm{B}}(0)$, where $\hat{\rho}_{\mathrm{B}}(0) = Z_{\mathrm{B}}^{-1}\exp(-\beta\hat{H}_{\mathrm{B}})$ and Z_{B} is the partition function of the bath. Because the bath consists of infinite degrees of freedom we assume the effects of the interaction with the TLS-NLO system on the bath to dissipate away quickly, such that the bath remains in thermal equilibrium for all times t: $\hat{W}_{\mathrm{I}}(t) = \hat{\rho}_{\mathrm{I}}(t)\hat{\rho}_B(0)$. Additionally an initial slip term is neglected, which occurs due to the sudden coupling of the system to the bath [1]. Finally we disregarded the Lamb-shift of the oscillation frequencies ω_{nm}.

4.3.2 Matrix elements

The Redfield tensors, Eq. (4.44), depend on the matrix elements y_{nm} of the NLO position operator in the TLS-NLO eigenbasis. Using Eq. (4.31) we rewrite y_{nm} in the form:

$$\begin{aligned}y_{nm} &= \langle n|y|m\rangle = {}_{\mathrm{eff}}\langle n|\exp(i\hat{S})\hat{y}\exp(-i\hat{S})|m\rangle_{\mathrm{eff}} \\ &\equiv {}_{\mathrm{eff}}\langle n|\hat{\tilde{y}}|m\rangle_{\mathrm{eff}}.\end{aligned} \tag{4.45}$$

The effective states are given in Eq. (4.29) as linear combinations of states of the $\{|j\mathrm{g}\rangle; |j\mathrm{e}\rangle\}$ basis. In the following we show the different building blocks for y_{nm}. We can distinguish between different situations. First there are matrix elements where neither the qubit nor the oscillator state is changed, namely:

$$\begin{aligned}\langle j\mathrm{g}|\hat{\tilde{y}}|j\mathrm{g}\rangle &= -2(L_{LO0}(\overline{g}) + L_{NLO0}(j,\overline{\alpha},\overline{g})), \\ \langle j\mathrm{e}|\hat{\tilde{y}}|j\mathrm{e}\rangle &= +2(L_{LO0}(\overline{g}) + L_{NLO0}(j,\overline{\alpha},\overline{g})),\end{aligned} \tag{4.46}$$

where $L_{LO0}(\overline{g}) = \overline{g}\varepsilon/\Delta_b\Omega$ and $L_{NLO0}(j,\overline{\alpha},\overline{g}) = -6\overline{\alpha}\,\overline{g}\varepsilon(2j+1)/\hbar\Delta_b\Omega^2$. These matrix elements contain contributions independent of the oscillator occupation number j for zeroth order in the nonlinearity $\overline{\alpha}$ and acquire a level dependence in first order.
A transition within the qubit is described by

$$\langle j\mathrm{g}|\hat{\tilde{y}}|j\mathrm{e}\rangle = L_{LO0+}(\overline{g}) + L_{NLO0+}(\overline{\alpha},\overline{g})(2j+1). \tag{4.47}$$

Here we introduced abbreviations, given in Appendix E, to show the actual order of the matrix elements involved. The notation is as follows: indices LO and NLO refer to the linear or nonlinear oscillator, respectively. An additional index number, Δj, indicates that the nonlinear oscillator state is changed by Δj quanta. We have elements where zero, one, two or three quanta are emitted or absorbed by the oscillator. Moreover, we introduce indices $+/-$ or g/e which correspond to the TLS transition g $\rightarrow$ e or to e $\rightarrow$ g, respectively, or to the qubit not changing from g or e configuration.
For the case $\Delta j = 1$:

$$\begin{aligned}\langle j\mathrm{g}|\hat{\tilde{y}}|(j+1)\mathrm{g}\rangle &= \sqrt{j+1}\left[1+(j+1)L_{NLO}(\overline{\alpha})+L_{LO1}(\overline{g}^2)+L_{NLO1\mathrm{g}}(j,\overline{\alpha},\overline{g}^2)\right],\\ \langle j\mathrm{e}|\tilde{y}|(j+1)\mathrm{e}\rangle &= \sqrt{j+1}\left[1+(j+1)L_{NLO}(\overline{\alpha})-L_{LO1}(\overline{g}^2)+L_{NLO1\mathrm{e}}(j,\overline{\alpha},\overline{g}^2)\right],\end{aligned} \tag{4.48}$$

$$\begin{aligned}\langle j\mathrm{g}|\hat{\tilde{y}}|(j+1)\mathrm{e}\rangle &= \sqrt{j+1}\left[L_{LO1+}(\overline{g}^2)+L_{NLO1+}(\overline{\alpha},\overline{g}^2)(j+1)\right],\\ \langle j\mathrm{e}|\tilde{y}|(j+1)\mathrm{g}\rangle &= \sqrt{j+1}\left[L_{LO1-}(\overline{g}^2)+L_{NLO1-}(\overline{\alpha},\overline{g}^2)(j+1)\right],\end{aligned} \tag{4.49}$$

describe processes where an oscillator quantum is absorbed. All the matrix elements in Eqs. (4.47), (4.48) and in (4.49) contain both zeroth-order as well as first-order contributions in the nonlinearity. Additionally, due to the fact that the states of the NLO are linear combinations of the linear oscillator states, see Eq. (4.7), additional transitions involving a change of the oscillator state by more than one quantum are allowed. They correspond to $\Delta j = 2$, $\Delta j = 3$ and read as

$$\begin{aligned}\langle j\mathrm{g}|\hat{\tilde{y}}|(j+2)\mathrm{g}\rangle &= \sqrt{(j+1)(j+2)}L_{NLO2}(\overline{\alpha},\overline{g}),\\ \langle j\mathrm{g}|\hat{\tilde{y}}|(j+2)\mathrm{e}\rangle &= \sqrt{(j+1)(j+2)}L_{NLO2+}(\overline{\alpha},\overline{g}),\\ \langle j\mathrm{e}|\hat{\tilde{y}}|(j+2)\mathrm{g}\rangle &= \sqrt{(j+1)(j+2)}L_{NLO2-}(\overline{\alpha},\overline{g}),\\ \langle j\mathrm{e}|\hat{\tilde{y}}|(j+2)\mathrm{e}\rangle &= -\sqrt{(j+1)(j+2)}L_{NLO2}(\overline{\alpha},\overline{g}),\\ \langle j\mathrm{g}|\hat{\tilde{y}}|(j+3)\mathrm{g}\rangle &= \sqrt{(j+1)(j+2)(j+3)}\left[L_{NLO3}(\overline{\alpha},\overline{g}^2)-L_{NLO}(\overline{\alpha})/2\right],\\ \langle j\mathrm{g}|\hat{\tilde{y}}|(j+3)\mathrm{e}\rangle &= \sqrt{(j+1)(j+2)(j+3)}L_{NLO3+}(\overline{\alpha},\overline{g}^2),\\ \langle j\mathrm{e}|\hat{\tilde{y}}|(j+3)\mathrm{g}\rangle &= \sqrt{(j+1)(j+2)(j+3)}L_{NLO3-}(\overline{\alpha},\overline{g}^2),\\ \langle j\mathrm{e}|\hat{\tilde{y}}|(j+3)\mathrm{e}\rangle &= \sqrt{(j+1)(j+2)(j+3)}\left[-L_{NLO3}(\overline{\alpha},\overline{g}^2)-L_{NLO}(\overline{\alpha})/2\right].\end{aligned} \tag{4.50}$$

Notice that all terms in Eq. (4.50) vanish when $\overline{\alpha} = 0$. The terms in Eqs. (4.48) and (4.50) involving no change in the qubit and a change in the oscillator by $\Delta j = 1$ and $\Delta j = 3$ quanta contain $\overline{g}$-independent nonlinear contributions. The interplay of nonlinearity and coupling in lowest order can be observed in $\langle j\mathrm{g}|\hat{\tilde{y}}|j\mathrm{e}\rangle$, and in the terms involving an oscillator level change by 2. Additionally at the degeneracy point, $\varepsilon = 0$, $L_{LO0}(\overline{g})$, $L_{NLO0}(j,\overline{\alpha},\overline{g})$, $L_{LO1\pm}(\overline{g}^2)$, $L_{NLO2}(\overline{\alpha},\overline{g})$, $L_{NLO1\pm}(\overline{\alpha},\overline{g}^2)$, $L_{NLO3\pm}(\overline{\alpha},\overline{g}^2)$, and parts of $L_{NLO1\{g/e\}}(j,\overline{\alpha},\overline{g}^2)$ vanish. We are now able to calculate the matrix elements y_{nm}. They are given in Appendix E.

4.3.3 Dissipative dynamics

To calculate $P(t)$ we have to solve the system of coupled differential equations Eq. (4.43). When several TLS-NLO levels are involved an exact solution can only be found numerically. Hence, in the remaining of this section we discuss three different approximation schemes, two based on the full secular approximation (FSA) applied to Eq. (4.43) and one based on a partial secular approximation (PSA). We then compare the so obtained analytical predictions with the exact numerical solution of Eq. (4.43).

Full secular approximation (FSA)

We define:

$$\rho_{nm}(t) \;=\; \exp(-i\omega_{nm}t)\sigma_{nm}(t), \tag{4.51}$$

which, inserted in Eq. (4.43), enables us to obtain a set of differential equations for $\dot{\sigma}_{nm}(t)$:

$$\dot{\sigma}_{nm}(t) = \pi \sum_{kl} \mathcal{L}_{nm,kl} \exp[i(\omega_{nm} - \omega_{kl})t]\sigma_{kl}(t). \tag{4.52}$$

The FSA consists of neglecting fast rotating terms in Eq. (4.52) such that only terms survive where $\omega_{nm} - \omega_{kl}$ vanishes. This allows an effective decoupling of diagonal and off-diagonal elements such that:

$$\dot{\sigma}_{nn}(t) \;=\; \pi \sum_{k} \mathcal{L}_{nn,kk}\sigma_{kk}(t), \tag{4.53a}$$

$$\dot{\sigma}_{nm}(t) \;=\; \pi\mathcal{L}_{nm,nm}\sigma_{nm}(t) \text{ for } n \neq m. \tag{4.53b}$$

The off-diagonal elements are determined by:

$$\sigma_{nm}(t) \;=\; \sigma^0_{nm} \exp(\pi\mathcal{L}_{nm,nm}t), \tag{4.54}$$

which results with Eq. (4.51) in

$$\rho_{nm}(t) \;=\; \rho^0_{nm} \exp(\pi\mathcal{L}_{nm,nm}t) \exp(-i\omega_{nm}t). \tag{4.55}$$

The separation of the oscillatory motion of the dynamics from the relaxation one allows us to divide Eq. (4.14) into two parts:

$$P(t) \;=\; P_{\text{relax}}(t) + P_{\text{dephas}}(t), \tag{4.56}$$

where $P_{\text{relax}}(t) = \sum_n p_{nn}(t)$ is the relaxation contribution and $P_{\text{dephas}}(t) = \sum_{n>m} p_{nm}(t)$ is the dephasing part. Inserting Eq. (4.55) in the last expression and using Eq. (4.15), we obtain:

$$P_{\text{dephas}}(t) = \sum_{n>m} p_{nm}(0) \exp(-\Gamma_{nm}t) \cos(\omega_{nm}t), \tag{4.57}$$

where the dephasing rates are determined by $\Gamma_{nm} \equiv -\pi\mathcal{L}_{nm,nm}$. The actual form of the dephasing coefficients $\mathcal{L}_{nm,nm}$ can be found in Appendix F and the initial conditions

$\rho^0_{nm} = \sigma^0_{nm} = \rho_{nm}(0)$ are defined in Eq. (4.39). The diagonal elements are more difficult to obtain, since the coupled system of differential equations in Eq. (4.53a) has to be solved. To proceed we restrict ourselves in this section again to the physical relevant low temperature case, such that the highest qubit-nonlinear oscillator state involved is the eigenstate $|4\rangle$. Calculating the rate coefficients accompanied with the five lowest eigenstates, we observe that there are only eight independent ones due to the structure of the rate coefficients. These are $\mathcal{L}_{00,11}$, $\mathcal{L}_{00,22}$, $\mathcal{L}_{11,22}$, $\mathcal{L}_{11,33}$, $\mathcal{L}_{11,44}$, $\mathcal{L}_{22,33}$, $\mathcal{L}_{22,44}$, and $\mathcal{L}_{33,44}$. In general they are determined by:

$$\mathcal{L}_{jj,kk} = 2G(\omega_{jk})N_{jk}y^2_{jk} \quad \text{with} \quad j < k, \tag{4.58}$$

where j and k adopt the above values. Furthermore, $\mathcal{L}_{00,33}$, $\mathcal{L}_{00,44}$, $\mathcal{L}_{33,00}$ and $\mathcal{L}_{44,00}$ are disregarded, because they are at least of order $\mathcal{O}(\overline{g}^4)$. The remaining rate coefficients are combinations of the above. We find that:

$$\mathcal{L}_{kk,jj} \;=\; \mathcal{L}_{jj,kk} + 2G(\omega_{jk})y^2_{jk} = (N_{jk}+1)2G(\omega_{jk})y^2_{jk}, \tag{4.59}$$

and

$$\begin{aligned}
\mathcal{L}_{00,00} &= -\mathcal{L}_{11,00} - \mathcal{L}_{22,00}, \\
\mathcal{L}_{11,11} &= -\mathcal{L}_{00,11} - \mathcal{L}_{22,11} - \mathcal{L}_{33,11} - \mathcal{L}_{44,11}, \\
\mathcal{L}_{22,22} &= -\mathcal{L}_{00,22} - \mathcal{L}_{11,22} - \mathcal{L}_{33,22} - \mathcal{L}_{44,22}, \\
\mathcal{L}_{33,33} &= -\mathcal{L}_{11,33} - \mathcal{L}_{22,33} - \mathcal{L}_{44,33}, \\
\mathcal{L}_{44,44} &= -\mathcal{L}_{11,44} - \mathcal{L}_{22,44} - \mathcal{L}_{33,44}.
\end{aligned} \tag{4.60}$$

Low temperature approximation (LTA)

Despite the above relations Eq. (4.53a) is too complicated to be solved analytically. Therefore an additional approximation is applied: we consider the factor $N_{nm}+1 = \frac{1}{2}\left[\coth(\hbar\beta\omega_{nm}/2)+1\right]$ with $n < m$ in Eq. (4.59) and use that

$$\lim_{x\to-\infty} \coth(x/2) = -1$$

is reached exponentially fast.
The terms containing this factor are neglected in the following. As we consider only the lowest five levels, this amounts to require $\max\{\omega_{nm}\} = |\omega_{14}| \gg k_bT$. Using Eq. (4.34) we observe that $\omega_{12} \propto \overline{g}$ and $\omega_{34} \propto \overline{g}$. For this reason and due to the structure of y_{nm} given in Eq. (E.1) the rates $\mathcal{L}_{11,22}$ and $\mathcal{L}_{33,44}$ are at least of order $\mathcal{O}(\overline{g}^3)$ and can be neglected. With Eq. (4.60) the rate matrix $\mathcal{L}_{\text{relax}}$ associated to Eq. (4.53a) becomes:

$$\mathcal{L}_{\text{relax}} = \begin{pmatrix}
0 & \mathcal{L}_{00,11} & \mathcal{L}_{00,22} & 0 & 0 \\
0 & -\mathcal{L}_{00,11} & 0 & \mathcal{L}_{11,33} & \mathcal{L}_{11,44} \\
0 & 0 & -\mathcal{L}_{00,22} & \mathcal{L}_{22,33} & \mathcal{L}_{22,44} \\
0 & 0 & 0 & -\mathcal{L}_{11,33} - \mathcal{L}_{22,33} & 0 \\
0 & 0 & 0 & 0 & -\mathcal{L}_{11,44} - \mathcal{L}_{22,44}
\end{pmatrix}.$$

The eigenvalues and eigenvectors of this matrix and the associated time evolution of the elements $\sigma_{nn}(t)$ are given in Appendix G. In contrast to the simple analytic expression for the dephasing part the relaxation rate is not easy to extract as $P_{\text{relax}}(t) = \sum_n p_{nn}(t)$ consists of a sum of several exponential functions, cf. Eq. (4.15) and Appendix G. However, an analytical formula for $P(t)$ can be provided using Eq. (4.56).

Smallest eigenvalue approximation (SEA)

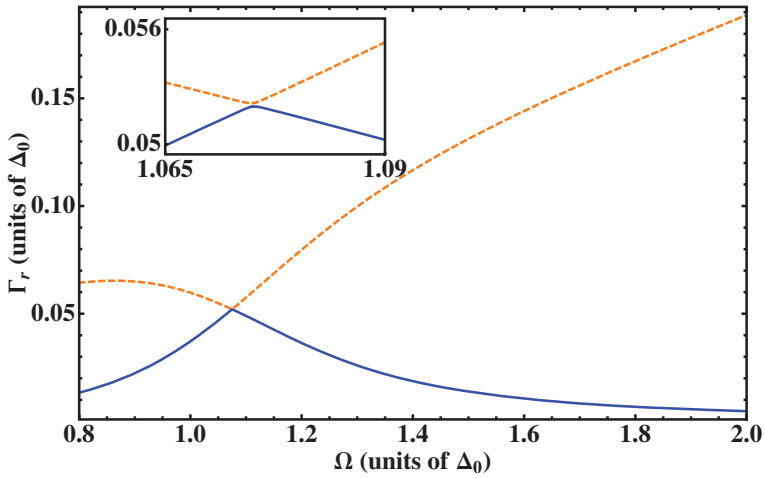

Figure 4.3: *The relaxation rate* Γ_r *given in Eq.* (4.62) *drawn against the oscillator frequency* Ω (*continuous blue line*). *We used* $\varepsilon = 0.5\Delta_0$, *corresponding to a frequency splitting* $\Delta_b = 1.118\Delta_0$, *coupling* $\overline{g} = 0.18\Delta_0$ *and the nonlinearity* $\overline{\alpha} = 0.02\hbar\Delta_0$. *The damping constant is* $\kappa = 0.0154$ *and* $\beta = 10(\hbar\Delta_0)^{-1}$. *At resonance* ($\Omega = \Delta_b - 3\overline{\alpha}/\hbar + \frac{\overline{g}^2\Delta_0^2}{\Delta_b^3}$) Γ_r *is maximal. For comparison also the second lowest eigenvalue is plotted* (*orange dashed line*). *The inset shows the two eigenvalues close to resonance.*

In order to get a better insight into the effect of the relaxation mechanism, we consider the long-time dynamics of the system. This means that the we direct our attention to the smallest eigenvalue of the relaxation coefficients, which dominates at long time, rather than to tackle the many relaxation contributions involved in the populations $\sigma_{nn}(t)$. We do not make the low temperature approximation discussed above. We restrict for simplicity to the three lowest qubit-NLO eigenstates $|0\rangle$, $|1\rangle$, $|2\rangle$ in Eq. (4.53a) and obtain using Eq. (4.60):

$$\mathcal{L}_{\text{relax}} = \begin{pmatrix} -\mathcal{L}_{11,00} - \mathcal{L}_{22,00} & \mathcal{L}_{00,11} & \mathcal{L}_{00,22} \\ \mathcal{L}_{11,00} & -\mathcal{L}_{00,11} - \mathcal{L}_{22,11} & \mathcal{L}_{11,22} \\ \mathcal{L}_{22,00} & \mathcal{L}_{22,11} & -\mathcal{L}_{00,22} - \mathcal{L}_{11,22} \end{pmatrix}. \quad (4.61)$$

We do not neglect $\mathcal{L}_{11,22}$ and $\mathcal{L}_{22,11}$, even if they are at least of order $\mathcal{O}(\overline{g}^3)$, because these contributions lift the degeneracy of the two lowest eigenvalues at resonance (see

Fig. 4.3). The smallest eigenvalue is:

$$\begin{aligned}\Gamma_{\rm r} \equiv & -\frac{\pi}{2}\Big\{-\sum_{n\neq m}\mathcal{L}_{nn,mm}+\Big[\Big(\sum_{n\neq m}\mathcal{L}_{nn,mm}\Big)^2-4(\mathcal{L}_{00,11}\mathcal{L}_{00,22}+\mathcal{L}_{11,00}\mathcal{L}_{00,22}\\ &+\mathcal{L}_{00,11}\mathcal{L}_{11,22}+\mathcal{L}_{11,00}\mathcal{L}_{11,22}+\mathcal{L}_{00,11}\mathcal{L}_{22,00}+\mathcal{L}_{11,22}\mathcal{L}_{22,00}+\mathcal{L}_{22,11}\mathcal{L}_{00,22}\\ &+\mathcal{L}_{11,00}\mathcal{L}_{22,11}+\mathcal{L}_{22,00}\mathcal{L}_{22,11})\Big]^{1/2}\Big\}. \end{aligned} \tag{4.62}$$

Additional detuning allows for a further simplification:
$\Gamma_r \approx \pi\mathcal{L}_{00,22}$ for $\Omega+3\overline{\alpha}/\hbar-\frac{\overline{g}^2\Delta_0^2}{\Delta_b^3}<\Delta_b$ and $\Gamma_r\approx\pi\mathcal{L}_{00,11}$ for $\Omega+3\overline{\alpha}/\hbar-\frac{\overline{g}^2\Delta_0^2}{\Delta_b^3}>\Delta_b$. In Fig. 4.3 the relaxation rate Γ_r in (4.62) is plotted as a function of the linear oscillator frequency Ω. It is maximal at resonance, whereas it decays for Ω being detuned from resonance. Additionally we plotted the second smallest eigenvalue of Eq. (4.61) for comparison (dashed orange line in Fig. 4.3).
In the long-time limit it then holds:

$$P_{\rm relax}(t)=(p_0-p_\infty)e^{-\Gamma_{\rm r}t}+p_\infty, \tag{4.63}$$

where, like in section 4.2.2, $p_0\equiv\sum_n p_{nn}(0)$. To obtain p_∞ we have in principle to find the steady-state solution of Eq. (4.53a). Here, we just assume for $t\to\infty$ a Boltzmann distribution for the TLS-NLO system, so that $\rho_{nn}(\infty)=Z^{-1}_{\rm TLS-NLO}\exp(-\beta\mathcal{E}_n)$ with $Z_{\rm TLS-NLO}=\sum_n\exp(-\beta\mathcal{E}_n)$. Thus,

$$p_\infty=\sum_n\sum_j\Big\{\cos\Theta\Big[\langle jg|n\rangle^2-\langle je|n\rangle^2\Big]+2\sin\Theta\langle jg|n\rangle\langle je|n\rangle\Big\}\rho_{nn}(\infty). \tag{4.64}$$

The formula for the long-time dynamics is then obtained,

$$P(t)=(p_0-p_\infty)\exp(-\Gamma_{\rm r}t)+p_\infty+\sum_{n>m}p_{nm}(0)\exp(-\Gamma_{nm}t)\cos(\omega_{nm}t). \tag{4.65}$$

To get further insight on the dominant frequencies we evaluate the Fourier transform of Eq. (4.65) according to

$$F(\omega)=2\int_0^\infty dt\cos\omega t P(t), \tag{4.66}$$

yielding

$$\begin{aligned}F(\omega) = & \ 2(p_0-p_\infty)\frac{\Gamma_{\rm r}}{\omega^2+\Gamma_{\rm r}^2}+2\pi p_\infty\delta(\omega)+\sum_{n<m}p_{nm}(0)\Gamma_{mn}\\ &\times\left[\frac{1}{\Gamma_{mn}^2+(\omega_{mn}+\omega)^2}+\frac{1}{\Gamma_{mn}^2+(\omega_{mn}-\omega)^2}\right].\end{aligned} \tag{4.67}$$

Partial secular approximation (PSA)

The PSA is an improvement to the FSA, where one accounts for corrections to the equations for the coherences due to dominant rotating terms $\omega_{nm} - \omega_{kl}$ in Eq. (4.52). The equation for the populations is still given by Eq. (4.53a). At low temperatures the dominant correction to the FSA comes from transitions involving the quasi-degenerate states $|1\rangle$ and $|2\rangle$. To solve the off-diagonal part we have to determine σ_{01}, σ_{02}, σ_{13}, σ_{23}, σ_{14}, and σ_{24}. With Eq. (4.52) the system of equations is:

$$\dot{\rho}_{nm}(t) = (-i\omega_{nm} + \pi\mathcal{L}_{nm,nm})\rho_{nm}(t) + \pi\mathcal{L}_{nm,jk}\rho_{jk}(t), \tag{4.68}$$

$$\dot{\rho}_{jk}(t) = \pi\mathcal{L}_{jk,nm}\rho_{nm}(t) + (-i\omega_{jk} + \pi\mathcal{L}_{jk,jk})\rho_{jk}(t) \tag{4.69}$$

with $\{(nm),(jk)\} = \{(01);(02)\}$,$\{(13);(23)\}$, or $\{(14);(24)\}$. The solution is:

$$\begin{aligned} \rho_{nm} &= c^{(+)}_{nm,jk} v^{(+)}_{nm,jk} \exp(\lambda^{(+)}_{nm,jk} t) + c^{(-)}_{nm,jk} v^{(-)}_{nm,jk} \exp(\lambda^{(-)}_{nm,jk} t), \\ \rho_{jk} &= c^{(+)}_{nm,jk} \exp(\lambda^{(+)}_{nm,jk} t) + c^{(-)}_{nm,jk} \exp(\lambda^{(-)}_{nm,jk} t), \end{aligned} \tag{4.70}$$

where the oscillation frequencies and the decay of the off-diagonal elements are given by [148]:

$$\lambda^{(+/-)}_{nm,jk} = \frac{1}{2}\left[\pi(\mathcal{L}_{nm,nm} + \mathcal{L}_{jk,jk}) - i(\omega_{nm} + \omega_{jk}) \pm R_{nm,jk}\right] \tag{4.71}$$

with

$$R_{nm,jk} = \sqrt{\left[\pi(\mathcal{L}_{nm,nm} - \mathcal{L}_{jk,jk}) - i(\omega_{nm} - \omega_{jk})\right]^2 + 4\pi^2 \mathcal{L}_{nm,jk}\mathcal{L}_{jk,nm}}. \tag{4.72}$$

The amplitudes of the oscillations are given through the coefficients:

$$c^{(+/-)}_{nm,jk} = \pm \frac{2\pi\mathcal{L}_{jk,nm}\rho^0_{nm} - \rho^0_{jk}\left[\pi(\mathcal{L}_{nm,nm} - \mathcal{L}_{jk,jk}) - i(\omega_{nm} - \omega_{jk}) \mp R_{nm,jk}\right]}{2R_{nm,jk}} \tag{4.73}$$

and

$$v^{(+/-)}_{nm,jk} = \frac{1}{2\pi\mathcal{L}_{jk,nm}}\left[\pi(\mathcal{L}_{nm,nm} - \mathcal{L}_{jk,jk}) - i(\omega_{nm} - \omega_{jk}) \pm R_{nm,jk}\right]. \tag{4.74}$$

We can calculate analytically the relaxation and dephasing part of $P(t)$. While the FSA allows a simple form for the dephasing rates, $\Gamma_{nm} = -\pi\mathcal{L}_{nm,nm}$, the PSA one is much more involved. As in case of the SEA the smallest eigenvalue dominates the dephasing behavior. The corresponding Bloch-Redfield tensors are found in Appendix F.

4.4 Numerical versus analytical predictions for dissipative qubit dynamics

In the following we compare the results for the dynamical quantity $P(t)$ and its Fourier transform, obtained by a numerical solution of Eq. (4.43), with the predictions of the approximations from section 4.3.

4.4.1 Low temperature

We start by focussing on low temperatures $\beta = 10/(\hbar\Omega)$ and compare the results for all three approaches (SEA, LTA, and PSA) to the numerical solution in Fig. 4.4. We recognize that the dynamics and the corresponding Fourier spectrum are well reproduced within the simple SEA approach as well as in the two LTA and PSA treatments and determined by the superposition of two oscillations. The best approximation is the PSA. In the following we use the SEA approach due to its simpler analytic form. To determine the effects of the nonlinearity onto the qubit dynamics we compare $P(t)$ and $F(\omega)$ with the corresponding linear case in Fig. 4.5. We choose $\Omega = \Delta_b$. Both in the nonlinear and in the corresponding linear case two oscillation frequencies are dominant. Due to the Bloch-Siegert shift, see Eq. (4.33), in both cases $\Omega = \Delta_b$ is not the exact resonance condition. However, in the nonlinear case the nonlinearity partly compensates the Bloch-Siegert shift, which also influences the relative peak heights, as we argued in section 4.2.2.

4.4.2 Higher temperatures

To investigate the influence of temperature we show in Fig. 4.6 $P(t)$ and the corresponding $F(\omega)$ for the same parameters as in Fig. 4.5, but at inverse temperature: $\beta = 3/(\hbar\Omega)$. By increasing the temperature higher oscillator levels are populated and influence the dynamics of the qubit. We calculated the corresponding equations for the long time dynamics within the SEA. The relaxation matrix $\mathcal{L}_{\text{relax}}$ for the rate Γ_{r} was calculated implementing higher levels, until $|8\rangle_{\text{eff}}$.
We plot for comparison also the linear oscillator case. We observe again the overall shift of the resonance frequencies to higher values and that a new shoulder arises in the Fourier spectrum. It corresponds to the transition frequency ω_{32} (see also Fig. 4.2 bottom). We checked numerically that the structure of the Fourier spectrum can be fully represented by summation of the six contributions in $P(t)$ with the frequencies ω_{10}, ω_{20}, ω_{32}, ω_{42}, ω_{13}, and ω_{14}. These six contributions arise due to the finite populations of the involved levels. Therefore the appearance of additional shoulders in the dynamics is a pure temperature effect, which is also seen in the corresponding linear case. The frequency shift induced by the nonlinearity is much larger for the higher levels. The effect of temperature is also reflected in the height of the dominating peaks, which is decreased for higher temperatures. The temperature can not influence which peak is dominant. This means by comparing Fig. 4.5 with Fig. 4.6 that in both figures in the nonlinear case the peak corresponding to ω_{10} dominates over the one corresponding to ω_{20}.
The use of a nonlinear oscillator instead of a linear one has advantages which rely in the fact that the energy spectrum of the nonlinear oscillator is not equidistant. Supposing that the TLS frequency Δ_b can be tuned, it is in case of the nonlinear oscillator possible to have the TLS in resonance with exactly one and only one nonlinear oscillator state transition. All other transitions are then off resonance/detuned. For the linear oscillator in resonance with the TLS the number of possible transitions is in principle infinite. Therefore we determine in the following the dynamics of the qubit

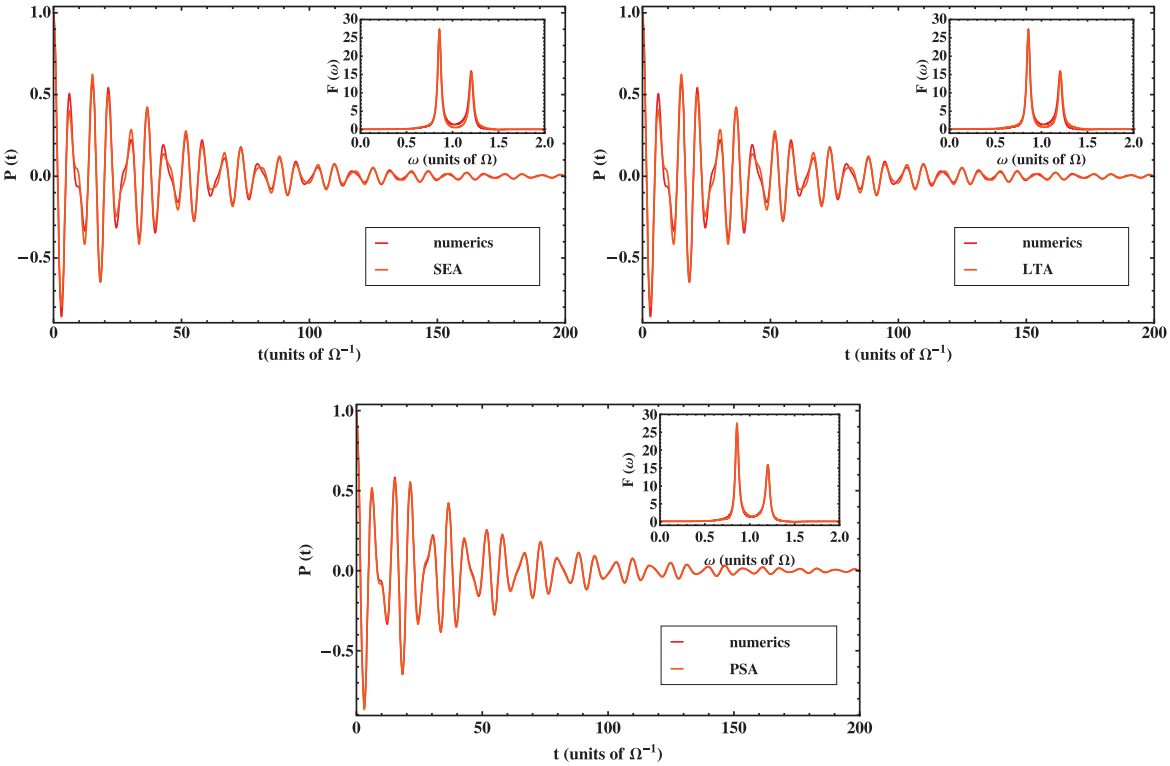

Figure 4.4: *Comparison of the behaviour of $P(t)$ and its Fourier transform $F(\omega)$ as obtained from the numerically exact solution (red line) and the three approximation schemes (orange line) discussed in the text. Top left: Smallest eigenvalue approximation (SEA), Top right: Low temperature approximation (LTA). Bottom: Partial secular approximation (PSA). The chosen parameters are: $\overline{\alpha} = 0.02\hbar\Omega$, $\overline{g} = 0.18\Omega$, $\varepsilon = 0\Omega$, $\kappa = 0.0154$ and $\beta = 10(\hbar\Omega)^{-1}$. The dynamics is well reproduced within all approximations, however, the agreement of the PSA with the exact numerics is the best. In the corresponding Fourier spectrum almost no deviations occur for all three approaches.*

by putting the qubit in resonance with the nonlinear oscillator transition $|3\rangle \rightarrow |2\rangle$, see Fig. 4.7.
We read off from Fig. 4.7 that the detuning compared to Fig. 4.6 results in the enhancement of the ω_{20}-peak, whereas the other dominating peak is shrinked. This is due to the different resonance conditions leading to opposite weights of the peaks for the nonlinear case in Fig. 4.7 compared to Fig. 4.6. However a peak corresponding to higher transitions is not seen. The reason for this is the small population of the higher oscillator levels involved.

4.5 Conclusions

To conclude, we determined the dynamics of a TLS which is coupled via a nonlinear oscillator to an environment described by an Ohmic spectral density. We restricted

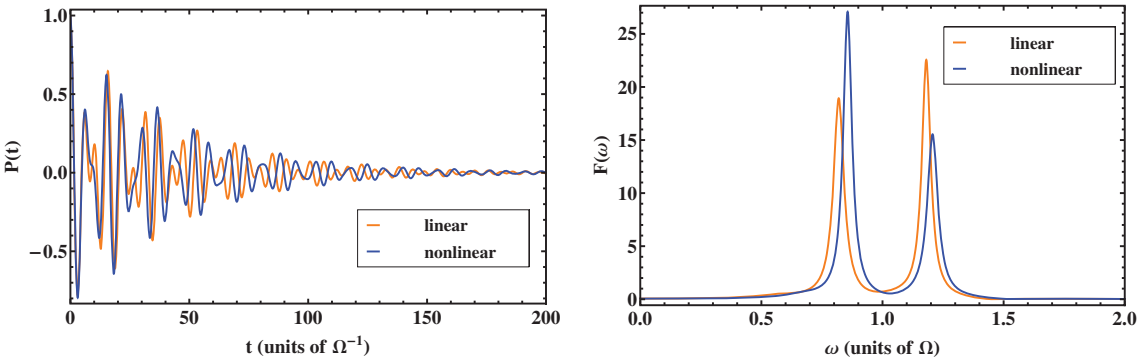

Figure 4.5: *Left:* $P(t)$ *for the linear (orange line) and nonlinear (blue line) case using the parameters:* $\overline{\alpha} = 0$ *or* $\overline{\alpha} = 0.02\hbar\Omega$*, respectively, and* $\overline{g} = 0.18\Omega$*,* $\kappa = 0.0154$*,* $\varepsilon = 0$*,* $\Delta_b = \Omega$*,* $\beta = 10(\hbar\Omega)^{-1}$*. Right: Corresponding Fourier transform* $F(\omega)$*.*

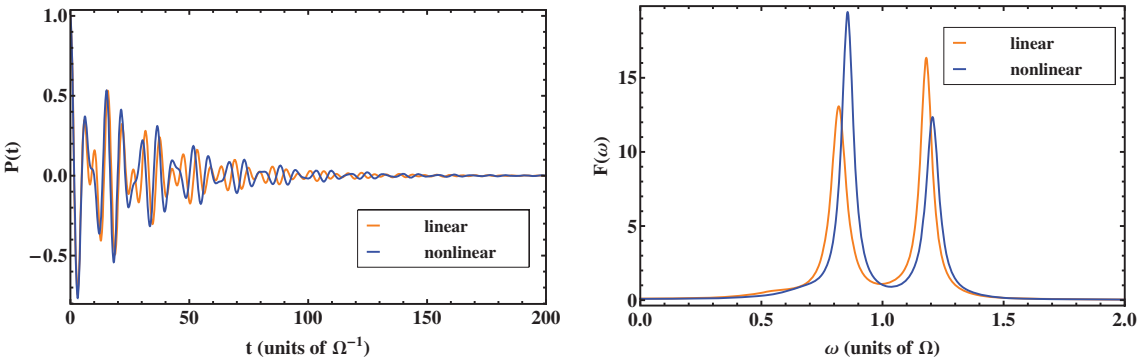

Figure 4.6: $P(t)$ *and its Fourier transform* $F(\omega)$ *for the parameters:* $\overline{\alpha} = 0.02\hbar\Omega$*,* $\overline{g} = 0.18\Omega$*,* $\kappa = 0.0154$*,* $\varepsilon = 0$*,* $\Delta_b = \Omega$ *as in Fig. 4.5, but* $\beta = 3(\hbar\Omega)^{-1}$*. For comparison we plotted the linear case in orange.*

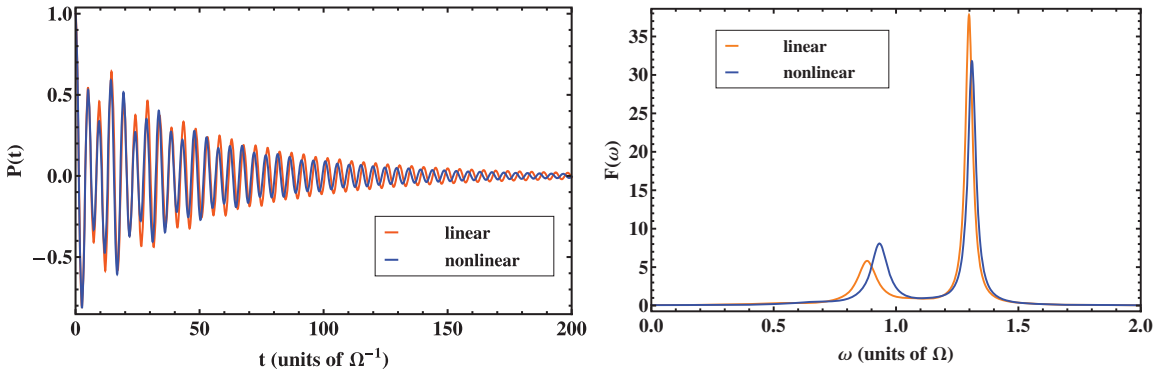

Figure 4.7: $P(t)$ *and its Fourier transform* $F(\omega)$ *for the parameters:* $\overline{\alpha} = 0.02\hbar\Omega$*,* $\overline{g} = 0.18\Omega$*,* $\kappa = 0.0154$*,* $\varepsilon = 0$*,* $\Delta_b = 1.18\Omega$*, corresponding to the oscillator transition from* $|3\rangle \rightarrow |2\rangle$*, and* $\beta = 3(\hbar\Omega)^{-1}$*. For comparison we plotted the linear case in orange.*

ourselves to the regime of weak nonlinearity, weak damping and moderate coupling of oscillator and TLS. To diagonalize the qubit-nonlinear-oscillator Hamiltonian we used Van Vleck perturbation theory, hence avoiding the use of the rotating wave approximation (RWA). Within the RWA and for vanishing nonlinearity our model would reduce to the Jaynes-Cummings Hamiltonian. In section 4.2.2, an analytical expression for the non-dissipative dynamics is given, which accounts for the infinite Hilbert space of the composed system. The influence of the nonlinearity onto the qubit dynamics is determined and compared to the linear case.
At low temperatures $k_BT < \hbar\Omega, \hbar\Delta_b$ this infinite Hilbert space can be truncated such that the transition processes between the ground state and the two first excited energy levels of the qubit-nonlinear-oscillator system dominate the dynamics. As in the linear case this yields a pronounced vacuum Rabi splitting.
To investigate the influence of the bath we solved the Bloch-Redfield Markovian master equation for the density-matrix of the qubit-nonlinear-oscillator system numerically. For an analytical treatment we considered three kinds of approximations: first a full secular approximation including a low temperature approximation, where all fast oscillating terms are neglected. Second an ansatz for the long-time dynamics allows a general expression for the relaxation and dephasing rates of the qubit. The third approximation was a partial secular approximation reproducing almost perfectly the exact numerical solution. A comparison of these three analytical approaches showed good agreement with the numerical solution. Finally, we investigated the effect of the non-equidistant energy spectrum of the nonlinear oscillator on the TLS dynamics. To do so, we allowed higher temperatures to populate higher levels and moreover we concentrated on the actual transition of the nonlinear oscillator from $|3\rangle \rightarrow |2\rangle$. We observed the rise of additional shoulders in the Fourier spectrum and showed that the shift in the transition frequencies is much larger if higher oscillator levels are involved.

Chapter 5

Effective bath approach

The results presented here have been published in [22].

The famous spin-boson model [1, 125, 130], introduced in section 2.2, consists of a two-level system (TLS) bilinearily coupled to a bath of harmonic oscillators. It allows to study the environmental influences on the coherent dynamics of a qubit. Reality is however often more complex, as the qubit might be coupled to other quantum systems besides to a thermal bath. For example, to read-out its state, a qubit is usually coupled to a read-out device.
In the following we mostly have in mind the flux qubit [75] read-out by a DC-SQUID. The latter mediates the dissipation originating from the surrounding electromagnetic bath and can be modeled both as a linear or nonlinear oscillator [75, 76, 77, 78, 104, 10, 88, 89, 11]. As shown in this chapter, this situation can be mapped, for weak TLS-read-out device coupling, to an effective spin-boson model.
From the theoretical side there are two different viewpoints to investigate the dynamics of a qubit coupled to an oscillator, with the latter in turn coupled to a thermal bath. The first way, demonstrated in chapter 4, is to consider the TLS and the oscillator as a single quantum system coupled to the bath, while the second, which is elaborated below, is an effective bath description where the effective environment seen by the qubit includes the oscillator and the original thermal bath. The mapping to an effective bath has been discussed for the case in which the TLS is coupled to a *harmonic* oscillator in [87]. Specifically, the spectral density of the effective bath acquires a broadened peak centered around the eigenfrequency of the oscillator. This case has been investigated in [93, 92, 91, 150, 147, 95, 151] by applying standard numerical and analytical methods established for the spin-boson model. All those works showed that the peaked structure of the effective bath is essential when the eigenfrequency of the TLS becomes comparable to the oscillator frequency.
So far the first approach was used in chapter 4 to describe a qubit-nonlinear oscillator (NLO) system in the deep quantum regime. Here the effects of the (harmonic) thermal reservoir can be treated using standard Born-Markov perturbation theory. The price to be paid, however, is that the Hilbert space of the qubit-nonlinear oscillator system is infinite, which requires for practical calculations its truncation invoking e.g. low

temperatures.
In contrast to the previous chapter we investigate here the case of a qubit-NLO system, with the latter being coupled to an Ohmic bath, within an effective bath description. Due to the nonlinearity of the oscillator, the mapping to a *linear* effective bath is not exact. In this case a temperature and nonlinearity dependent effective spectral density well captures the NLO influence on the qubit dynamics.
The chapter is organized as follows: In section 5.1 we introduce the model with the relevant quantities. In section 5.2 the mapping procedure is investigated and the effective spectral density for the corresponding linear case is given. Afterwards the mapping procedure is applied to the case of a qubit coupled to a nonlinear quantum oscillator. As a consequence of the mapping the determination of the effective spectral density is directly related to the knowledge of the susceptibility of the oscillator. We show how the susceptibility can be obtained from the steady-state response of a quantum Duffing oscillator in section 5.2.3. In section 5.3 the steady-state response of the dissipative quantum Duffing oscillator is reviewed and its susceptibility is put forward. The related effective spectral density is derived in section 5.4. In section 5.5 the qubit dynamics is investigated by applying the non-interacting blip approximation (NIBA) to the kernels of the generalized master equation which governs the dynamics of the population difference of the qubit. In section 5.6 an analytical formula for the qubit's population difference is derived. A comparison with the results of chapter 4, obtained within the first approach, is shown in section 5.7. Further analogies and differences with respect to the linear case are discussed. In section 5.8 conclusions are drawn.

5.1 Qubit-nonlinear oscillator-bath Hamiltonian

We consider a composed system built of a qubit, which is the system of interest, coupled to a nonlinear quantum oscillator (NLO), see Fig. 5.1. To read-out the qubit state we couple the qubit linearly to the oscillator with the coupling constant g, such that via the intermediate NLO dissipation also enters the qubit dynamics.

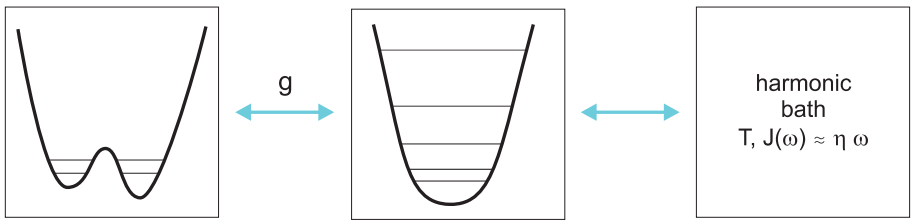

Figure 5.1: *Schematic representation of the composed system built of a qubit, an intermediate nonlinear oscillator and an Ohmic bath.*

The Hamiltonian of the composed system reads:

$$\hat{H}_{\rm tot} = \hat{H}_{\rm S} + \hat{H}_{\rm NLO} + \hat{H}_{\rm S+NLO} + \hat{H}_{\rm NLO+B} + \hat{H}_{\rm B}, \tag{5.1}$$

where

$$\begin{aligned}
\hat{H}_{\rm S} &= \frac{\hat{p}^2}{2\mu} + U(\hat{q}), \\
\hat{H}_{\rm NLO} &= \frac{1}{2M}\hat{P}_y^2 + \frac{1}{2}M\Omega^2\hat{y}^2 + \frac{\alpha}{4}\hat{y}^4, \\
\hat{H}_{\rm S+NLO} &= g\hat{y}\hat{q}, \\
\hat{H}_{\rm NLO+B} &= \sum_j \left[-c_j\hat{x}_j\hat{y} + \frac{c_j^2}{2m_j\omega_j^2}\hat{y}^2 \right], \\
\hat{H}_{\rm B} &= \sum_j \left[\frac{\hat{p}_j^2}{2m_j} + \frac{1}{2}m_j\omega_j^2\hat{x}_j^2 \right].
\end{aligned} \tag{5.2}$$

Here $\hat{H}_{\rm S}$ represents the qubit Hamiltonian, where μ is the particle's mass and $U(q)$ a one-dimensional double well potential with minima at $q = \pm q_0/2$. $\hat{H}_{\rm NLO}$ is the NLO Hamiltonian, see Eq. (1.29), where the parameter $\alpha > 0$ accounts for the nonlinearity. When the oscillator represents a SQUID used to read-out the qubit, the oscillator frequency Ω corresponds to the SQUID's plasma frequency. The dissipation on the NLO is modeled in the following by coupling it to an Ohmic bath, characterized by the spectral density [1], given in Eq. (2.12):

$$J(\omega) = \frac{\pi}{2}\sum_{j=1}^{\mathcal{N}} \frac{c_j^2}{m_j\omega_j}\delta(\omega - \omega_j) = \eta\omega = M\gamma\omega. \tag{5.3}$$

In the classical limit it corresponds to a white noise source, where η is a friction coefficient with dimensions mass times frequency.
In the following focus will be on the qubit dynamics in the presence of the dissipative nonlinear oscillator. Namely we will study the time evolution of the qubit's position as described by:

$$q(t) := {\rm Tr}\{\hat{\rho}_{\rm tot}(t)\hat{q}\} = {\rm Tr}_{\rm S}\{\hat{\rho}_{\rm red}(t)\hat{q}\}, \tag{5.4}$$

where $\hat{\rho}_{\rm tot}$ and $\hat{\rho}_{\rm red}$ are the total and reduced density operators, respectively. The latter is defined as:

$$\hat{\rho}_{\rm red} := {\rm Tr}_{\rm B}{\rm Tr}_{\rm NLO}\{\hat{\rho}_{\rm tot}\}, \tag{5.5}$$

where the trace over the degrees of freedom of the bath and of the oscillator is taken. In Fig. 5.2 the two different approaches to determine the qubit dynamics are depicted. In the first approach, which is elaborated in chapter 4, one first determines the eigenstates and eigenvalues of the composed qubit-oscillator system and then includes environmental effects via standard Born-Markov perturbation theory. The second approach exploits an effective description for the environment surrounding the qubit based on a mapping procedure. This will be investigated in the next section.

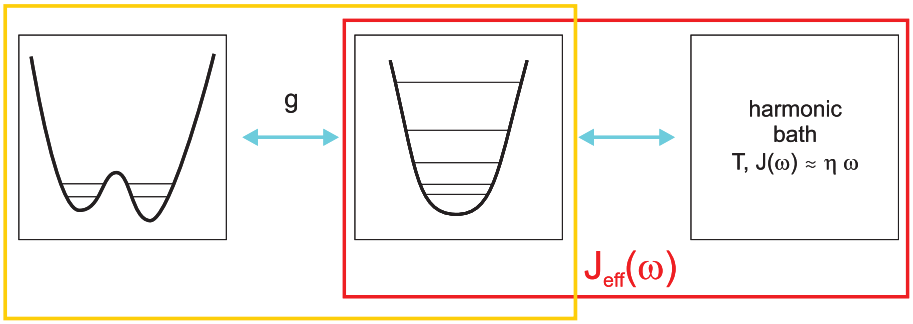

Figure 5.2: *Schematic representation of the complementary approaches available to evaluate the qubit dynamics: In the first approach one determines the eigenvalues and eigenfunctions of the composite qubit plus oscillator system (yellow box) and accounts afterwards for the harmonic bath characterized by the Ohmic spectral density $J(\omega)$. In the effective bath description one considers an environment built of the harmonic bath and the nonlinear oscillator (red box). In the harmonic approximation the effective bath is fully characterized by its effective spectral density $J_{\rm eff}(\omega)$.*

5.2 Mapping to an effective bath

The main aim is to evaluate the qubit's evolution described by $q(t)$. This can be achieved within an effective description using a mapping procedure. Thereby the oscillator and the Ohmic bath are put together, as depicted in Fig. 5.2, to form an effective bath. The effective Hamiltonian

$$\hat{H}_{\rm eff} \;=\; \hat{H}_{\rm S} + \hat{H}_{\rm Beff} \tag{5.6}$$

is chosen such that, after tracing out the bath degrees of freedom, the same dynamical equations for $q(t)$ are obtained as from the original Hamiltonian $\hat{H}_{\rm tot}$. Due to the nonlinear character of the oscillator an exact mapping implies that $\hat{H}_{\rm Beff}$ represents a nonlinear environment. We show in the following subsection using linear response theory that a linear approximation for $\hat{H}_{\rm Beff}$ is justified for weak coupling g. Then Eq. (5.6) describes an effective spin-boson problem, introduced in section 2.2, where

$$\hat{H}_{\rm Beff} \;=\; \frac{1}{2}\sum_{j=1}^{\mathcal{N}}\left[\frac{\hat{P}_j^2}{m_j} + m_j\omega_j^2\left(\hat{X}_j - \frac{d_j}{m_j\omega_j^2}\hat{q}\right)^2\right], \tag{5.7}$$

and the associated spectral density is:

$$J_{\rm eff}(\omega) = \frac{\pi}{2}\sum_{j=1}^{\mathcal{N}}\frac{d_j^2}{m_j\omega_j}\delta(\omega-\omega_j). \tag{5.8}$$

The Hamiltonian, Eq. (5.6), with Eq. (5.7) leads to coupled equations of motion [1, 125]:

$$\begin{aligned} \mu\ddot{\hat{q}}(t) + U'(\hat{q}) + \sum_{j=1}^{\mathcal{N}} \left(\frac{d_j^2}{m_j\omega_j^2}\hat{q} \right) &= \sum_{j=1}^{\mathcal{N}} d_j \hat{X}_j, \\ m_j\ddot{\hat{X}}_j + m_j\omega_j^2\hat{X}_j &= d_j\hat{q}, \end{aligned}$$

where $U'(\hat{q}) = \frac{d}{dq}U(\hat{q})$. By formally integrating the second equation of motion and inserting the solution into the first equation the well-known Langevin equation, derived in section 2.1.1, for the operator $\hat{q}$ is obtained. This, in turn, allows to obtain the Langevin equation for $q_{\text{eff}}(t) := \text{Tr}\{\hat{\rho}_{\text{eff}}\hat{q}(t)\}$ [1]:

$$\mu\ddot{q}_{\text{eff}} + \mu\int_0^t dt'\gamma_{\text{eff}}(t-t')\dot{q}_{\text{eff}} + \langle U'(\hat{q})\rangle_{\text{eff}} = 0, \tag{5.9}$$

with the effective damping kernel $\gamma_{\text{eff}}(t-t')$.
Notice that $\langle \dots \rangle_{\text{eff}}$ indicates the expectation value taken with respect to $\hat{\rho}_{\text{eff}}$, which is the density operator associated to $\hat{H}_{\text{eff}}$ [1]. In Laplace space, defined by

$$\begin{aligned} y(t) &= \frac{1}{2\pi i}\int_{\mathcal{C}} d\lambda y(\lambda)\exp(\lambda t), \\ y(\lambda) &= \int_0^\infty dt y(t)\exp(-\lambda t), \end{aligned} \tag{5.10}$$

we obtain from Eq. (5.9) the equation of motion:

$$\mu\lambda^2 q_{\text{eff}}(\lambda) + \mu\lambda\gamma_{\text{eff}}(\lambda)q_{\text{eff}}(\lambda) + \langle U'(\lambda)\rangle_{\text{eff}} = 0. \tag{5.11}$$

The real part $\gamma'_{\text{eff}}(\omega) = \text{Re}[\hat{\gamma}(\lambda = -i\omega)]$ of the effective damping kernel $\gamma_{\text{eff}}(t)$ is related to the spectral density via [1]:

$$\gamma'_{\text{eff}}(\omega) = \frac{J_{\text{eff}}(\omega)}{\mu\omega}. \tag{5.12}$$

The mapping for the case of zero nonlinearity α and Ohmic damping has already been discussed in [87]. There the influence of both the intermediate harmonic oscillator and the bath is embedded into an effective peaked spectral density given by:

$$J_{\text{eff}}^{\text{HO}}(\omega) = \frac{g^2\gamma\omega}{M(\Omega^2-\omega^2)^2 + M\gamma^2\omega^2}, \tag{5.13}$$

showing Ohmic low frequency behaviour $J_{\text{eff}}^{\text{HO}}(\omega) \underset{\omega\to 0}{\longrightarrow} g^2\gamma\omega/(M\Omega^4)$.

5.2.1 Equation of motion for the nonlinear Hamiltonian

As discussed above, the mapping requires the knowledge of the *reduced* dynamics of the system described by the variable $q(t)$. Therefore we start from the coupled equations of motion derived from the Hamiltonian $\hat{H}_{\rm tot}$ given in Eq. (5.1):

$$\mu\ddot{\hat{q}} + U'(\hat{q}) = -g\hat{y}, \tag{5.14a}$$

$$M\ddot{\hat{y}} + \eta\dot{\hat{y}} + M\Omega^2\hat{y} + \alpha\hat{y}^3 \;=\; -g\hat{q} + \hat{\xi}(t). \tag{5.14b}$$

According to Eq. (5.3), $\eta = M\gamma$ is the damping coefficient and

$$\hat{\xi}(t) = \sum_{j=1}^{\mathcal{N}} c_j \left[x_j^{(0)} \cos(\omega_j t) + \frac{p_j^{(0)}}{m_j\omega_j} \sin(\omega_j t) \right] - M\gamma\delta(t)\hat{y}(0) \tag{5.15}$$

a fluctuating force originating from the coupling to the bath. In order to eliminate $\hat{y}$ from the first equation of motion, we have to calculate $\hat{y}[\hat{q}(t)]$ from the second equation.

In the following we look at equations of motion for the expectation values resulting from Eqs. (5.14a) and (5.14b), i.e., we look at the evolution of $q(t) := \mathrm{Tr}\{\hat{\rho}_{\rm tot}\hat{q}(t)\}$ and $y(t) := \mathrm{Tr}\{\hat{\rho}_{\rm tot}\hat{y}(t)\}$. Since we want to calculate $y(t)$ we turn back to Eq. (5.1) and treat the coupling term $\hat{H}_{\rm S+NLO}$ as a perturbation, $gy_0q_0 \ll \hbar\Omega$, where we introduced the oscillator length $y_0 = \sqrt{\hbar/(M\Omega)}$. Then the use of linear response theory in this perturbation is justified and we find:

$$y(t) = \langle\hat{y}(t)\rangle_0 - \frac{i}{\hbar}\int_{-\infty}^{\infty} dt'\theta(t-t')\langle[\hat{y}(t),\hat{y}(t')]\rangle_0 g\langle\hat{q}(t')\rangle_0\theta(t') + \mathcal{O}(\alpha g^2), \tag{5.16}$$

where $\langle\ldots\rangle_0$ denotes the expectation value in the absence of the coupling g, which we assume it has been switched on at time $t_0 = 0$.

Notice that for a *linear* system, as for example the damped harmonic oscillator, the linear response *becomes exact*, such that the neglected corrections are at least of order $\mathcal{O}(\alpha g^2)$. Moreover, the time evolution of the expectation values is the same as in *the classical case*; this fact corresponds to the Ehrenfest theorem [1]. For *nonlinear* systems the expression in Eq. (5.16) is an approximation, because all orders in the perturbation are nonvanishing[1] .

In Laplace space, Eq. (5.16) yields:

$$\delta y(\lambda) = \chi(\lambda) g\langle\hat{q}(\lambda)\rangle_0 + \mathcal{O}(\alpha g^2), \tag{5.17}$$

where $\delta y(\lambda) = y(\lambda) - \langle\hat{y}(\lambda)\rangle_0$ and where $\chi(\lambda)$ is the Laplace transform of the response function or susceptibility:

$$\chi(t-t') = -\frac{i}{\hbar}\theta(t-t')\langle[\hat{y}(t),\hat{y}(t')]\rangle_0. \tag{5.18}$$

[1] An extension of the concept of linear response in case of nonlinear systems is the so called Volterra expansion, which provides a systematic perturbation series in the forcing [152].

Since $q(\lambda) - \langle\hat{q}(\lambda)\rangle_0 = \mathcal{O}(g)$, from Eqs. (5.14a) and (5.17) it follows:

$$\mu\lambda^2 q(\lambda) + g^2\chi(\lambda)q(\lambda) + \mathcal{O}(\alpha g^3, g^3) = -\langle U'(\lambda)\rangle - g\langle\hat{y}(\lambda)\rangle_0. \tag{5.19}$$

That is, we have a normalization of the mass, and a damping-like term due to the coupled equations of motion. The effect of the nonlinearity is embedded in the response function χ.
We assume in the following that in the absence of the coupling to the qubit the NLO and bath are in thermal equilibrium, which yields $\langle\hat{y}(t)\rangle_0 = 0$ for all times, and thus also: $\langle\hat{y}(\lambda)\rangle_0 = 0$.

5.2.2 Mapping of the equations of motion and generic form for the effective spectral density

By comparison of Eqs. (5.11) and (5.19) we can conclude that they yield the same dynamics if:

$$\langle U'(\lambda)\rangle_{\text{eff}} = \langle U'(\lambda)\rangle, \tag{5.20}$$

and the effective bath is chosen such that:

$$g^2\frac{\chi(\lambda)}{\mu\lambda} \;=\; \gamma_{\text{eff}}(\lambda). \tag{5.21}$$

By comparing the last equations with the relation in Eq. (5.12) and replacing $\lambda = -i\omega$ it follows:

$$J_{\text{eff}}(\omega) = -g^2\chi''(\omega), \tag{5.22}$$

where $\chi''(\omega)$ is the imaginary part of the susceptibility in Fourier space. We have now reduced the problem of finding the effective spectral density to that of determining the corresponding susceptibility. Notice that for a linear system the classical and quantum susceptibility coincide and are independent of the driving amplitude! In this case it is possible to calculate $\chi(\omega)$ directly from the classical equations of motion. For a generic nonlinear system, however, the classical and quantum susceptibilities differ.

5.2.3 Linear susceptibility of a Duffing oscillator

In order to evaluate the linear susceptibility, we solve the auxiliary problem of calculating the susceptibility of a quantum Duffing oscillator (DO), i.e., of the nonlinear quantum oscillator in Eq. (5.2) additionally driven by a periodic force with driving amplitude F and driving frequency ω_{ex}. The corresponding equation of motion is:

$$M\ddot{\hat{y}} + \eta\dot{\hat{y}} + M\Omega^2\hat{y} + \alpha\hat{y}^3 = -F\theta(t - t_0)\cos(\omega_{ex}t) + \hat{\xi}(t). \tag{5.23}$$

Application of linear response theory in the driving yields the equation for the expectation value of the position of the oscillator:

$$y(t) = \langle \hat{y}(t) \rangle_0 - \frac{i}{\hbar} \int_{t_0}^{\infty} dt' \theta(t-t') \langle [\hat{y}(t), \hat{y}(t')] \rangle_0 F \cos(\omega_{ex} t') + \mathcal{O}(F^2). \tag{5.24}$$

Using the symmetry properties of the susceptibility $\chi(\omega)$ we obtain in the steady-state limit:

$$\begin{aligned} y_{\rm st}(t) = \lim_{t_0 \to -\infty} y(t) &= \langle \hat{y}(t) \rangle_0 + F \cos(\omega_{ex} t) \chi'(\omega_{ex}) + F \sin(\omega_{ex} t) \chi''(\omega_{ex}) + \mathcal{O}(F^3) \\ &\equiv A \cos(\omega_{ex} t + \phi) + \mathcal{O}(F^3). \end{aligned} \tag{5.25}$$

Here the presence of the Ohmic bath implies $\lim_{t_0 \to -\infty} \langle \hat{y}(t) \rangle_0 = 0$. Notice that due to symmetry inversion of the NLO, corrections of $\mathcal{O}(F^2)$ vanish in Eq. (5.25). In Eq. (5.25) A and ϕ are the amplitude and phase of the steady-state response. It follows $\chi(\omega) = \frac{A}{F} \exp(-i\phi)$, such that $\chi''(\omega) = -\frac{A}{F} \sin\phi$.

5.3 Steady-state dynamics of a Duffing oscillator

So far we have reduced the problem of finding the effective spectral density to the one of determining the steady-state response of the Duffing oscillator in terms of the amplitude A and the phase ϕ. These quantities were derived in chapter 3 and [18], using the framework of a Bloch-Redfield-Floquet description of the dynamics of the DO. The results in chapter 3 are applicable in a wide range of driving frequencies around the one-photon resonance regime $\omega_{ex} = \Omega + \frac{3\alpha y_0^4}{4\hbar} \equiv \Omega_1$ for strong enough nonlinearities: $\frac{y_0 F}{2\sqrt{2}} \ll \frac{3}{4}\alpha y_0^4 \ll \hbar\Omega$.
As illustrated in chapter 3 and Ref. [18] the amplitude and phase are fully determined by the knowledge of the matrix elements of the stationary density matrix of the Duffing oscillator in the Floquet basis, see e.g. Eqs. (3.98)-(3.100) and (3.103) in chapter 3. There the master equation yielding the elements of the stationary density matrix is analytically solved in the low temperature regime $k_B T \ll \hbar\Omega$ imposing a partial secular approximation, yielding Eq. (3.103), and restricting to spontaneous emission processes only. Here we follow the same line of reasoning as in chapter 3 to evaluate the amplitude and phase: we impose the same partial secular approximation and consider low temperatures $k_B T < \hbar\Omega$. However, we include now both emission and absorption processes, i.e., we use the full dissipative transition rates as in Eq. (3.95) of chapter 3. The imaginary part of the linear susceptibility χ follows from the so obtained *nonlinear* susceptibility χ_{NL} in the limit of vanishing driving amplitudes:

$$\begin{aligned} \chi''(\omega_{ex}) &= \lim_{F \to 0} \chi''_{NL}(\omega_{ex}) \\ &= -\frac{y_0^4 J(\omega_{ex}) n_1^4(0) \frac{2\Omega_1}{|\omega_{ex}| + \Omega_1}}{y_0^4 J^2(\Omega_1) n_1^4(0) (2n_{th}(\Omega_1)+1)^2 + 4\hbar^2 (|\omega_{ex}| - \Omega_1)^2}, \end{aligned} \tag{5.26}$$

where

$$n_1(0) \;=\; \left[1 - \frac{3}{8\hbar\Omega}\alpha y_0^4\right]. \tag{5.27}$$

For consistency also $n_1^4(0)$ has to be treated up to first order in α only.
Moreover, we used the spectral density $J(\omega) = M\gamma\omega$ and the Bose function

$$n_{th}(\omega) = \frac{1}{2}\left[\coth\left(\frac{\hbar\omega}{2k_BT}\right) - 1\right], \tag{5.28}$$

which determine the weight of the emission and absorption processes.

5.4 Effective spectral density for a nonlinear system

The effective spectral density follows from Eqs. (5.22) and (5.26). It reads:

$$J_{\text{eff}}(\omega_{ex}) \;=\; g^2 \frac{\gamma\omega_{ex} n_1^4(0)\frac{2\Omega_1}{|\omega_{ex}|+\Omega_1}}{M\gamma^2\Omega_1^2(2n_{th}(\Omega_1)+1)^2 n_1^4(0) + 4M\Omega^2(|\omega_{ex}|-\Omega_1)^2}. \tag{5.29}$$

As in case of the effective spectral density $J_{\text{eff}}^{\text{HO}}$, Eq. (5.13), we observe Ohmic behaviour at low frequency. In contrast to the linear case, the effective spectral density is peaked at the shifted frequency $\Omega_1 = \Omega + \frac{3}{4\hbar}\alpha y_0^4$. Its shape approaches the Lorentzian one of the linear effective spectral density, but with peak at the shifted frequency, as shown in Fig. 5.3.

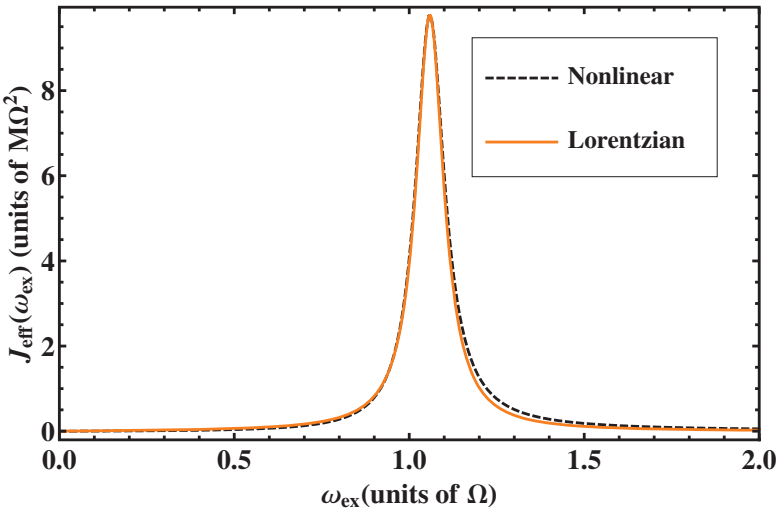

Figure 5.3: *Comparison of the effective spectral density* $J_{\text{eff}}(\omega)$ *and a Lorentz curve. The parameters are:* $\Omega = 1.0$, $y_0^4\alpha/(\hbar\Omega) = 0.08$ and $\gamma/\Omega = 0.097$, $\beta = 10(\hbar\Omega)^{-1}$.

While in chapter 3 and in [20, 18] the amplitude of the oscillator showed an antiresonant to resonant transition depending on the ratio of driving amplitude F and damping γ the effective spectral density displays only resonant behaviour.

5.5 Qubit dynamics

In the following we derive the dynamics of a qubit coupled to this effective nonlinear bath. Therefore we identify the system Hamiltonian $\hat{H}_{\rm S}$ introduced in Eq. (5.1) with the one of a qubit, denoted in the following as $\hat{H}_{\rm TLS}$. This is verified at low energies if the barrier height of the double well potential $U(\hat{q})$ is larger than the energy separation of the ground and first excited levels in each well. In this case the relevant Hilbert space can be restricted to the two-dimensional space spanned by the ground state vectors $|L\rangle$ and $|R\rangle$ in the left and right potential well, respectively [1]. We start defining the actual form of the qubit Hamiltonian and its interaction with the nonlinear oscillator and afterwards introduce its dynamical quantity of interest, the population difference $P(t)$.

5.5.1 Qubit

The Hamiltonian of the TLS (qubit), given in the localized basis $\{|L\rangle, |R\rangle\}$, is, see Eq. (1.23):

$$\hat{H}_{\rm TLS} = -\frac{\hbar}{2}\left(\varepsilon\sigma_z + \Delta_0\sigma_x\right), \tag{5.30}$$

where σ_i, $i = x, z$, are the corresponding Pauli matrices. The energy bias ε accounts for an asymmetry between the two wells and Δ_0 is the tunneling amplitude. The bias ε can be tuned for a superconducting flux qubit by application of an external flux $\Phi_{\rm ext}$ and vanishes at the so-called degeneracy point [74]. For $\varepsilon \gg \Delta_0$ the states $|L\rangle$ and $|R\rangle$ are eigenstates of $\hat{H}_{\rm TLS}$, corresponding to clockwise and counterclockwise currents, respectively.
The interaction in Eq. (5.2), defined already in Eq. (1.31), is conveniently rewritten as:

$$\begin{aligned} \hat{H}_{\rm TLS-NLO} &= g\hat{q}\hat{y} \\ &= \frac{g}{2\sqrt{2}} q_0\sigma_z y_0(\hat{a} + \hat{a}^\dagger) \\ &:= \hbar\overline{g}\sigma_z(\hat{a} + \hat{a}^\dagger). \end{aligned} \tag{5.31}$$

Likewise we express the nonlinear oscillator Hamiltonian as:

$$\begin{aligned}\hat{H}_{\mathrm{NLO}} &= \hbar\Omega\left(\hat{j}+\frac{1}{2}\right)+\frac{\alpha}{4}\hat{y}^4 \\ &= \hbar\Omega\left(\hat{j}+\frac{1}{2}\right)+\frac{\alpha y_0^4}{16}(\hat{a}+\hat{a}^\dagger)^4 \\ &:= \hbar\Omega\left(\hat{j}+\frac{1}{2}\right)+\frac{\overline{\alpha}}{4}(\hat{a}+\hat{a}^\dagger)^4.\end{aligned} \tag{5.32}$$

5.5.2 Population difference

The dynamics of a qubit is usually characterized in terms of the population difference $P(t)$ between the $|R\rangle$ and $|L\rangle$ states of the qubit, as defined in section 2.3:

$$\begin{aligned}P(t) &:= \langle\sigma_z\rangle \\ &= \mathrm{Tr}_{\mathrm{TLS}}\{\sigma_z\hat{\rho}_{\mathrm{red}}(t)\} \\ &= \langle \mathrm{R}|\hat{\rho}_{\mathrm{red}}(t)|\mathrm{R}\rangle - \langle \mathrm{L}|\hat{\rho}_{\mathrm{red}}(t)|\mathrm{L}\rangle,\end{aligned} \tag{5.33}$$

where $\hat{\rho}_{\mathrm{red}}(t)$ is the reduced density matrix of the TLS,

$$\hat{\rho}_{\mathrm{red}}(t) = \mathrm{Tr}_B\{\hat{\rho}_{\mathrm{eff}}(t)\}. \tag{5.34}$$

It is found after tracing out the degrees of freedom of the effective bath from the total density matrix $\hat{\rho}_{\mathrm{eff}}(t) = \exp^{-\frac{\mathrm{i}}{\hbar}\hat{H}_{\mathrm{eff}}t}\,\hat{\rho}_{\mathrm{eff}}(0)\exp^{\frac{\mathrm{i}}{\hbar}\hat{H}_{\mathrm{eff}}t}$. It follows that in the two level approximation $q_{\mathrm{eff}}(t) = \frac{q_0}{2}P(t)$, where $q_{\mathrm{eff}}(t)$ is the position operator expectation value introduced in section 5.2.
As we mapped the nonlinear system onto an effective spin-boson model, the evaluation of the population difference $P(t)$ of the TLS is possible using standard approximations developed for the spin-boson model [91, 92, 147]. Assuming a factorized initial condition $\hat{\rho}_{\mathrm{eff}}(0) = \hat{\rho}_{\mathrm{TLS}}(0)\exp(-\beta\hat{H}_{\mathrm{Beff}})/Z$, the population difference $P(t)$ fulfills the generalized master equation (GME) [1, 132]

$$\dot{P}(t) = -\int_0^t dt'[K^s(t-t')P(t') + K^a(t')], \quad t>0 \tag{5.35}$$

where $K^s(t-t')$ and $K^a(t-t')$ are symmetric and antisymmetric with respect to the bias, respectively. They are represented as a series in the tunneling amplitude. As an exact solution neither analytically nor numerically is available, due to the complicated form of the exact kernel, we impose in the following the so-called Non-Interacting Blip Approximation (NIBA) [1, 125] illustrated in section 2.3. Applying NIBA corresponds to truncating the exact kernels to first order in Δ_0^2 and is therefore perturbative in the tunneling amplitude of the qubit. It is justified in various regimes: it is exact at zero damping, otherwise it is only an approximation which works at best for zero bias and/or large damping and/or high temperature [1]. One finds within the NIBA

$$\begin{aligned}K^s(t) &= \Delta_0^2\exp(-S(t))\cos(R(t)), \\ K^a(t) &= \Delta_0^2\exp(-S(t))\sin(R(t)),\end{aligned} \tag{5.36}$$

where $S(\tau)$ and $R(\tau)$ are the real and imaginary part of the bath correlation function:

$$Q(\tau) = S(\tau) + iR(\tau) = \int_0^\infty d\omega \frac{G_{\text{eff}}(\omega)}{\omega^2} \left[\coth\left(\frac{\beta\hbar\omega}{2}(1-\cos(\omega t))\right) + i\sin(\omega t)\right], \tag{5.37}$$

where $G_{\text{eff}}(\omega) = \frac{q_0^2}{\pi\hbar} J_{\text{eff}}(\omega)$. In particular, upon introducing the dimensionless constant $\varsigma = \frac{\bar{g}^2}{\Omega^3}\frac{\gamma}{\pi} n_1^4(0)$, we obtain:

$$G_{\text{eff}}(\omega) \;=\; 2\varsigma\Omega^2 \frac{\omega \frac{2\Omega_1}{|\omega|+\Omega_1}}{\overline{\gamma}^2 + (|\omega| - \Omega_1)^2}, \tag{5.38}$$

where we used $\Omega_1 n_1^2(0) = \Omega + \mathcal{O}(\overline{\alpha}^2)$, and $\overline{\gamma}_{th} := \frac{2n_{th}(\Omega_1)+1}{2}\gamma$. Consequently, the dynamics of the qubit is fully determined by the knowledge of the correlation function $Q(\tau)$ and hence of the effective spectral density derived in section 5.4.
We now consider the qubit dynamics for the case of the effective nonlinear bath. Therefore we determine the actual form of the correlation functions $S(\tau)$ and $R(\tau)$. From Eq. (5.38) it follows:

$$\begin{aligned} S(\tau) &= X\tau + L\left[\exp(-\overline{\gamma}_{th}\tau)\cos(\Omega_1\tau) - 1\right] + Z\exp(-\overline{\gamma}_{th}\tau)\sin(\Omega_1\tau), \\ R(\tau) &= I - \exp(-\overline{\gamma}_{th}\tau)\left[N\sin(\Omega_1\tau) + I\cos(\Omega_1\tau)\right], \end{aligned} \tag{5.39}$$

where

$$\begin{aligned} I &= \frac{2\pi\varsigma\Omega^2}{\Omega_1^2 + \overline{\gamma}_{th}^2} \\ N &= -I\left(\frac{\Omega_1}{\overline{\gamma}_{th}} - \frac{\overline{\gamma}_{th}}{\Omega_1}\right) \\ X &= \frac{2}{\hbar\beta} I \\ L &= -\frac{I}{\overline{\gamma}_{th}} \frac{1}{\cosh(\beta\hbar\Omega_1) - \cos(\beta\hbar\overline{\gamma}_{th})}\left[\Omega_1 \sinh(\beta\hbar\Omega_1) - \overline{\gamma}_{th}\sin(\beta\hbar\overline{\gamma}_{th})\right] \\ Z &= -\frac{I}{\overline{\gamma}_{th}} \frac{1}{\cosh(\beta\hbar\Omega_1) - \cos(\beta\hbar\overline{\gamma}_{th})}\left[\overline{\gamma}_{th} \sinh(\beta\hbar\Omega_1) + \Omega_1\sin(\beta\hbar\overline{\gamma}_{th})\right]. \end{aligned} \tag{5.40}$$

Here we have neglected the contribution coming from the Matsubara term, which is verified if the temperature is high enough [1], i.e., $k_B T \gg \hbar\overline{\gamma}/(2\pi)$. Moreover, we applied in the contributions of the poles lying in the vicinity of $\pm\Omega_1$ the approximation: $2\Omega_1/(2\Omega_1 \pm i\overline{\gamma}_{th}) \approx 1$. This corresponds effectively to neglect certain $\mathcal{O}(\overline{\gamma}_{th})$ contributions.

5.6 Analytical solution for the nonlinear peaked spectral density

In this section we derive an analytical formula for the population difference $P(t)$ for the symmetric case ($\varepsilon = 0$), requiring weak damping strengths γ, such that a *weak*

damping approximation of the NIBA kernels is verified, specifically $\gamma/(2\pi\Omega) \ll 1$. As this calculation is analogue to the one illustrated in detail in [147], we only define the relevant quantities and give the main results.
Due to the convolutive form of Eq. (5.35) this integro-differential equation is solved by applying Laplace transform. In Laplace space it reads:

$$P(\lambda) = \frac{1 - \frac{1}{\lambda}K^a(\lambda)}{\lambda + K^s(\lambda)}, \tag{5.41}$$

where $P(\lambda) = \int_0^\infty dt \exp(-\lambda t)P(t)$ and analogously for $K^{a/s}(\lambda)$.
Consequently, the dynamics of $P(t)$ is determined if the poles of

$$\lambda + K^s(\lambda) = 0 \tag{5.42}$$

are found and the corresponding back transformation is applied. We transform the kernels in Eq. (5.36) in Laplace space and expand them up to first order in the damping. This procedure is called weak damping approximation (WDA) [147]. One obtains:

$$\begin{aligned} K^{(s)}(\lambda) &= \Delta_0^2 \int_0^\infty d\tau \exp(-\lambda\tau) \exp(-S_0(\tau)) \left\{\cos(R_0(\tau))[1 - S_1(\tau)]\right. \\ &\quad \left. - \sin(R_0(\tau))R_1(\tau)\right\}, \\ K^{(a)}(\lambda) &= 0, \end{aligned} \tag{5.43}$$

where the indices $\{0, 1\}$ denote the actual order in the damping. Specifically,

$$S(\tau) = S_0(\tau) + S_1(\tau) + \mathcal{O}(\gamma^2), \tag{5.44}$$
$$R(\tau) = R_0(\tau) + R_1(\tau) + \mathcal{O}(\gamma^2), \tag{5.45}$$

where

$$\begin{aligned} S_0(\tau) &= Y[\cos(\Omega_1\tau) - 1], \\ S_1(\tau) &= A\tau\cos(\Omega_1\tau) + B\tau + C\sin(\Omega_1\tau), \\ R_0(\tau) &= W\sin(\Omega_1\tau), \\ R_1(\tau) &= V\left(1 - \cos(\Omega_1\tau) - \frac{\Omega_1\tau}{2}\sin(\Omega_1\tau)\right). \end{aligned} \tag{5.46}$$

The zeroth order coefficients in the damping are given by:

$$\begin{aligned} Y &= -W\frac{\sinh(\beta\hbar\Omega_1)}{\cosh(\beta\hbar\Omega_1) - 1} \\ W &= \frac{4\overline{g}^2 n_1^4(0)}{\Omega_1\Omega(2n_{th}(\Omega_1) + 1)}, \end{aligned} \tag{5.47}$$

and the first order coefficients by:

$$\begin{aligned} A &= -\overline{\gamma}_{th} Y, \\ B &= \frac{2}{\hbar\beta} V \\ C &= -V \frac{\beta\hbar\Omega_1 + \sinh(\beta\hbar\Omega_1)}{(\cosh(\beta\hbar\Omega_1) - 1)(2n_{th}(\Omega_1) + 1)} \\ V &= \frac{2\overline{g}^2 n_1^4(0)\gamma}{\Omega_1^2 \Omega}. \end{aligned}$$

With this we are able to solve the pole equation for $P(t)$, Eq. (5.42), as an expansion up to first order in the damping around the solutions λ_p of the non-interacting pole equation, i.e., $\lambda^* = \lambda_p - \gamma\kappa_p + i\gamma\upsilon + \mathcal{O}(\gamma^2)$, as $\gamma/\Omega \ll 1$. Following Nesi et al. [147] the kernel is rewritten in the compact form:

$$K^{(s)}(\lambda) = \sum_{n=0}^{\infty} \int_0^{\infty} d\tau \exp(-\lambda\tau) \left\{ \Delta_{n,c}^2 \cos(n\Omega_1 t)[1 - S_1(\tau)] + \Delta_{n,s}^2 \sin(n\Omega_1 t) R_1(\tau) \right\}, \tag{5.48}$$

where

$$\begin{aligned} \Delta_{n,c} &= \Delta_0 \exp(Y/2) \sqrt{(2 - \delta_{n,0})(-i)^n J_n(u_0) \cosh\left(n \frac{\hbar\beta\Omega_1}{2}\right)}, \\ \Delta_{n,s} &= \Delta_0 \exp(Y/2) \sqrt{(2 - \delta_{n,0})(-i)^n J_n(u_0) \sinh\left(n \frac{\hbar\beta\Omega_1}{2}\right)}, \end{aligned} \tag{5.49}$$

and

$$\begin{aligned} u_0 &= i\sqrt{Y^2 - W^2} \\ &= i \left(\frac{4\overline{g}^2 n_1^4(0)}{(2n_{th}(\Omega_1) + 1)\Omega_1 \Omega} \right) \frac{1}{\sinh(\beta\hbar\Omega_1/2)}. \end{aligned} \tag{5.50}$$

To obtain analytical expressions, we observe that in the considered parameter regime where $\overline{g}/\Omega \ll 1$ and $\beta\hbar\Omega_1 > 1$ it holds $|u_0| < 1$. Following [147] this allows effectively a truncation to the $n = 0$ and $n = 1$ contributions in $K^{(s)}(\lambda)$ as the argument of the Bessel functions is small, leading to the following approximations:

$$\begin{aligned} \Delta_{0,c}^2 &= \Delta_0^2 \exp(Y) J_0(u_0) \approx \Delta_0^2 \exp(Y) \\ &\approx \Delta_0^2 \exp\left(-\frac{4\overline{g}^2 n_1^6(0)}{\Omega^2} \right) \approx \Delta_0^2 \left(1 - \frac{4\overline{g}^2 n_1^6(0)}{\Omega^2} \right) \\ \Delta_{1,c}^2 &= \Delta_0^2 \exp(Y) \sqrt{Y^2 - W^2} \cosh(\beta\hbar\Omega_1/2), \\ &\approx \Delta_0^2 \frac{4\overline{g}^2 n_1^6(0)}{\Omega^2}, \end{aligned} \tag{5.51}$$

where corrections of order $\mathcal{O}(\overline{g}^4/\Omega^4)$ have been neglected. Notice also that as our theory only accounts for corrections up to linear order in the nonlinearity $\overline{\alpha}$ we expand $n_1^6(0) = 1 - 6(3\overline{\alpha}/(2\hbar\Omega)) + \mathcal{O}(\overline{\alpha}^2)$. Solving the undamped pole equation yields:

$$\begin{aligned} \lambda_p^2 \equiv \lambda_\pm^2 &= -\frac{\Delta_{0,c}^2 + \Delta_{1,c}^2 + \Omega_1^2}{2} \pm \sqrt{\left(\frac{\Delta_{0,c}^2 - \Omega_1^2}{2}\right)^2 + \frac{\Delta_{1,c}^2}{2}\left(\Delta_{0,c}^2 + \frac{{\Delta_{1,c}}^2}{2} + \Omega_1^2\right)} \\ &:= -\Omega_\pm^2. \end{aligned} \tag{5.52}$$

The last two equations allow to determine the oscillation frequency. Finally, within the WDA the qubit's population difference is obtained as:

$$\begin{aligned} P(t) &= \exp(-\gamma\kappa_- t)\frac{\lambda_-^2 + \Omega_1^2}{\lambda_-^2 - \lambda_+^2}\left[\cos(\Omega_- t) - \frac{\gamma\kappa_-}{\Omega_-}\sin(\Omega_- t)\right] \\ &\quad + \exp(-\gamma\kappa_+ t)\frac{\lambda_+^2 + \Omega_1^2}{\lambda_+^2 - \lambda_-^2}\left[\cos(\Omega_+ t) - \frac{\gamma\kappa_+}{\Omega_+}\sin(\Omega_+ t)\right], \end{aligned} \tag{5.53}$$

where $\kappa_\pm = \kappa(\lambda_\pm)$, which is derived in detail in Eq. (B.1.) of [147]. Note that for a consistent treatment if $\mathcal{O}(\overline{g}^2)$ is kept we implicitly require $\gamma \ll \overline{g}$, as only the first order in the damping is taken into account.
We consider two possible resonance cases: First we choose the resonance condition $\Omega_1 = \Delta_{0,c}$, such that the oscillation frequencies are, to lowest order in $\overline{g}/\Omega$ and $\overline{\alpha}/(\hbar\Omega)$,

$$\begin{aligned} \Omega_\pm &= \Omega_1 \mp \frac{\Delta_{1,c}}{2} \\ &\approx \Omega + \frac{3}{\hbar}\overline{\alpha} \mp \overline{g}(1 - \frac{3}{2\hbar\Omega}\overline{\alpha}). \end{aligned} \tag{5.54}$$

As a consequence we obtain a nonlinearity-decreased vacuum Rabi splitting:

$$\hbar(\Omega_- - \Omega_+) = 2\hbar\overline{g}(1 - 3\overline{\alpha}/(2\hbar\Omega)), \tag{5.55}$$

which is in the same form also obtained in chapter 4. For comparison with chapter 4 we choose as second condition $\Delta_0 = \Omega$, such that to lowest order in $\overline{g}/\Omega$ and $\overline{\alpha}/(\hbar\Omega)$ we obtain:

$$\begin{aligned} \Omega_\pm &= \Omega + \frac{3\overline{\alpha}}{2\hbar} \mp \overline{g}\left(1 - \frac{9\overline{\alpha}}{4\hbar\Omega}\right), \\ \Omega_- - \Omega_+ &= 2\overline{g}(1 - 9\overline{\alpha}/(4\hbar\Omega)), \end{aligned} \tag{5.56}$$

which also agrees with the results of chapter 4.

5.7 Qubit dynamics within different approaches

We show in Fig. 5.4 a comparison of the analytic WDA formula Eq. (5.53), the numerical solution of the NIBA Eq. (5.35), denoted by NIBA, and the results obtained

in chapter 4 from a numerical solution of the Bloch-Redfield equations referred to as TLS-NLO approach. We observe that the dynamics is dominated by two frequencies and well reproduced within all three approaches. In the Fourier spectrum we observe tiny deviations of the resonance frequencies. There are two different reasons for these deviations: First the coupling strength $\overline{g}$ is large enough, that higher orders in the coupling yield a finite contribution in the effective bath description. Second Eq. (5.52) has to be expanded in both the nonlinearity and the coupling $\overline{g}$, which is not possible in the numerical program. However, as we derived above when expanding the analytic formula, we find up to lowest order in the coupling $\overline{g}$ and in the nonlinearity $\overline{\alpha}$ the same results. We emphasize that this small discrepancy is also seen for the corresponding linear system in the work of Hausinger et al. [148] when comparing the NIBA results in [147] with those of the Bloch-Redfield procedure. To clarify the above statements

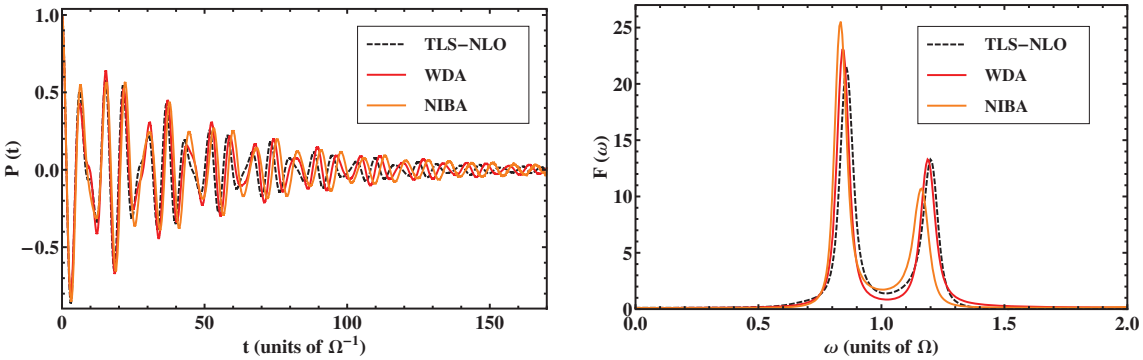

Figure 5.4: *Left: Comparison of the behaviour of $P(t)$ as obtained from the numerical solution of the Bloch-Redfield equations based on the TLS-NLO approach, chapter 4, the numerical solution of the NIBA equation, Eq. (5.35), and the analytical formula provided in Eq. (5.53). The chosen parameters are: $\overline{\alpha} = 0.02(\hbar\Omega)$, $\overline{g} = 0.18\Omega$, $\varepsilon = 0$, $\gamma/(2\pi\Omega) = 0.0154$ and $\beta = 10(\hbar\Omega)^{-1}$. The dynamics agree within all three approaches. Right: Corresponding Fourier transform of $P(t)$.*

we consider also the case that the coupling is weak, i.e., $\overline{g} \ll \gamma, \Omega_1$. In the regime where the coupling is much weaker than the nonlinearity ($\hbar\overline{g} \ll \overline{\alpha}$), Eq. (4.32) given in chapter 4 has to be expanded differently. Note that in this regime the results of Eq. (4.41) in chapter 4 are not applicable. A proper expansion allows in this regime to neglect $\mathcal{O}(\overline{g}^2)$ or higher if $\mathcal{O}(\overline{\alpha}^2)$ is neglected. The transition frequencies, when choosing $\Omega = \Delta_0$, are then determined by Eq. (4.32) of chapter 4:

$$\begin{aligned} \Omega_\pm &= \Omega + \frac{3}{2\hbar}\overline{\alpha} \mp \frac{1}{2}\sqrt{9\overline{\alpha}^2/\hbar^2} \\ &= \begin{cases} \Omega, \\ \Omega_1 = \Omega + 3\overline{\alpha}/\hbar. \end{cases} \end{aligned} \tag{5.57}$$

Applying also an expansion of Eq. (5.52) consistent with this parameter regime, we obtain:

$$-\Omega_\pm^2 = \frac{1}{2}\left(-\Omega^2 - \Omega_1^2 \pm \Omega^2 \mp \Omega_1^2\right), \tag{5.58}$$

such that:

$$\begin{aligned} \Omega_+ &= \Omega \\ \Omega_- &= \Omega_1 = \Omega + 3\overline{\alpha}/\hbar. \end{aligned} \tag{5.59}$$

The transition frequencies in Eqs. (5.57) and (5.59) coincide, and in Fig. 5.5 there is no deviation observed when comparing the three different approaches.

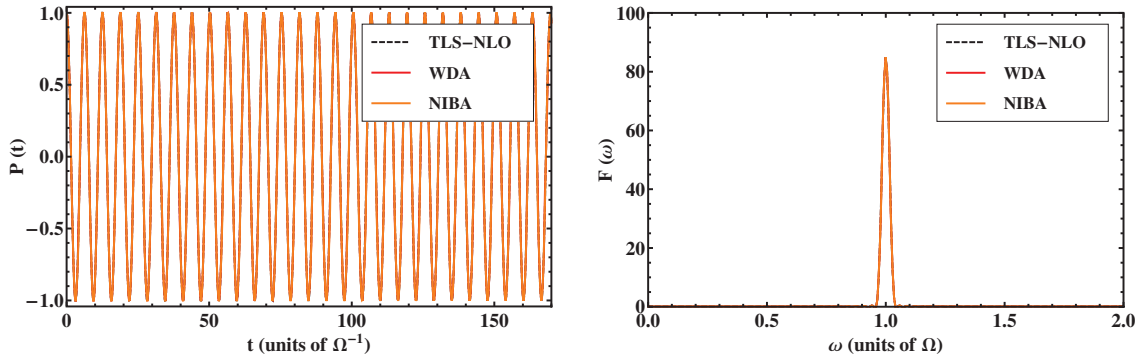

Figure 5.5: *Left: As in Fig. 5.4 but a weaker TLS-NLO coupling constant* $\overline{g} = 0.0018\Omega$. *Right: Corresponding Fourier transform of* $P(t)$.

5.7.1 Influence on the qubit dynamics due to the nonlinearity- A comparison of the NIBA for linear and nonlinear effective spectral densities

In this last section we want to address the effects of the nonlinearity on the qubit dynamics. The comparison of linear versus nonlinear case is done at level of the numerical solution of the NIBA equation and shown in Fig. 5.6. As already obtained in chapter 4, we observe that the transition frequencies are shifted to higher values compared to the linear case. Specifically, as it can be seen from Eqs. (5.54) and (5.56), the reduction is linear in $\overline{\alpha}$ for terms involving both nonlinearity and coupling. As a consequence also the amplitudes associated to the transitions are modified. Moreover, we observe a decrease of the vacuum Rabi splitting compared to the linear case. Consequently, the effect of the nonlinearity of the read-out device can be observed in the qubit dynamics.

5.8 Conclusions

In this chapter we determined the dynamics of a qubit coupled via a nonlinear oscillator (NLO) to an Ohmic bath within an effective bath description. We investigated an approximate mapping procedure based on linear response theory, which is applicable in case of weak nonlinearities and small to moderate qubit-NLO coupling. We

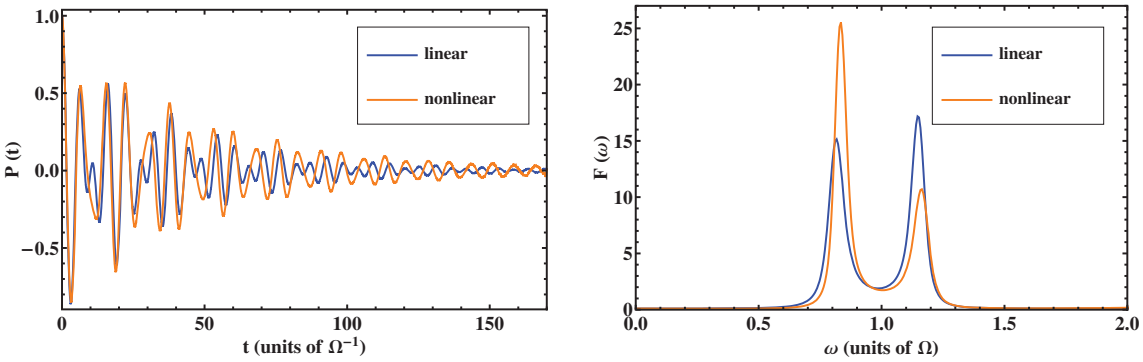

Figure 5.6: *Left:* $P(t)$ *within the NIBA when using the linear and the nonlinear effective spectral densities, Eqs. (5.13) and (5.29) respectively. Parameters are:* $\overline{\alpha} = 0.02(\hbar\Omega)$ *or* $\overline{\alpha} = 0$ *respectively,* $\overline{g} = 0.18\Omega$, $\varepsilon = 0\Omega$, $\gamma/(2\pi\Omega) = 0.0154$ *and* $\beta = 10(\hbar\Omega)^{-1}$. *Right: Corresponding Fourier transform of* $P(t)$. *The effect of the nonlinearity is to increase the resonance frequencies with respect to the linear case. As a consequence the relevant peak heights change.*

determined the effective spectral density in terms of the qubit-oscillator coupling and the linear susceptibility of a nonlinear oscillator. The susceptibility was calculated for practical purposes from the periodically driven counterpart of the original nonlinear oscillator, yielding an analytical expression for the effective spectral density valid at low temperatures. The so obtained spectral density shows resonant behaviour, specifically almost a Lorentzian form for the considered parameter regime, and is peaked at a shifted frequency, namely at the one-photon resonance between ground state and first excited state of the nonlinear oscillator. Moreover, this effective spectral density acquires a temperature dependence and behaves Ohmic at low frequencies. Based on the effective spectral density the qubit dynamics is investigated within the NIBA approximation. In addition an analytical formula for the qubit dynamics is provided, which describes correctly the dynamics at low damping. These results were compared to the numerical solution in chapter 4, where the Bloch-Redfield equations for the density matrix of the coupled qubit nonlinear oscillator system (TLS-NLO) are solved. These latter equations have the same regime of validity as those of the effective bath approach, namely weak nonlinearities $\overline{\alpha}/(\hbar\Omega) \ll 1$, small qubit-nonlinear oscillator coupling $\overline{g}/\Omega \ll 1$ and low temperatures $k_B T/(\hbar\Omega) \ll 1$. In this regime we expect an overall agreement of the two approaches. Exemplarily the predictions of the two approaches were analyzed for two possible coupling strengths $\overline{g}$. We emphasize that parameters like temperature and damping and especially the strength of the coupling $\overline{g}$ and nonlinearity $\overline{\alpha}$ determine the appropriate form of the expansions in the different regime of parameters. Due to the tunability of the parameters various qubit dynamics are possible. In special, near at at resonance the same analytical results are predicted within the two approaches up to first order in the coupling and nonlinearity. In agreement with chapter 4 we observed the following effects due to the nonlinearity: In the regime $\overline{g} \gg \overline{\alpha}/\hbar$ a vacuum Rabi splitting is observed. The transition frequencies of

the two dominating peaks are shifted to larger values compared to the linear case. As a consequence also the amplitudes of the coherent oscillations of the population difference $P(t)$ are modified. Moreover, the vacuum Rabi splitting is decreased due to the nonlinearity.
We conclude that, as in case of the corresponding linear system [147, 148], the effective bath description provides an alternative approach to investigate the complex dynamics of the qubit dissipative NLO system.

Chapter 6

Conclusions and perspectives

The main aim of this thesis was to clarify the effects on the qubit dynamics of the coupling to a read-out device, a DC-SQUID, which is modeled as a nonlinear oscillator in the deep quantum regime. The latter, in turn, is coupled to an Ohmic environment. To this extent we also investigated the interplay of driving and nonlinearity on the dynamics of dissipative quantum oscillators.
In the introduction we first gave an insight into the various experimental realisations starting from the classical regime and ending up in the deep quantum regime. Additionally an overview of the corresponding theoretical research achievements was presented. To account for dissipative effects within a quantum description we introduced in chapter 2 the Ullersma-Caldeira-Leggett model, the Feynman-Vernon path integral formalism and focussed on the famous spin-boson model. In the last part of chapter 2 we defined the dynamical quantity of interest, the qubit's population difference, whose evolution characterizes the qubit dynamics.
In this thesis we elaborated two complementary approaches to describe the qubit-nonlinear oscillator-bath system and showed their agreement. The first is based on considering the qubit and SQUID as composite system. In a second step dissipative effects are included. This procedure is perturbative in the qubit-SQUID coupling and in the nonlinearity of the SQUID. This approach is based on degenerate perturbation theory, in particular van Vleck perturbation theory, thereby focussing on the case that the qubit transition frequency between its two eigenstates is at or in the vicinity of a certain transition of two nonlinear oscillator levels. The second approach to describe the qubit-nonlinear oscillator-bath system is based on the following observation: As the SQUID mediates the dissipation, which originates from the bath, to the qubit, the qubit sees an effective environment formed by SQUID and bath. Due to the fact that the SQUID acts as a 'band pass' for the environmental frequencies, the qubit feels an effective bath characterized by an effective spectral density of structured form; i.e., the spectral density is peaked at the SQUID's eigenfrequency. Consequently, the second approach is based on this effective bath description.
To determine the effective spectral density associated with the SQUID acting as nonlinear undriven oscillator, the knowledge about the behaviour of a dissipative nonlinear quantum oscillator is essential. In chapter 3 we therefore developed two different ap-

proaches to describe the dissipative dynamics of the quantum Duffing oscillator, which is the driven counterpart of our nonlinear quantum oscillator. The first approach is based on the exact Floquet states of the driven harmonic oscillator. It is applicable off resonance, i.e., when the driving frequency is far off the frequency associated to a certain transition between two nonlinear oscillator levels. It is thus perturbative in the driving and in the nonlinearity and the energy scale associated with the driving can overcome the shift introduced by the nonlinearity. The second approach in contrast is applicable at and in the vicinity of such an N-photon resonance. It is perturbative in both driving and nonlinearity and in particular the energy scale of the driving is smaller than the one introduced by the nonlinearity. In the regime of low driving amplitudes both approaches can be combined to cover a large range of driving frequencies. In contrast to previous works [16, 17, 18, 19], the application of a rotating wave approximation has been avoided. We calculated the nonlinear response of the dissipative system for the special case of a one-photon resonance by solving a Born-Markov-Floquet master equation and determined the characteristic antiresonance, which originates from the very special degeneracy of the nonlinear oscillator. An extension of the first approach including dissipation is a very hard task as shown in detail in chapter 3. It remains to be clarified, whether a full analytical solution of the dissipative dynamics can be given for this approach at all. We want to emphasize that while the classical counterpart of the Duffing oscillator exhibits hysteresis, the quantum system can show an antiresonant response and so a completly different behaviour. This is a first indicator of how important nonlinear systems are, when transitions between the quantum and classical regime are investigated.

In chapter 4 we focussed on the composed qubit-nonlinear oscillator system and determined first the corresponding eigensystem in analytic form up to first order in the nonlinearity and up to second order in the qubit-oscillator coupling. This allowed us to derive the effects of the nonlinearity on the qubit dynamics as well as on the Bloch-Siegert shift. Moreover, the nonlinearity results in an decreased vacuum Rabi splitting. We observed in the low temperature regime that the qubit dynamics is dominated by the transition frequencies between the ground state and the two first excited energy levels. Additionally, the transition frequencies of the composite system are shifted to higher values compared to the corresponding linear case and also the weights of the transitions are modified due to the nonlinearity. Via a Born-Markov master equation, restricting to weak coupling to the bath, we accounted for dissipative effects and derived three different analytical approaches, covering the qubit dynamics. The first was a full secular approximation, where on top a low temperature approximation was applied. Within the second approach an ansatz for the long time dynamics is obtained, which yields approximate general expressions for the relaxation and dephasing rates of the qubit. The third approach is a partial secular approximation showing almost perfect agreement with the exact numerical solution. A comparison of these analytical approaches with the numeric solution showed good agreement.

Chapter 5 is dedicated to the effective bath description. As, due to the nonlinearity of the SQUID, an exact mapping of the composite SQUID-bath system to an effective bath is not possible, we investigated an approximate mapping procedure based

on linear response theory. Then the effective spectral density can be related to the susceptibility of the nonlinear oscillator, so that an analytic expression for the effective spectral density is obtained. To determine the susceptibility of a nonlinear quantum oscillator we considered its driven counterpart, the nonlinear quantum Duffing oscillator within linear response theory in the driving amplitude. The so obtained effective spectral density is peaked at a shifted frequency compared to the linear case and becomes temperature-dependent. Having derived the actual form of the effective spectral density, the qubit dynamics can be investigated both numerically and analytically using standard procedures elaborated for the spin-boson problem. An analytic formula for the population difference, covering the qubit dynamics, is derived in the weak damping regime using the non-interacting blip approximation. The formula allows us an easy insight in the qubit's behaviour. A comparison of the numerical solution with the analytic formula showed good agreement. Moreover, a direct comparison with the approach of chapter 4 based on the Bloch-Redfield equations is performed. In agreement with chapter 4 we observed that the transition frequencies are shifted to higher values compared to the linear case. Consequently, also the amplitudes of the coherent oscillations entering the qubit's population difference are modified.
Both complementary approaches, introduced in Fig. 1.1, capture very well the qubit dynamics and agree nicely up to first order in the qubit-oscillator coupling and nonlinearity.
We want to emphasize that, to our knowledge, this is the first time that the quantum Duffing oscillator has been investigated beyond a rotating wave approximation and the first time that an effective spectral density for a SQUID acting as nonlinear oscillator has been derived. We also compared the linear and nonlinear effective spectral densities, originating when the SQUID is treated either as linear or nonlinear oscillator, respectively. The overall results for the qubit dynamics show a shift to higher transition frequencies compared to the linear case and as a consequence modifications of the weights of the oscillation amplitudes. This means that within both approaches the effect of the nonlinearity can be observed in the qubit dynamics.
Hopefully the use of nonlinear effects will allow to improve read-out schemes. This is already the case for SQUIDs used as a Josepson bifurcation amplifiers in the semiclassical regime. But additional new relaxation mechanisms could also occur: Due to the non-equidistant energy spectrum of the nonlinear quantum oscillator the SQUID could possible no more act as a band pass for a certain frequency as in the linear case, but a whole bunch of frequencies originating from the nonlinear oscillator could influence the qubit dynamics. However, due to the complexity of the system, which offers different dynamical regimes, there is still a large variety of possibilities to improve qubit read-out.
We hopefully convinced the reader that nonlinear oscillators are an interesting topic to study. First, they give insight into the classical to quantum transition, as their system's response changes completely. Second, quantum computation architectures, for example qubit read-out devices, could also benefit from the use of nonlinear behaviours. We are looking forward to see the first realisation of a qubit-nonlinear SQUID-system in the deep quantum regime. I wish that this work can help to clarify the understanding

of the behaviour of coupled nonlinear systems including dissipative effects, and that quantum computation issues can benefit from this work.

Appendix A

Fourier components

In this appendix we evaluate the matrix elements of the perturbation $\hat{V}_\alpha$ on the Floquet basis of the driven linear oscillator as well as the Fourier coefficients $v_{kj}^{(n)}$.

$$
\begin{aligned}
{}_0\langle\phi_k(t)|\hat{V}_\alpha|\phi_j(t)\rangle_0 &= \frac{\alpha}{4}\int_{-\infty}^{\infty} dy'dy''\ {}_0\langle\phi_k(t)|y'\rangle\langle y'|\hat{y}^4|y''\rangle\langle y''|\phi_j(t)\rangle_0 \qquad \text{(A.1)}\\
&= \frac{\alpha}{4}\int_{-\infty}^{\infty} dy\overline{\phi}_k(y)\left[y+\xi(t)\right]^4\overline{\phi}_j(y)\\
&= \frac{\alpha}{4}\int_{-\infty}^{\infty} dy\overline{\phi}_k(y)\left[y^4+4\xi(t)y^3+6\xi(t)^2y^2\right.\\
&\quad \left.+4\xi(t)^3y+\xi(t)^4\right]\overline{\phi}_j(y)\\
&= \sum_n \exp(-in\omega_{ex}t)\underbrace{{}_0\langle\phi_k(t)|\hat{V}_\alpha|\phi_j(t)\rangle_0^{(n)}}_{\equiv v_{kj}^{(n)}}. \qquad \text{(A.2)}
\end{aligned}
$$

The Fourier coefficients $v_{kj}^{(n)}$ are given, using the notation $A_\xi \equiv \frac{F}{M(\omega_{ex}^2-\Omega^2)}$, by:

$$
\begin{aligned}
v_{kj}^{(0)} &= \frac{\alpha}{4}\left[\delta_{kj}\left(\frac{3}{2}(2j+1)y_0^2A_\xi^2+\frac{3}{2}(j(j+1)+\frac{1}{2})y_0^4+\frac{3}{8}A_\xi^4\right)\right. \qquad \text{(A.3)}\\
&\quad +\delta_{k,j+2}\left(\frac{3}{2}y_0^2A_\xi^2+y_0^4(j+\frac{3}{2})\right)\sqrt{(j+1)(j+2)}\\
&\quad +\delta_{k,j-2}\left(\frac{3}{2}y_0^2A_\xi^2+y_0^4(j-\frac{1}{2})\right)\sqrt{j(j-1)}\\
&\quad +\delta_{k,j+4}\frac{y_0^4}{4}\sqrt{(j+1)(j+2)(j+3)(j+4)}\\
&\quad \left.+\delta_{k,j-4}\frac{y_0^4}{4}\sqrt{j(j-1)(j-2)(j-3)}\ \right],
\end{aligned}
$$

$$
\begin{aligned}
v_{kj}^{(\pm 1)} &= \frac{\alpha}{4}\left[\delta_{k,j+1}\left(\frac{3}{2\sqrt{2}}\sqrt{j+1}y_0A_\xi^3+\frac{3!\sqrt{2}}{4}(j+1)\sqrt{j+1}A_\xi y_0^3\right)\right. \\
&+\delta_{k,j-1}\left(\frac{3}{2\sqrt{2}}\sqrt{j}y_0A_\xi^3+\frac{3!\sqrt{2}}{4}j\sqrt{j}A_\xi y_0^3\right) \\
&+\delta_{k,j+3}\sqrt{(j+3)(j+2)(j+1)}\frac{2^{3/2}}{4}y_0^3A_\xi \\
&\left.+\delta_{k,j-3}\sqrt{j(j-1)(j-2)}\frac{2^{3/2}}{4}y_0^3A_\xi\right],
\end{aligned}
\tag{A.4}
$$

$$
\begin{aligned}
v_{kj}^{(\pm 2)} &= \frac{\alpha}{4}\left[\delta_{kj}\left(\frac{3}{4}(2j+1)y_0^2A_\xi^2+\frac{1}{4}A_\xi^4\right)\right. \\
&+\delta_{k,j+2}\frac{3}{4}y_0^2A_\xi^2\sqrt{(j+1)(j+2)} \\
&\left.+\delta_{k,j-2}\frac{3}{4}y_0^2A_\xi^2\sqrt{j(j-1)}\right],
\end{aligned}
\tag{A.5}
$$

$$
\begin{aligned}
v_{kj}^{(\pm 3)} &= \frac{\alpha}{4}\left[\delta_{k,j+1}\frac{1}{2\sqrt{2}}\sqrt{j+1}y_0A_\xi^3\right. \\
&\left.+\delta_{k,j-1}\frac{1}{2\sqrt{2}}\sqrt{j}y_0A_\xi^3\right],
\end{aligned}
\tag{A.6}
$$

$$
v_{kj}^{(\pm 4)} = \frac{\alpha}{4}\left[\frac{1}{16}A_\xi^4\right]\delta_{kj}. \tag{A.7}
$$

Appendix B

Rotating wave approximation for a driven linear oscillator

The quantum Duffing oscillator has mainly been studied within a rotating wave approximation (RWA), applicable if the driving amplitude is not large and the driving frequency is in the vicinity of the eigenfrequency of the nonlinear oscillator. To give a first insight we consider this approximation for the linear case. By applying the transformation $R = \exp(i\omega_{ex}\hat{a}^\dagger\hat{a}t)$ to the time-dependent Hamiltonian of the driven harmonic oscillator and neglecting all fast rotating terms we result in:

$$\hat{H}_{\text{RWA}}|\phi_{j,\ \text{RWA}}\rangle = \epsilon_{j,\ \text{RWA}}|\phi_{j,\ \text{RWA}}\rangle, \tag{B.1}$$

where

$$\hat{H}_{\text{RWA}} = \hbar(\Omega + \frac{1}{2} - \omega_{ex})\hat{j} + \frac{y_0 F}{2\sqrt{2}}(\hat{a} + \hat{a}^\dagger) \tag{B.2}$$

$$|\phi_{j,\ \text{RWA}}(t)\rangle = \exp(i\omega_{ex}\hat{a}^\dagger\hat{a}t)|\phi_j(t)\rangle. \tag{B.3}$$

The structure of the Hamiltonian is the same as obtained within the exact Floquet treatment, see Eq. (3.48), if we set $\alpha = 0$, $j = n$ and $n' = k$. The driving term is treated by defining the translation-operator [13] to exactly diagonalize $\hat{H}_{\text{RWA}}$[1]: The quasienergies obtain a global energy shift proportional to the driving and the deviation of eigenfrequency and driving frequency:

$$\epsilon_{j,\ \text{RWA}} = \hbar\left(\Omega + \frac{1}{2} - \omega_{ex}\right) j + \frac{F^2}{8M\Omega(\omega_{ex} - \Omega)}. \tag{B.4}$$

The eigenstates are obtained by applying a translation operator:

$$\begin{aligned} |\phi_{j,\ \text{RWA}}\rangle &= \exp\left[\frac{y_0 F}{2\sqrt{2}\hbar(\Omega - \omega_{ex})}(\hat{a} - \hat{a}^\dagger)\right]|j\rangle \\ &= |j\rangle + \frac{y_0 F\sqrt{j}}{2\sqrt{2}\hbar(\Omega - \omega_{ex})}|j-1\rangle - \frac{y_0 F\sqrt{j+1}}{2\sqrt{2}\hbar(\Omega - \omega_{ex})}|j+1\rangle + \mathcal{O}(F^2). \end{aligned} \tag{B.5}$$

[1] Applying conventional time-independent perturbation theory yields identical results, but is not that compact, as by using the translation operator method combined with certain commutation relations exact results in all orders are obtained.

In the second line the states are determined in first order. The approximate Floquet states are determined by applying the transformation

$$|\phi_j(t)\rangle \quad = \quad \exp(-i\omega_{ex}\hat{a}^\dagger\hat{a}t)|\phi_{j,\ \mathrm{RWA}}\rangle, \tag{B.6}$$

which fixes the actual time dependence of the Floquet states. We point out that in the vicinity of a resonance the energies in RWA are well described as: $(\omega_{ex}^2 - \Omega^2) \simeq (\omega_{ex} - \Omega)2\Omega$ and diverging at exact resonance. Moreover, as seen in Appendix D, choosing a resonance condition is not equivalent to applying a RWA, as there also the counterrotating terms exist, see e.g. Eq. (D.6). However, parts of the contributions are equal, see Eq. (D.7)[2]. In contrast to the exact solution, given in section 3.2.1, both the energies and the states acquire only contributions proportional to the difference of frequencies. A relevant quantity is the matrix element of the position operator:

$$\begin{aligned} y_{lk}(t) &= \frac{y_0}{\sqrt{2}}\langle\phi_l(t)|(\hat{a}+\hat{a}^\dagger)|\phi_k(t)\rangle \\ &= \frac{y_0}{\sqrt{2}}\langle\phi_{l,\ \mathrm{RWA}}|\exp(i\omega_{ex}\hat{a}^\dagger\hat{a}t)(\hat{a}+\hat{a}^\dagger)\exp(-i\omega_{ex}\hat{a}^\dagger\hat{a}t)|\phi_{k,\ \mathrm{RWA}}\rangle \\ &= \frac{y_0}{\sqrt{2}}\left[\exp(-i\omega_{ex}t)\langle\phi_{l,\ \mathrm{RWA}}|\hat{a}|\phi_{k,\ \mathrm{RWA}}\rangle + \exp(+i\omega_{ex}t)\langle\phi_{l,\ \mathrm{RWA}}|\hat{a}^\dagger|\phi_{k,\ \mathrm{RWA}}\rangle\right] \\ &= \frac{y_0}{\sqrt{2}}\sqrt{k}\delta_{l,k-1}\exp(-i\omega_{ex}t) + \frac{y_0}{\sqrt{2}}\sqrt{l}\delta_{l,k+1}\exp(i\omega_{ex}t) - \frac{F}{2M\Omega(\Omega-\omega_{ex})}\cos(\omega_{ex}t), \end{aligned} \tag{B.7}$$

where we used some commutator relations. For comparison with the exact result, see Eq. (3.108), we express $y_{lk}(t)$ in the ψ-basis:

$$\begin{aligned} y_{lk}(t) \quad &= \quad \frac{y_0}{\sqrt{2}}\langle\psi_l(t)|(\hat{a}+\hat{a}^\dagger)|\psi_k(t)\rangle \\ &= \quad \frac{y_0}{\sqrt{2}}\sqrt{k}\delta_{l,k-1}\exp(-i[\omega_{ex}+\Omega]t) + \frac{y_0}{\sqrt{2}}\sqrt{l}\delta_{l,k+1}\exp(i[\omega_{ex}+\Omega]t) \\ &\quad -\frac{F}{2M\Omega\hbar(\Omega-\omega_{ex})}\cos(\omega_{ex}t). \end{aligned} \tag{B.8}$$

First we observe a different time-dependence of the undriven contributions, and these terms are not slowly oscillating. Second the driving dependent coefficients enter with a different weight compared to the exact result, proportional only to $\omega_{ex} - \Omega$.
However, the counterrotating terms for the driven harmonic oscillator are essential for the following reasons:

1. For strictly linear systems, especially the harmonic oscillator Ehrenfest theorem is fulfilled, such that the quantum mechanical observables coincide with the classical ones. This is no more valid, for the reasons mentioned above, when a rotating wave approximation is applied.

[2] $\frac{F}{2\sqrt{2}My_0\Omega} = \frac{y_0F}{2\sqrt{2}\hbar}$

2. As the oscillator is not coupled to bath leading to dissipation and accounting for a finite temperature the transitions from a certain level either upwards or downwards are equal probable, as the spectrum of the oscillator is equidistant. Hence the question arises, whether a RWA treatment of the harmonic oscillator is appropriate and valid at all. As the inclusion of counterrotating terms results in the classical equations we have to consider the full dynamics for the linear oscillator.

Appendix C

Van Vleck perturbation theory

In the following we give a basic introduction of the Van Vleck perturbation theory [141, 142, 143, 144]. It allows to calculate eigenenergies and eigenfunctions of Hamiltonians $\hat{H}$ whose spectrum is splitted into well-defined manifolds (denoted by Greek indices) [142, 143, 144, 153, 154]. Within Van Vleck perturbation theory an effective Hamiltonian $\hat{H}_{\rm eff} = \exp(i\hat{S})\hat{H}\exp(-i\hat{S})$ is constructed whose spectrum is the same as that of the original Hamiltonian

$$\hat{H} \;=\; \hat{H}^{(0)} + \hat{V}, \tag{C.1}$$

but only connects almost degenerate levels within a given manifold. The eigenstates are then calculated from the eigenstates of the effective Hamiltonian via a back transformation. For time-dependent Hamiltonians one introduces an effective Floquet Hamiltonian $\hat{\mathcal{H}}_{\rm eff}$ in the composite Hilbert space $\mathcal{R}\otimes\mathcal{T}$. The effective quasienergies up to second order in the perturbation are determined by:

$$\begin{aligned}\langle\langle i,\alpha|\hat{\mathcal{H}}_{\rm eff}|j,\alpha\rangle\rangle &= E_{i,\alpha}\delta_{ij} + \langle\langle i,\alpha|\hat{V}|j,\alpha\rangle\rangle \\ &+\frac{1}{2}\sum_{k,\gamma\neq\alpha}\langle\langle i,\alpha|\hat{V}|k,\gamma\rangle\rangle\langle\langle k,\gamma|\hat{V}|j,\alpha\rangle\rangle\left[\frac{1}{E_{i,\alpha}-E_{k,\gamma}}+\frac{1}{E_{j,\alpha}-E_{k,\gamma}}\right] \\ &= E_{i,\alpha}\delta_{ij} + \langle\langle i,\alpha|\hat{V}|j,\alpha\rangle\rangle + \langle\langle i,\alpha|(\hat{R}\hat{V})^{\dagger}\hat{V}|j,\alpha\rangle\rangle + \langle\langle i,\alpha|\hat{V}(\hat{R}\hat{V})|j,\alpha\rangle\rangle,\end{aligned} \tag{C.2}$$

where we introduced the reduced resolvent:

$$\hat{R} \;=\; \sum_{k,\gamma}{}' |k,\gamma\rangle\rangle\langle\langle k,\gamma|/(E-E_{k,\gamma}). \tag{C.3}$$

The prime over the sum denotes that all the states belonging to the manifold α under consideration are excluded from the sum. The states of the original Floquet Hamiltonian $\hat{\mathcal{H}}$ are given by applying a back transformation connecting different manifolds:

$\exp(-i\hat{S})|j,\alpha\rangle\rangle = (1 - i\hat{S}^{(1)} - i\hat{S}^{(2)} + i\hat{S}^{(1)}i\hat{S}^{(1)}/2 + \dots)|j,\alpha\rangle\rangle$, where:

$$\begin{aligned}
\langle\langle i,\alpha|i\hat{S}^{(1)}|j,\beta\rangle\rangle &= \frac{\langle\langle i,\alpha|\hat{V}|j,\beta\rangle\rangle}{E_{i,\alpha} - E_{j,\beta}} \qquad \text{(C.4)}\\
\langle\langle i,\alpha|i\hat{S}^{(2)}|j,\beta\rangle\rangle &= \frac{\langle\langle i,\alpha|\hat{V}|k,\gamma\rangle\rangle\langle\langle k,\gamma|\hat{V}|j,\beta\rangle\rangle}{2(E_{j,\beta} - E_{i,\alpha})}\left[\frac{1}{E_{k,\gamma} - E_{i,\alpha}} + \frac{1}{E_{k,\gamma} - E_{j,\beta}}\right]\\
&\quad + \sum_k \frac{1}{E_{j,\beta} - E_{i,\alpha}} \frac{\langle\langle i,\alpha|\hat{V}|k,\beta\rangle\rangle\langle\langle k,\beta|\hat{V}|j,\beta\rangle\rangle}{E_{k,\beta} - E_{i,\alpha}}\\
&\quad + \sum_k \frac{1}{E_{j,\beta} - E_{i,\alpha}} \frac{\langle\langle i,\alpha|\hat{V}|k,\alpha\rangle\rangle\langle\langle k,\alpha|\hat{V}|j,\beta\rangle\rangle}{E_{k,\alpha} - E_{j,\beta}}.
\end{aligned}$$

The construction using the reduced resolvent is more easily comparable to conventional degenerate perturbation theory [155, 156]. After identification of the degenerate levels the modifications to the eigenvectors are given by calculating all possible matrix elements from the degenerate levels out of the manifold.

C.1 Van Vleck perturbation theory within the undriven qubit-NO system

As we consider in chapter 4 a time-independent problem, the notation $|\dots\rangle\rangle$ is no more adequate and replaced in the following by $|\dots\rangle$. Here the perturbation $\hat{H}_{\text{Int}}$ is proportional to $\hat{a} + \hat{a}^\dagger$. Therefore we consider first the action of this operator on arbitrary nonlinear oscillator states $|l\rangle, |m\rangle$:

$$\begin{aligned}
\langle l|\hat{a} + \hat{a}^\dagger|m\rangle &= \langle l|\Big[\sqrt{m}|m-1\rangle_0 + a_2^{(m)}\sqrt{m+2}|m+1\rangle_0 + a_{-2}^{(m)}\sqrt{m-2}|m-3\rangle_0\\
&\quad + a_{-4}^{(m)}\sqrt{m-4}|m-5\rangle_0 + a_4^{(m)}\sqrt{m+4}|m+3\rangle_0 + \sqrt{m+1}|m+1\rangle_0\\
&\quad + a_2^{(m)}\sqrt{m+3}|m+3\rangle_0 + a_{-2}^{(m)}\sqrt{m-1}|m-1\rangle_0 + a_{-4}^{(m)}\sqrt{m-3}|m-3\rangle_0\\
&\quad + a_4^{(m)}\sqrt{m+5}|m+5\rangle_0\Big] + \mathcal{O}(\overline{\alpha}^2), \qquad \text{(C.5)}
\end{aligned}$$

where $|l\rangle_0$ denotes an eigenstates of the linear oscillator. Now we have different cases:

$$\begin{aligned}
l = m-1 \;:&\quad \langle m-1|(\hat{a} + \hat{a}^\dagger)|m\rangle = \sqrt{m} + a_{-2}^{(m)}\sqrt{m-1} + a_2^{(m-1)}\sqrt{m+1} + \mathcal{O}(\overline{\alpha}^2),\\
l = m-3 \;:&\quad \langle m-3|(\hat{a} + \hat{a}^\dagger)|m\rangle = a_{-2}^{(m)}\sqrt{m-2} + a_{-4}^{(m)}\sqrt{m-3} + a_2^{(m-3)}\sqrt{m}\\
&\qquad + a_4^{(m-3)}\sqrt{m+1} + \mathcal{O}(\overline{\alpha}^2),\\
l = m-5 \;:&\quad \langle m-5|(\hat{a} + \hat{a}^\dagger)|m\rangle = a_{-4}^{(m)}\sqrt{m-4} + a_4^{(m-5)}\sqrt{m} + \mathcal{O}(\overline{\alpha}^2) = 0,\\
l = m+1 \;:&\quad \langle m+1|(\hat{a} + \hat{a}^\dagger)|m\rangle = \sqrt{m+1} + a_{-2}^{(m+1)}\sqrt{m} + a_2^{(m)}\sqrt{m+2} + \mathcal{O}(\overline{\alpha}^2),\\
l = m+3 \;:&\quad \langle m+3|(\hat{a} + \hat{a}^\dagger)|m\rangle = a_{-2}^{(m+3)}\sqrt{m+1} + a_{-4}^{(m+3)}\sqrt{m} + a_2^{(m)}\sqrt{m+3}\\
&\qquad + a_4^{(m)}\sqrt{m+4} + \mathcal{O}(\overline{\alpha}^2),\\
l = m+5 \;:&\quad \langle m+5|(\hat{a} + \hat{a}^\dagger)|m\rangle = a_{-4}^{(m+5)}\sqrt{m+1} + a_4^{(m)}\sqrt{m+5} + \mathcal{O}(\overline{\alpha}^2) = 0.
\end{aligned} \qquad \text{(C.6)}$$

Due to the manifold structure we only have to consider for Van Vleck perturbation theory the matrix elements involving $l = m \pm 1$, $l = m \pm 3$. Therefore we introduce the notations:

$$n_1(j) = \sqrt{j+1}\left(1 + \frac{\sqrt{j}a_{-2}^{(j+1)}}{\sqrt{j+1}} + \frac{a_2^{(j)}\sqrt{j+2}}{\sqrt{j+1}}\right) = \sqrt{j+1}\left[1 - \frac{3}{2\hbar\Omega}\overline{\alpha}(j+1)\right], \quad \text{(C.7)}$$

$$\begin{aligned} n_3(j,\overline{\alpha}) &= a_{-2}^{(j)}\sqrt{j-2} + a_{-4}^{(j)}\sqrt{j-3} + a_2^{(j-3)}\sqrt{j} + a_4^{(j-3)}\sqrt{j+1} \\ &= \frac{\overline{\alpha}}{4\hbar\Omega}\sqrt{j(j-1)(j-2)}. \end{aligned} \quad \text{(C.8)}$$

The non-vanishing matrix elements for the transformation matrix are in first order:

$$\begin{aligned} iS^{(1)}_{(j-1)\mathrm{e},j\mathrm{e}} &= \frac{\langle \mathrm{e}, j-1|\hat{H}_{\mathrm{Int}}|\mathrm{e},j\rangle}{E_{\mathrm{e}(j-1)} - E_{\mathrm{e}j}} = \frac{\overline{g}\frac{\varepsilon}{\Delta_b}n_1(j-1)}{\Omega + \frac{3}{2\hbar}\overline{\alpha}\cdot 2j} \\ &= \frac{\overline{g}\varepsilon\sqrt{j}}{\Delta_b\Omega}\left[1 - \frac{9}{2\hbar\Omega}\overline{\alpha}j\right] + \mathcal{O}(\overline{\alpha}^2), \end{aligned} \quad \text{(C.9)}$$

$$\begin{aligned} iS^{(1)}_{\mathrm{g}j,(j+1)\mathrm{g}} &= \frac{\langle \mathrm{g}, j|\hat{H}_{\mathrm{Int}}|\mathrm{g},j+1\rangle}{E_{\mathrm{g}j} - E_{\mathrm{g}(j+1)}} = -\frac{\overline{g}\frac{\varepsilon}{\Delta_b}n_1(j)}{\Omega + \frac{3}{2\hbar}\overline{\alpha}\cdot 2(j+1)} \\ &= -\frac{\overline{g}\varepsilon\sqrt{j+1}}{\Delta_b\Omega}\left[1 - \frac{9}{2\hbar\Omega}\overline{\alpha}(j+1)\right] + \mathcal{O}(\overline{\alpha}^2), \end{aligned}$$

$$\begin{aligned} iS^{(1)}_{\mathrm{g}j,(j+1)\mathrm{e}} &= \frac{\langle \mathrm{g}, j|\hat{H}_{\mathrm{Int}}|\mathrm{e},j+1\rangle}{E_{\mathrm{g}j} - E_{\mathrm{e}(j+1)}} = \frac{\overline{g}\frac{\Delta_0}{\Delta_b}n_1(j)}{\Delta_b + \Omega + \frac{3}{2\hbar}\overline{\alpha}\cdot 2(j+1)} \\ &= \frac{\overline{g}\Delta_0\sqrt{j+1}}{\Delta_b(\Delta_b+\Omega)}\left[1 - \frac{3\overline{\alpha}(j+1)(\Delta_b+3\Omega)}{2\hbar\Omega(\Delta_b+\Omega)}\right] + \mathcal{O}(\overline{\alpha}^2), \end{aligned}$$

$$iS^{(1)}_{j\mathrm{e},(j+3)\mathrm{e}} = \frac{\langle \mathrm{e}, j|\hat{H}_{\mathrm{Int}}|\mathrm{e},j+3\rangle}{E_{\mathrm{e}j} - E_{\mathrm{e}(j+3)}} = \frac{\overline{g}\frac{\varepsilon}{\Delta_b}n_3(j+3,\overline{\alpha})}{3\Omega} + \mathcal{O}(\overline{\alpha}^2),$$

$$iS^{(1)}_{j\mathrm{g},(j+3)\mathrm{g}} = \frac{\langle \mathrm{g}, j|\hat{H}_{\mathrm{Int}}|\mathrm{g},j+3\rangle}{E_{\mathrm{g}j} - E_{\mathrm{g}(j+3)}} = -\frac{\overline{g}\frac{\varepsilon}{\Delta_b}n_3(j+3,\overline{\alpha})}{3\Omega} + \mathcal{O}(\overline{\alpha}^2),$$

$$iS^{(1)}_{j\mathrm{g},(j+3)\mathrm{e}} = \frac{\langle \mathrm{g}, j|\hat{H}_{\mathrm{Int}}|\mathrm{e},j+3\rangle}{E_{\mathrm{g}j} - E_{\mathrm{e}(j+3)}} = \frac{\overline{g}\frac{\Delta_0}{\Delta_b}n_3(j+3,\overline{\alpha})}{\Delta_b + 3\Omega} + \mathcal{O}(\overline{\alpha}^2),$$

$$iS^{(1)}_{j\mathrm{e},(j+3)\mathrm{g}} = \frac{\langle \mathrm{e}, j|\hat{H}_{\mathrm{Int}}|\mathrm{g},j+3\rangle}{E_{\mathrm{e}j} - E_{\mathrm{g}(j+3)}} = \frac{\overline{g}\frac{\Delta_0}{\Delta_b}n_3(j+3,\overline{\alpha})}{-\Delta_b + 3\Omega} + \mathcal{O}(\overline{\alpha}^2).$$

Due to the fact that $n_3(j,\overline{\alpha})$ is a purely nonlinear contribution, we can reduce the possible contributions for the second order of the transformation matrix. Restricting

to lowest order in the nonlinearity the non-vanishing contributions are either combinations of involving twice $n_1(j)$ and expanding this afterwards to first order in the nonlinearity or combinations of both $n_1(j)$ and $n_3(j,\overline{\alpha})$, while $n_1(j)$ is reduced in this case to the zeroth order in the nonlinearity, because $n_3(j,\overline{\alpha})$ is already of first order in the nonlinearity. For the second order we obtain:

$$
\begin{aligned}
iS^{(2)}_{j\mathrm{e},(j+2)\mathrm{g}} &= \frac{1}{E_{\mathrm{g}(j+2)}-E_{\mathrm{e}j}} \qquad\qquad (C.10)\\
&\left[\frac{\langle \mathrm{e},j|\hat{H}_{\mathrm{Int}}|\mathrm{e},j+1\rangle\langle \mathrm{e},j+1|\hat{H}_{\mathrm{Int}}|\mathrm{g},j+2\rangle}{E_{\mathrm{e}(j+1)}-E_{\mathrm{e}j}}+\frac{\langle \mathrm{e},j|\hat{H}_{\mathrm{Int}}|\mathrm{g},j+1\rangle\langle \mathrm{g},j+1|\hat{H}_{\mathrm{Int}}|\mathrm{g},j+2\rangle}{E_{\mathrm{g}(j+1)}-E_{\mathrm{g}(j+2)}}\right]\\
&+\frac{\langle \mathrm{e},j|\hat{H}_{\mathrm{Int}}|\mathrm{e},j-1\rangle\langle \mathrm{e},j-1|\hat{H}_{\mathrm{Int}}|\mathrm{g},j+2\rangle}{2(E_{\mathrm{g}(j+2)}-E_{\mathrm{e}j})}\left[\frac{1}{E_{\mathrm{e}(j-1)}-E_{\mathrm{e}j}}+\frac{1}{E_{\mathrm{e}(j-1)}-E_{\mathrm{g}(j+2)}}\right]\\
&+\frac{\langle \mathrm{e},j|\hat{H}_{\mathrm{Int}}|\mathrm{g},j-1\rangle\langle \mathrm{g},j-1|\hat{H}_{\mathrm{Int}}|\mathrm{g},j+2\rangle}{2(E_{\mathrm{g}(j+2)}-E_{\mathrm{e}j})}\left[\frac{1}{E_{\mathrm{g}(j-1)}-E_{\mathrm{e}j}}+\frac{1}{E_{\mathrm{g}(j-1)}-E_{\mathrm{g}(j+2)}}\right]\\
&+\frac{\langle \mathrm{e},j|\hat{H}_{\mathrm{Int}}|\mathrm{g},j+3\rangle\langle \mathrm{g},j+3|\hat{H}_{\mathrm{Int}}|\mathrm{g},j+2\rangle}{2(E_{\mathrm{g}(j+2)}-E_{\mathrm{e}j})}\left[\frac{1}{E_{\mathrm{g}(j+3)}-E_{\mathrm{e}j}}+\frac{1}{E_{\mathrm{g}(j+3)}-E_{\mathrm{g}(j+2)}}\right]\\
&+\frac{\langle \mathrm{e},j|\hat{H}_{\mathrm{Int}}|\mathrm{e},j+3\rangle\langle \mathrm{e},j+3|\hat{H}_{\mathrm{Int}}|\mathrm{g},j+2\rangle}{2(E_{\mathrm{g}(j+2)}-E_{\mathrm{e}j})}\left[\frac{1}{E_{\mathrm{e}(j+3)}-E_{\mathrm{e}j}}+\frac{1}{E_{\mathrm{e}(j+3)}-E_{\mathrm{g}(j+2)}}\right]\\
&=\frac{2\hbar^2\overline{g}^2\varepsilon\Delta_0\sqrt{(j+1)(j+2)}}{\Delta_b^2\hbar^2\Omega(2\Omega-\Delta_b)}\left[1+\frac{3\overline{\alpha}(2j+3)(\Delta_b-3\Omega)}{\hbar\Omega(2\Omega-\Delta_b)}\right]\\
&+\frac{\overline{g}^2(2j+3)\sqrt{(j+1)(j+2)}\overline{\alpha}\Delta_0\varepsilon(\Delta_b-5\Omega)}{12\hbar\Omega^2\left(\Delta_b^4-4\Omega\Delta_b^3+\Omega^2\Delta_b^2+6\Omega^3\Delta_b\right)}+\mathcal{O}(\overline{\alpha}^2),
\end{aligned}
$$

$$
\begin{aligned}
iS^{(2)}_{j\mathrm{g},(j+2)\mathrm{g}} &= \qquad\qquad (C.11)\\
&\frac{\langle \mathrm{g},j|\hat{H}_{\mathrm{Int}}|\mathrm{g},j+1\rangle\langle \mathrm{g},j+1|\hat{H}_{\mathrm{Int}}|\mathrm{g},j+2\rangle}{2(E_{\mathrm{g}(j+2)}-E_{\mathrm{g}j})}\left[\frac{1}{E_{\mathrm{g}(j+1)}-E_{\mathrm{g}j}}+\frac{1}{E_{\mathrm{g}(j+1)}-E_{\mathrm{g}(j+2)}}\right]\\
&+\frac{\langle \mathrm{g},j|\hat{H}_{\mathrm{Int}}|\mathrm{e},j+1\rangle\langle \mathrm{e},j+1|\hat{H}_{\mathrm{Int}}|\mathrm{g},j+2\rangle}{(E_{\mathrm{g}(j+2)}-E_{\mathrm{g}j})(E_{\mathrm{e}(j+1)}-E_{\mathrm{g}j})}\\
&+\frac{\langle \mathrm{g},j|\hat{H}_{\mathrm{Int}}|\mathrm{g},j-1\rangle\langle \mathrm{g},j-1|\hat{H}_{\mathrm{Int}}|\mathrm{g},j+2\rangle}{2(E_{\mathrm{g}(j+2)}-E_{\mathrm{g}j})}\left[\frac{1}{E_{\mathrm{g}(j-1)}-E_{\mathrm{g}j}}+\frac{1}{E_{\mathrm{g}(j-1)}-E_{\mathrm{g}(j+2)}}\right]\\
&+\frac{\langle \mathrm{g},j|\hat{H}_{\mathrm{Int}}|\mathrm{g},j+3\rangle\langle \mathrm{g},j+3|\hat{H}_{\mathrm{Int}}|\mathrm{g},j+2\rangle}{2(E_{\mathrm{g}(j+2)}-E_{\mathrm{g}j})}\left[\frac{1}{E_{\mathrm{g}(j+3)}-E_{\mathrm{g}j}}+\frac{1}{E_{\mathrm{g}(j+3)}-E_{\mathrm{g}(j+2)}}\right]\\
&+\frac{\langle \mathrm{g},j|\hat{H}_{\mathrm{Int}}|\mathrm{e},j+3\rangle\langle \mathrm{e},j+3|\hat{H}_{\mathrm{Int}}|\mathrm{g},j+2\rangle}{2(E_{\mathrm{g}(j+2)}-E_{\mathrm{g}j})}\left[\frac{1}{E_{\mathrm{e}(j+3)}-E_{\mathrm{g}j}}+\frac{1}{E_{\mathrm{e}(j+3)}-E_{\mathrm{g}(j+2)}}\right]\\
&+\frac{\langle \mathrm{g},j|\hat{H}_{\mathrm{Int}}|\mathrm{e},(j-1)\rangle\langle \mathrm{e},j-1|\hat{H}_{\mathrm{Int}}|\mathrm{g},(j+2)\rangle}{(E_{\mathrm{g}(j+2)}-E_{\mathrm{g}j})(E_{\mathrm{e}(j-1)}-E_{\mathrm{g}(j+2)})}\\
&=\frac{\hbar\overline{g}^2\sqrt{(j+1)(j+2)}}{2\Delta_b^2\Omega}\left[\frac{3\overline{\alpha}\varepsilon^2}{2\hbar^2\Omega^2}+\frac{\Delta_0^2}{\hbar(\Delta_b+\Omega)}\left(1-\frac{3\overline{\alpha}((2j+3)\Delta_b+\Omega(3j+4))}{\hbar(\Delta_b+\Omega)\Omega}\right)\right]\\
&+\frac{\overline{g}^2\sqrt{(j+1)(j+2)}\overline{\alpha}}{8\hbar\Delta_b^2\Omega^2}\left(\frac{2\varepsilon^2}{\Omega}+\frac{\left((2j+3)\Delta_b^2+3(j-1)\Omega\Delta_b-3(j+6)\Omega^2\right)\Delta_0^2}{(\Delta_b-3\Omega)\left(\Delta_b^2+4\Omega\Delta_b+3\Omega^2\right)}\right)+\mathcal{O}(\overline{\alpha}^2),
\end{aligned}
$$

$$
\begin{aligned}
&iS^{(2)}_{j\mathrm{e},(j+2)\mathrm{e}} = \qquad\qquad (C.12)\\
&\frac{\langle \mathrm{e},j|\hat{H}_{\mathrm{Int}}|\mathrm{e},j+1\rangle\langle \mathrm{e},j+1|\hat{H}_{\mathrm{Int}}|\mathrm{e},j+2\rangle}{2(E_{\mathrm{e}(j+2)}-E_{\mathrm{e}j})}\left[\frac{1}{E_{\mathrm{e}(j+1)}-E_{\mathrm{e}j}}+\frac{1}{E_{\mathrm{e}(j+1)}-E_{\mathrm{e}(j+2)}}\right]\\
&+\frac{\langle \mathrm{e},j|\hat{H}_{\mathrm{Int}}|\mathrm{g},j+1\rangle\langle \mathrm{g},j+1|\hat{H}_{\mathrm{Int}}|\mathrm{e},j+2\rangle}{(E_{\mathrm{e}(j+2)}-E_{\mathrm{e}j})(E_{\mathrm{g}(j+1)}-E_{\mathrm{e}(j+2)})}\\
&+\frac{\langle \mathrm{e},j|\hat{H}_{\mathrm{Int}}|\mathrm{g},j-1\rangle\langle \mathrm{g},j-1|\hat{H}_{\mathrm{Int}}|\mathrm{e},j+2\rangle}{2(E_{\mathrm{e}(j+2)}-E_{\mathrm{e}j})}\left[\frac{1}{E_{\mathrm{g}(j-1)}-E_{\mathrm{e}j}}+\frac{1}{E_{\mathrm{g}(j-1)}-E_{\mathrm{e}(j+2)}}\right]\\
&+\frac{\langle \mathrm{e},j|\hat{H}_{\mathrm{Int}}|\mathrm{e},j-1\rangle\langle \mathrm{e},j-1|\hat{H}_{\mathrm{Int}}|\mathrm{e},j+2\rangle}{2(E_{\mathrm{e}(j+2)}-E_{\mathrm{e}j})}\left[\frac{1}{E_{\mathrm{e}(j-1)}-E_{\mathrm{e}j}}+\frac{1}{E_{\mathrm{e}(j-1)}-E_{\mathrm{g}(j+2)}}\right]\\
&+\frac{\langle \mathrm{e},j|\hat{H}_{\mathrm{Int}}|\mathrm{e},j+3\rangle\langle \mathrm{e},j+3|\hat{H}_{\mathrm{Int}}|\mathrm{e},j+2\rangle}{2(E_{\mathrm{e}(j+2)}-E_{\mathrm{e}j})}\left[\frac{1}{E_{\mathrm{e}(j+3)}-E_{\mathrm{g}j}}+\frac{1}{E_{\mathrm{e}(j+3)}-E_{\mathrm{e}(j+2)}}\right]\\
&+\frac{\langle \mathrm{e}j|\hat{H}_{\mathrm{Int}}|\mathrm{g},j+3\rangle\langle \mathrm{g}j+3|\hat{H}_{\mathrm{Int}}|\mathrm{e},j+2\rangle}{(E_{\mathrm{e}(j+2)}-E_{\mathrm{e}j})(E_{\mathrm{g}(j+3)}-E_{\mathrm{e}j})}\\
&=\frac{\hbar^2\overline{g}^2\sqrt{(j+1)(j+2)}}{\Delta_b^2 2\hbar\Omega}\left[-\frac{\Delta_0^2}{\hbar(\Omega+\Delta_b)}\left(1-\frac{3\overline{\alpha}(\Delta_b(2j+3)+\Omega(3j+5))}{\hbar(\Delta_b+\Omega)\Omega}\right)+\frac{3\overline{\alpha}\varepsilon^2}{\hbar^2\Omega^2}\right]\\
&+\frac{\overline{g}^2\overline{\alpha}\sqrt{(j+1)(j+2)}}{8\hbar\Delta_b^2\Omega^2}\left(-\frac{(3+2j)\Delta_b^2+3(4+j)\Delta_b\Omega-3(j-3)\Omega^2}{\Delta_b^3+\Delta_b^2\Omega-9\Omega^2\Delta_b-9\Omega^3}\right.\\
&\left.+\frac{2\varepsilon^2}{\Omega}\right)+\mathcal{O}\left(\overline{\alpha}^2\right),
\end{aligned}
$$

$$
\begin{aligned}
&iS^{(2)}_{j\mathrm{g},j\mathrm{e}} = \qquad\qquad (C.13)\\
&\frac{\langle \mathrm{g},j|\hat{H}_{\mathrm{Int}}|\mathrm{g},j-1\rangle\langle \mathrm{g},j-1|\hat{H}_{\mathrm{Int}}|\mathrm{e},j\rangle}{2(E_{\mathrm{e}j}-E_{\mathrm{g}j})}\left[\frac{1}{E_{\mathrm{g}(j-1)}-E_{\mathrm{g}j}}+\frac{1}{E_{\mathrm{g}(j-1)}-E_{\mathrm{e}j}}\right]\\
&+\frac{\langle \mathrm{g},j|\hat{H}_{\mathrm{Int}}|\mathrm{e},j+1\rangle\langle \mathrm{e},j+1|\hat{H}_{\mathrm{Int}}|\mathrm{e},j\rangle}{2(E_{\mathrm{e}j}-E_{\mathrm{g}j})}\left[\frac{1}{E_{\mathrm{e}(j+1)}-E_{\mathrm{g}j}}+\frac{1}{E_{\mathrm{e}(j+1)}-E_{\mathrm{e}j}}\right]\\
&+\frac{\langle \mathrm{g},j|\hat{H}_{\mathrm{Int}}|\mathrm{e},j-1\rangle\langle \mathrm{e},j-1|\hat{H}_{\mathrm{Int}}|\mathrm{e},j\rangle}{(E_{\mathrm{e}j}-E_{\mathrm{g}j})(E_{\mathrm{e}(j-1)}-E_{\mathrm{e}j})}+\frac{\langle \mathrm{g},j|\hat{H}_{\mathrm{Int}}|\mathrm{g},j+1\rangle\langle \mathrm{g},j+1|\hat{H}_{\mathrm{Int}}|\mathrm{e},j\rangle}{(E_{\mathrm{e}j}-E_{\mathrm{g}j})(E_{\mathrm{g}(j+1)}-E_{\mathrm{g}j})}\\
&=\frac{\overline{g}^2\Delta_0\varepsilon}{\hbar\Delta_b^2\Omega(\Delta_b+\Omega)}\left[-\frac{\hbar(2j+1)}{2}+\frac{3\overline{\alpha}(2j^2+2j+1)(2\Delta_b+3\Omega)}{2\Omega(\Delta_b+\Omega)}\right]+\mathcal{O}\left(\overline{\alpha}^2\right),
\end{aligned}
$$

$$
\begin{aligned}
&iS^{(2)}_{\mathrm{jg},(j+2)\mathrm{e}} = \qquad\qquad (C.14)\\
&\frac{\langle \mathrm{g},j|\hat{H}_{\mathrm{Int}}|\mathrm{g},j+1\rangle\langle \mathrm{g},j+1|\hat{H}_{\mathrm{Int}}|\mathrm{e},j+2\rangle}{2(E_{\mathrm{e}(j+2)}-E_{\mathrm{g}j})}\left[\frac{1}{E_{\mathrm{g}(j+1)}-E_{\mathrm{g}j}}+\frac{1}{E_{\mathrm{g}(j+1)}-E_{\mathrm{e}(j+2)}}\right]\\
&+\frac{\langle \mathrm{g},j|\hat{H}_{\mathrm{Int}}|\mathrm{e},j+1\rangle\langle \mathrm{e},j+1|\hat{H}_{\mathrm{Int}}|\mathrm{e},j+2\rangle}{2(E_{\mathrm{e}(j+2)}-E_{\mathrm{g}j})}\left[\frac{1}{E_{\mathrm{e}(j+1)}-E_{\mathrm{g}j}}+\frac{1}{E_{\mathrm{e}(j+1)}-E_{\mathrm{e}(j+2)}}\right]\\
&+\frac{\langle \mathrm{g},j|\hat{H}_{\mathrm{Int}}|\mathrm{g},j-1\rangle\langle \mathrm{g},j-1|\hat{H}_{\mathrm{Int}}|\mathrm{e},j+2\rangle}{2(E_{\mathrm{e}(j+2)}-E_{\mathrm{g}j})}\left[\frac{1}{E_{\mathrm{g}(j-1)}-E_{\mathrm{g}j}}+\frac{1}{E_{\mathrm{g}(j-1)}-E_{\mathrm{e}(j+2)}}\right]\\
&+\frac{\langle \mathrm{g},j|\hat{H}_{\mathrm{Int}}|\mathrm{e},j+3\rangle\langle \mathrm{e},j+3|\hat{H}_{\mathrm{Int}}|\mathrm{e},j+2\rangle}{2(E_{\mathrm{e}(j+2)}-E_{\mathrm{g}j})}\left[\frac{1}{E_{\mathrm{e}(j+3)}-E_{\mathrm{g}j}}+\frac{1}{E_{\mathrm{e}(j+3)}-E_{\mathrm{e}(j+2)}}\right]\\
&+\frac{\langle \mathrm{g},j|\hat{H}_{\mathrm{Int}}|\mathrm{e},j-1\rangle\langle \mathrm{e},j-1|\hat{H}_{\mathrm{Int}}|\mathrm{e},j+2\rangle}{(E_{\mathrm{e}(j+2)}-E_{\mathrm{g}j})(E_{\mathrm{e}(j-1)}-E_{\mathrm{e}(j+2)})}+\frac{\langle \mathrm{g},j|\hat{H}_{\mathrm{Int}}|\mathrm{g},j+3\rangle\langle \mathrm{g},j+3|\hat{H}_{\mathrm{Int}}|\mathrm{e},j+2\rangle}{(E_{\mathrm{e}(j+2)}-E_{\mathrm{g}j})(E_{\mathrm{g}(j+3)}-E_{\mathrm{g}j})}\\
&=\frac{\hbar^2\overline{g}^2\varepsilon\Delta_0\sqrt{(j+1)(j+2)}}{2\Delta_b^2\hbar(2\Omega+\Delta_b)}\left[-\frac{2\Delta_b}{\hbar\Omega(\Omega+\Delta_b)}+\frac{3\overline{\alpha}\Delta_b(2j+3)(2\Delta_b^2+9\Delta_b\Omega+8\Omega^2)}{\hbar^2\Omega^2(\Omega+\Delta_b)^2(2\Omega+\Delta_b)}\right]\\
&+\frac{g^2(2j+3)\sqrt{(j+1)(j+2)}\overline{\alpha}\Delta_0\varepsilon(\Delta_b+6\Omega)}{24\hbar\Delta_b^2\Omega^2\left(\Delta_b^2+5\Omega\Delta_b+6\Omega^2\right)}+\mathcal{O}\left(\overline{\alpha}^2\right),
\end{aligned}
$$

$$
\begin{aligned}
&iS^{(2)}_{\mathrm{jg},(j+4)\mathrm{g}} = \qquad\qquad (C.15)\\
&\frac{\langle \mathrm{g},j|\hat{H}_{\mathrm{Int}}|\mathrm{g},j+1\rangle\langle \mathrm{g},j+1|\hat{H}_{\mathrm{Int}}|\mathrm{g},j+4\rangle}{2(E_{\mathrm{g}(j+4)}-E_{\mathrm{g}j})}\left[\frac{1}{E_{\mathrm{g}(j+1)}-E_{\mathrm{g}j}}+\frac{1}{E_{\mathrm{g}(j+1)}-E_{\mathrm{g}(j+4)}}\right]\\
&+\frac{\langle \mathrm{g},j|\hat{H}_{\mathrm{Int}}|\mathrm{e},j+1\rangle\langle \mathrm{e},j+1|\hat{H}_{\mathrm{Int}}|\mathrm{g}(j+4)\rangle}{2(E_{\mathrm{g}(j+4)}-E_{\mathrm{g}j})}\left[\frac{1}{E_{\mathrm{e}(j+1)}-E_{\mathrm{g}j}}+\frac{1}{E_{\mathrm{e}(j+1)}-E_{\mathrm{g}(j+4)}}\right]\\
&+\frac{\langle \mathrm{g},j|\hat{H}_{\mathrm{Int}}|\mathrm{g},j+3\rangle\langle \mathrm{g},j+3|\hat{H}_{\mathrm{Int}}|\mathrm{g}(j+4)\rangle}{2(E_{\mathrm{g}(j+4)}-E_{\mathrm{g}j})}\left[\frac{1}{E_{\mathrm{g}(j+3)}-E_{\mathrm{g}j}}+\frac{1}{E_{\mathrm{g}(j+3)}-E_{\mathrm{g}(j+4)}}\right]\\
&+\frac{\langle \mathrm{g},j|\hat{H}_{\mathrm{Int}}|\mathrm{e},j+3\rangle\langle \mathrm{e},j+3|\hat{H}_{\mathrm{Int}}|\mathrm{g}j+4\rangle}{(E_{\mathrm{g}(j+4)}-E_{\mathrm{g}j})(E_{\mathrm{e}(j+3)}-E_{\mathrm{g}j})}\\
&=\frac{\overline{g}^2\sqrt{(j+1)(j+2)(j+3)(j+4)}\overline{\alpha}\Delta_0^2\left(\Delta_b^2-3\Omega^2\right)}{8\hbar\Delta_b^2\Omega^2\left(\Delta_b^3+\Omega\Delta_b^2-9\Omega^2\Delta_b-9\Omega^3\right)}+\mathcal{O}(\overline{\alpha}^2),
\end{aligned}
$$

$$
\begin{aligned}
&iS^{(2)}_{\mathrm{jg},(j+4)\mathrm{e}} = \qquad\qquad (C.16)\\
&\frac{\langle \mathrm{g},j|\hat{H}_{\mathrm{Int}}|\mathrm{g},j+1\rangle\langle \mathrm{g},j+1|\hat{H}_{\mathrm{Int}}|\mathrm{e},j+4\rangle}{2(E_{\mathrm{e}(j+4)}-E_{\mathrm{g}j})}\left[\frac{1}{E_{\mathrm{g}(j+1)}-E_{\mathrm{g}j}}+\frac{1}{E_{\mathrm{g}(j+1)}-E_{\mathrm{e}(j+4)}}\right]\\
&+\frac{\langle \mathrm{g},j|\hat{H}_{\mathrm{Int}}|\mathrm{e},j+1\rangle\langle \mathrm{e},j+1|\hat{H}_{\mathrm{Int}}|\mathrm{e},j+4\rangle}{2(E_{\mathrm{e}(j+4)}-E_{\mathrm{g}j})}\left[\frac{1}{E_{\mathrm{e}(j+1)}-E_{\mathrm{g}j}}+\frac{1}{E_{\mathrm{e}(j+1)}-E_{\mathrm{e}(j+4)}}\right]\\
&+\frac{\langle \mathrm{g},j|\hat{H}_{\mathrm{Int}}|\mathrm{g},j+3\rangle\langle \mathrm{g},j+3|\hat{H}_{\mathrm{Int}}|\mathrm{e},j+4\rangle}{2(E_{\mathrm{e}(j+4)}-E_{\mathrm{g}j})}\left[\frac{1}{E_{\mathrm{g}(j+3)}-E_{\mathrm{g}j}}+\frac{1}{E_{\mathrm{g}(j+3)}-E_{\mathrm{e}(j+4)}}\right]\\
&+\frac{\langle \mathrm{g},j|\hat{H}_{\mathrm{Int}}|\mathrm{e},j+3\rangle\langle \mathrm{e},j+3|\hat{H}_{\mathrm{Int}}|\mathrm{e},j+4\rangle}{2(E_{\mathrm{e}(j+4)}-E_{\mathrm{g}j})}\left[\frac{1}{E_{\mathrm{e}(j+3)}-E_{\mathrm{g}j}}+\frac{1}{E_{\mathrm{e}(j+3)}-E_{\mathrm{e}(j+4)}}\right]\\
&=-\frac{\overline{g}^2\sqrt{(j+1)(j+2)(j+3)(j+4)}\overline{\alpha}\Delta_0\varepsilon(2\Delta_b+5\Omega)}{6\hbar\Omega^2\left(\Delta_b^4+8\Omega\Delta_b^3+19\Omega^2\Delta_b^2+12\Omega^3\Delta_b\right)}+\mathcal{O}(\overline{\alpha}^2),
\end{aligned}
$$

$$
\begin{aligned}
&iS^{(2)}_{\mathrm{je},(j+4)\mathrm{g}} = \qquad\qquad (C.17)\\
&\frac{\langle \mathrm{e},j|\hat{H}_{\mathrm{Int}}|\mathrm{e},j+1\rangle\langle \mathrm{e},j+1|\hat{H}_{\mathrm{Int}}|\mathrm{g},j+4\rangle}{2(E_{\mathrm{g}(j+4)}-E_{\mathrm{e}j})}\left[\frac{1}{E_{\mathrm{e}(j+1)}-E_{\mathrm{e}j}}+\frac{1}{E_{\mathrm{e}(j+1)}-E_{\mathrm{g}(j+4)}}\right]\\
&+\frac{\langle \mathrm{e},j|\hat{H}_{\mathrm{Int}}|\mathrm{g},j+3\rangle\langle \mathrm{g},j+3|\hat{H}_{\mathrm{Int}}|\mathrm{g},j+4\rangle}{2(E_{\mathrm{g}(j+4)}-E_{\mathrm{e}j})}\left[\frac{1}{E_{\mathrm{g}(j+3)}-E_{\mathrm{e}j}}+\frac{1}{E_{\mathrm{g}(j+3)}-E_{\mathrm{g}(j+4)}}\right]\\
&+\frac{\langle \mathrm{e},j|\hat{H}_{\mathrm{Int}}|\mathrm{e},j+3\rangle\langle \mathrm{e},j+3|\hat{H}_{\mathrm{Int}}|\mathrm{g},j+4\rangle}{(E_{\mathrm{g}(j+4)}-E_{\mathrm{e}j})(E_{\mathrm{e}(j+3)}-E_{\mathrm{e}j})}+\frac{\langle \mathrm{e},j|\hat{H}_{\mathrm{Int}}|\mathrm{g},j+1\rangle\langle \mathrm{g},j+1|\hat{H}_{\mathrm{Int}}|\mathrm{g},j+4\rangle}{(E_{\mathrm{g}(j+4)}-E_{\mathrm{e}j})(E_{\mathrm{g}(j+1)}-E_{\mathrm{g}(j+4)})}\\
&=-\frac{\overline{g}^2\sqrt{(j+1)(j+2)(j+3)(j+4)}\overline{\alpha}\Delta_0\varepsilon(5\Delta_b-12\Omega)}{12\hbar\Delta_b^2\Omega^2\left(\Delta_b^2-7\Omega\Delta_b+12\Omega^2\right)}+\mathcal{O}(\overline{\alpha}^2),
\end{aligned}
$$

$$
\begin{aligned}
&iS^{(2)}_{\mathrm{je},(j+4)\mathrm{e}} = \qquad\qquad (C.18)\\
&\frac{\langle \mathrm{e},j|\hat{H}_{\mathrm{Int}}|\mathrm{e},j+1\rangle\langle \mathrm{e},j+1|\hat{H}_{\mathrm{Int}}|\mathrm{e},j+4\rangle}{2(E_{\mathrm{e}(j+4)}-E_{\mathrm{e}j})}\left[\frac{1}{E_{\mathrm{e}(j+1)}-E_{\mathrm{e}j}}+\frac{1}{E_{\mathrm{e}(j+1)}-E_{\mathrm{e}(j+4)}}\right]\\
&+\frac{\langle \mathrm{e},j|\hat{H}_{\mathrm{Int}}|\mathrm{g},j+3\rangle\langle \mathrm{g},j+3|\hat{H}_{\mathrm{Int}}|\mathrm{e},j+4\rangle}{2(E_{\mathrm{e}(j+4)}-E_{\mathrm{e}j})}\left[\frac{1}{E_{\mathrm{g}(j+3)}-E_{\mathrm{e}j}}+\frac{1}{E_{\mathrm{g}(j+3)}-E_{\mathrm{e}(j+4)}}\right]\\
&+\frac{\langle \mathrm{e},j|\hat{H}_{\mathrm{Int}}|\mathrm{e},j+3\rangle\langle \mathrm{e},j+3|\hat{H}_{\mathrm{Int}}|\mathrm{e},j+4\rangle}{2(E_{\mathrm{e}(j+4)}-E_{\mathrm{e}j})}\left[\frac{1}{E_{\mathrm{e}(j+3)}-E_{\mathrm{e}j}}+\frac{1}{E_{\mathrm{e}(j+3)}-E_{\mathrm{e}(j+4)}}\right]\\
&+\frac{\langle \mathrm{e},j|\hat{H}_{\mathrm{Int}}|\mathrm{g},j+1\rangle\langle \mathrm{g},j+1|\hat{H}_{\mathrm{Int}}|\mathrm{e},j+4\rangle}{2(E_{\mathrm{e}(j+4)}-E_{\mathrm{e}j})(E_{\mathrm{g}(j+1)}-E_{\mathrm{e}(j+4)})}\\
&=-\frac{\overline{g}^2\sqrt{(j+1)(j+2)(j+3)(j+4)}\overline{\alpha}\Delta_0^2\left(\Delta_b^2-3\Omega^2\right)}{8\hbar\Delta_b^2\Omega^2\left(\Delta_b^3+\Omega\Delta_b^2-9\Omega^2\Delta_b-9\Omega^3\right)}+\mathcal{O}(\overline{\alpha}^2),
\end{aligned}
$$

Appendix D

Comparison for the states

As seen in section 3.5.1, App II yields away from resonance the same quasienergies as App I expanded up to second order in the driving amplitude F. In the following we determine whether the states behave in the same way. For simplicity we compare the two approaches for the case of the driven linear oscillator. This corresponds in the perturbative approach, App II, to expand to zeroth order in the nonlinearity and first order in the driving.

D.1 Floquet states in App I

According to Eq. (3.25) the Floquet states of the driven linear oscillator $\{|\phi_j(t)\rangle_0\}$ can be obtained from those of the undriven linear oscillator $\{|j\rangle_0\}$ by applying a time-dependent translation:

$$\hat{U}(\xi(t)) \;=\; \exp\left(-\frac{\xi(t)}{y_0\sqrt{2}}(\hat{a}-\hat{a}^\dagger)\right), \tag{D.1}$$

and accounting for a driving dependent phase

$$\exp(-i\theta(F^2,t))\exp\left(\frac{i}{\hbar}\left[-\frac{M}{2}\xi(t)\dot{\xi}(t)+M\dot{\xi}(t)y\right]\right), \tag{D.2}$$

see Eq. (3.30). Here $\hat{a}^\dagger$ and $\hat{a}$ are the usual creation/annihilation operator related to the linear oscillator. To compare to the results of App II we give the Floquet states from App I up to first order in the driving amplitude and zeroth order in the nonlinearity using:

$$\begin{aligned}\hat{U}(\xi(t))\exp(-i\theta(F^2,t))\exp\left(\frac{i}{\hbar}\left[-\frac{M}{2}\xi(t)\dot{\xi}(t)+M\dot{\xi}(t)y\right]\right) = \\ \left[1+\frac{\xi(t)}{y_0\sqrt{2}}(\hat{a}^\dagger-\hat{a})+\mathcal{O}(F^2)\right]\exp\left(\frac{i}{\hbar}\left[-\frac{M}{2}\xi(t)\dot{\xi}(t)+M\dot{\xi}(t)y\right]\right).\end{aligned} \tag{D.3}$$

We obtain:

$$\begin{aligned}|\phi_j(t)\rangle_0 &= \hat{U}(\xi(t))\exp(-i\theta(F^2,t))\exp\left(\frac{i}{\hbar}\left[-\frac{M}{2}\xi(t)\dot{\xi}(t)+M\dot{\xi}(t)y\right]\right)|j\rangle_0 \\ &= \left[|j\rangle_0+\frac{\xi(t)}{y_0\sqrt{2}}\left(\sqrt{j+1}|j+1\rangle_0-\sqrt{j}|j-1\rangle_0\right)+\mathcal{O}(F^2)\right] \\ &\quad\times\exp\left(\frac{i}{\hbar}\left[-\frac{M}{2}\xi(t)\dot{\xi}(t)+M\dot{\xi}(t)y\right]\right). \end{aligned} \tag{D.4}$$

As the second term in the last equation is a pure phase and not entering any observable, we neglect it in the following.
In the composite Hilbert space $\mathcal{R}\otimes\mathcal{T}$ the Floquet state corresponding to $\epsilon^{(0)}_{j,0}$ is:

$$\begin{aligned}|\phi_{j,0}\rangle\rangle_0 &= |j,0\rangle\rangle_0+\frac{F}{2\sqrt{2}My_0(\omega_{ex}^2-\Omega^2)}\left(\sqrt{j+1}|j+1,-1\rangle\rangle_0\right. \\ &\quad\left.+\sqrt{j+1}|j+1,+1\rangle\rangle_0-\sqrt{j}|j-1,-1\rangle\rangle_0-\sqrt{j}|j-1,+1\rangle\rangle_0\right). \end{aligned} \tag{D.5}$$

D.2 Floquet states in App II

In App II the counterpart of Eq. (D.5) is the state:

$$\begin{aligned}|-_{j,0}\rangle\rangle_0 &= |j,0\rangle\rangle_0+\frac{F}{2\sqrt{2}My_0\Omega}\left(\frac{\sqrt{j+1}|j+1,+1\rangle\rangle_0}{\omega_{ex}-\Omega}-\frac{\sqrt{j+1}|j+1,-1\rangle\rangle_0}{\omega_{ex}+\Omega}\right. \\ &\quad\left.-\frac{\sqrt{j}|j-1,-1\rangle\rangle_0}{\omega_{ex}-\Omega}+\frac{\sqrt{j}|j-1,+1\rangle\rangle_0}{\omega_{ex}+\Omega}\right). \end{aligned} \tag{D.6}$$

Note that by reducing to the linear case not only the energies $E_{j,0}$ and $E_{j+1,+1}$ but also $E_{j-1,-1}$ are equal if $\Omega\approx\omega_{ex}$. These are the dominant contributions, as $1/(\Omega-\omega_{ex})\gg 1$ if $\Omega\approx\omega_{ex}$:

$$|-_{j,0}\rangle\rangle_0\cong|j,0\rangle\rangle_0+\frac{F}{2\sqrt{2}My_0\Omega}\left(\frac{\sqrt{j+1}|j+1,+1\rangle\rangle_0}{\omega_{ex}-\Omega}-\frac{\sqrt{j}|j-1,-1\rangle\rangle_0}{\omega_{ex}-\Omega}\right). \tag{D.7}$$

D.2.1 Comparison

By comparing the states we see that the exact linear oscillator Floquet states from App I are proportional to $\xi(t)$ and hence are obtained as a linear combination of rotating and anti-rotating contributions. This accounts for the fact that the spectrum of the underlying oscillator is equidistant. Consequently the driving can excite both upwards and downwards transitions $|j\rangle_0\to|j+1\rangle_0$, $|j\rangle_0\to|j-1\rangle_0$ with the same weight. In contrast, App II in a vicinity of an N-photon resonance includes rotating and anti-rotating terms but with different weights. In fact, by choosing a resonance condition certain transitions are preferred, namely those within the resonant levels and those lying closest to these, giving the dominant contributions (see Eq. D.7). The

actual form for the states in App II is determined by the structure of the quasienergy-spectrum, i.e., by the resonance condition determining the structure of the manifold. As the manifold structure of App II is crucially depending on a finite nonlinearity to obtain a doublet, a reduction to the linear case is not possible. It would destroy the ordering of the manifolds, as not only $E_{j,0}$ and $E_{j+1,1}$ but also $E_{j+n,n}$, $n > 1$ and $E_{j-n,-n}$, $n \geq 1$, become degenerate. The way of treating the Floquet Hamiltonian thus results in different symmetry properties and weights for the corresponding states.

Appendix E

Oscillator matrix elements

Here we give the explicit form of the functions L_{LO} and L_{NLO} introduced in section 4.3.2 and derive the corresponding matrix elements y_{nm}. The zeroth order contributions in the nonlinearity in section 4.3.2 are denoted by:

$$L_{LO1}(\overline{g}^2) = \frac{\overline{g}^2\Delta_0^2(2\Delta_b+3\Omega)}{2\Omega\Delta_b^2(\Omega+\Delta_b)^2}, \qquad L_{LO0+}(\overline{g}) = \frac{\overline{g}\Delta_0}{\Delta_b(\Omega+\Delta_b)},$$
$$L_{LO1+}(\overline{g}^2) = \frac{4\overline{g}^2\varepsilon\Delta_0}{\Delta_b^2(\Delta_b^2+3\Omega\Delta_b+2\Omega^2)}, \qquad L_{LO1-}(\overline{g}^2) = -\frac{4\overline{g}^2\varepsilon\Delta_0}{\Delta_b^2\Omega(\Delta_b-2\Omega)}.$$

The term independent of $\overline{g}$ is $L_{NLO}(\overline{\alpha}) = -3\overline{\alpha}/2\hbar\Omega$.
The terms linear in $\overline{\alpha}$ and $\overline{g}$ are given by:

$$\begin{aligned}
L_{NLO0+}(\overline{\alpha},\overline{g}) &= -\frac{3\overline{\alpha}\,\overline{g}\Delta_0(\Delta_b+2\Omega)}{\hbar\Delta_b\Omega(\Delta_b+\Omega)^2},\\
L_{NLO2+}(\overline{\alpha},\overline{g}) &= \frac{3\overline{\alpha}\,\overline{g}}{4}\frac{\Delta_0(\Delta_b^2+6\Delta_b\Omega+13\Omega^2)}{\hbar\Omega(\Delta_b+\Omega)^2(\Delta_b^2+3\Delta_b\Omega)},\\
L_{NLO2-}(\overline{\alpha},\overline{g}) &= -\frac{3\overline{\alpha}\,\overline{g}\Delta_0}{\hbar\Delta_b(\Delta_b-3\Omega)(\Delta_b+\Omega)},\\
L_{NLO2}(\overline{\alpha},\overline{g}) &= -\frac{4\overline{\alpha}\,\overline{g}\varepsilon}{\hbar\Delta_b\Omega^2}.
\end{aligned}$$

Finally, the terms linear in $\overline{\alpha}$ but quadratic in $\overline{g}$ are:

$$L_{NLO1g}(j,\overline{\alpha},\overline{g}^2) = -\frac{6\varepsilon^2\overline{\alpha}\,\overline{g}^2}{\hbar\Delta_b^2\Omega^3}$$
$$-\frac{3\overline{\alpha}\,\overline{g}^2\Delta_0^2[14(j+1)\Delta_b^3-\Omega^2\Delta_b(88+92j)-(3+5j)\Omega\Delta_b^2-(89j+87)\Omega^3]}{4\hbar\Omega^2\Delta_b^2(\Omega+\Delta_b)^3(\Delta_b-3\Omega)},$$
$$L_{NLO1e}(j,\overline{\alpha},\overline{g}^2) = -\frac{6\varepsilon^2\overline{\alpha}\,\overline{g}^2}{\hbar\Delta_b^2\Omega^3}$$
$$-\frac{3\overline{\alpha}\,\overline{g}^2\Delta_0^2[-14(j+1)\Delta_b^3+(5j+7)\Delta_b^2\Omega+\Omega^2\Delta_b(92j+96)+\Omega^3(89j+91)]}{4\hbar\Delta_b^2\Omega^2(\Delta_b-3\Omega)(\Delta_b+\Omega)^3},$$

$$
\begin{aligned}
L_{NLO1+}(\overline{\alpha},\overline{g}^2) &= -\frac{2\overline{\alpha}\,\overline{g}^2\Delta_0\varepsilon(4\Delta_b^4+29\Omega\Delta_b^3+51\Omega^2\Delta_b^2-80\Delta_b\Omega^3-124\Omega^4)}{\hbar\Omega^2(\Delta_b-2\Omega)(\Delta_b^3+3\Delta_b^2\Omega+2\Delta_b\Omega^2)^2},\\
L_{NLO1-}(\overline{\alpha},\overline{g}^2) &= +\frac{6\overline{\alpha}\,\overline{g}^2\varepsilon\Delta_0(9\Delta_b^3+\Delta_b^2\Omega-56\Omega^2\Delta_b-36\Delta_b^3)}{\hbar\Omega^2(\Delta_b^2+3\Omega\Delta_b+2\Omega^2)(\Delta_b^2-2\Delta_b\Omega)^2},\\
L_{NLO3}(\overline{\alpha},\overline{g}^2) &= \frac{\overline{\alpha}\,\overline{g}^2\Delta_0^2(14\Delta_b^3+25\Delta_b^2\Omega-130\Omega^2\Delta_b-261\Omega^3)}{8\hbar\Delta_b^2\Omega^2(\Delta_b+\Omega)^2(\Delta_b^2-9\Omega^2)},\\
L_{NLO3+}(\overline{\alpha},\overline{g}^2) &= \frac{\overline{\alpha}\,\overline{g}^2\Delta_0\varepsilon(\Delta_b^3+3\Omega\Delta_b^2+74\Omega^2\Delta_b+216\Omega^3)}{3\hbar\Delta_b^2\Omega(\Delta_b+2\Omega)^2(\Delta_b^3+8\Delta_b^2\Omega+19\Omega^2\Delta_b+12\Omega^3)},\\
L_{NLO3-}(\overline{\alpha},\overline{g}^2) &= -\frac{\overline{\alpha}\,\overline{g}^2\Delta_0\varepsilon(24\Delta_b^3-239\Omega\Delta_b^2+814\Omega^2\Delta_b-936\Omega^3)}{3\hbar\Delta_b^2\Omega^2(\Delta_b-2\Omega)^2(\Delta_b^2-7\Delta_b\Omega+12\Omega^2)}.
\end{aligned}
$$

We can now give the expressions for y_{nm} using $\tan\eta_j = \frac{2|\Delta(j)|}{\delta_j}$, where $0 \le \eta_j < \pi$:

$$
\begin{aligned}
y_{2j+1,2j+1} &= -L_{NLO0}(j+1,\overline{\alpha},\overline{g}) + L_{NLO0}(j,\overline{\alpha},\overline{g}) \\
&\quad -\cos\eta_j[2L_{LO0}(\overline{g}) + L_{NLO0}(j+1,\overline{\alpha},\overline{g}) + L_{NLO0}(j,\overline{\alpha},\overline{g})] \\
&\quad +\sqrt{j+1}\sin\eta_j\left[L_{LO1-}(\overline{g}^2) + (j+1)L_{NLO1-}(\overline{\alpha},\overline{g}^2)\right], \\
y_{2j+1,2j+2} &= [2L_{LO0}(\overline{g}) + L_{NLO0}(j,\overline{\alpha},\overline{g}) + L_{NLO0}(j+1,\overline{\alpha},\overline{g})]\sin\eta_j \\
&\quad +\sqrt{j+1}\cos\eta_j\left[L_{LO1-}(\overline{g}^2) + (j+1)L_{NLO1-}(\overline{\alpha},\overline{g}^2)\right], \\
y_{2j+1,2j+3} &= \cos\frac{\eta_j}{2}\cos\frac{\eta_{j+1}}{2}\sqrt{j+2}\left[1 + (j+2)L_{NLO}(\overline{\alpha}) + L_{LO1}(\overline{g}^2)\right. \\
&\quad \left.+L_{NLO1\mathrm{g}}(j+1,\overline{\alpha},g^2)\right], \\
&\quad +\cos\frac{\eta_j}{2}\sin\frac{\eta_{j+1}}{2}\left[L_{LO0+}(\overline{g}) + L_{NLO0+}(\overline{\alpha},\overline{g})(2(j+1)+1)\right] \\
&\quad +\sin\frac{\eta_j}{2}\cos\frac{\eta_{j+1}}{2}\sqrt{(j+1)(j+2)}L_{NLO2-}(\overline{\alpha},\overline{g}) \\
&\quad +\sin\frac{\eta_j}{2}\sin\frac{\eta_{j+1}}{2}\sqrt{j+1}\left[1 + (j+1)L_{NLO}(\overline{\alpha}) - L_{LO1}(\overline{g}^2)\right. \\
&\quad \left.+L_{NLO1\mathrm{e}}(j,\overline{\alpha},\overline{g}^2)\right], \\
y_{2j+1,2j+4} &= \cos\frac{\eta_j}{2}\cos\frac{\eta_{j+1}}{2}\left[L_{LO0+}(\overline{g}) + L_{NLO0+}(\overline{\alpha},\overline{g})(2(j+1)+1)\right] \\
&\quad -\cos\frac{\eta_j}{2}\sin\frac{\eta_{j+1}}{2}\sqrt{j+2}\left[1 + (j+2)L_{NLO}(\overline{\alpha}) + L_{LO1}(\overline{g}^2)\right. \\
&\quad \left.+L_{NLO1\mathrm{g}}(j+1,\overline{\alpha},\overline{g}^2)\right] \\
&\quad +\sin\frac{\eta_j}{2}\cos\frac{\eta_{j+1}}{2}\left[1 + (j+1)L_{NLO}(\overline{\alpha}) - L_{LO1}(\overline{g}^2) + L_{NLO1\mathrm{e}}(j,\overline{\alpha},\overline{g}^2)\right] \\
&\quad -\sin\frac{\eta_j}{2}\sin\frac{\eta_{j+1}}{2}\sqrt{(j+1)(j+2)}L_{NLO2-}(\overline{\alpha},\overline{g}), \\
y_{2j+1,2j+5} &= \cos\frac{\eta_j}{2}\cos\frac{\eta_{j+2}}{2}\sqrt{(j+2)(j+3)}L_{NLO2}(\overline{\alpha},\overline{g}) \\
&\quad +\cos\frac{\eta_j}{2}\sin\frac{\eta_{j+2}}{2}\sqrt{j+2}\left[L_{LO1+}(\overline{g}^2) + (j+2)L_{NLO1+}(\overline{\alpha},\overline{g}^2)\right] \\
&\quad +\sin\frac{\eta_j}{2}\cos\frac{\eta_{j+2}}{2}\sqrt{(j+1)(j+2)(j+3)}L_{NLO3-}(\overline{\alpha},\overline{g}^2) \\
&\quad -\sin\frac{\eta_j}{2}\sin\frac{\eta_{j+2}}{2}L_{NLO2}(\overline{\alpha},\overline{g})\sqrt{(j+1)(j+2)}, \\
y_{2j+1,2j+6} &= -\cos\frac{\eta_j}{2}\sin\frac{\eta_{j+2}}{2}\sqrt{(j+2)(j+3)}L_{NLO2}(\overline{\alpha},\overline{g}) \\
&\quad +\cos\frac{\eta_j}{2}\cos\frac{\eta_{j+2}}{2}\sqrt{j+2}\left[L_{LO1+}(\overline{g}^2) + (j+2)L_{NLO1+}(\overline{\alpha},\overline{g}^2)\right] \\
&\quad -\sin\frac{\eta_j}{2}\sin\frac{\eta_{j+2}}{2}\sqrt{(j+1)(j+2)(j+3)}L_{NLO3-}(\overline{\alpha},\overline{g}^2) \\
&\quad -\sin\frac{\eta_j}{2}\cos\frac{\eta_{j+2}}{2}L_{NLO2}(\overline{\alpha},\overline{g})\sqrt{(j+1)(j+2)}, \\
y_{2j+1,2j+7} &= +\cos\frac{\eta_j}{2}\cos\frac{\eta_{j+3}}{2}\sqrt{(j+2)(j+3)(j+4)}\left[L_{NLO3}(\overline{\alpha},\overline{g}^2) - L_{NLO}(\overline{\alpha})/2\right] \\
&\quad +\cos\frac{\eta_j}{2}\sin\frac{\eta_{j+3}}{2}\sqrt{(j+2)(j+3)}L_{NLO2+}(\overline{\alpha},\overline{g}) \\
&\quad +\sin\frac{\eta_j}{2}\sin\frac{\eta_{j+3}}{2}\sqrt{(j+1)(j+2)(j+3)}\left[-L_{NLO3}(\overline{\alpha},\overline{g}^2) - L_{NLO}(\overline{\alpha})/2\right],
\end{aligned}
\tag{E.1}
$$

$$
\begin{aligned}
y_{2j+1,2j+8} &= -\cos\frac{\eta_j}{2}\sin\frac{\eta_{j+3}}{2}\sqrt{(j+2)(j+3)(j+4)}\left[L_{NLO3}(\overline{\alpha},\overline{g}^2)-L_{NLO}(\overline{\alpha})/2\right]\\
&\quad+\cos\frac{\eta_j}{2}\cos\frac{\eta_{j+3}}{2}\sqrt{(j+2)(j+3)}L_{NLO2+}(\overline{\alpha},\overline{g})\\
&\quad+\sin\frac{\eta_j}{2}\cos\frac{\eta_{j+3}}{2}\sqrt{(j+1)(j+2)(j+3)}\left[-L_{NLO3}(\overline{\alpha},\overline{g}^2)-L_{NLO}(\overline{\alpha})/2\right],\\
y_{2j+1,2j+9} &= \cos\frac{\eta_j}{2}\sin\frac{\eta_{j+4}}{2}\sqrt{(j+2)(j+3)(j+4)}L_{NLO3+}(\overline{\alpha},\overline{g}^2),\\
y_{2j+1,2j+10} &= \cos\frac{\eta_j}{2}\cos\frac{\eta_{j+4}}{2}\sqrt{(j+2)(j+3)(j+4)}L_{NLO3+}(\overline{\alpha},\overline{g}^2),
\end{aligned}
$$

and

$$
\begin{aligned}
y_{2j+2,2j+2} &= L_{NLO0}(j,\overline{\alpha},\overline{g})-L_{NLO0}(j+1,\overline{\alpha},\overline{g})+(2L_{LO0}(\overline{g})\\
&\quad+L_{NLO0}(j,\overline{\alpha},\overline{g})+L_{NLO0}(j+1,\overline{\alpha},\overline{g}))\cos\eta_j-\sin\eta_j\sqrt{j+1}\\
&\quad\times\left[L_{LO1-}(\overline{g}^2)+(j+1)L_{NLO1-}(\overline{\alpha},\overline{g}^2)\right],\\
y_{2j+2,2j+3} &= -\sin\frac{\eta_j}{2}\cos\frac{\eta_{j+1}}{2}\sqrt{j+2}\left[1+(j+2)L_{NLO}(\overline{\alpha})+L_{LO1}(\overline{g}^2)\right.\\
&\quad\left.+L_{NLO1\mathrm{g}}(j+1,\overline{\alpha},\overline{g}^2)\right],\\
&\quad-\sin\frac{\eta_j}{2}\sin\frac{\eta_{j+1}}{2}\left[L_{LO0+}(\overline{g})+L_{NLO0+}(\overline{\alpha},\overline{g})(2(j+1)+1)\right]\\
&\quad+\cos\frac{\eta_j}{2}\cos\frac{\eta_{j+1}}{2}\sqrt{(j+1)(j+2)}L_{NLO2-}(\overline{\alpha},\overline{g})\\
&\quad+\cos\frac{\eta_j}{2}\sin\frac{\eta_{j+1}}{2}\sqrt{j+1}\left[1+(j+1)L_{NLO}(\overline{\alpha})-L_{LO1}(\overline{g}^2)\right.\\
&\quad\left.+L_{NLO1\mathrm{e}}(j,\overline{\alpha},\overline{g}^2)\right],\\
y_{2j+2,2j+4} &= \sin\frac{\eta_j}{2}\sin\frac{\eta_{j+1}}{2}\sqrt{j+2}\left[1+(j+2)L_{NLO}(\overline{\alpha})+L_{LO1}(\overline{g}^2)\right.\\
&\quad\left.+L_{NLO1\mathrm{g}}(j+1,\overline{\alpha},\overline{g}^2)\right]\\
&\quad-\sin\frac{\eta_j}{2}\cos\frac{\eta_{j+1}}{2}\left[L_{LO0+}(\overline{g})+L_{NLO0+}(\overline{\alpha},\overline{g})(2(j+1)+1)\right]\\
&\quad-\cos\frac{\eta_j}{2}\sin\frac{\eta_{j+1}}{2}\sqrt{(j+1)(j+2)}L_{NLO2-}(\overline{\alpha},\overline{g})\\
&\quad+\cos\frac{\eta_j}{2}\cos\frac{\eta_{j+1}}{2}\sqrt{j+1}\left[1+(j+1)L_{NLO}(\overline{\alpha})-L_{LO1}(\overline{g}^2)\right.\\
&\quad\left.+L_{NLO1\mathrm{e}}(j,\overline{\alpha},\overline{g}^2)\right],\\
y_{2j+2,2j+5} &= -\sin\frac{\eta_j}{2}\cos\frac{\eta_{j+2}}{2}\sqrt{(j+2)(j+3)}L_{NLO2}(\overline{\alpha},\overline{g})\\
&\quad-\sin\frac{\eta_j}{2}\sin\frac{\eta_{j+2}}{2}\sqrt{j+2}\left[L_{LO1+}(\overline{g}^2)+L_{NLO1+}(\overline{\alpha},\overline{g}^2)(j+2)\right]\\
&\quad+\cos\frac{\eta_j}{2}\cos\frac{\eta_{j+2}}{2}\sqrt{(j+1)(j+2)(j+3)}L_{NLO3-}(\overline{\alpha},\overline{g}^2)\\
&\quad-\cos\frac{\eta_j}{2}\sin\frac{\eta_{j+2}}{2}\sqrt{(j+2)(j+3)}L_{NLO2}(\overline{\alpha},\overline{g}),
\end{aligned}
\tag{E.2}
$$

$$
\begin{aligned}
y_{2j+2,2j+6} &= \sin\frac{\eta_j}{2}\sin\frac{\eta_{j+2}}{2}\sqrt{(j+2)(j+3)}L_{NLO2}(\overline{\alpha},\overline{g}) \\
&\quad -\sin\frac{\eta_j}{2}\cos\frac{\eta_{j+2}}{2}\sqrt{j+2}\left[L_{LO1+}(\overline{g}^2)+L_{NLO1+}(\overline{\alpha},\overline{g}^2)(j+2)\right] \\
&\quad -\cos\frac{\eta_j}{2}\sin\frac{\eta_{j+2}}{2}\sqrt{(j+1)(j+2)(j+3)}L_{NLO3-}(\overline{\alpha},\overline{g}^2) \\
&\quad -\cos\frac{\eta_j}{2}\cos\frac{\eta_{j+2}}{2}\sqrt{(j+2)(j+3)}L_{NLO2}(\overline{\alpha},\overline{g}), \\
y_{2j+2,2j+7} &= -\sin\frac{\eta_j}{2}\cos\frac{\eta_{j+3}}{2}\sqrt{(j+2)(j+3)(j+4)}\left[L_{NLO3}(\overline{\alpha},\overline{g}^2)-L_{NLO}(\overline{\alpha})/2\right] \\
&\quad -\sin\frac{\eta_j}{2}\sin\frac{\eta_{j+3}}{2}\sqrt{(j+2)(j+3)}L_{NLO2+}(\overline{\alpha},\overline{g}) \\
&\quad +\cos\frac{\eta_j}{2}\sin\frac{\eta_{j+3}}{2}\sqrt{(j+1)(j+2)(j+3)}\left[-L_{NLO3}(\overline{\alpha},\overline{g}^2)-L_{NLO}(\overline{\alpha})/2\right], \\
y_{2j+2,2j+8} &= +\sin\frac{\eta_j}{2}\sin\frac{\eta_{j+3}}{2}\sqrt{(j+2)(j+3)(j+4)}\left[L_{NLO3}(\overline{\alpha},g^2)-L_{NLO}(\overline{\alpha})/2\right] \\
&\quad -\sin\frac{\eta_j}{2}\cos\frac{\eta_{j+3}}{2}\sqrt{(j+2)(j+3)}L_{NLO2+}(\overline{\alpha},\overline{g}) \\
&\quad +\cos\frac{\eta_j}{2}\cos\frac{\eta_{j+3}}{2}\sqrt{(j+1)(j+2)(j+3)}\left[-L_{NLO3}(\overline{\alpha},\overline{g}^2)-L_{NLO}(\overline{\alpha})/2\right], \\
y_{2j+2,2j+9} &= -\sin\frac{\eta_j}{2}\sin\frac{\eta_{j+4}}{2}\sqrt{(j+2)(j+3)(j+4)}L_{NLO3+}(\overline{\alpha},\overline{g}^2), \\
y_{2j+2,2j+10} &= -\sin\frac{\eta_j}{2}\cos\frac{\eta_{j+4}}{2}\sqrt{(j+2)(j+3)(j+4)}L_{NLO3+}(\overline{\alpha},\overline{g}^2).
\end{aligned}
$$

The matrix elements including the ground state are calculated separately because of its special form:

$$
\begin{aligned}
y_{00} &= -2(L_{LO0}(\overline{g})+L_{NLO0}(0,\overline{\alpha},\overline{g})), \qquad \text{(E.3)} \\
y_{01} &= \cos\frac{\eta_0}{2}\left[1+L_{NLO}(\overline{\alpha})+L_{LO1}(\overline{g}^2)+L_{NLO1g}(0,\overline{\alpha},\overline{g}^2)\right]+\sin\frac{\eta_0}{2}\left[L_{LO0+}(\overline{g})\right. \\
&\quad \left.+L_{NLO0+}(\overline{\alpha},\overline{g})\right], \\
y_{02} &= -\sin\frac{\eta_0}{2}\left[1+L_{NLO}(\overline{\alpha})+L_{LO1}(\overline{g}^2)+L_{NLO1g}(0,\overline{\alpha},\overline{g}^2)\right]+\cos\frac{\eta_0}{2}\left[L_{LO0+}(\overline{g})\right. \\
&\quad \left.+L_{NLO0+}(\overline{\alpha},\overline{g})\right], \\
y_{03} &= \cos\frac{\eta_1}{2}\sqrt{2}L_{NLO2}(\overline{\alpha},\overline{g})+\sin\frac{\eta_1}{2}\left[L_{LO1+}(\overline{g}^2)+L_{NLO1+}(\overline{\alpha},\overline{g}^2)\right], \\
y_{04} &= -\sin\frac{\eta_1}{2}\sqrt{2}L_{NLO2}(\overline{\alpha},\overline{g})+\cos\frac{\eta_1}{2}\left[L_{LO1+}(\overline{g}^2)+L_{NLO1+}(\overline{\alpha},\overline{g}^2)\right], \\
y_{05} &= \cos\frac{\eta_2}{2}\sqrt{3}\left[L_{NLO3}(\overline{\alpha},\overline{g}^2)-L_{NLO}(\overline{\alpha})/2\right]+\sin\frac{\eta_2}{2}\sqrt{2}L_{NLO2+}(\overline{\alpha},\overline{g}), \\
y_{06} &= -\sin\frac{\eta_2}{2}\sqrt{3}\left[L_{NLO3}(\overline{\alpha},\overline{g}^2)-L_{NLO}(\overline{\alpha})/2\right]+\cos\frac{\eta_2}{2}\sqrt{2}L_{NLO2+}(\overline{\alpha},\overline{g}), \\
y_{07} &= \sin\frac{\eta_3}{2}\sqrt{3}L_{NLO3+}(\overline{\alpha},\overline{g}^2), \\
y_{08} &= \cos\frac{\eta_3}{2}\sqrt{3}L_{NLO3+}(\overline{\alpha},\overline{g}^2).
\end{aligned}
$$

Appendix F

Rate coefficients for the off-diagonal density matrix elements

We give the rate coefficients occurring in the Bloch-Redfield equation, Eq. (4.43), for the reduced density matrix,

$$\mathcal{L}_{01,01} = \frac{2\kappa}{\hbar\beta} y_{00} y_{11} - \frac{\kappa}{\hbar\beta} y_{00}^2 - \frac{\kappa}{\hbar\beta} y_{11}^2 - \frac{1}{2}\mathcal{L}_{00,11}, \tag{F.1}$$

$$\mathcal{L}_{02,02} = \frac{2\kappa}{\hbar\beta} y_{00} y_{22} - \frac{\kappa}{\hbar\beta} y_{00}^2 - \frac{\kappa}{\hbar\beta} y_{22}^2 - \frac{1}{2}\mathcal{L}_{00,22}, \tag{F.2}$$

$$\mathcal{L}_{03,03} = \frac{2\kappa}{\hbar\beta} y_{00} y_{33} - \frac{\kappa}{\hbar\beta} y_{00}^2 - \frac{\kappa}{\hbar\beta} y_{33}^2 - \frac{1}{2}\mathcal{L}_{11,33} - \frac{1}{2}\mathcal{L}_{22,33}, \tag{F.3}$$

$$\mathcal{L}_{04,04} = \frac{2\kappa}{\hbar\beta} y_{00} y_{44} - \frac{\kappa}{\hbar\beta} y_{00}^2 - \frac{\kappa}{\hbar\beta} y_{44}^2 - \frac{1}{2}\mathcal{L}_{11,44} - \frac{1}{2}\mathcal{L}_{22,44}, \tag{F.4}$$

$$\mathcal{L}_{12,12} = \frac{2\kappa}{\hbar\beta} y_{11} y_{22} - \frac{\kappa}{\hbar\beta} y_{11}^2 - \frac{\kappa}{\hbar\beta} y_{22}^2 - \frac{1}{2}\mathcal{L}_{00,11} - \frac{1}{2}\mathcal{L}_{00,22}, \tag{F.5}$$

$$\mathcal{L}_{13,13} = \frac{2\kappa}{\hbar\beta} y_{11} y_{33} - \frac{\kappa}{\hbar\beta} y_{11}^2 - \frac{\kappa}{\hbar\beta} y_{33}^2 - \frac{1}{2}\mathcal{L}_{00,11} - \frac{1}{2}\mathcal{L}_{11,33} - \frac{1}{2}\mathcal{L}_{22,33}, \tag{F.6}$$

$$\mathcal{L}_{14,14} = \frac{2\kappa}{\hbar\beta} y_{11} y_{44} - \frac{\kappa}{\hbar\beta} y_{11}^2 - \frac{\kappa}{\hbar\beta} y_{44}^2 - \frac{1}{2}\mathcal{L}_{00,11} - \frac{1}{2}\mathcal{L}_{11,44} - \frac{1}{2}\mathcal{L}_{22,44}, \tag{F.7}$$

$$\mathcal{L}_{23,23} = \frac{2\kappa}{\hbar\beta} y_{22} y_{33} - \frac{\kappa}{\hbar\beta} y_{22}^2 - \frac{\kappa}{\hbar\beta} y_{33}^2 - \frac{1}{2}\mathcal{L}_{00,22} - \frac{1}{2}\mathcal{L}_{11,33} - \frac{1}{2}\mathcal{L}_{22,33}, \tag{F.8}$$

$$\mathcal{L}_{24,24} = \frac{2\kappa}{\hbar\beta} y_{22} y_{44} - \frac{\kappa}{\hbar\beta} y_{22}^2 - \frac{\kappa}{\hbar\beta} y_{44}^2 - \frac{1}{2}\mathcal{L}_{00,22} - \frac{1}{2}\mathcal{L}_{11,44} - \frac{1}{2}\mathcal{L}_{22,44}, \tag{F.9}$$

$$\mathcal{L}_{34,34} = \frac{2\kappa}{\hbar\beta} y_{33} y_{44} - \frac{\kappa}{\hbar\beta} y_{33}^2 - \frac{\kappa}{\hbar\beta} y_{44}^2 - \frac{1}{2}\mathcal{L}_{11,33} - \frac{1}{2}\mathcal{L}_{22,33} - \frac{1}{2}\mathcal{L}_{11,44} - \frac{1}{2}\mathcal{L}_{22,44}, \tag{F.10}$$

$$\begin{aligned}\mathcal{L}_{01,02} &= \frac{\kappa}{\hbar\beta}(y_{00}y_{12} - y_{12}y_{22}) - G(\omega_{02})N_{02}y_{01}y_{02} - G(\omega_{12})N_{12}y_{11}y_{12} \\ &\quad -G(\omega_{32})N_{32}y_{13}y_{23} - G(\omega_{42})N_{42}y_{14}y_{24}, \end{aligned} \tag{F.11}$$

$$\begin{aligned}\mathcal{L}_{02,01} &= \frac{\kappa}{\hbar\beta}(y_{00}y_{12} - y_{12}y_{11}) - G(\omega_{01})N_{01}y_{01}y_{02} - G(\omega_{21})N_{21}y_{22}y_{12} \\ &\quad -G(\omega_{31})N_{31}y_{13}y_{23} - G(\omega_{41})N_{41}y_{14}y_{24}, \end{aligned} \tag{F.12}$$

$$\begin{aligned}\mathcal{L}_{13,23} &= \frac{\kappa}{\hbar\beta}(y_{33}y_{12} - y_{12}y_{22}) - G(\omega_{12})N_{12}(y_{11}y_{12} - y_{12}y_{33}) \\ &\quad -G(\omega_{02})N_{02}y_{01}y_{02} - G(\omega_{32})N_{32}y_{13}y_{23} - G(\omega_{42})N_{42}y_{14}y_{24}, \end{aligned} \tag{F.13}$$

$$\begin{aligned}\mathcal{L}_{23,13} &= \frac{\kappa}{\hbar\beta}(y_{33}y_{12} - y_{12}y_{11}) - G(\omega_{21})N_{21}(y_{22}y_{12} - y_{12}y_{33}) \\ &\quad -G(\omega_{01})N_{01}y_{01}y_{02} - G(\omega_{31})N_{31}y_{13}y_{23} - G(\omega_{41})N_{41}y_{14}y_{24}, \end{aligned} \tag{F.14}$$

$$\begin{aligned}\mathcal{L}_{14,24} &= \frac{\kappa}{\hbar\beta}(y_{44}y_{12} - y_{12}y_{22}) - G(\omega_{12})N_{12}(y_{11}y_{12} - y_{12}y_{44}) \\ &\quad -G(\omega_{02})N_{02}y_{01}y_{02} - G(\omega_{32})N_{32}y_{13}y_{23} - G(\omega_{42})N_{42}y_{14}y_{24}, \end{aligned} \tag{F.15}$$

$$\begin{aligned}\mathcal{L}_{24,14} &= \frac{\kappa}{\hbar\beta}(y_{44}y_{12} - y_{12}y_{11}) - G(\omega_{21})N_{21}(y_{22}y_{12} - y_{12}y_{44}) \\ &\quad -G(\omega_{01})N_{01}y_{01}y_{02} - G(\omega_{31})N_{31}y_{13}y_{23} - G(\omega_{41})N_{41}y_{14}y_{24}. \end{aligned} \tag{F.16}$$

Appendix G

Diagonal reduced density matrix elements

The solutions of the FSA master equation, Eq. (4.53a), for the diagonal elements within the low temperature approximation, Eq. (4.61), read:

$$
\begin{aligned}
&\sigma_{00}(t) = \\
&\sigma^0_{00} + \sigma^0_{11} + \sigma^0_{22} + \sigma^0_{33} + \sigma^0_{44} \\
&- \exp(-\pi\mathcal{L}_{00,11}t)\left(\sigma^0_{11} + \sigma^0_{33}\frac{\mathcal{L}_{11,33}}{-\mathcal{L}_{00,11}+\mathcal{L}_{11,33}+\mathcal{L}_{22,33}} + \sigma^0_{44}\frac{\mathcal{L}_{11,44}}{-\mathcal{L}_{00,11}+\mathcal{L}_{11,44}+\mathcal{L}_{22,44}}\right) \\
&- \exp(-\pi\mathcal{L}_{00,22}t)\left(\sigma^0_{22} + \sigma^0_{33}\frac{\mathcal{L}_{22,33}}{-\mathcal{L}_{00,22}+\mathcal{L}_{11,33}+\mathcal{L}_{22,33}} + \sigma^0_{44}\frac{\mathcal{L}_{22,44}}{-\mathcal{L}_{00,22}+\mathcal{L}_{11,44}+\mathcal{L}_{22,44}}\right) \\
&+ \exp(-\pi(\mathcal{L}_{11,33}+\mathcal{L}_{22,33})t)\sigma^0_{33}\left(\frac{\mathcal{L}_{00,22}-\mathcal{L}_{11,33}}{-\mathcal{L}_{00,22}+\mathcal{L}_{11,33}+\mathcal{L}_{22,33}} + \frac{\mathcal{L}_{11,33}}{-\mathcal{L}_{00,11}+\mathcal{L}_{11,33}+\mathcal{L}_{22,33}}\right) \\
&+ \exp(-\pi(\mathcal{L}_{11,44}+\mathcal{L}_{22,44})t)\sigma^0_{44}\left(\frac{\mathcal{L}_{00,22}-\mathcal{L}_{11,44}}{-\mathcal{L}_{00,22}+\mathcal{L}_{11,44}+\mathcal{L}_{22,44}} + \frac{\mathcal{L}_{11,44}}{-\mathcal{L}_{00,11}+\mathcal{L}_{11,44}+\mathcal{L}_{22,44}}\right),
\end{aligned}
\tag{G.1}
$$

$$
\begin{aligned}
\sigma_{11}(t) \;=\; &- \exp(-\pi\mathcal{L}_{00,11}t)\sigma^0_{11} \\
&- \exp(-\pi(\mathcal{L}_{00,11}+\mathcal{L}_{11,33}+\mathcal{L}_{22,33})t)\sigma^0_{33}\frac{\mathcal{L}_{11,33}}{-\mathcal{L}_{00,11}+\mathcal{L}_{11,33}+\mathcal{L}_{22,33}} \\
&- \exp(-\pi(\mathcal{L}_{00,11}+\mathcal{L}_{11,44}+\mathcal{L}_{22,44})t)\sigma^0_{44}\frac{\mathcal{L}_{11,44}}{-\mathcal{L}_{00,11}+\mathcal{L}_{11,44}+\mathcal{L}_{22,44}},
\end{aligned}
\tag{G.2}
$$

$$
\begin{aligned}
\sigma_{22}(t) \;=\; &- \exp(-\pi\mathcal{L}_{00,22}t)\sigma^0_{22} \\
&- \exp(-\pi(\mathcal{L}_{00,22}+\mathcal{L}_{11,33}+\mathcal{L}_{22,33})t)\sigma^0_{33}\frac{\mathcal{L}_{22,33}}{-\mathcal{L}_{00,22}+\mathcal{L}_{11,33}+\mathcal{L}_{22,33}} \\
&- \exp(-\pi(\mathcal{L}_{00,22}+\mathcal{L}_{11,44}+\mathcal{L}_{22,44})t)\sigma^0_{44}\frac{\mathcal{L}_{22,44}}{-\mathcal{L}_{00,22}+\mathcal{L}_{11,44}+\mathcal{L}_{22,44}},
\end{aligned}
\tag{G.3}
$$

$$
\sigma_{33}(t) = \exp(-\pi(\mathcal{L}_{11,33}+\mathcal{L}_{22,33})t)\sigma^0_{33}, \tag{G.4}
$$

$$
\sigma_{44}(t) = \exp(-\pi(\mathcal{L}_{11,44}+\mathcal{L}_{22,44})t)\sigma^0_{44}. \tag{G.5}
$$

Bibliography

[1] U. Weiss, *Quantum Dissipative Systems,* Series in modern Condensed Matter Physics Vol. 13, 3rd ed. (Singapore: World Scientific, 2008).

[2] P. Ullersma, Physica **32**, 27,56,74,90 (1966).

[3] R. Zwanzig, Journal of Statistical Physics **9**, 215 (1973).

[4] A. O. Caldeira and A. J. Leggett, Physica A: Statistical and Theoretical Physics **121**, 587 (1983).

[5] A. O. Caldeira and A. J. Leggett, Annals of Physics **149**, 374 (1983).

[6] A. H. Nayfeh and D. T. Mook, *Nonlinear Oscillations*, Wiley Classics Libary Edition, A Wiley-Interscience Publication (John Wiley & Sons, Inc. New York - Chichester - Brisbane - Toronto - Singapore, 1995).

[7] D. W. Jordan and P. Smith, *Nonlinear ordinary differential equations, An introduction to dynamical systems*, 3rd ed. (Oxford University Press, Oxford, 1999).

[8] I. Siddiqi *et al.*, Physical Review B **73**, 054510 (2006).

[9] I. Siddiqi *et al.*, Physical Review Letters **94**, 027005 (2005).

[10] J. C. Lee, W. D. Oliver, K. K. Berggren, and T. P. Orlando, Physical Review B **75**, 144505 (2007).

[11] T. Picot, A. Lupaşcu, S. Saito, C. J. P. M. Harmans, and J. E. Mooij, Physical Review B **78**, 132508 (2008).

[12] I. Katz, R. Lifshitz, A. Retzker, and R. Straub, New Journal of Physics **10**, 125023 (2008).

[13] C. C. Tannoudji, B. Diu, and F. Laloë, *Quantenmechanik*, Vol. I,II, 2nd ed. (Walter de Gruyter Berlin - New York, 1999).

[14] F. Schwabl, *Quantenmechanik*, 6th ed. (Springer Verlag Berlin - Heidelberg - New York, 2005).

[15] M. Rigo, G. Alber, F. Mota-Furtado, and P. F. O'Mahony, Physical Review A **55**, 1665 (1997).

[16] M. I. Dykman and M. V. Fistul, Physical Review B **71**, 140508 (2005).

[17] V. Peano and M. Thorwart, Chemical Physics **322**, 135 (2006).

[18] V. Peano and M. Thorwart, New Journal of Physics **8**, 21 (2006).

[19] V. Peano and M. Thorwart, Physical Review B **70**, 235401 (2004).

[20] C. Vierheilig and M. Grifoni, Chemical Physics **375**, 216 (2010), Stochastic processes in Physics and Chemistry (in honor of Peter Hänggi).

[21] C. Vierheilig, J. Hausinger, and M. Grifoni, Physical Review A **80**, 052331 (2009).

[22] C. Vierheilig, D. Bercioux, and M. Grifoni, Phys. Rev. A **83**, 012106 (2011).

[23] C. Frammelsberger, *Spectral density of a qubit in a nonlinear environment*, in *Workshop Report VII of the Graduiertenkolleg*, edited by C. Frammelsberger and C. Strunk, Graduiertenkolleg 638, Nichtlinearität und Nichtgleichgewicht in kondensierter Materie, p. 117, 2007.

[24] C. Frammelsberger, *The dissipative quantum Duffing oscillator*, in *Workshop Report VIII of the Graduiertenkolleg*, edited by H. Diehl and C. Strunk, Graduiertenkolleg 638, Nichtlinearität und Nichtgleichgewicht in kondensierter Materie, p. 15, 2008.

[25] W. J. Cunnigham, *Introduction to nonlinear analysis,* Electrical and electronic engineering series (McGraw-Hill Verlag, 1958).

[26] F. Kneubühl, *Lineare und nichtlineare Schwingungen und Wellen,* Teubner Studienbücher Physik (Teubner Verlag Stuttgart, 1995).

[27] A. Polyamin and V. Zaitsev, *Handbook of exact solutions for ordinary differential equations* (CRC Press, 1995).

[28] C. Hayashi, *Nonlinear oscillations in physical systems* (McGraw-Hill, Inc., 1965).

[29] S. Alridge (a), R. Lifshitz (b), and M. C. Cross (b), *Nonlinear Dynamics of Nanosystems* (Wiley VCH Verlag GmbH & Co. KGaA Weinheim, 2010), chap. 7,8, (a) The Duffing Oscillator for Nanoelectromechanical Systems and (b) Nonlinear Dynamcis of Nanomechanical Resonators, pp. 203-266.

[30] H. W. C. Postma, I. Kozinsky, A. Husain, and M. L. Roukes, Applied Physics Letters **86**, 223105 (2005).

[31] A. N. Cleland and M. L. Roukes, Applied Physics Letters **69**, 2653 (1996).

[32] R. G. Knobel and A. N. Cleland, Nature **424**, 291 (2003).

[33] K. L. Ekinci, X. M. H. Huang, and M. L. Roukes, Applied Physics Letters **84**, 4469 (2004).

[34] A. N. Cleland and M. R. Geller, Physical Review Letters **93**, 070501 (2004).

[35] H. B. Peng, C. W. Chang, S. Aloni, T. D. Yuzvinsky, and A. Zettl, Physical Review Letters **97**, 087203 (2006).

[36] W. Zhang, R. Baskaran, and K. L. Turner, Sensors and Actuators A: Physical **102**, 139 (2002).

[37] A. N. Cleland and M. L. Roukes, Nature **392**, 160 (1998).

[38] E. Buks and B. Yurke, Physical Review E **74**, 046619 (2006).

[39] R. Almog, S. Zaitsev, O. Shtempluck, and E. Buks, Physical Review Letters **98**, 078103 (2007).

[40] J. S. Aldridge and A. N. Cleland, Physical Review Letters **94**, 156403 (2005).

[41] B. Yurke, D. S. Greywall, A. N. Pargellis, and P. A. Busch, Physical Review A **51**, 4211 (1995).

[42] D. S. Greywall, B. Yurke, P. A. Busch, A. N. Pargellis, and R. L. Willett, Physical Review Letters **72**, 2992 (1994).

[43] K. C. Schwab and M. L. Roukes, Physics Today **58**, 36 (2005).

[44] S. M. Carr, W. E. Lawrence, and M. N. Wybourne, Physical Review B **64**, 220101 (2001).

[45] M. Blencowe, Physics Reports **395**, 159 (2004).

[46] I. Katz, A. Retzker, R. Straub, and R. Lifshitz, Physical Review Letters **99**, 040404 (2007).

[47] M. I. Dykman, Physical Review E **75**, 011101 (2007).

[48] P. D. Drummond and D. F. Walls, Journal of Physics A: Mathematical and General **13**, 725 (1980).

[49] I. Serban and F. K. Wilhelm, Physical Review Letters **99**, 137001 (2007).

[50] L.-Z. Guo, Z.-G. Zheng, and X.-Q. Li, Europhysics Letters **90**, 10011 (2010).

[51] A. D. Armour, M. P. Blencowe, and K. C. Schwab, Physical Review Letters **88**, 148301 (2002).

[52] A. N. Cleland and M. R. Geller, Physical Review Letters **93**, 070501 (2004).

[53] S. Etaki *et al.*, Nature Physics **4**, 785 (2008).

[54] E. Boaknin *et al.*, arXiv:cond-mat/0702445v1 (2007).

[55] M. Metcalfe *et al.*, Physical Review B **76**, 174516 (2007).

[56] P. D. Nation, M. P. Blencowe, and E. Buks, Physical Review B **78**, 104516 (2008).

[57] M. A. Nielson and I. L. Chuang, *Quantum Computation and Quantum Information* (Cambridge University Press, 2000).

[58] C. Monroe, D. M. Meekhof, B. E. King, W. M. Itano, and D. J. Wineland, Physical Review Letters **75**, 4714 (1995).

[59] N. A. Gershenfeld and I. L. Chuang, Science **275**, 350 (1997).

[60] T. Yoshie *et al.*, Nature **432**, 200 (2004).

[61] A. Faraon *et al.*, Nature Physics **4**, 859 (2008).

[62] J. P. Reithmaier *et al.*, Nature **432**, 197 (2004).

[63] J. M. Raimond, M. Brune, and S. Haroche, Reviews of Modern Physics **73**, 565 (2001).

[64] T. P. Orlando *et al.*, Physical Review B **60**, 15398 (1999).

[65] Y. Nakamura, Y. A. Pashkin, and J. S. Tsai, Nature **398**, 786 (1999).

[66] Y. Makhlin, G. Schön, and A. Shnirman, Reviews of Modern Physics **73**, 357 (2001).

[67] D. Vion *et al.*, Science **296**, 886 (2002).

[68] E. Collin *et al.*, Physical Review Letters **93**, 157005 (2004).

[69] A. Blais, R.-S. Huang, A. Wallraff, S. M. Girvin, and R. J. Schoelkopf, Physical Review A **69**, 062320 (2004).

[70] A. Wallraff *et al.*, Nature **431**, 162 (2004).

[71] D. I. Schuster *et al.*, Physical Review Letters **94**, 123602 (2005).

[72] A. Wallraff *et al.*, Physical Review Letters **95**, 060501 (2005).

[73] D. I. Schuster *et al.*, Nature **445**, 515 (2007).

[74] A. Wallraff *et al.*, Physical Review Letters **99**, 050501 (2007).

[75] J. E. Mooij *et al.*, Science **285**, 1036 (1999).

[76] I. Chiorescu, Y. Nakamura, C. J. P. M. Harmans, and J. E. Mooij, Science **299**, 1869 (2003).

[77] I. Chiorescu *et al.*, Nature **431**, 159 (2004).

[78] J. Johansson *et al.*, Physical Review Letters **96**, 127006 (2006).

[79] J. Clarke and F. K. Wilhelm, Nature **453**, 1031 (2008).

[80] A. Blais *et al.*, Physical Review A **75**, 032329 (2007).

[81] A. A. Houck *et al.*, Nature **449**, 328 (2007).

[82] L. S. Bishop *et al.*, Nature Physics **5**, 105 (2009).

[83] J. M. Fink *et al.*, Nature **454**, 315 (2008).

[84] A. Lupaşcu, C. J. M. Verwijs, R. N. Schouten, C. J. P. M. Harmans, and J. E. Mooij, Physical Review Letters **93**, 177006 (2004).

[85] N. Boulant *et al.*, Physical Review B **76**, 014525 (2007).

[86] A. Lupascu, S. Saito, T. Picot, P. C. de Groot, and C. J. P. M. Harmans, Nature Physics **3**, 119 (2007).

[87] A. Garg, J. N. Onuchic, and V. Ambegaokar, The Journal of Chemical Physics **83**, 4491 (1985).

[88] L. Tian, S. Lloyd, and T. P. Orlando, Physical Review B **65**, 144516 (2002).

[89] C. van der Wal, F. Wilhelm, C. Harmans, and J. Mooij, The European Physical Journal B **31**, 111 (2003).

[90] M. Thorwart, E. Paladino, and M. Grifoni, Chemical Physics **296**, 333 (2004).

[91] M. C. Goorden, M. Thorwart, and M. Grifoni, Physical Review Letters **93**, 267005 (2004).

[92] M. C. Goorden, M. Thorwart, and M. Grifoni, The European Physical Journal B - Condensed Matter and Complex Systems **45**, 405 (2005).

[93] F. K. Wilhelm, S. Kleff, and J. von Delft, Chemical Physics **296**, 345 (2004).

[94] S. Kleff, S. Kehrein, and J. von Delft, Physica E: Low-dimensional Systems and Nanostructures **18**, 343 (2003).

[95] S. Kleff, S. Kehrein, and J. von Delft, Physical Review B **70**, 014516 (2004).

[96] I. Serban and F. K. Wilhelm, arXiv:0905.3045v1 (2009).

[97] I. Serban, M. I. Dykman, and F. K. Wilhelm, Physical Review A **81**, 022305 (2010).

[98] H. Nakano, S. Saito, K. Semba, and H. Takayanagi, Physical Review Letters **102**, 257003 (2009).

[99] K. Kakuyanagi *et al.*, arXiv:1004.0182v2 (2010).

[100] B. D. Josephson, Physics Letters **1**, 251 (1962).

[101] M. Tinkham, *Introduction to superconductivity*, 2nd ed. (McGraw-Hill, Inc., 1996).

[102] C. H. van der Wal *et al.*, Science **290**, 773 (2000).

[103] A. J. Leggett, Contemporary Physics **25**, 583 (1984).

[104] A. Lupaşcu, C. J. P. M. Harmans, and J. E. Mooij, Physical Review B **71**, 184506 (2005).

[105] V. Peano Cavasola, *Interplay of driving, nonlinearity and dissipation in nanoscale and ultracold atom systems*, PhD thesis, Universität Düsseldorf, 2007, http://docserv.uni-duesseldorf.de/servlets/DocumentServlet?id=3399.

[106] R. Vijay, M. H. Devoret, and I. Siddiqi, Review of Scientific Instruments **80**, 111101 (2009).

[107] G. Burkard, D. P. DiVincenzo, P. Bertet, I. Chiorescu, and J. E. Mooij, Physical Review B **71**, 134504 (2005).

[108] H. Grabert, P. Schramm, and G.-L. Ingold, Physics Reports **168**, 115 (1988).

[109] P. Hänggi, *Lecture Notes in Physics Vol. 484* (Springer Verlag, 1997), chap. Generalized Langevin Equations: A Useful Tool for the Perplexed Modeller of Nonequilibrium Fluctuations?, p. 15.

[110] R. P. Feynman and F. L. Vernon, Annals of Physics **24**, 118 (1963).

[111] H. Kleinert, *Path Integrals in Quantum Mechanics, Statistics, Polymer Physics, and Financial Markets*, 3rd ed. (World Scientific New Jersey - London - Singapore - Shanghai - Hong Kong - Taipei - Bangalore, 2004).

[112] G.-L. Ingold, *Lecture Notes in Physics: Coherent Evolution in Noisy Environments* (Springer Berlin - Heidelberg, 2002), chap. Path Integrals and Their Application to Dissipative Quantum Systems, p. 1.

[113] W. H. Louisell, *Quantum Statistical Properties of Radiation* (Wiley, New York, 1973).

[114] R. Blümel *et al.*, Physical Review Letters **62**, 341 (1989).

[115] R. Blümel *et al.*, Physical Review A **44**, 4521 (1991).

[116] K. Blum, *Density Matrix Theory and Applications*, 2nd ed. (Plenum Press, New York - London, 1996).

[117] S. Kohler, T. Dittrich, and P. Hänggi, Physical Review E **55**, 300 (1997).

[118] S. Kohler, R. Utermann, P. Hänggi, and T. Dittrich, Physical Review E **58**, 7219 (1998).

[119] R. P. Feynman and A. R. Hibbs, *Quantum mechanics and Path Integrals* (McGraw-Hill Book Company New York - St. Louis - San Francisco - Toronto - London - Sydney, 1965).

[120] L. S. Schulman, *Techniques and Applications of Path Integrals* (Wiley & Sons New York, 1961).

[121] S. Kohler, *The interplay of chaos and dissipation in driven quantum systems*, PhD thesis, Universität Augsburg, 1999, Shaker Verlag Aachen, http://www.icmm.csic.es/sigmundkohler/Dissertation.html.

[122] N. Makri and D. E. Makarov, The Journal of Chemical Physics **102**, 4600 (1995).

[123] A. J. Leggett and A. Garg, Physical Review Letters **54**, 857 (1985).

[124] A. J. Leggett *et al.*, Reviews of Modern Physics **59**, 1 (1987).

[125] A. J. Leggett *et al.*, Reviews of Modern Physics **67**, 725 (1995).

[126] E. P. M. Grifoni and U. Weiss, The European Physical Journal B **10**, 719 (1999).

[127] R. Görlich, M. Sassetti, and U. Weiss, Europhysics Letters **10**, 507 (1989).

[128] A. G. Redfield, IBM Journal of Research and Development **1**, 19 (1957).

[129] L. Hartmann, I. Goychuk, M. Grifoni, and P. Hänggi, Physical Review E **61**, R4687 (2000).

[130] M. Grifoni and P. Hänggi, Physics Reports **304**, 229 (1998).

[131] M. Grifoni, M. Winterstetter, and U. Weiss, Physical Review E **56**, 334 (1997).

[132] M. Grifoni, M. Sassetti, and U. Weiss, Physical Review E **53**, R2033 (1996).

[133] G. Floquet, Annales Scientifiques de l'École Normale Supérieure **12**, 47 (1883).

[134] J. H. Shirley, Physical Review **138**, B979 (1965).

[135] H. Sambe, Physical Review A **7**, 2203 (1973).

[136] I. Tittonen, M. Lippmaa, and J. Javanainen, Physical Review A **53**, 1112 (1996).

[137] K. Husimi, Progress of Theoretical Physics **9**, 381 (1953).

[138] A. M. Perelomov and V. S. Popov, Theoretical and Mathematical Physics **3**, 582 (1970).

[139] H. P. Breuer and M. Holthaus, Zeitschrift für Physik D Atoms, Molecules and Clusters **11**, 1 (1989).

[140] T. Dittrich *et al.*, *Quantum Transport and Dissipation* (Wiley VCH Weinheim - Berlin - New York - Chichester - Brisbane - Singapore - Toronto, 1998).

[141] I. Shavitt and L. T. Redmon, The Journal of Chemical Physics **73**, 5711 (1980).

[142] D. C.-T. J. Dupont-Roc and G. Grynberg, *Atom-Photon Interactions: Basic Processes and Applications* (Wiley, New York, 1992).

[143] P. R. Certain and J. O. Hirschfelder, The Journal of Chemical Physics **52**, 5977 (1970).

[144] B. Kirtman, The Journal of Chemical Physics **49**, 3895 (1968).

[145] R. Graham and R. Hübner, Annals of Physics **234**, 300 (1994).

[146] I. S. Gradshteyn and I. M. Ryzhik, *Tables of integrals, series and products* (Academic Press, New York and London, 1971).

[147] F. Nesi, M. Grifoni, and E. Paladino, New Journal of Physics **9**, 316 (2007).

[148] J. Hausinger and M. Grifoni, New Journal of Physics **10**, 115015 (2008).

[149] F. Bloch and A. Siegert, Physical Review **57**, 522 (1940).

[150] M. C. Goorden and F. K. Wilhelm, Physical Review B **68**, 012508 (2003).

[151] F. Brito and A. O. Caldeira, New Journal of Physics **10**, 115014 (2008).

[152] V. Volterra, *Theory of functionals and of integral and integro-differential equations* (Dover Publications (New York), 1959).

[153] P. R. Certain, D. R. Dion, and J. O. Hirschfelder, The Journal of Chemical Physics **52**, 5987 (1970).

[154] P. K. Aravind and J. O. Hirschfelder, The Journal of Physical Chemistry **88**, 4788 (1984).

[155] W. Nolting, *Grundkurs Theoretische Physik 5/2*, 4th ed. (Springer Verlag, Berlin, 2002).

[156] A. J. Stone, *The Theory of Intermolecular Forces* (Clarendon Press, Oxford, 1997).

Acknowledgements

I want to thank all the people, who supported me during the work on my thesis.

First of all I would like to thank Milena Grifoni, my supervisor, for her continuous support, her patience and her talent to motivate. Due to her positive attitude I enjoyed the pleasing working atmosphere within our group. I would also like to thank Johannes Hausinger and Dario Bercioux for many helpful discussions. It was a pleasure for me to work with you all.
I am also grateful to our secretary Lizy Lazar, who tried to help whenever there was any problem, in particular: „bürokratische Hürden zu überwinden“. Within the group „Quantum Transport and Dissipation“ I met a lot of kind people and found new friends. I will also never forget our group trips (cycling, hiking, snowshoeing, ...). I would also like to thank my colleagues in the office during the last years, Peter, Christoph and Björn. We had a lot of fun together. In particular, Christoph and me, both Bavarians, felt that we had the duty to teach our Prussian something about dialect, local culture, ...
I also want to thank my parents, who gave me the possibility to study and supported me during my whole life. For my husband Clemens: Thank you for your numerous encouragements. I would have never managed without you ... .
To my husband Clemens and my friends Nikolaus and Andrea, who were so kind and brave as to patiently read this theoretical work: Thank you a lot! Just a small sidemark: Without you, I would never have known, what this thesis and the works of Shakespeare have in common. Hence ... .
I would also like to thank for the financial support by the DFG under the funding programs GRK 638 and SFB 631.

Publications

Publications

C. Vierheilig, D. Bercioux, M. Grifoni: *Dynamics of a qubit coupled to a dissipative nonlinear quantum oscillator: an effective bath approach*, Physical Review A **83**, 012106 (2011)

C. Vierheilig, M. Grifoni: *The dissipative quantum Duffing oscillator: a comparison of Floquet based approaches*, Chemical Physics **375**, 216 (2010)

C. Vierheilig, J. Hausinger, M. Grifoni: *Dissipative dynamics of a qubit coupled to a nonlinear oscillator*, Physical Review A **80**, 052331 (2009)

C. Frammelsberger, M. Grifoni: *The dissipative quantum Duffing oscillator*, Workshop Report VIII of the Graduiertenkolleg 2008

C. Frammelsberger, M. Grifoni: *Spectral density of a qubit in a nonlinear environment*, Workshop Report VII of the Graduiertenkolleg 2007

Conference contributions

DPG-Frühjahrstagung 2010, Regensburg:
C. Vierheilig, J. Hausinger, M. Grifoni: *Dissipative dynamics of a qubit coupled to a nonlinear undriven or driven oscillator* (Poster)

Solid State Based Quantum Information Processing QIP 2009, Herrsching:
C. Vierheilig, M. Grifoni: *Dissipative properties of a qubit coupled to a nonlinear oscillator* (Poster)

DPG-Frühjahrstagung 2009, Dresden:
C. Frammelsberger, M. Grifoni: *The dissipative quantum Duffing oscillator* (Poster)

Graduiertenkolleg Workshop 2008, Velburg:
C. Frammelsberger, M. Grifoni: *The dissipative quantum Duffing oscillator* (Vortrag)

DPG-Frühjahrstagung 2008, Berlin:
C. Frammelsberger, J. Hausinger, M. Grifoni: *Dynamics of a qubit in a linear/nonlinear structured environment* (Poster)

Graduiertenkolleg Workshop 2007, Frauenchiemsee:
C. Frammelsberger, M. Grifoni: *Spectral density of a qubit in a nonlinear environment* (Vortrag)